REPORT NO.
UCB/EERC-80/08
APRIL 1980

EARTHQUAKE ENGINEERING RESEARCH CENTER

STUDY OF X-BRACED STEEL FRAME STRUCTURES UNDER EARTHQUAKE SIMULATION

by

YUSOF GHANAAT

Report to
American Iron and Steel Institute
and
National Science Foundation

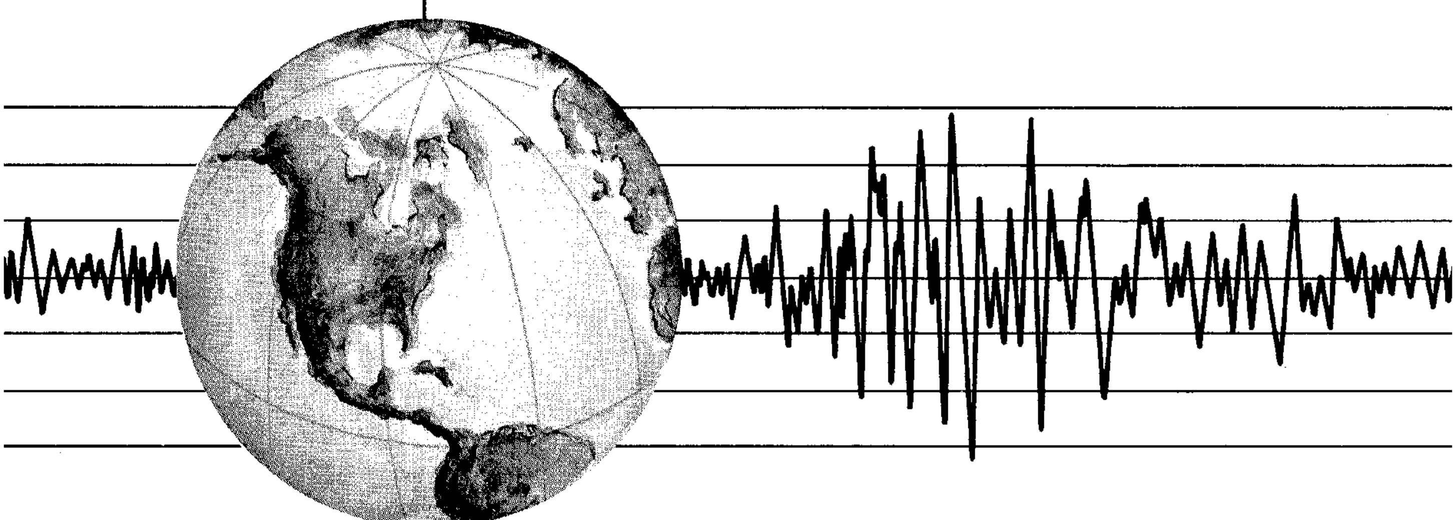

COLLEGE OF ENGINEERING

UNIVERSITY OF CALIFORNIA · Berkeley, California

50272-101

REPORT DOCUMENTATION PAGE

1. REPORT NO. NSF/RA-800194

2.

3. Recipient's Accession No. PB81 122335

4. Title and Subtitle
Study of X-Braced Steel Frame Structures Under Earthquake Simulation

5. Report Date
April 1980

6.

7. Author(s)
Yusof Ghanaat

8. Performing Organization Rept. No.
UCB/EERC-80/08

9. Performing Organization Name and Address
Earthquake Engineering Research Center
University of California, Richmond Field Station
47th and Hoffman Blvd.
Richmond, California 94804

10. Project/Task/Work Unit No.

11. Contract(C) or Grant(G) No.
(C)
(G) PFR-7908257

12. Sponsoring Organization Name and Address
National Science Foundation
1800 G Street, N.W.
Washington, D. C. 20550

13. Type of Report & Period Covered

14.

15. Supplementary Notes

16. Abstract (Limit: 200 words)

Diagonal steel bracing systems are intended to limit lateral displacements of buildings when subjected to wind or other lateral loadings. Many existing buildings with such bracing were designed on the basis of nominal building code requirements for wind, with no consideration of the function of ductility in seismic response. Although the seismic behavior of such structures has been studied analytically, no experiments had been performed previously for verification of the analytical results.

This report presents experimental shaking table test results on the seismic performance of a model three-story building frame, both unbraced and with three different wind bracing systems; and correlates these results with analytical predictions. Considerable compression buckling and tension yielding of the diagonal bracing members were observed in the tests, but the bracing provided significant reductions in the lateral displacements when compared with the unbraced frame response.

Analytical techniques employing three different hysteresis models to represent the three types of bracing systems are shown to predict the response of braced frames with excellent accuracy. Analytical response predictions for the unbraced frame, employing concentrated bilinear plastic hinges for all members including joint connections, also are shown to be very accurate for the levels of nonlinearity encountered.

The results of this study indicate that diagonal bracing systems such as pipe and double angle braces are very effective in reducing lateral displacements of buildings for moderate earthquakes and that their energy dissipation will be significant if their compressive capacity is not less than 50 percent of their tension capacity. Consequently, damage to both the primary structural members as well as non-structural components can be reduced by the use of appropriate light weight diagonal bracing systems.

18. Availability Statement:
Release Unlimited

19. Security Class (This Report)

20. Security Class (This Page)

21. No. of Pages

22. Price

(See ANSI–Z39.18)

See Instructions on Reverse

OPTIONAL FORM 272 (4–77)
(Formerly NTIS–35)
Department of Commerce

STUDY OF X-BRACED STEEL FRAME STRUCTURES UNDER EARTHQUAKE SIMULATION

By

Yusof Ghanaat

Report to

American Iron and Steel Institute

and

National Science Foundation

Report No. UCB/EERC 80/08
Earthquake Engineering Research Center
University of California
Berkeley, California

April 1980

ABSTRACT

Diagonal steel bracing systems are intended to limit lateral displacements of buildings when subjected to wind or other lateral loadings. Many existing buildings with such bracing were designed on the basis of nominal building code requirements for wind, with no consideration of the function of ductility in seismic response. Although the seismic behavior of such structures has been studied analytically, no experiments had been performed previously for verification of the analytical results.

This report presents experimental results on the seismic performance of a model three-story building frame, both unbraced and with three different wind bracing systems; and correlates these results with analytical predictions. The experimental investigation was carried out on the shaking table of the U.C. Berkeley Earthquake Simulator Laboratory. Considerable compression buckling and tension yiedling of the diagonal bracing members were observed in the tests, but the bracing provided significant reductions in the lateral displacements when compared with the unbraced frame response.

Analytical techniques employing three different hysteresis models to represent the three types of bracing systems are shown to predict the response of braced frames with excellent accuracy. The mathematical model of the rod braces simulated both tension yielding and elastic buckling with tension rod rupture mechanism included; pipe and double angle bracing members included both tension yeilding and post-buckling behavior; residual elongation and reduction of compressive capacity with the number of cycles was considered in the double angle model. Analytical response predictions for the unbraced frame, employing concentrated bilinear plastic hinges for all members including joint connections, also are shown to be

very accurate for the levels of nonlinearity encountered.

The results of this study indicate that diagonal bracing systems such as pipe and double angle braces are very effective in reducing lateral displacements of buildings for moderate earthquakes and that their energy dissipation will be significant if their compressive capacity is not less than 50 percent of their tension capacity. Consequently, damage to both the primary structural members as well as non-structural components can be reduced by the use of appropriate light weight diagonal bracing systems.

ACKNOWLEDGMENTS

The support of the American Iron and Steel Institute in fabrication of the test structures and of the National Science Foundation in funding the research program described herein is gratefully acknowledged.

The author is grateful to Professor Graham Powell and his students for developing a very suitable nonlinear program, DRAIN-2D, used extensively in the analytical portion of this research. Thanks are also extended to Professor Egor P. Popov and his former student Dr. Charles W. Roeder, and also to Professor Subhash C. Goel and Dr. Ashok K. Jain for their post-buckling truss elements developed for use in DRAIN-2D program.

The author wishes to express his deep appreciation to Professor Ray W. Clough for his supervision, patience and support throughout the course of this study. In addition, he would like to extend his appreciation to Professor Jack G. Bouwkamp and Professor C. D. Mote for serving as members of his thesis committee. Particularly, Professor Bouwkamp's valuable guidance on design of the bracing members is gratefully acknowledged.

The University of California, Berkeley, Earthquake Engineering Research Center and the Computer Center of the Berkeley Campus provided excellent facilities for carrying out this research program. The assistance of many individuals in the Earthquake Simulator Laboratory and elsewhere is gratefully acknowledged. Special thanks are due to Mr. David Steere whose extensive efforts in instrument calibration and operation of the shaking table itself made a successful test program possible.

The manuscript was typed by Ms. Ruth Horning; numerous figures were prepared by Mr. Larry Bell.

Finally, but most sincerely, the author would like to acknowledge the loyalty, encouragement, and understanding of his fiancee, Shahrzad, which gave this study a purpose beyond its mere academic value.

TABLE OF CONTENTS

LIST OF TABLES

LIST OF FIGURES

EL CENTRO SPAN 100 TEST - ROD BRACED STRUCTURE

EL CENTRO SPAN 1000 - ROD BRACED STRUCTURE

EL CENTRO SPAN 950 - ROD BRACED STRUCTURE

PACOIMA EARTHQUAKE (1.129 G) - ROD BRACED STRUCTURE

Page

Page

PACOIMA SPAN 400 - UNBRACED STRUCTURE

1. INTRODUCTION

1.1 Background

Diagonal steel bracing systems are frequently used to control the lateral displacements of buildings that are designed for wind or other lateral loadings. Many existing buildings of this type were designed on the basis of nominal building code requirements, with no consideration for modern concepts of ductility. When such structures are subjected to earthquake motions of even moderate intensity, the bracing members typically yield in tension and/or buckle in compression. Some analytical studies have been made of the seismic behavior of buildings with diagonal bracing designed for wind, but experimental research on this subject has not previously been done.

Assuming an elastic resistance mechanism, Clough and Jenschke[1] used computer procedures to study the seismic behavior of two buildings with supplemental diagonal braces; also some evidence about their dynamic behavior was obtained from observation of actual earthquake performance (see Reference 1). Inelastic behavior of braced frame structures is closely related to the hysteretic behavior of the bracing members. This behavior makes the response of a braced frame more difficult than that of an unbraced frame because of the complicated buckling-yielding mechanism. The earliest analytical studies of the inelastic behavior of braced frames were based on the assumption of a "slip-type" behavior for the bracing members. The slip model assumes the presence of two cross braces with each alternately becoming inactive during the application of cyclic loading. Hanson and Fan[2], Workman[3], and Goel and Hanson[4] employed this model in their analyses, in which an elasto-plastic resistance mechanism was assumed in tension only for the slender bracing members and the compression capacity of these members was neglected. This model is not too unrealistic for extremely slender braces, but it cannot be justified for braces having small to moderate slenderness ratios. Hence obtaining a model with a more realistic hysteresis behavior for the bracing members became the object of many later studies.

The cyclic behavior of individual bracing members with different slenderness ratios has been studied both analytically and experimentally by many investigators, in Japan and in the United States. These studies have been summarized and reported fully by Popov, Takanashi, and Roeder(5). The results of these studies indicate that the general cyclic behavior of less slender braces differs significantly from the slip model; in particular it exhibits considerable energy dissipation in the inelastic response. These studies also suggest that the plastic rotation due to inelastic behavior in the post-buckling range is concentrated in a region near the middle of the brace. Many analytical studies have been performed to calculate the general cyclic behavior of bracing members, but most of them are either excessively complex or otherwise impractical for analysis of large structures. One simple method of analyzing the inelastic behavior of a braced frame was proposed by Nilforoushan(6). His analysis was based on a straight line segment approximation of the general hysteretic behavior of a brace, and included the post-buckling behavior. The general force-displacement behavior of the brace is approximated by a series of straight lines selected to get the best fit. Nilforoushan used this model to perform dynamic analyses of several concentriclly K-braced structures (in concentrically K-braced frames, the center line intersection of the braces intersects the center line of the beam). A similar hysteresis model was developed by Roeder and Popov[7], and was adapted for use in the program DRAIN-2D[8]. They used this model to analyze the dynamic behavior of an eccentric braced structure. Note that the eccentric braces employed by Roeder and Popov were quite heavy and differ greatly from the wind bracing members which are the subject of the present study; the eccentric braces deliberately introduce large eccentricities between the brace-beam connection and the beam-column joint (i.e. the center line of the brace does not intersect the center line intersection of the beam and column), to ensure that the eccentric beam element yields in shear while preventing buckling of the brace. An alternative mathematical hysteresis model was developed later by Singh[9], which consisted of fewer linear segments. Subsequently, Jain and Goel[10] presented another hysteresis model which represents the post-buckling behavior of bracing members in a more realistic manner, and includes the residual elongation in tension and reduction in compressive capacity as a function of the number of cycles.

All of these studies were limited either to experimental study of the individual members or to analytical studies of complete frames which were not verified by experimental results. The purpose of the present investigation was to perform dynamic tests on a building frame with diagonal wind bracing systems, and to correlate these results with computer analyses.

1.2 Objectives and Scope

The specific objective of this research was to obtain experimental data on the seismic performance of a building frame having three different diagonal wind bracing systems, and to correlate these results with computer analyses. The actual response results were also utilized to demonstrate the effectiveness of an existing nonlinear structural program in the analysis of diagonal bracing systems. Of particular interest was the adequacy of the available bracing elements in that program. The experimental and analytical responses were then used to compare the performances of the bracing systems.

2. TEST FACILITIES

2.1 Earthquake Simulator

The test program was carried out at the Earthquake Simulator Laboratory, located at the Richmond Field Station of the University of California, Berkeley. The primary facility at this laboratory is a 20-ft square shaking table and its associated control systems. A complete description of this has been reported by Rea and Penzien[11]. A brief description along with the new modifications is given here.

The reinforced, post-tensioned concrete shaking table shown in Fig. 2.1.1b is able to move independently in one horizontal component and in the vertical direction; and is driven by three 50 kip, and four 20 kip hydraulic actuators, respectively. During the test operation the dead weight of the shaking table (100 kips) and of the test structure are balanced by differential air pressure which frees the vertical actuators from carrying any static load.

The capabilities for both the horizontal and vertical motions of the table are illustrated in Fig. 2.1.2. At frequencies lower than one cps, the intensity of motion is limited by the actuator strokes; at intermediate frequencies from 1 to 4 cps, by the maximum actuator velocity; at frequencies greater than 4 cps, by the maximum actuator force capabilities and the oil column resonance of the drive system.

The command signals of the table are in the form of analog displacement time histories on magnetic tape which are usually obtained through a double integration of acceleration time histories. The shaking table was originally operating with only an active stabilization system to resist overturning moments. Recently a passive stabilization system consisting of four vertical stabilizers was installed; this is described below.

Passive Stabilizers

The vertical active actuators do not have sufficient force capacity to resist the overturning forces that would be generated by the largest structures that were envisioned for testing on the table. Thus it was planned to install a passive stabilization system for the shaking table that would have a larger overturning moment capacity than the active system provided.

A vertical passive stabilizer system increases the shaking table stiffness and overturning moment capacity in its pitching mode. The effect of the passive stabilizer system on the pitching mode stiffness was determined from frequency response functions for the unloaded table and from the maximum pitch of the table while it was subjecting a three-story steel frame to the El Centro ground motion.

The horizontal motion causes the table to pitch. Pitch frequency response for the table without the passive stabilizers and with the passive stabilizers at operating pressures of 100, 500, 1000, and 1500 psi are shown in Fig. 2.1.3. The pitch resonant frequency of the table before the passive stabilizers were installed was 13.0 cps. The passive stabilizers for operating pressure above 100 psi, increase the pitch resonant frequency to 26 cps.

2.2 Data Acquisition System

A data acquisition system consists of a NOVA 1200 mini-computer and a NEFF System 620 Analog-Digital processor, whose prime function is the collection of data during a test. The NOVA mini-computer is equipped with a Diablo 31 magnetic disk unit, which is capable of digitally sampling up to 128 data channels at rates up to 155 samples per second, per channel. Transducer signals in analog form pass through an Analog-Digital processor. The digitized data are then temporarily stored on the magnetic disk before being transferred to tape by a Wang 9-track magnetic tape drive for permanent storage.

Limited data reduction for immediate evaluation of test results can be performed on the mini-computer, but for major data reduction operations the CDC 6400 Computer System at the Berkeley Campus is utilized. In order to be compatible with the CDC system, a conversion to 7-track magnetic tape must be carried out on the data. An extra magnetic tape drive system has recently been installed for the mini-computer to perform this conversion at the Earthquake Simulator Laboratory. The transformed data are then generally displayed in a graphical form using the Calcomp Plotting system at the computer center at the Berkeley campus.

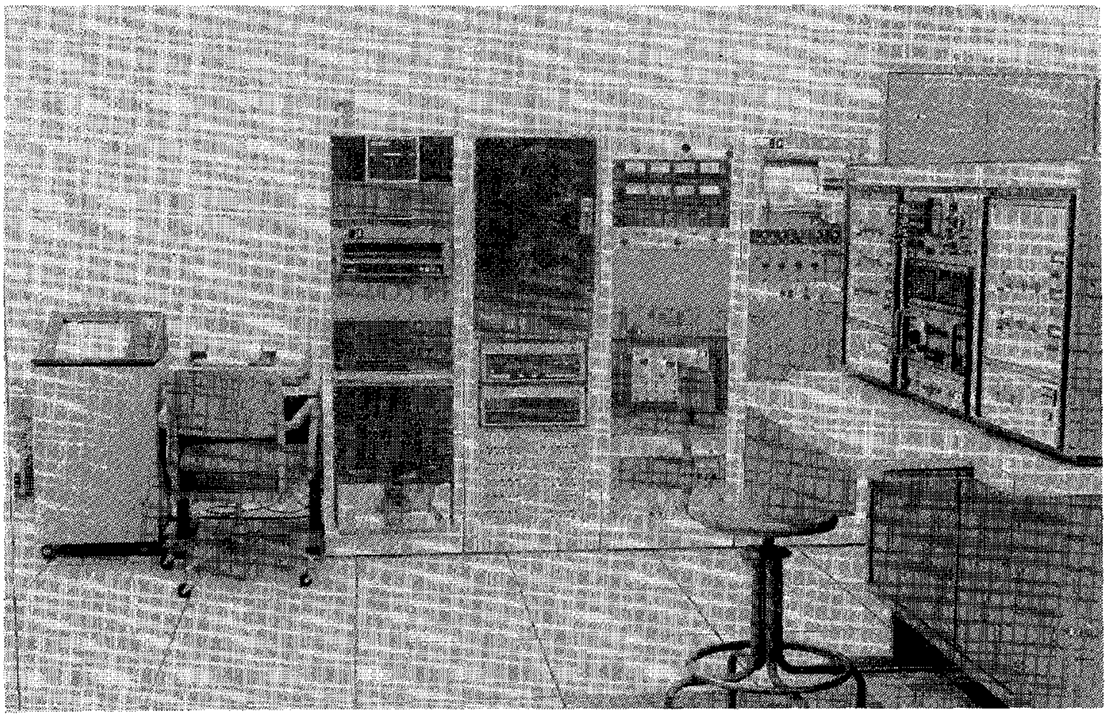

a. Control Room

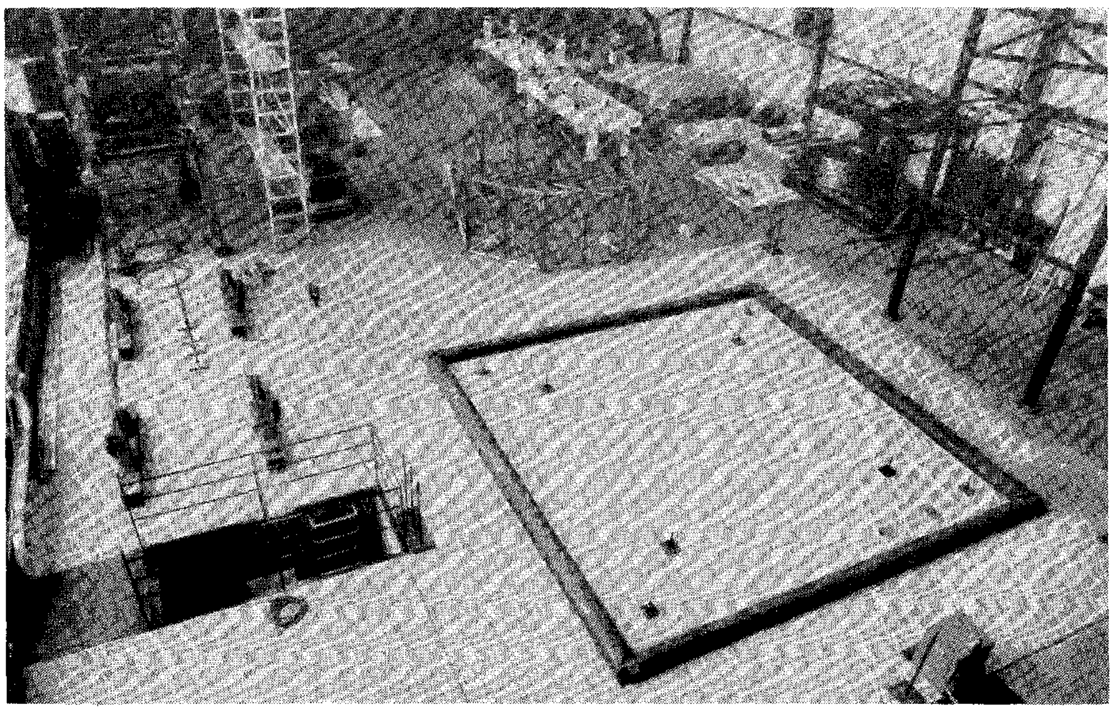

b. Shaking Table

Fig. 2.1.1 Test Facility

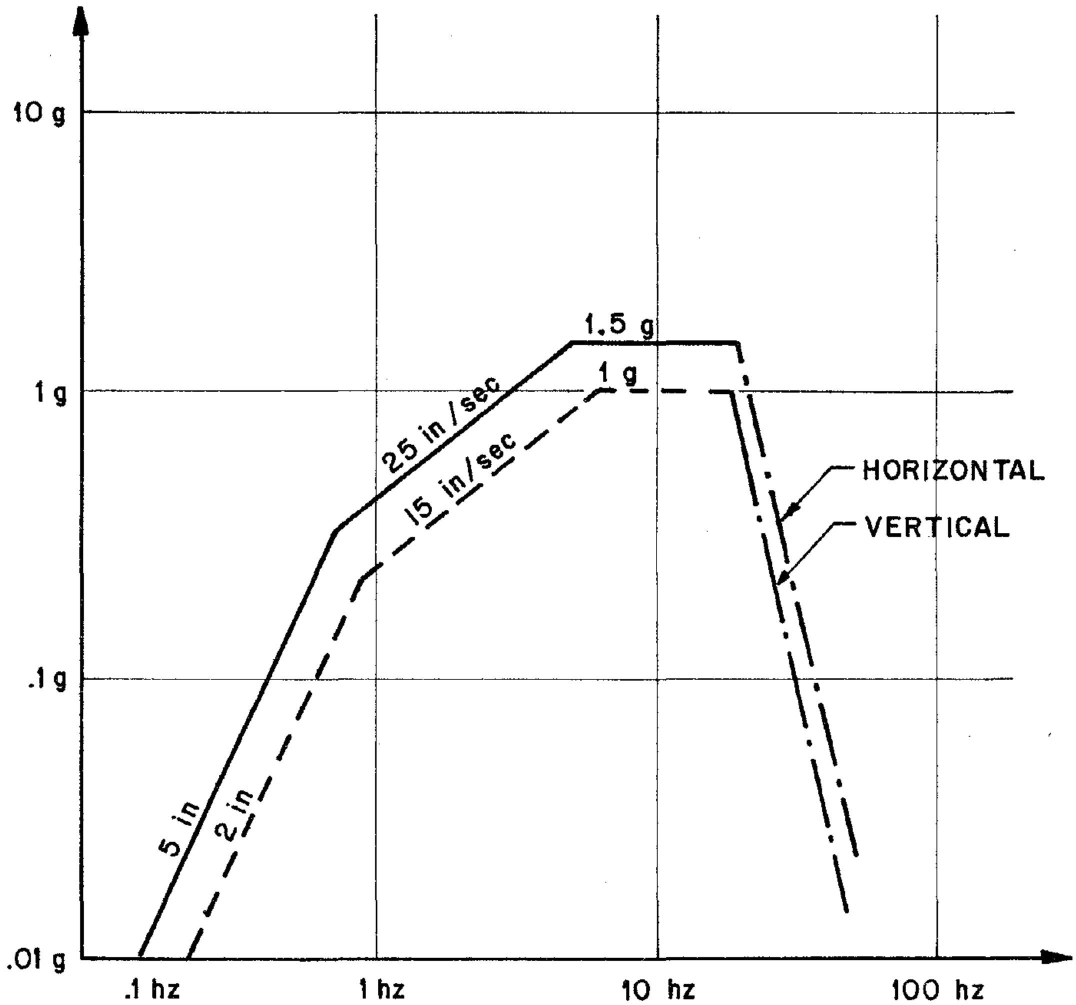

Fig. 2.1.2 Shaking Table Motion Capabilities
(after D. Rea and J. Penzien)

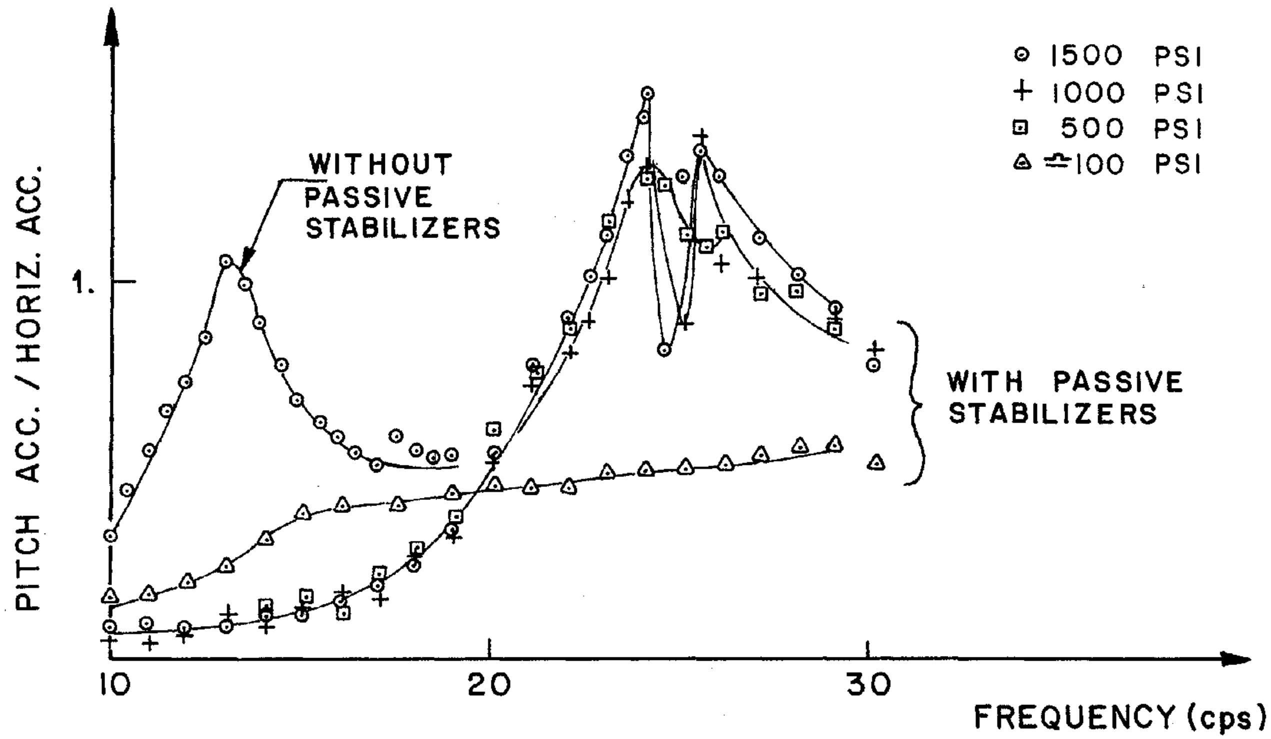

Fig. 2.1.3 Pitch Frequency Responses for Unloaded Table

3. TEST STRUCTURES

3.1 Moment Resistant Steel Frame Model

The three-story moment resistant steel frame test structure of Reference 12 was designed as a 6/10 scale model of typical building construction. This is 6 x 12 ft in plan, 17 ft - 4 in. high, and was fabricated from A36 wide flange sections; W5x16 for columns and W6x12 for girders. The first floor, second floor, and the third floor heights are 6 ft - 8 in., 5 ft - 4 in., and 5 ft - 4 in., respectively. Each floor system was supplemented with enough crossing beams and angle braces to resemble a rigid floor diaphragm. The connections of the cross beams to columns were initially provided by gusset plates and high strength bolts. However, in this investigation the gusset plates were welded to the columns in order to obtain a shear resistant joint in the plane of the columns' weak axes (Fig. 3.2.3).

The original lateral bracing system consisted of 1/2 in. diameter rods with turnbuckles, arranged in an X pattern at each story across the 6 ft dimension of the frame (corresponding to the weak axis of the columns). In the second and third test series, these braces were replaced by 3/4 in. diameter pipe X-braces, and 1 x 1 x 1/8 in. double angle X-braces, respectively. Each pipe or double angle X-brace unit was welded together at the center and to connections at the ends. Figure 3.1.1 and 3.1.2 show the test frame with rod and double angle braces, and Fig. 3.1.3 demonstrates the front elevation of the test frame with pipe braces. Note that concrete blocks were supported at each floor to provide appropriate seismic loads during tests.

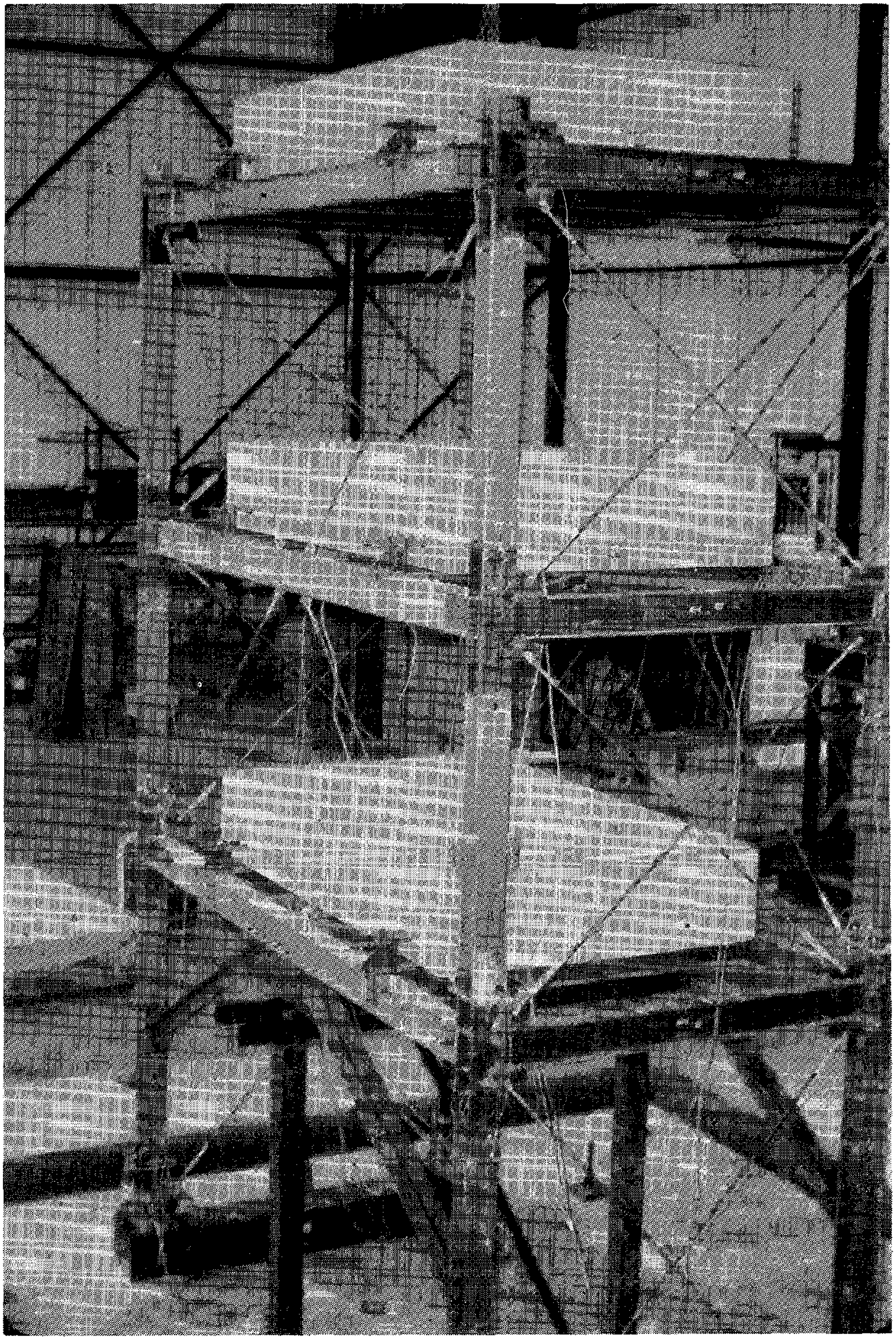

Fig. 3.1.1 Test Structure with Rod Braces on the Shaking Table

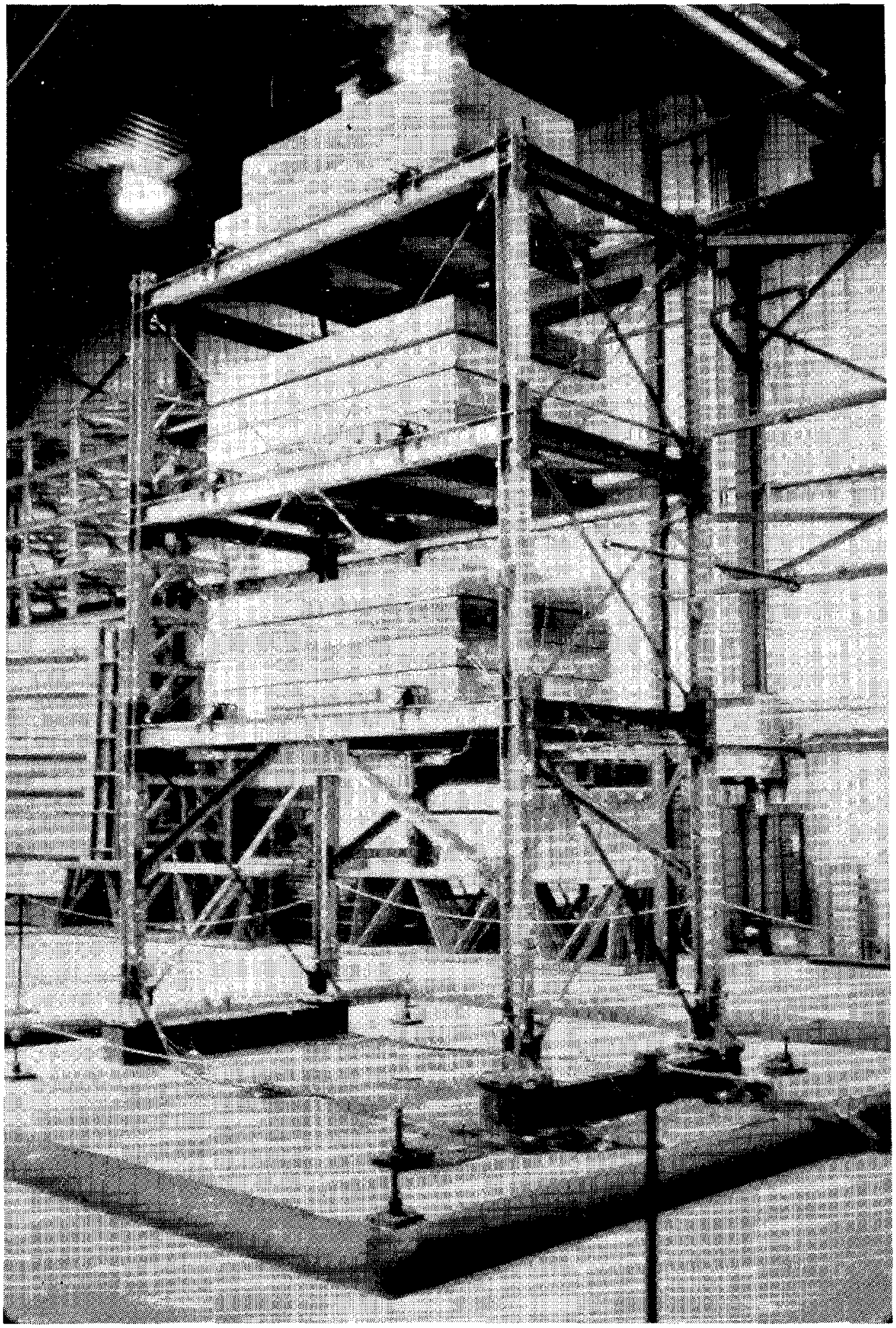

Fig. 3.1.2 Test Structure with Double Angle Braces on the Shaking Table

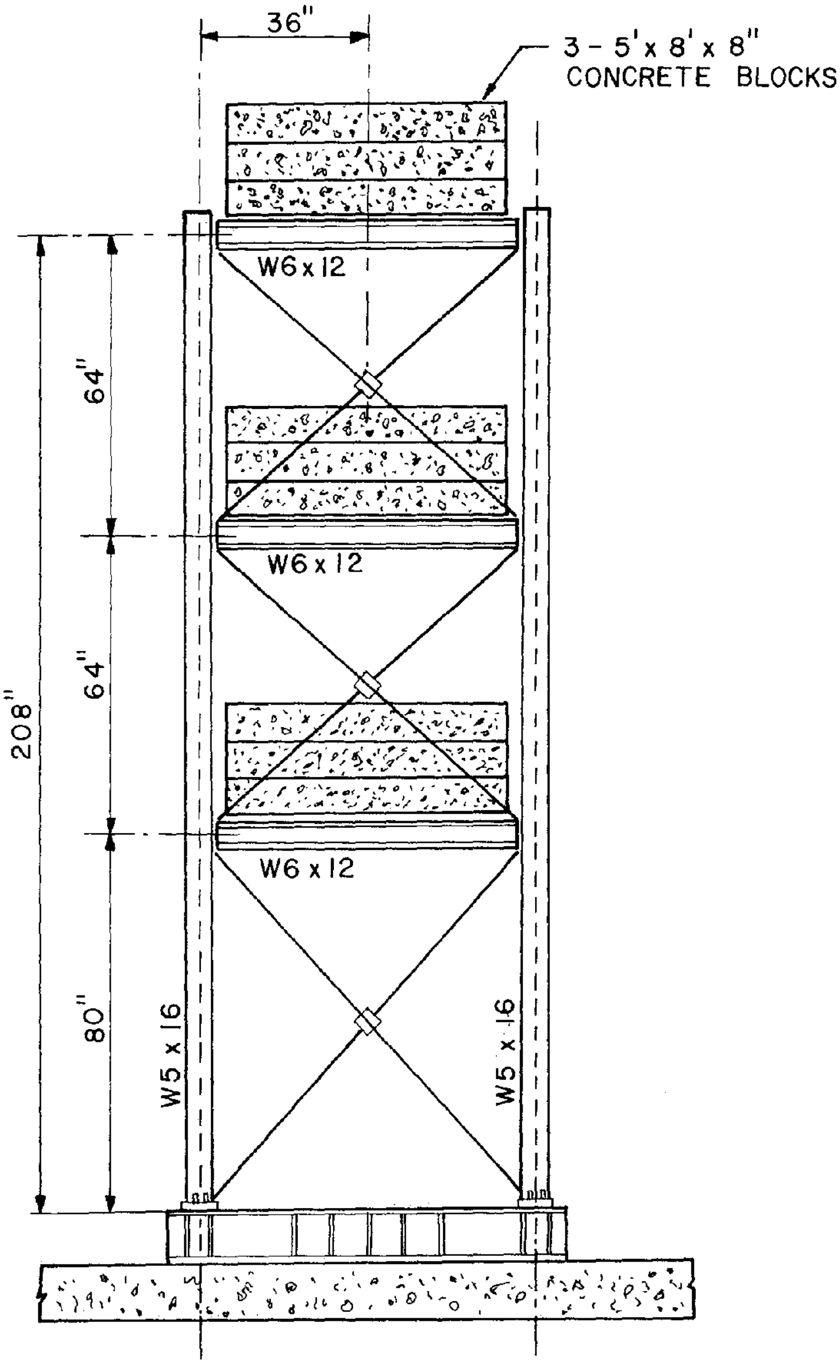

Fig. 3.1.3 Front Elevation of the Test Structure with Pipe Braces

3.2 Design Criteria of the Bracing Members

Bracing members were initially designed for wind loading of a typical steel frame building on the basis of the Uniform Building Code[13]. The designed bracing members were then reduced for use on the scaled prototype test structure using a geometric ratio of 6/10. The wind load pressure was assumed to be 20 lb/ft^2 constant over the height of building.

Rod X-braces - The diagonal rod X-braces of Reference 12 were supplied originally to control lateral or torsional motions of the frame. These diagonals were made the subject of the present research during test series 1 by mounting the structure on the shaking table at 90° to its previous orientation. The half-inch rod-turnbuckle braces which had a slenderness ratio of $KL/r = 370$ and buckling capacity of $P_e = 80$ lb turned out to satisfy the Uniform Building Code requirements for tension members subjected to wind loading. The rod braces were attached to the steel frame by clevis joints and half-inch diameter pins.

Pipe X-braces - In test series 2, the rod X-braces were replaced by 3/4-in. diameter pipe diagonal X-braces. These diagonal braces were designed as compression members on the basis of the AISC[14] specification (slenderness ratio should be smaller than 200). The maximum experimental compressive load P_{max} was very close to that calculated by the formulas recommended by AISI[15]. For tubular sections AISI recommends:

$$P_{max} = \frac{\pi^2 EA}{[KL/r]^2} \qquad C_c < KL/r \leq 200 \tag{3.1}$$

$$\text{where} \quad C_c = \sqrt{\frac{2\pi^2 E}{\sigma_y}} \tag{3.2}$$

KL/r is effective slenderness ratio and A is area of the cross section. The slenderness ratio of the pipe braces welded at their mid-span intersection was KL/r = 125; the theoretical buckling load was 6.3 kips and the tensile yield load was 14 kips. Figure 3.2.1 illustrates the details of the pipe diagonal braces with their connections. The connections and details were designed such that they exceed the elastic capacity of the pipe sections. Thus, ductile performance of the bracing members was possible. For attachment purposes, each pipe was flattened at its ends and was welded to connection plates. The attachment of the connection plates to the steel frame was then accomplished by means of one 3/4 in. and two 1/2 in. diameter high-strength bolts. Figures 3.2.3 and 3.2.4 show these connection attachments to the beam-to-column joint and to the column base joint, respectively.

Double angle X-braces - Double angle (L 1 x 1 x 1/8) diagonal X-braces were tested in test series three. These braces were also designed as compression members according to AISC specifications. The maximum experimental compressive load P_{cr} was closely related to that calculated by the formulas recommended by AISC. For compressive members AISC recommends;

$$P_{cr} = \frac{\left[1 - \frac{(KL/_{r})^{2}}{2C_c^{2}}\right] \sigma_y \cdot A}{\frac{5}{3} + \frac{3(KL/r)}{8C_c} - \frac{(KL/r)^{3}}{8C_c^{3}}} \qquad KL/r < C_c \qquad (3.3)$$

The slenderness ratio of double angle braces welded at their mid-span intersection was KL/r = 86; the theoretical buckling load was 8.8 kips and the measured tensile yield load was 24 kips. Figure 3.2.2 shows the details of the double angle braces with their corresponding connections.

Double angle diagonals were welded together at their centers and to the 1/4 in. thick connection plates at the ends. Again, one 3/4 in. and two 1/2 in. diameter high-strength bolts were supplied for the attachment of the braces to the steel frame (See Figs. 3.2.3 and 3.2.4).

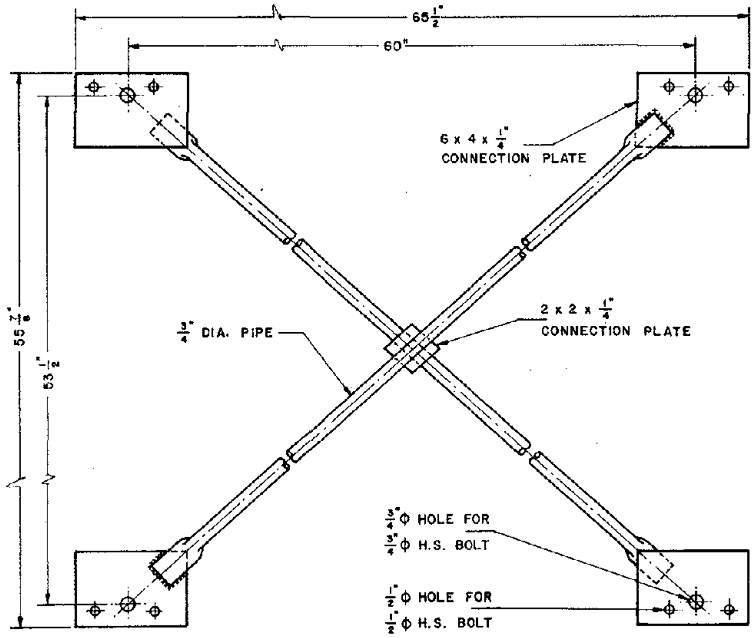

2nd and 3rd Floor Brace

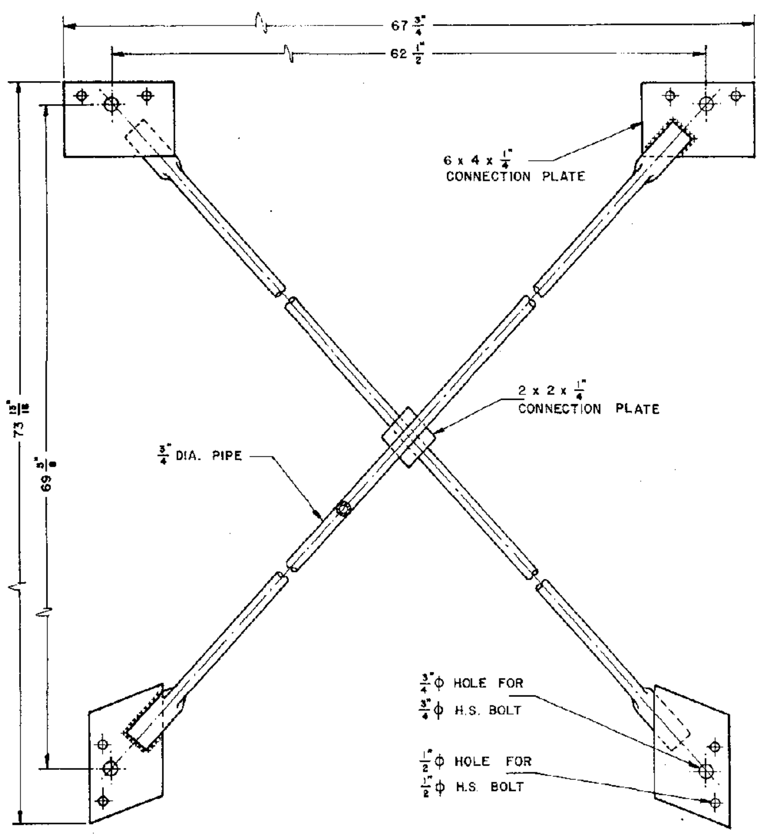

1st Floor Brace

Fig. 3.2.1 Details of the Pipe Diagonal Braces

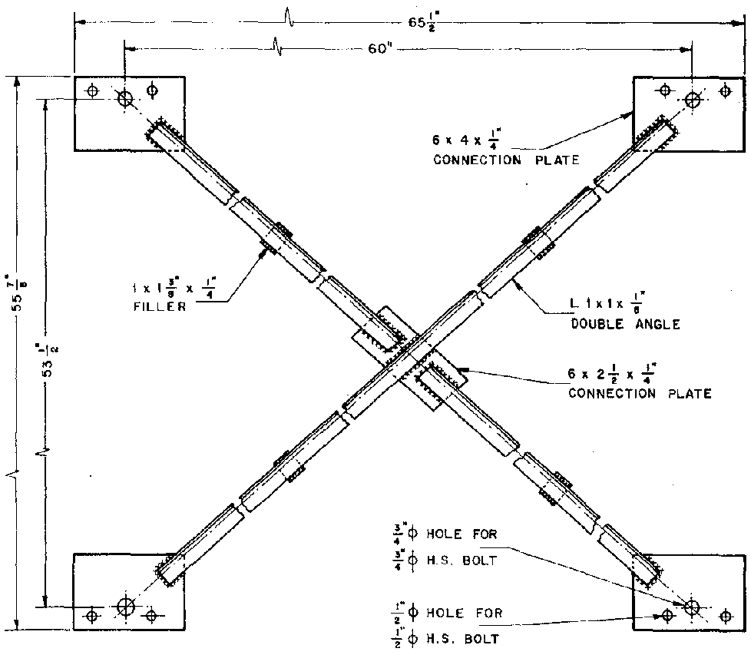

2nd and 3rd Floor Brace

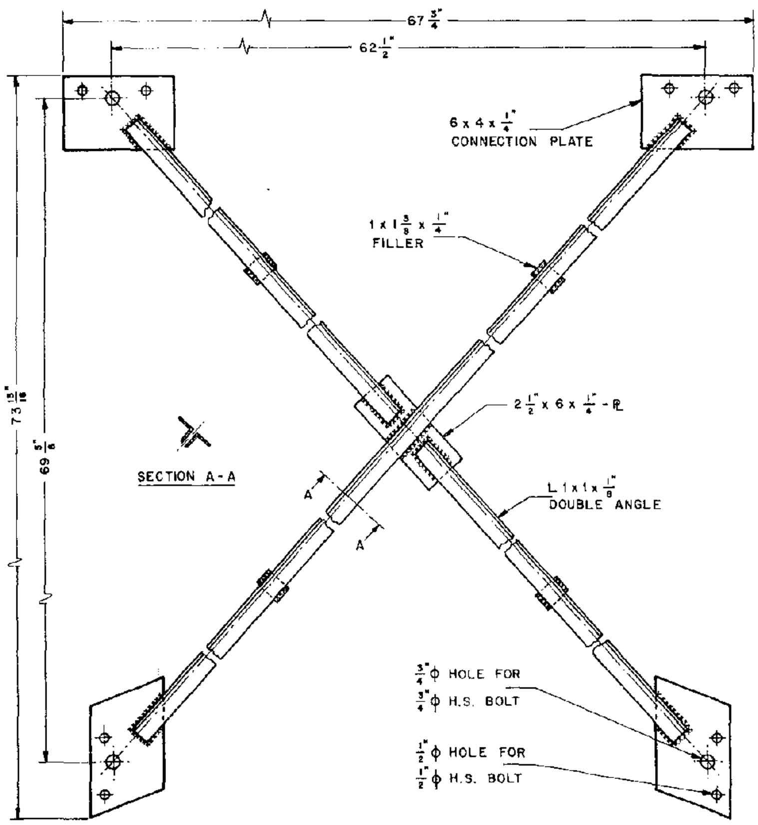

1st Floor Brace

Fig. 3.2.2 Details of the Double Angle Diagonal Braces

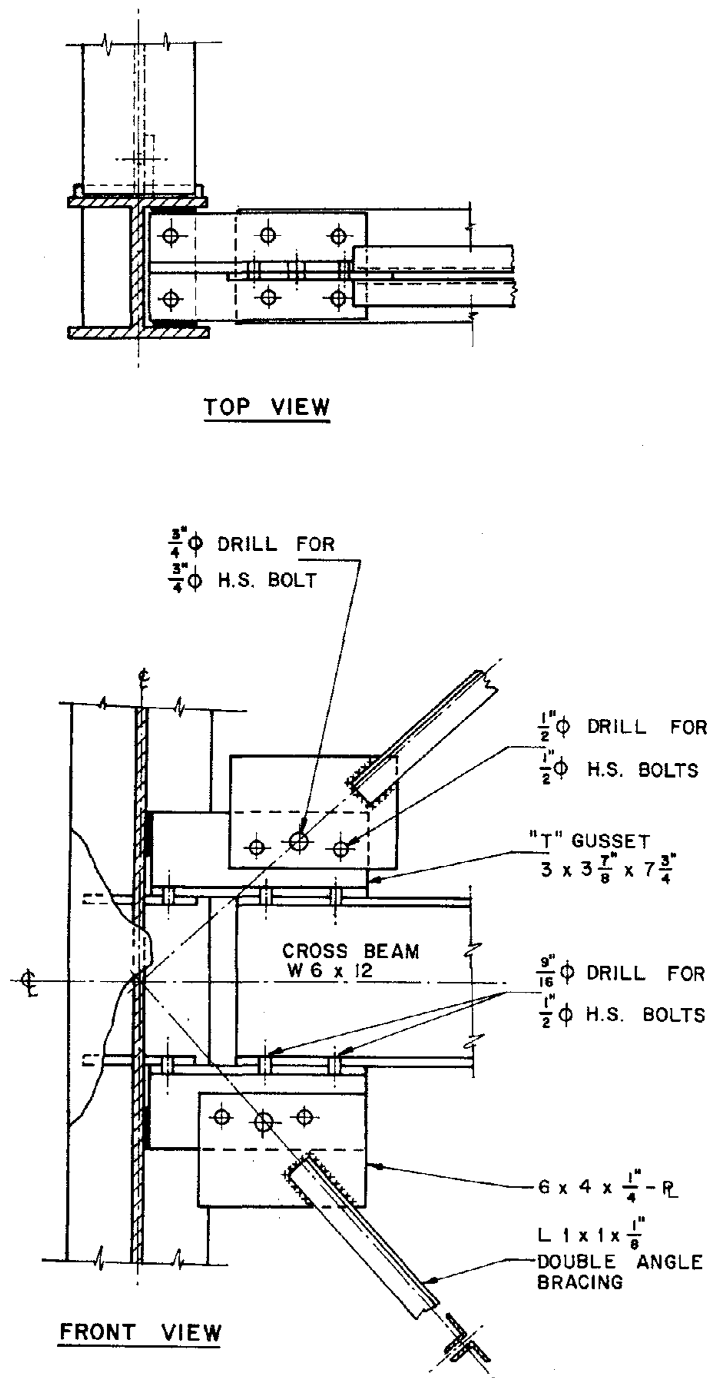

Fig. 3.2.3 Details of Cross Beam-to-Column Connection

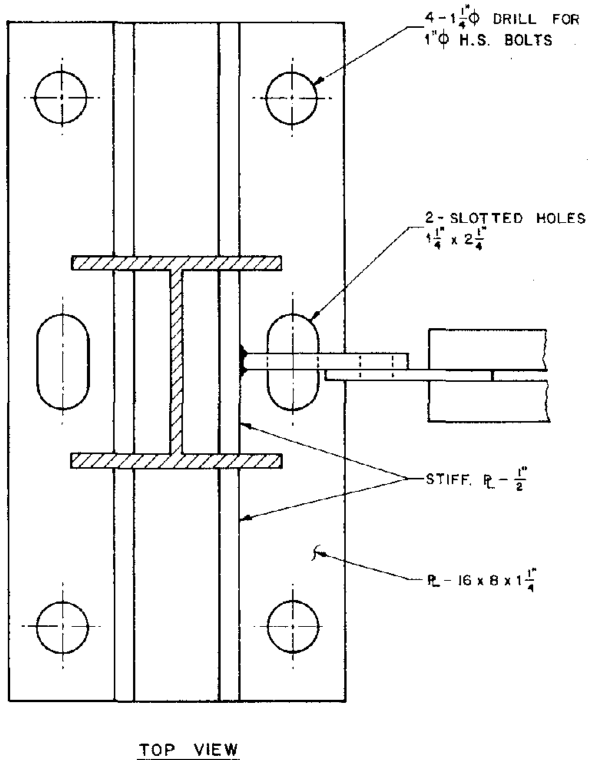

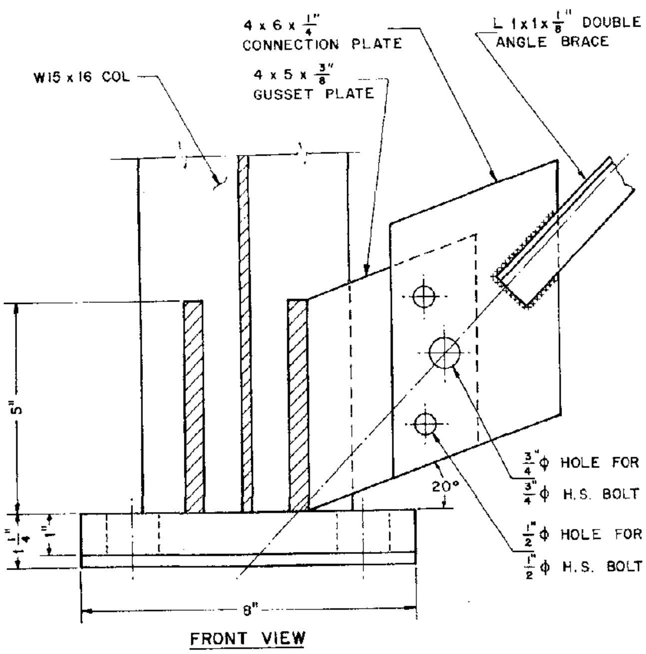

Fig. 3.2.4 Details of Column Base Connection

4. INSTRUMENTATION

The Earthquake Simulator data acquisition system was described in Chapter 2. Dynamic response measurements of the test structures and the shaking table are discussed here.

The motions of the shaking table and the dynamic response of the test structure were measured by 96 channels of instrumentation during the rod bracing tests, of which 36 channels were devoted to monitoring the shaking table parameters. The scanning rate of the data acquisition system was 52 samples per second, per channel.

During tests of the pipe and double angle bracing system, the total number of instrumentation channels was 104 of which 32 channels were used to measure the shaking table quantities. The sampling rate of the test data was about 50 samples per second, per channel. Finally, in tests of the unbraced frame, a total of 75 channels were monitored to measure dynamic response of the structure, and the scanning rate was the same as before (50 samples/sec /channel).

The measured response quantities included accelerations and displacements of each floor, forces and deformations of selected columns, and also forces and deformations of the bracing members. The measurement procedures used for these quantities are described individually. Complete lists of the data channels used with the different test structures are given in Appendix A.

4.1 Acceleration Measurement

Accelerations in the shaking direction were measured at each floor level. An accelerometer was mounted at the center of the concrete weight on both the first and second floors. The third floor was provided with two accelerometers which were located at two column ends so as to measure possible twist accelerations as well as the longitudinal acceleration.

Two types of accelerometer were used in testing. One was the Kistler Model 305T non-pendulous, force balance, servo accelrometer, with a Kistler Model 515T servo amplifier attached. The second type was the Statham Model A39TCB-5-500 resistive bridge accelerometer which used strain gage conditioning circuits. Both types of accelerometers were set to measure a data range of ± 5 g.

4.2 Displacement Measurement

Houston Scientific Model 1800-15A potentiometers were employed to measure the total horizontal displacements of each floor of the structure. The potentiometers were mounted on an independent fixed frame, located outside the shaking table, and their wires were attached to the test structure at each floor level. One potentiometer was used for each of the first two floors; for the third floor two potentiometers were utilized to distinguish between twist and horizontal displacements. The travel range of these instruments was ± 15 in. Also, another potentiometer with a travel range of ± 7.5 in. was employed to measure the total displacement of rod braces of the first floor.

4.3 Force Measurement

The global forces such as floor shears and overturning moments were computed from inertia forces at each floor level calculated from the corresponding measured accelerations. All local member axial forces, shears and moments were derived from readings of strain gages mounted in the elastic regions of the various structural members.

Axial strains were determined by averaging measurements from two strain gages attached on opposite faces of a section. Flexural strains were obtained from the differences of readings given by four strain gages placed on flange tips of a column section. Moments at two points within a member were directly computed from the indicated flexural strains, using a nominal section modulus S and a value of 29,600 ksi for modulus of elasticity E. Shear forces were then obtained from the calculated moments, by assuming a linear moment variation within any member.

The locations of axial and flexural strain gages are depicted in Fig. 4.3.1. These elastic gages were manufactured by Micro-Measurements, and the selected model was EA-06-250-BG-120 with option L and W.

The bracing member axial forces were derived from readings of post-yield gages of type YL-10, produced by Tokyo-Sokki Kenkyujo Co., as long as no yielding was indicated at the location of the strain gages. Figures 4.4.1, 4.4.2, and 4.4.3 show the locations of these strain gages for the various bracing members.

4.4 Local Deformation Measurement

It was expected that forces beyond the elastic limits of certain members would develop during moderate and strong shakings of the test structures. Hence, appropriate instruments were installed to measure local deformations of the most critical members which were believed to be the first floor columns and the first floor diagonal cross bracing members.

Two types of local deformation were measured for the columns, both within what can be considered the plastic hinge at the member ends. One type of measurement was the post-yield flexural strain which also was used to compute the average curvature of the member; the other quantity was the average member rotation, measured over a gage length of 12.5 inches. The post-yield strain gage locations are shown in Figs. 4.4.1, 4.4.2 and 4.4.3 for the various test structures. Flexural strains were obtained by averaging the differential strains from four strain gages (Tokyo-Sokki Kenkujo, Model YL-10) mounted on the flange tips of the column end sections. Curvatures were computed from the flexural strains and the width of the section.

Average column end rotations were measured by pairs of Sanborn Direct Current Displacement Transducers (DCDT) Model 7DCDT-500, mounted in aluminum frames as shown in Fig. 4.4.4. The DCDTs have a travel range of ± 0.5 in. and the distance between the opposed pair was 12.5 in.

Plastic deformations were expected to occur in the mid-section of the pipe and double angle X-braces. These sections were instrumented by four Tokyo-Sokki Kenkujo Model YL-10 post-yield strain gages arranged in the patterns shown in Figs. 4.4.2 and 4.4.3. Axial strains and flexural strains were obtained by averaging and/or differencing the strains measured with specific gages.

4.5 Noise Level and Accuracy of the Experimental Data

The accuracy of response measurement is governed by three prime parameters; input noise, instrument exactness, and the Data Acquisition System (DAS) resolution.

Input noise is caused by mechanical vibrations of the shaking table, which produced a high frequency resonant vibration in the test structure during idle operation of the shaking table, and was superimposed on any dynamic motions applied to the table. The instrument accuracy is characterized by accuracies in gage factor, shunt calibration, nonlinearity (whichever is applicable), and installation of the instrument in the test structure. The Data Acquisition System, which consists of amplifier, scanner, and analog-to-digital converter, controls the accuracy in the process of sampling experimental data.

These sources of errors are discussed for the various transducers in the following paragraphs. In addition, an example illustration of the overall accuracy for the worst estimate, corresponding to the least intense input signal is presented for each type of response. It should be noticed that the maximum error estimate is computed by the square root of the sum of the square of all the extreme errors. However, the overall error for most cases is much lower than that estimated for the worst case. Thus, the accuracy of experimental data can be considered very good.

Post-yield strain measurement

The strain response due to the input noise was obtained from a one-second zero reading of all post-yield gages during idle operation of the shaking table. The mean amplitude of the strain noise was 0.007 milli in./in., with the extreme amplitude of 0.014 milli in./in. The largest extreme amplitude of strain was observed in the first floor bracing members; this was considered to be due to the sensitivity of these members to high frequency input noise.

In addition, a gage factor tolerance of 0.5 percent and an error of 1.0 percent in the shunt calibration may cause a significant offset of the measurement axis of the strain gage components. Although precise evaluation of the accuracy in the strain gage installation is difficult, it is reasonably assumed that the error of this kind is not more than a few percent.

The El Centro span 100 input signal with a maximum table acceleration of 0.067 g which produced an extreme strain value of 0.375 milli in./in. was chosen to estimate the maximum error. Based on a 0.2 percent error caused by the DAS, the overall error for these gages is about 5.5 percent; given by 3.7 percent (= 100 x .014/.375), 4 percent (gage error), and 0.2 percent (DAS). It is interesting to note that the error caused by input noise when the structure was subjected to the Pacoima span 300 input motion (max acc = 0.37 g) was only 0.06 percent.

Elastic strain measurement

The mean amplitude strain of 0.007 milli in./in. with the extreme amplitude strain of 0.0015 milli in./in. was computed for sixteen elastic strain gages mounted in the test structure during the application of input noise. The same conservative error of 4 percent is assumed for the error associated with the gage factor tolerance, shunt calibration, and the strain gage installation. The DAS error is also assumed to be 0.2 percent as before.

As an example, the estimate of the greatest overall measurement error for a peak strain Of 0.066 milli in./in. corresponding to the El Centro span 100 input signal is 4.6 percent; given by 2.3 percent (= 100 x .0015/.066) (input noise), 4 percent (gage error), and 0.2 percent (DAS).

Acceleration measurement

The accelerometers used are the most accurate instruments available in the Earthquake Simulator Laboratory. The greatest error associated with the input noise, in the acceleration was 1.6 percent.

According to the manufacturer's catalogue, this instrument has a nonlinearity of only 0.01 percent. But, significant error may arise from misalignment of the sensitive axis of the instrument when it is installed. However, this kind of error is not more than a few percent and it can be assumed to be about 1 percent for a carefully installed accelerometer.

As an example, an estimate of the greatest overall measurement error with a 0.2 percent error caused by the DAS, is about 2 percent.

Displacement measurement

Slide wire potentiometers were used to measure the floor displacements of the test structures. The displacement response due to the input noise had a mean amplitude of 0.007 in., with an extreme amplitude of 0.008 in. The associated error caused by input noise for a peak displacement of 0.558 in. during the El Centro excitation with a peak acceleration of 0.067 g was estimated about 1.4 percent.

This transducer (according to the manufacturer's report) has a guaranteed nonlinearity of less than ± 1 percent, but the error resulting from the installation of the transducer, could be significant. For a carefully installed potentiometer this error can be assumed to be not more than 2 percent. Then, the greatest overall displacement error could be about 2.5 percent.

DCDT displacement transducers were employed to measure the column rotations. These transducers have an accuracy of ± 0.5 percent of their total stroke range. Their input noise error was negligible. The only significant error that might arise would be due to poor installation, so that the DCDT is offset with respect to its location and/or direction. A reasonable possible error of this kind is assumed to be about 2 percent. Therefore, the overall measurement error can be about 2 percent.

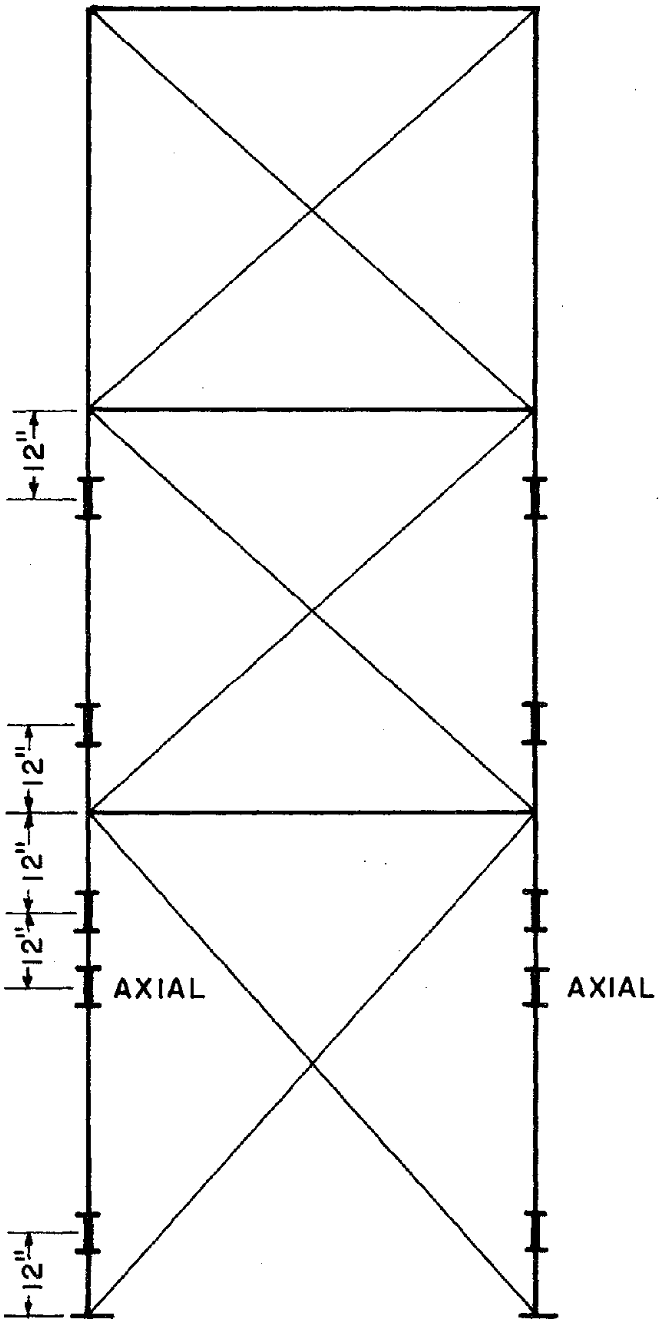

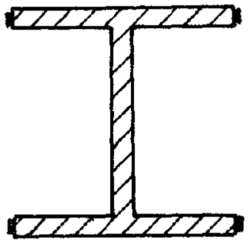

Four Flexural Strain Gages
to Form a 4 Arm Bridge
(1 Data Channel)

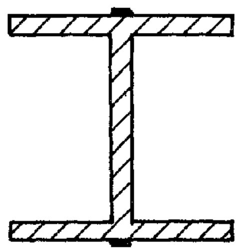

Two Axial Gages to Form a
2 Arm Bridge (1 Data Channel)

Fig. 4.3.1 Elastic Flexural and Axial Strain Gage Stations

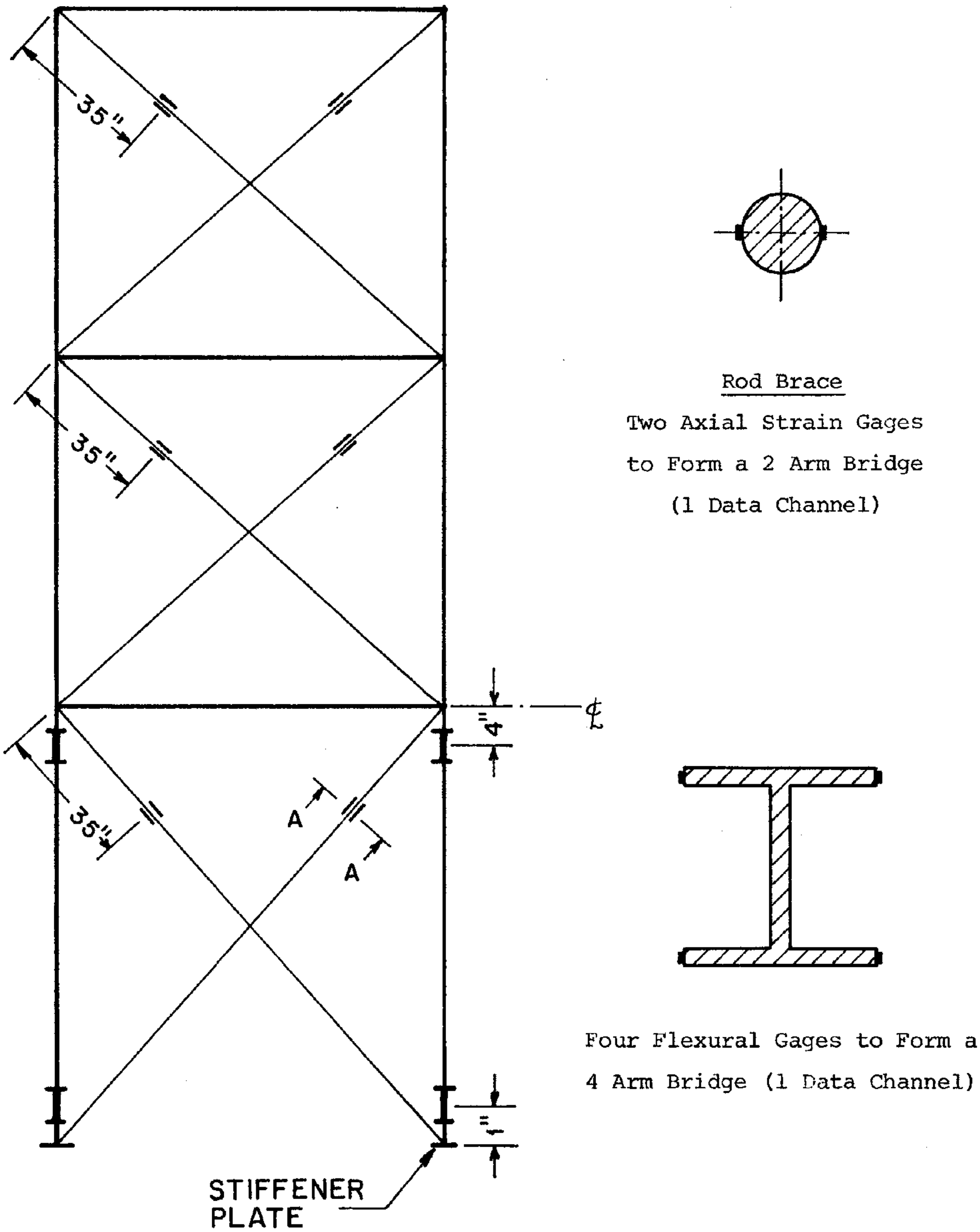

Fig. 4.4.1 Post-Yield Flexural and Axial Strain Gage Stations

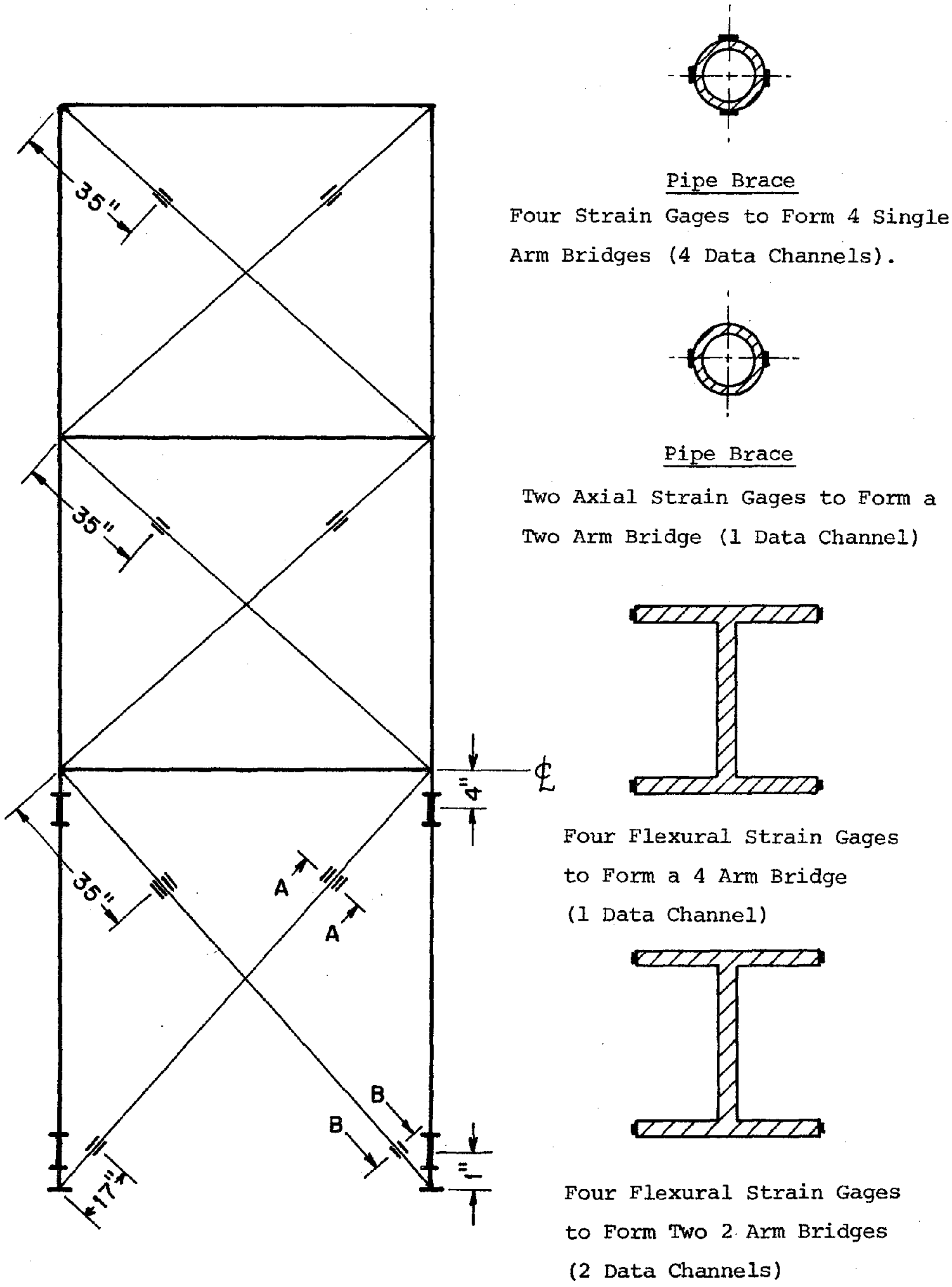

Fig. 4.4.2 Post-Yield Flexural and Axial Strain Gage Stations

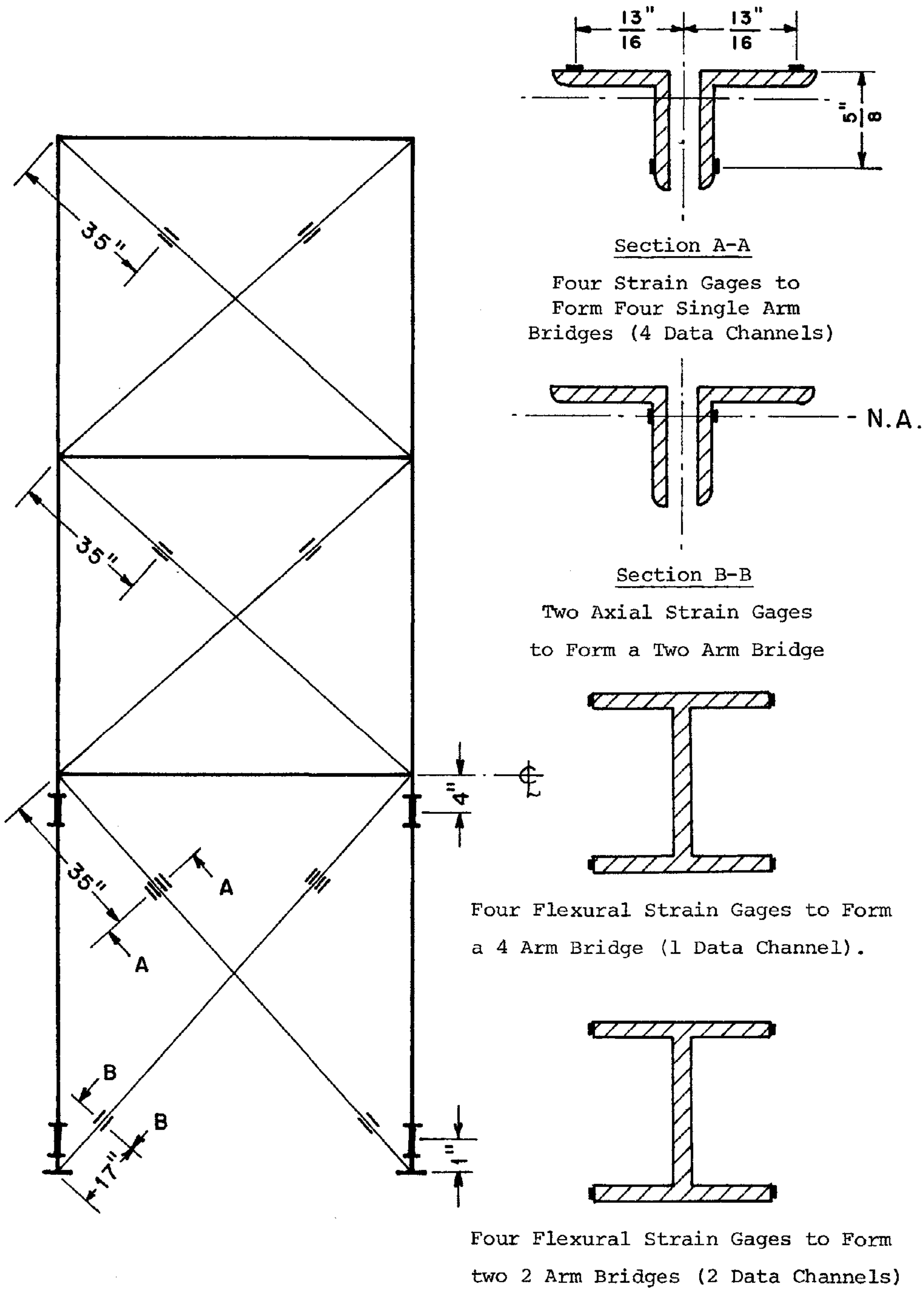

Fig. 4.4.3 Post-Yield Flexural and Axial Strain Gage Stations

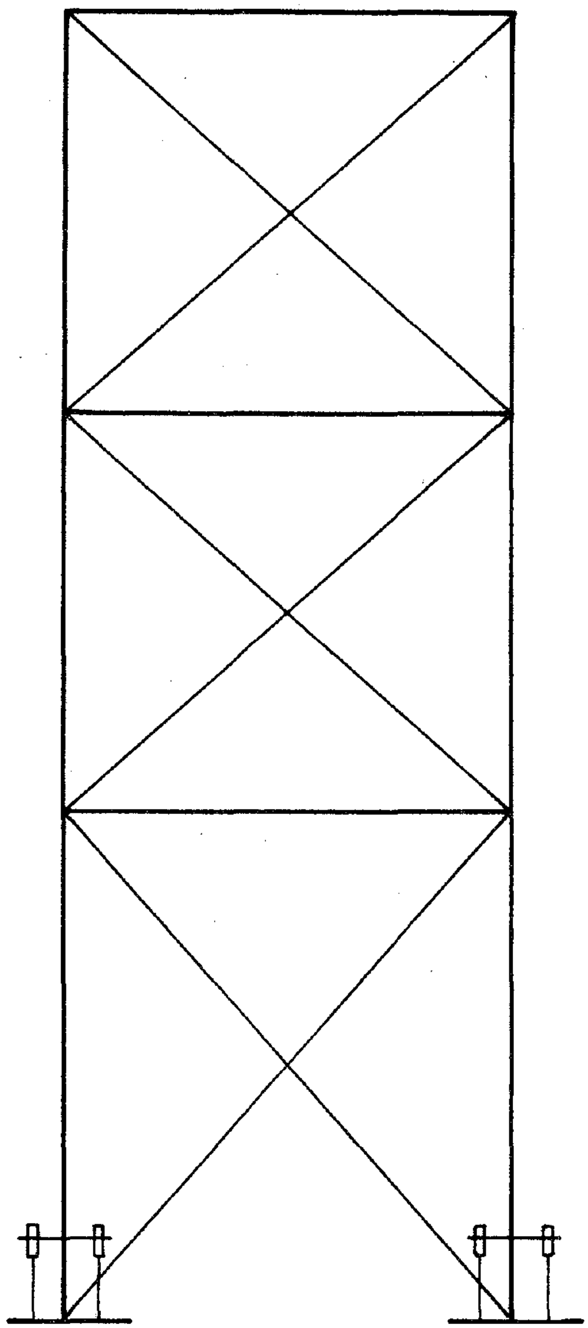

Fig. 4.4.4 DCDT Transducer Stations

5. EXPERIMENTAL STUDY

In this chapter, the shaking table testing of three different bracing systems and the unbraced frame structure is discussed. The principal command signals used during this study were derived from the El Centro 1940 N-S and the Pacoima Dam 1971 S74W earthquake records. Each of these signals was applied to each test structure for a wide range of intensities; results of some specific tests of each structure are reported here.

5.1 Rod X-Bracing Tests

As was mentioned earlier, the slenderness ratio of the half inch rod-turnbuckle braces was very large ($KL/r = 370$) so their buckling capacity was low ($P_e = 80$ lb). Accordingly, all braces were pretensioned to about 2500 lb (40 percent of yield) before testing, to insure initial participation of both members in each panel. The horizontal components of the 1940 El Centro N-S and the 1971 Pacoima Dam S74W records were used for six different test runs (see Table 5.1.A). The first three tests, during which the dead load per floor of the structure was 8 kips, did not introduce any damage in the bracing members. In this series of tests, the maximum table acceleration and displacement were 0.775 g and 5.0 in., respectively, but the induced maximum lateral force was not sufficient to rupture the braces. However, alternate yielding in tension and buckling were observed in the rod braces.

In the second series of test runs one more concrete block was added to each floor, so that the dead weight of each floor was 12 kips. The structure was first subjected to an El Centro span 50 test with a peak acceleration of 0.033 g, which introduced a linear structural response. Then the El Centro span 950 motion, with a peak acceleration of 0.833 g, was applied to the structure. Three of the four rod braces at the first floor level ruptured and severe "necking" occurred in the fourth brace; also, all of the first floor columns yielded at their bottom ends.

After this test, the first floor braces were replaced by new rods, and it was decided to subject the structure to the scaled Pacoima Dam earthquake motion. The peak table acceleration was about 1.129 g. Although the peak table acceleration of this test and the resulting story shear forces were higher than during the previous test, only two braces ruptured, one in the first floor and another in the second floor. The performance here was better because the new first floor braces had different material properties; the rupture strength was 90 ksi-milli in./in. compared with 45 ksi-milli in./in.

Table 5.1.A

Rod Bracing Tests

	Test No.	Input Signal	Max. Table Acc. (g)	Weight/Flr (Kips)	Comments
Test series 1	1	EC 100	0.063	8	Linear response
	2	EC 400	0.280	8	Linear response
	3	EC 1000	0.775	8	Nonlinear response No damage
	4	EC 50	0.033	12	Linear response
	5	EC 950	0.833	12	Nonlinear response 3 rod braces ruptured
Test series 2	6	PACOIMA	1.129	12	Nonlinear response 2 rod braces ruptured

5.1a Rod Bracing Subjected to El Centro Span 100

The El Centro earthquake signal with a "span" setting of 100 (corresponding to a peak table acceleration of 0.063 g) was applied to the test structure incorporating the rod diagonal braces. The span setting is a control system setting indicating the "intensity" of the input signal. This is linearly proportional to the table displacement. This application of ground motion caused a linear structural response. The table horizontal motion is shown in Fig. 5.1a.1. The story and table accelerations, represented by Fig. 5.1a.2 indicate a dominant first mode vibration. The time histories of the north and south frame accelerations at the third floor level demonstrate a close match which implies a symmetric structural response. The fundamental frequency of the structure, calculated using the FRMSTC program[16], a static load analysis program for multi-story buildings, was about 4.23 cps (see Fig. 6.1a.4).

The story displacements relative to the shaking table and shear forces are shown in Fig. 5.1a.3 and Fig. 5.1a.4, respectively. The maximum first floor shear was about 2.73 kips, and the maximum axial force induced in the first floor braces was estimated to be about ± 1.7 kips, which was lower than the pre-tension load of the braces (2.5 kips). Thus, as was observed during the test, these braces did not lose their pre-tension loads and actively participated in the compression direction as well as in tension.

The strain time history graphs of the first floor rod braces shown in Fig. 5.1a.5 also show the linear behavior of these members. The maximum strain indicated is less than the rod's yielding strain. Therefore, the measured strains were used to compute the axial forces in the rods.

5.1b Rod Bracing Subjected to El Centro Span 1000

In this test, the El Centro signal with a peak acceleration of 0.775 g was employed; also, the structure was loaded with concrete blocks weighing 8 kips per floor. The resulting maximum shear force in each resisting frame was 13 kips. This lateral force was not sufficient to rupture the braces, but caused alternate yielding in tension and buckling in compression. The applied table motion is shown in Fig. 5.1b.1, and the floor absolute acceleration and relative displacement time histories are shown in Fig. 5.1b.2 and Fig. 5.1b.3, respectively. The frequency change in these plots compared with the EC 100 test results was due to the nonlinear nature of the response.

The floor shears are presented in Fig. 5.1b.4, in which the bottom graph displays the first floor shear (solid line) and also the portion of this shear which was resisted by the braces (dashed line) at this floor level. The first floor shear force is plotted versus the first floor displacement in Fig. 5.1b.5, which also represents the combined force-displacement of the first floor rod diagonals. These results show that during the early stage of response, while the braces retained their pre-tension, they provided an efficient dual path for resisting the lateral forces. At this time, they resisted 80 to 85 percent of the lateral loads. After compression buckling and tension yielding occurred, however, the compression diagonal became ineffective; the tension diagonal then supplied only about 50 percent of the resistance with the rest being carried by the moment-resisting frame. During this stage, the diagonals alternately went slack and were subjected to tensile impact which produced additional elongation (see Fig 5.1b.5 and Fig.5.1b.6). At this time, story shear forces less than about 6 kips were carried entirely by columns while the braces remained slack as may be deduced by comparing the bottom two curves of Fig. 5.1b.4. The column moment-strain loops, presented in Fig. 5.1b.7 show that minor yielding occurred at the bottom end of the first floor columns.

5.1c Rod Bracing Subjected to El Centro Span 950

The El Centro span 1000 excitation described above, which induced a peak lateral force of 13 kips per frame did not cause any rod to rupture. Accordingly, in order to provide a really damaging test, the frame was loaded with additional concrete blocks (to a total weight of 12 kips per floor) and was subjected to the El Centro span 950 excitation with a peak acceleration of 0.833 g (Fig. 5.1c.1). The general behavior during this test resembled the previous El Centro response, but the increased force levels ruptured three rod braces in the first floor, and caused yielding and "necking" of the other first and second story braces. In addition, the first floor columns experienced significant yielding.

The first ruptures occurred simultaneously in two tension rods, similarly oriented in opposite end frames, as shown in the strain time history plots of the first floor rods (Fig. 5.1c.6). At this time the story relative displacement was 0.8 in., but it reached 2.38 inches by the end of this excursion. The first floor column moment-strain plots (Fig. 5.1c.7) demonstrate the significant column yielding which was induced during this test. The permanent strain at the bottom end of the column, according to this hysteresis plot, was estimated to be about 0.33 percent. The next rupture occurred a few cycles after the first, when the frame excursion in the opposite direction reached a displacement of 1.22 in. at the first story level. At this time, only one of the two rods left in the first story ruptured, but the other rod suffered significant yielding and necking.

The rupture of braces combined with the yielding of the first floor columns reduced the structure frequency considerably. This can be clearly observed in floor acceleration time histories (Fig. 5.1c.2). In general, all floor relative displacements became larger in this test (Fig. 5.1c.3) than in the preceding one. As may be seen, the first floor displacement particularly increased with respect to that of the previous test (Fig. 5.1c.4); this was expected because the column yielding and bracing failure occurred in the first floor.

5.1d <u>Rod Bracing Subjected to the Pacoima Earthquake</u>

After the El Centro earthquake tests, the damaged rod braces were replaced, and the structure was subjected to the Pacoima Dam earthquake with a peak acceleration of 1.129 g (see Fig. 5.1d.1). The dead load of the structure again was supplemented by concrete blocks weighing 12 kips per floor. The general behavior during this test resembled the El Centro response, but the rupture mechanism of rod braces was different. Only two rod braces ruptured, one in the first floor, and the other in the second floor but these ruptures were accompanied by significant yielding and necking of the other first and second floor braces. The first floor rod rupture occurred during a large story displacement of 2 in. During the return swing from this maximum excursion, the tension rod at the second floor level of the opposite end frame ruptured. At this time the displacement of the second floor relative to the first floor and to the shaking table were about 0.8 in. and 2 in., respectively.

The floor acceleration time histories shown in Fig. 5.1d.2 demonstrate the nonlinear behavior of the response. The first and second mode of vibration are present, and the change of frequency due to nonlinear behavior of the structure is quite evident. The third floor acceleration time history contains a high frequency impulsive type signal which was caused by defective installation of the third floor accelerometers. These accelerometers had been attached to the top ends of the columns and, therefore, picked up the high frequency vibration of the rods installed in the lateral direction.

The floor shear forces associated with inertia forces determined from the masses and accelerations measured at the floors are displayed in Fig. 5.1d.5. The high frequency signal imposed on shear time histories also was caused by the spurious signals recorded by the third floor accelerometers. The bottom graph depicts the first floor shear and the portion of this shear that was resisted by the diagonals of the first floor. This graph shows that the major portion of the first floor shear was resisted by the diagonal. Their resisting shear forces were as high as 13 kips, and the rods were very effective for lateral story shears up to 15 kips. This effective performance was mainly due to the higher strength of these rods in comparison with the diagonals of the previous tests.

The strain time-history plots of the first floor rod braces are shown in Fig. 5.1d.6. Although, the general behavior of the rod braces during this test resembled the El Centro response, they showed some peculiar behavior of their own. As was mentioned before, the first floor rod braces of this test were stronger than those used in the El Centro tests and they had different yield properties. The tension yielding occurred not only in their weak sections (threaded portion of rods), but it also occurred along the half-inch diameter section of the rods. However, only one rod brace of the first floor ruptured. This peculiar behavior of the first floor diagonals introduced a more severe "pinching" effect in the story displacement hysteresis loops, associated with slack in the braces (see Fig. 5.1d.7).

A detailed examination of the rod diagonal strain time histories shown in Fig. 5.1d.6 may explain the behavior mechanism of the braces. The two upper graphs are the strain time histories of cross braces located in the front frame, and the two lower graphs are the strain time histories of those in the opposite end frame. Three different states can be recognized in the response. During the elastic response, both cross braces efficiently participated in controlling the lateral displacements as well as carrying a substantial portion of the lateral forces; they did not lose their pre-tension loads during this stage. In the second stage, as the response built up and the forces increased, the compression braces lost their pre-tension loads and buckled elastically. During this interval, the cross braces buckled alternately and the slackening mechanism was initiated. Finally, in the last stage, the tension braces yielded as the compression braces buckled. In this stage, the yielded braces remained slack for a longer period of time and the pinching effect was initiated in the hysteresis loops. Also, as the diagonals alternately went slack they were then subjected to tensile impact which produced additional elongation. The first floor rod braces of the opposite frame (two lower graphs) behaved similarly, except that the tension brace in this frame ruptured.

The hysteresis moment - strain plots for the bottom end of the first floor column are illustrated in Fig. 5.1d.8. A significant yielding occurred at the bottom end of this column, and the maximum moment was measured to be about 196 kips-in. The shift of the hysteresis plots to the right was associated with a residual strain of 1.25 milli in./in., and this distortion occurred as the tension rod of the first floor ruptured.

The floor relative dispacements shown in Fig. 5.1d.3 were about 10 percent smaller than those of the El Centro span 950. This was expected because the damage during this test was less. However, the second floor displacement relative to the first floor displacement (drift) shown in Fig. 5.1d.4 was higher, because one rod brace of the second floor ruptured during this test.

5.2 Pipe Bracing Tests

After the rod diagonal bracing tests, the same steel frame structure was equipped with 3/4 in. pipe braces and subjected to a series of simulated earthquakes with the El Centro and the Pacoima Dam earthquake motions. The slenderness ratio of the pipe diagonal bracers welded at their mid-span intersection was $KL/r = 125$ at the first story level, and $KL/r = 107$ at the second and third story levels. The tests performed on the pipe braced structure are listed in Table 5.2.A, in which a summary of the test results and the peak accelerations of the input signals are included.

In the first test series, the structure was subjected to eight tests, with gradually increased input signals. The structural response was linear for input signals up to a peak acceleration of 0.2 g, and no pipe buckling and/or tension yielding was observed. Pipe buckling was intitiated during an El Centro span 400 test having a peak acceleration of 0.28 g. The maximum first story shear during this test was about 17 kips, but the columns remained elastic. In subsequent test runs, the peak acceleration of the table motion reached 0.5 g, and this induced compression buckling and tension yielding of all the first floor pipe braces. In addition, yielding occurred in the first floor columns.

In the second test series, all damaged pipe braces of the first floor were replaced by new members. Then the structure was subjected to the Pacoima earthquake motion with a peak acceleration of 0.068 g which induced a linear response. After this input signal, the Pacoima span 600 signal with a peak acceleration of 0.812 g was applied to the structure. This strong table motion caused significant buckling and tension yielding in all the first floor pipe diagonals. In addition, the second floor pipe diagonals also buckled and significant yielding was induced in the first floor columns. The maximum first story shear force during this test was about 26.7 kips. Figure 5.2.1 is a photograph of the first and second floor buckled pipe diagonal braces. The tension yielding of the first floor pipes is also shown. In the following subsections the experimental results obtained during some of the tests are discussed.

Table 5.2.A

Pipe Bracing Tests

	Test No.	Input Signal	Max. Table Acc. (g)	Weight/Flr (Kips)	Comments
Test series 1	1	EC 100	0.067	17	Linear response
	2	PAC 50	0.074	17	Linear response
	3	EC 300	0.202	17	Linear response
	4	EC 400	0.283	17	Nonlinear response 1st pipe buckling
	5	PAC 200	0.235	17	Minor pipe buckling
	6	PAC 300	0.373	17	Pipe buckling Minor col. yielding
	7	PAC 400	0.475	17	Pipe buckling & yielding Col. yielding
	8	EC 650	0.503	17	Pipe buckling & yielding Col. yielding
Test series 2	9	PAC 50	0.068	17	Linear response
	10	PAC 600	0.812	17	Pipe buckling & yielding Col. yielding

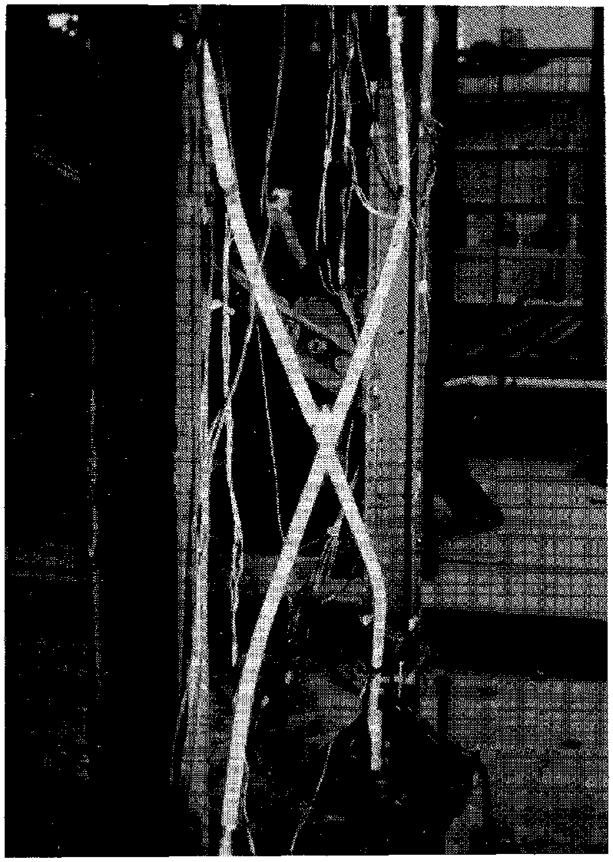

1st Floor Buckled Pipe

2nd Floor Buckled Pipe

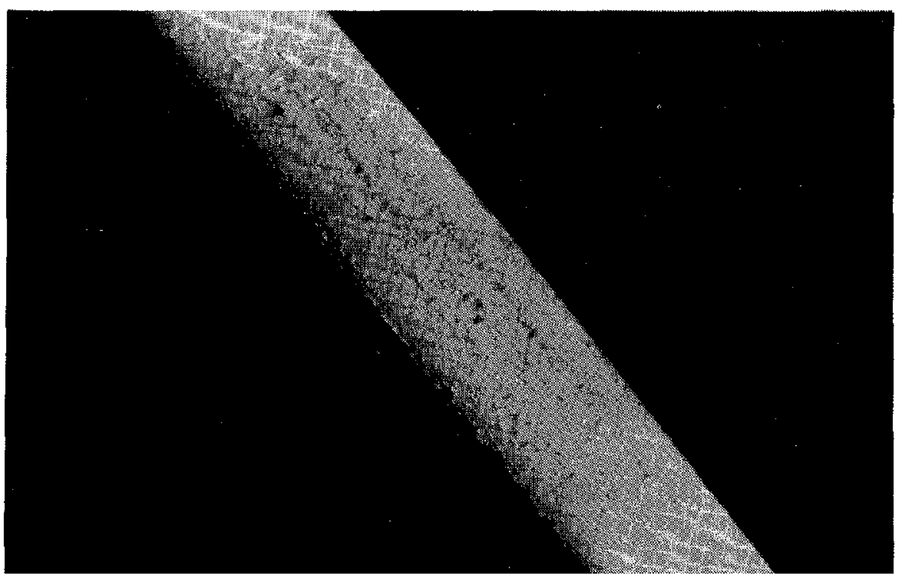

Fig. 5.2.1 Photographs of Compression Buckling and Tension Yielding of Pipe Diagonal Braces

5.2a Pipe Bracing Subjected to El Centro Span 100

The response of the test structure with pipe diagonal braces to the El Centro span 100 test (with a peak acceleration of 0.067 g) was within the elastic range. The fundamental frequency of the structure measured from its free vibration response was 3.63 cps. The typical floor acceleration and relative displacement time histories, shown in Fig. 5.2a.1 and Fig 5.2a.2, respectively, demonstrate that this fundamental frequency dominates the structural response. It is interesting to note that the maximum third floor displacement relative to the table was only 0.13 in. due to the table motion having a peak displacement of 0.5 in.

Figure 5.2a.3 displays the strain time histories of four strain gages mounted at the mid-span section of the first floor pipes. All four time histories are in phase and have the same sign, which indicates that no buckling was induced in the pipe diagonals. The maximum axial force of the first floor pipe diagonals was 2.7 kips which was only 45 percent of its buckling load. The story shear forces are shown in Fig. 5.2a.4, in which the bottom graph displays both the first floor shear and the portion of the first floor shear that was resisted by the first floor pipe diagonals. This graph indicates that more than 90 percent of the first floor shear force was resisted by the diagonals. Therefore, these elastic results show that the pipe diagonals were very efficient in carrying the lateral forces as well as controlling the lateral displacements. Their effectiveness and efficiency in the nonlinear cases are discussed in the following paragraphs.

5.2b Pipe Bracing Subjected to El Centro Span 400

The application of the El Centro span 400 signal (with peak acceleration of 0.283 g) to the pipe braced structure caused a nonlinear response. This nonlinear response was initiated when the first floor pipe diagonals buckled in compression and yielded in tension. No column yielding occurred, because the moment induced at the bottom end of the first floor columns was never more than 35 percent of the yielding moment of the columns.

The shaking table and the floor acceleration time histories shown in Fig. 5.2b.1 indicate that the first mode of vibration is dominant. The second mode of vibration which appeared in the first floor acceleration record can be explained by looking at the second mode shape of buildings of this type (see Fig. 6.1a.4). The contribution of the second mode to the structural response is highest at the first floor level.

The time histories of floor displacements relative to the shaking table are shown in Fig. 5.2b.2. The maximum first floor relative displacement is about 19 percent of the maximum table displacement, whereas this was only 13 percent during the El Centro span 100 test. The increase was expected because the first floor stiffness was reduced when the pipe diagonals buckled and/or yielded.

The floor shear forces are shown in Fig. 5.2b.3, in which the bottom frame displays both the first floor shear and the portion of this shear resisted by the pipe diagonals. This graph shows that, despite the pipe buckling, the first floor diagonals resisted about 90 percent of the first floor lateral forces. The figure is not very different from the corresponding one for the El Centro span 100 test, except for the larger amplitudes and a frequency decrease of 9 percent. In fact, the buckling and yielding of the first floor pipe diagonals as shown in Fig. 5.2b.4 were not drastic, and the change of stiffness at the end of the response was negligible. The buckling and yielding loads were about 6 and 14 kips, respectively. The hysteresis plots of Fig. 5.2b.5 demonstrate the combined force-displacement behavior of the first floor pipe bracing. These hysteresis plots show that the buckling and yielding of the diagonals occurred only during the first four seconds of the response. The pipe braces were quite effective for this intensity of input signal, and no pinching behavior was developed in the hysteresis loops. Therefore, the loss of strength was almost negligible. The second floor shear forces were not sufficient to cause any brace buckling at this level. Note that the buckling capacity of the second and third floor diagonals was higher due to their lower slenderness ratios.

5.2c Pipe Bracing Subjected to Pacoima Span 400

In this test, the frame was loaded with 17 kips of concrete blocks per floor as before and was subjected to the Pacoima earthquake excitation with a peak acceleration of 0.475 g . The theoretical buckling load of the braces as mentioned earlier was 6 kips and the tensile yield load was 14 kips. Before performing this test, however, the braces had suffered buckling and yielding in earlier tests; it is estimated that the residual buckling strength of the damaged first floor braces was only about 3 kips.

The floor accelerations and displacements shown in Fig. 5.2c.1 and Fig. 5.2c.2, respectively, are similar to those of the previous tests. The fundamental frequency of the structure measured at the end of this test was 2 cps (about 55 percent of the elastic case). The floor drift time histories (story to story displacement) show that the ratio of first floor drift to second floor drift is much higher than that observed in the El Centro span 400 test (see Fig. 5.2c.3). This reduced stiffness was expected, because the buckling and yielding of the diagonals were more severe in this test, especially at the first floor level.

The resulting maximum first story shear force was 28.36 kips, which resulted in tension yielding and compressive buckling of the braces. Despite their alternate buckling during response cycles, the first floor braces resisted 75 to 80 percent of the lateral load in the initial response stage (see Fig. 5.2c.4), and effectively controlled the lateral displacement. However, as tensile yield deformations gradually accumulated, the bracing efficiency diminished and a pinching effect was developed in the force-displacement curves (see Fig. 5.2c.5) due to the slack resulting from tensile yield. The slope of this force-displacement curve at the end of the excitation was only 53 percent of its initial slope; this indicates a significan strength loss of the first floor braces. Also, the resisting force capacity of the braces was as low as 45 to 50 percent of the lateral load at this stage. The pipe bracing behavior became, therefore, somewhat similar to that of the rod braced system, but the much more open hysteresis loops show that the pipe braces continue to absorb significant energy while buckling.

The first floor columns yielded at their bottom ends as the buckling and tension yielding of the braces occurred. The hysteresis loops of the moment-curvature diagram for the bottom ends of the first floor columns are shown in Fig. 5.2c.6.

5.2d Pipe Bracing Subjected to Pacoima Span 600

After the test described above was completed, the damaged pipe braces were replaced. Then, to provide a more damaging test, the frame was subjected to the Pacoima earthquake excitation with a peak acceleration of 0.812 g (see Fig. 5.2d.1, bottom frame). The general behavior during this test resembled the Pacoima span 400 response, but the increased force levels were such that the second floor pipe braces also buckled and a residual distortion remained at the bottom end of the first floor columns.

The typical floor acceleration and relative displacement time histories are shown in Fig. 5.2d.1 and Fig. 5.2d.2, in which the change of response frequency due to the nonlinear behavior of the structure is evident. The fundamental response frequency measured at the end of this test was about 1.95 cps; this represents a reduction of 46 percent with respect to the elastic case. The floor drifts shown in Fig. 5.2d.3 indicate a larger first and second floor response than was obtained in the Pacoima span 400 response. This was expected, because the plastic deformations at the first floor level were larger and therefore the loss of strength was greater. In addition, larger second floor drifts were caused by the buckling of braces at this level.

The floor shear forces are shown in Fig. 5.2d.4. Although the general features of these plots are similar to those of the Pacoima span 400 test, a careful study of them identifies three distinct phases. Phase one was associated with the elastic response. In this phase the maximum first floor shear was smaller than 15 kips. The pipe braces did not buckle during this interval and effectively resisted up to 90 percent of the lateral forces. In phase two, as the first floor shear forces became larger than 15 kips, the compressive braces buckled. At this time the efficiency of the pipe braces decreased, and they resisted only about 70 to 80 percent of the lateral forces (see Fig. 5.2d.4). Finally, in phase three as tensile yield deformations accumulated, the bracing efficiency diminished drastically, and a pinching effect was developed in the force-displacement curves(see Fig. 5.2d.5). During this interval the braces resisted about 60 percent of the lateral forces as the pinching initiated, and their contribution decreased to about 35 percent of the total lateral force at the end of this test.

The force-displacement hysteresis loops show that the slope of these curves as the excitation ended was only 35 percent of its initial slope; this indicates the great damage which occurred in the braces during this test. Accordingly, the first floor column yielded significantly, and a residual distortion was developed at their bottom ends (see Fig. 5.2d.6).

5.3 Double Angle Diagonal Bracing Tests

Angle sections are frequently used as diagonal bracing members in many braced steel frame buildings. Therefore, to complete the task of this investigation, the steel frame test structure was provided with 1x1x1/8 in. double angle diagonal braces. The double angle cross braces were welded together at the center and to connections at the ends using 1/4 in. thick gusset plates. The test structure was subjected to motions simulating the El Centro and the Pacoima Dam earthquake records with different intensities. Two series of tests were performed: in series 1, the structure was loaded with 12 kips per floor, and in series 2, the load per floor was increased to 17 kips. The tests performed and a summary of results are shown in Table 5.3.A.

In test series 1, the double angle braces intially had no filler plates between their ends and the middle crossing point. Hence, the double angles did not act together, and the buckling occurred in the direction of each single angle z-axis. The slenderness ratio of the single angles with respect to their z-axis was $KL/r = 230$, and the angle buckling was initiated during the application of the El Centro span 500 test. At this time, the maximum resulting first floor shear was about 13 kips, and the buckling load was estimated to be about 2.5 kips per angle. Then it was decided to modify the braces so that they would act together as a composite member. For this purpose, each pair of angles was welded together through a 1/4 in. thick filler plate at the sections midway between the end and the center crossing (i.e. at quarter-span of the full diagonal length). After this modification, the first buckling of the first floor braces was initiated when the El Centro span 700 signal was applied to the structure with a peak acceleration of

0.485 g. The slenderness ratio of these combined double angle diagonal braces was KL/r = 86 as they buckled with respect to their y-axis. At this time, the maximum first floor shear was about 20 kips, and the buckling load was estimated to be about 9 kips. In subsequent tests of this series, the intensity of excitation was increased to a peak acceleration of 0.820 g, which caused significant buckling and tension yielding in the diagonal braces of the first floor level. The first floor columns also yielded during this test, but no buckling occurred in the second floor braces.

After test series 1, all the damaged first floor diagonals were replaced and the structure was loaded with concrete blocks weighting 17 kips per floor, to produce a more destructive test. Note that the new set of diagonal braces was also interconnected using 1/4 in. filler plates at their quarter span sections. The structure was first subjected to the El Centro span 100 signal and then to the Pacoima span 100 to provide elastic response data. Finally, a very intense Pacoima span 800 test with a peak acceleration of 1.314 g was applied to the structure; this produced extensive nonlinear response. During this test, all the first floor double angle diagonals buckled and were damaged significantly. A photograph of the first floor braces is shown in Fig 5.3.1. The intensity of this motion was such that the lateral forces were sufficient to cause buckling in the second floor diagonals as well (KL/r = 72). The buckled second floor brace is shown in Fig. 5.3.2. Also a photograph of the local buckling of the angle legs which eventually ruptured during test series 1 is shown in Fig. 5.3.2 (bottom frame). A detailed discussion of the structural behavior during these tests follows.

Table 5.3.A

Double Angle Bracing Tests

Test No.	Input Signal	Max. Table Acc. (g)	Wt./Flr (Kips)	Comments
1	EC 100	0.062	12	wo/filler, linear response
2	EC 300	0.192	12	wo/filler, linear response
3	PAC 200	0.244	12	wo/filler, linear response
4	EC 500	0.336	12	wo/filler, angle buckling initiated
5	PAC 350	0.458	12	wo/filler, angle buckling
6	EC 500	0.330	12	w/filler, linear response
7	EC 700	0.485	12	w/filler, angle buckling intiated
8	EC 900	0.689	12	w/filler, angle buckling
9	EC 1000	0.820	12	w/filler, angle buckling minor col. yielding
10	PAC 600	0.772	12	w/filler, angle buckling minor col. yielding
11	EC 100	0.068	17	w/filler, linear response
12	PAC 100	0.127	17	w/filler, linear response
13	PAC 800	1.314	17	w/filler, angle buckling significant col. yielding

SOUTH FRAME

NORTH FRAME

Fig. 5.3.1 Photographs of the 1st Floor Buckled Double Angle Diagonal Braces

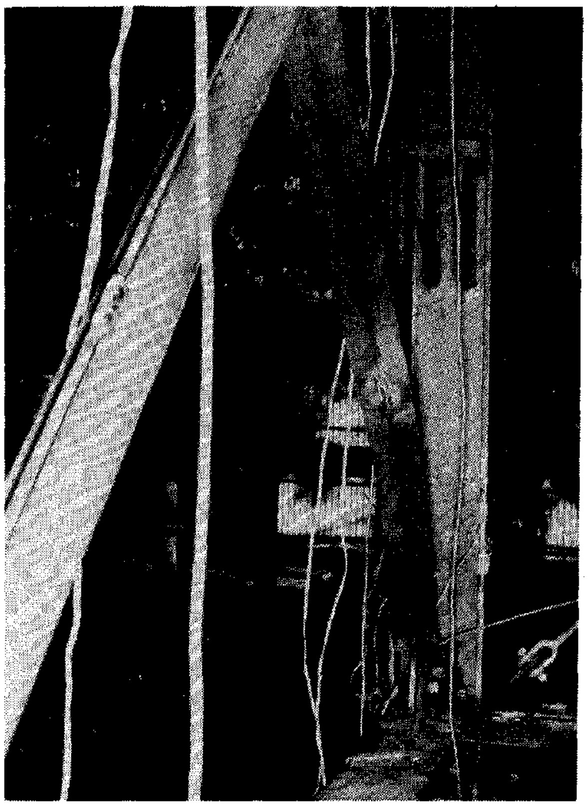

2nd Floor Buckled Angle

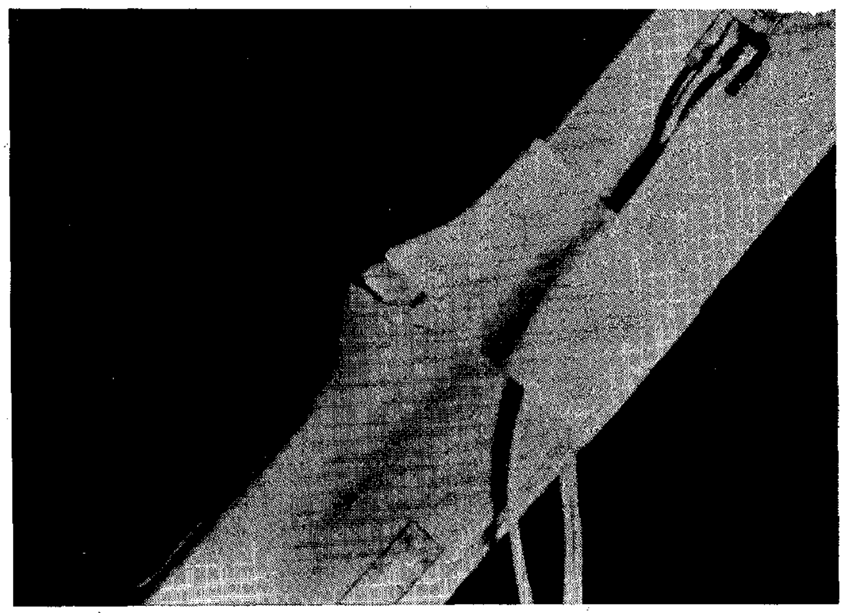

1st Floor Damaged Angle

Fig. 5.3.2 Photographs of Buckled and Damaged Double Angle Braces

5.3a Double Angle Bracing Subjected to El Centro Span 100

In this test the structure was loaded with concrete blocks weighing 17 kips per floor, and the angle pairs were welded together through 1/4 in. filler plates to insure combined action. The El Centro span 100 signal with a peak acceleration of 0.068 g was applied to the structure, producing a linear structural response. The general behavior during this test was similar to that of the previous braced structure tests using identical excitation. However, the stronger double angle braces reduced the force level developed in the columns and the lateral displacement of the floors.

Time-histories of the floor accelerations and displacements are shown in Fig. 5.3a.1 and Fig. 5.3a.2, respectively. As in the previous tests, the first mode of vibration dominates the structural response. The fundamental frequency during this test was calculated by frequency analysis of the first floor acceleration record using the Fast Fourier Transform (FFT) routine. This frequency was about 3.75 cps which was 15 percent and 20 percent higher, respectively, than the fundamental frequency of the pipe and the rod braced structures under identical loading.

The floor shear time histories shown in Fig. 5.3a.3 indicate that the double angle braces resisted more than 90 percent of the lateral forces (see the bottom frame).

5.3b Double Angle Bracing Subjected to El Centro Span 900

This test was performed during test series 1, while the structure was loaded with 12 kips per floor. The slenderness ratio of the combined double angle diagonals welded at their mid-span intersection was $KL/r = 86$ at the first floor level, and $KL/r = 72$ at the second and third floor levels. The braced frame was subjected to the El Centro span 900 signal with a peak acceleration of 0.689 g. This excitation induced compression buckling and tension yielding in all the first floor double angle braces. The buckling load for the first cycle was estimated to be about 8.5 kips, and it reduced to about 6 kips in the subsequent cycles. No buckling and/or yielding occurred in the upper floor braces, and all beams and columns responded within their elastic range.

The time histories of the floor accelerations and displacements, in which the first mode of vibration is dominant and the frequency change due to the nonlinear behavior of the braces is not significant, are shown in Fig. 5.3b.1 and Fig. 5.3b.2, respectively. Also it may be noted that the floor relative displacements are quite small.

The floor shear forces are displayed in Fig. 5.3b.3. The maximum first floor shear was about 20 kips which was sufficient to cause brace buckling and yielding. The bottom frame in this figure indicates that about 88 to 93 percent of the first floor shear was resisted by the double angle diagonals. Indeed, the first floor angle braces buckled only during two response cycles as the first floor shear became larger than 16 kips (see Fig. 5.3b.3, bottom frame). The force-displacement hysteresis loops for the diagonal braces are shown in Fig. 5.3b.4 for successive time intervals of 4 seconds. As was mentioned earlier the initial buckling load was estimated to be about 8.5 kips, whereas the buckling load for the subsequent cycles decreased to about 6 kips; in addition, the brace yielded in tension (see the upper left frame). The subsequent lateral force level was such that the bracing diagonals remained within their elastic range. The post-buckling displacement and tension yielding of the first floor diagonals were not severe enough to produce a pinching effect in the force-displacement curves; also the strength loss of the diagonals due to two induced buckling cycles was negligible. Accordingly, no significant frequency change can be seen in the response time histories.

The hysteresis loops of the first floor shear versus displacement are shown in Fig. 5.3b.5. These curves also include the combined force-displacement contribution of the double angle diagonals. The flat portion of the curve in the first four second time interval (upper left frame) demonstrates the buckling of the diagonals.

These results indicate that despite the buckling of the diagonals, the damage was minor, and the strength loss of the first floor diagonals was negligible. Therefore, the bracing system efficiently resisted the lateral forces and controlled the lateral displacement during this excitation.

5.3c Double Angle Bracing Subjected to Pacoima Span 800

After test series 1, the damaged first floor double angle diagonals were replaced and the structure with a dead load of 17 kips per floor was subjected to the Pacoima Dam earthquake motion with a peak acceleration of 1.314 g. The intensity of this excitation was so great that the resulting lateral forces induced buckling of the first and second floor diagonals, and yielding of the first floor columns. Photographs of the buckled double angle braces are shown in Fig. 5.3.1 and Fig. 5.3.2.

The time histories of table and floor accelerations, displayed in Fig. 5.3c.1, illustrate the frequency change associated with the non-linear structural response. The measured frequency of the damaged structure was 2 cps, a 47 percent reduction from the initial elastic frequency. The high frequency component in the third floor acceleration signal was found to be a disturbance produced by poor installation of the third floor accelerometers. It is believed that the actual third floor acceleration was not more than 2 g, and the large amplitudes of the peak acceleration in the record were the result of that installation. The three floor displacement time histories shown in Fig. 5.3c.2 are identical in form and have almost the same amplitude. This was expected because the major plastic deformations were concentrated in the first floor level, including plastic hinges formed at the base of the first floor columns (see also the floor drift shown in Fig. 5.3c.3). The two third floor displacement time histories indicate that the displacements of the two end frames were nearly identical and, thus, that structural symmetry was preserved.

The first and second floor double angle diagonals buckled with respect to their Y-axis in a direction perpendicular to the plane of the frame because they were completely restrained by the tensile braces. The initial buckling load was estimated to be about 9.3 and 12 kips for the first and second floor braces, respectively. The maximum compressive force developed in the third floor braces was only 7 kips, so they never buckled. The buckling of the first floor diagonals was repreated in subsequent response cycles at lower force levels, and the post-buckling displacements were such that the plastic hinges developed in the mid-span section of these braces.

The floor shear forces are shown in Fig. 5.3c.4. The bottom frame in this figure displays the first floor shear and the portion of this shear that was resisted by the first floor braces. This graph demonstrates that more than 90 percent of the total lateral force was resisted by the braces before they buckled. As the buckling initiated, the brace force resisting capacity decreased to 70 to 80 percent of the total lateral force, and when they were considerably damaged, this contribution dropped to as low as 30 to 40 percent of the total. The first floor shear versus displacement curves which are shown in Fig. 5.3c.5, also include force-displacement hysteresis loops of the combined diagonals. The flat portions of these curves are associated with brace buckling and yielding, and the pinching type behavior in the lower left curve is due to the accumulated tensile yield deformations. The bracing efficiency diminished as the pinching developed, and the lateral first floor stiffness decreased to about 14 percent of its initial value (see the lower right curve). Accordingly, the first floor column yielded significantly as the bracing strength diminished, and a residual distortion was developed at the bottom ends of columns. The first floor column moment-curvature hysteresis loops are shown in Fig. 5.3c.6.

5.4 Unbraced Steel Frame Tests

One of the objectives of this investigation was to compare the performance of different diagonal bracing systems and study their benefits and disadvantages with respect to the unbraced steel frame structure. Thus, for the final test series the diagonal braces were removed, and the basic moment-resistant steel frame was subjected to the El Centro and the Pacoima Dam earthquake motions. The dead load of the structure was supplied by concrete blocks weighing 17 kips per floor. The tests performed on the unbraced frame and a summary of the results are given in Table 5.4.A.

The response of the steel frame to excitations with peak accelerations up to 0.2 g was within the elastic range. The resulting lateral forces were much less than those of the braced structures because the unbraced structure was softer. However, the floor displacments and the column force levels were much higher.

Eight tests were performed, ending with the Pacoima span 400 signal with a peak acceleration of 0.481 g. This table motion induced significant yielding in the first floor columns including a residual distortion; the maximum third floor displacement was more than 4 inches. At this stage it was decided to terminate the tests, because a stronger excitation might have caused serious damage to the frame or even collapse. The results of one elastic and one inelastic test are discussed in the following subsections.

Table 5.4.A

Unbraced Frame Tests

Test No.	Input Signal	Max. Table Acc. (g)	Wt./Flr (Kips)	Comments
1	EC 100	0.064	17	Linear response
2	PAC 50	0.063	17	Linear response
3	EC 200	0.123	17	Linear response
4	EC 300	0.193	17	Linear response
5	PAC 200	0.235	17	Minor col. yielding
6	EC 400	0.268	17	Minor col. yielding
7	PAC 300	0.364	17	Col. yielding
8	PAC 400	0.481	17	Col. yielding w/residual distortion

5.4a Unbraced Frame Subjected to El Centro Span 100

The unbraced steel frame was loaded to 17 kips per floor and was subjected to the El Centro earthquake with a peak acceleration of 0.064 g. The response of the structure to this excitation was within the elastic range as had been expected. The fundamental frequency of the unbraced structure measured by a free vibration test was 1.45 cps. This free vibration test was performed when the shaking table was resting on its static supports. However, the response frequency during a simulated earthquake test was smaller due to table-structure interaction. Therefore, to determine this frequency, a Fast Fourier Transform analysis was performed on the first floor acceleration history. The calculated frequency was found to be 1.186 cps, a reduction of 18 percent, which was due to the flexibility of the table actuator system.

The time histories of floor accelerations, displacements, drifts, and shears are shown in Fig. 5.4a.1 to Fig. 5.4a.4. These results show that the unbraced frame had larger floor displacements and drifts than the braced structures, as would be expected. Also the column force levels were larger. However, the total floor shears were smaller in the unbraced frame because the floor accelerations were not amplified so much in this flexible structure.

5.4b Unbraced Frame Subjected to Pacoima Span 400

The last earthquake motion applied to the unbraced frame was the Pacoima Dam signal with a peak acceleration of 0.481 g. The dead weight of the structure was 17 kips per floor as before. This input motion caused inelastic structural response and induced a residual distortion at the bases of the first floor columns.

The floor accelerations shown in Fig. 5.4b.1 demonstrate the importance of the second mode of vibration in this structure. The floor displacements were very large in general, especially at the third floor where the peak displacement was twice as large as the maximum of the shaking table motion. The time histories of floor displacements shown in Fig. 5.4b.2 demonstrate that the first mode of vibration is dominant in the displacement response. The fundamental frequency calculated from the response history was about 1.04 cps, a 12 percent reduction with respect to the elastic case. The floor drifts are shown in Fig. 5.4b.3, which demonstrates that the drifts of the higher floors are larger than for the braced structures. The moment-curvature hysteresis loops of the columns show their yielding mechanism; the residual distortion is indicated by the shift of these curves from the center (see Fig. 5.4b.4).

These results show that for the unbraced frame lateral movement is very large because of its insufficient stiffness. The nonlinear behavior of the structure is associated with column yielding. During the application of a strong earthquake signal to an unbraced frame, the formation of plastic hinges at the bases of the columns should be expected; and these plastic hinges could cause the structure to collapse if the dead load were close to its critical buckling load.

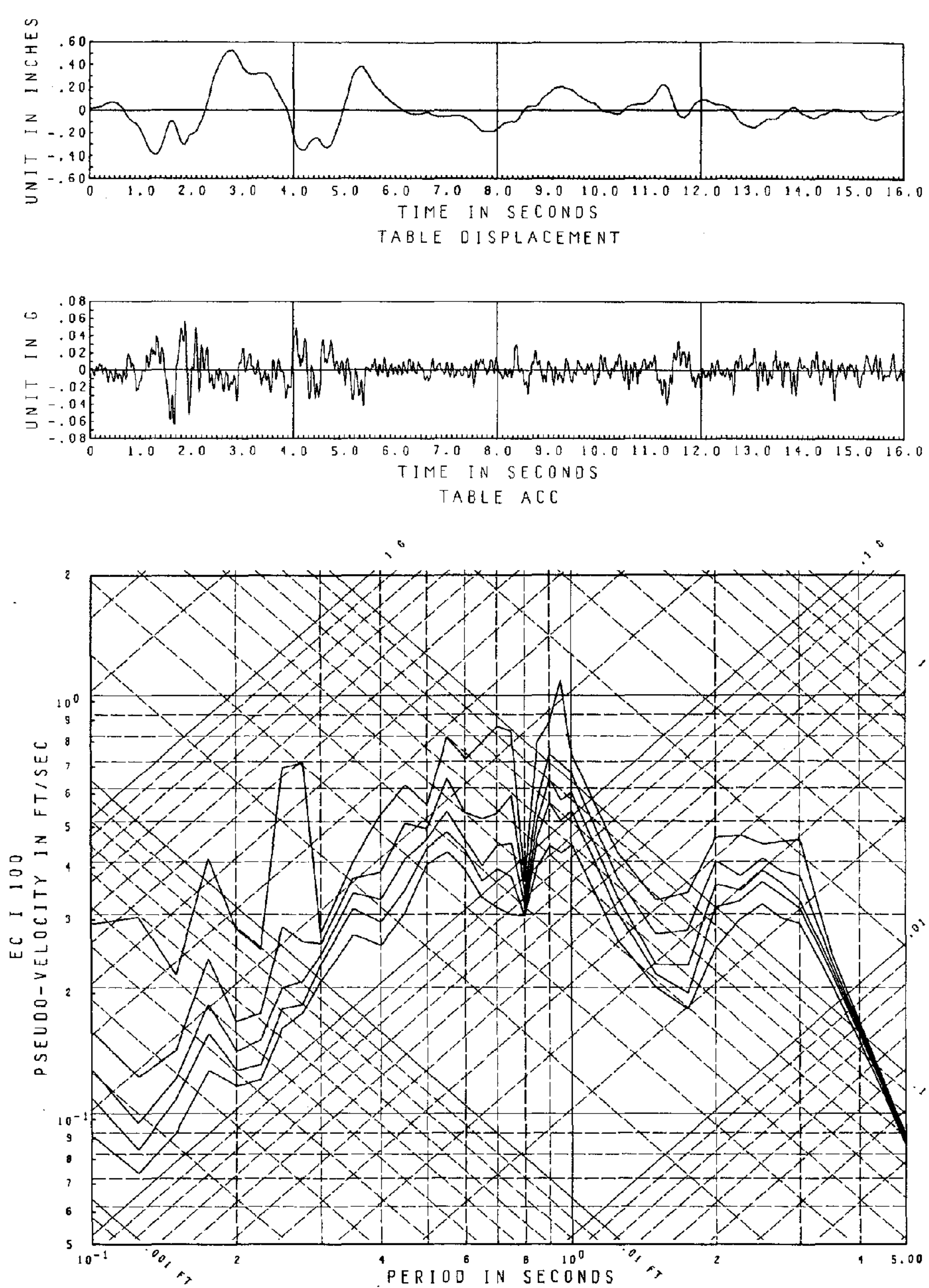

Damping = .00, .01, .02, .03, .05 Critical

Fig. 5.1a.1 El Centro Span 100 Horizontal Table Motion

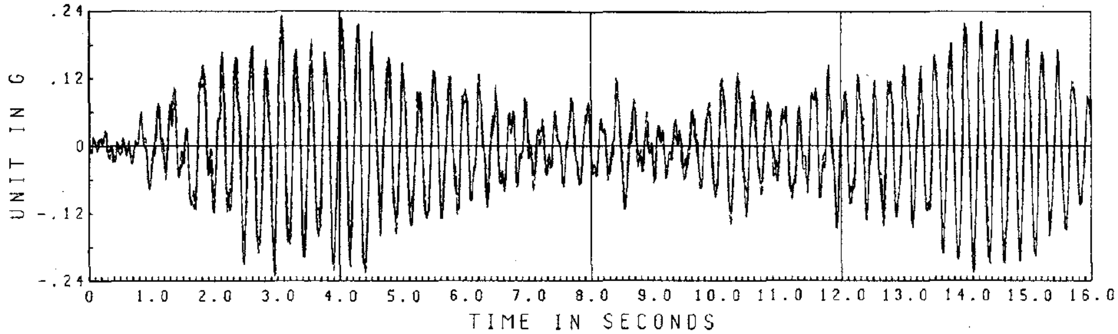

SOLID LINE = 3RD FLOOR ACC. NA DASHED LINE = 3RD FLR ACC. SA

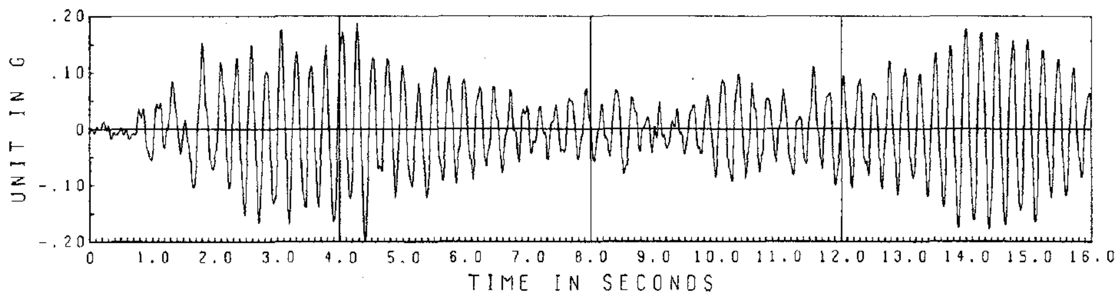

2ND FL. ABSOLUTE ACCELERATION

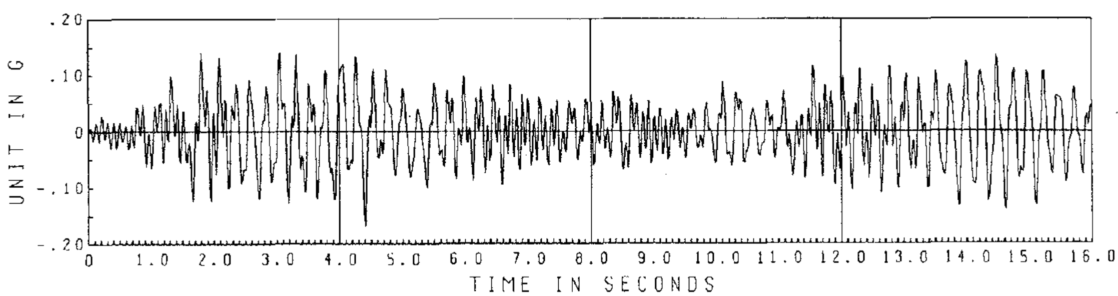

1ST FL. ABSOLUTE ACCELERATION

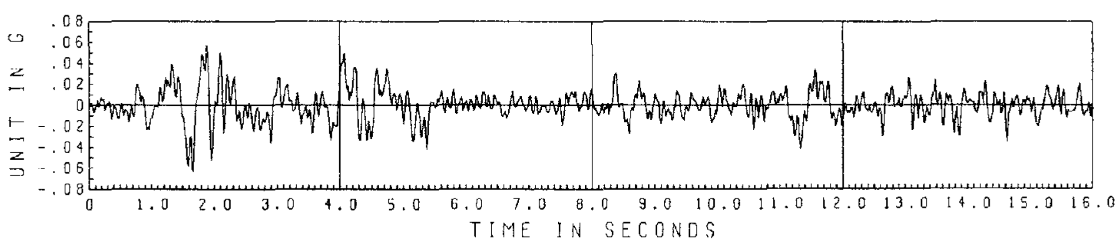

TABLE ACC

EL CENTRO SPAN 100

TEST RESULTS OF ROD BRACING

Fig. 5.1a.2 Table and Floor Accelerations

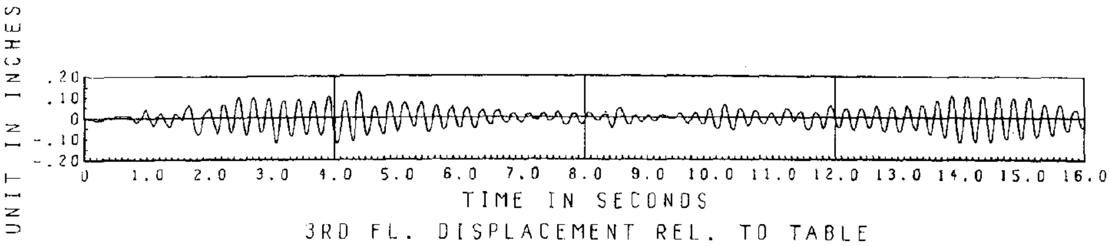

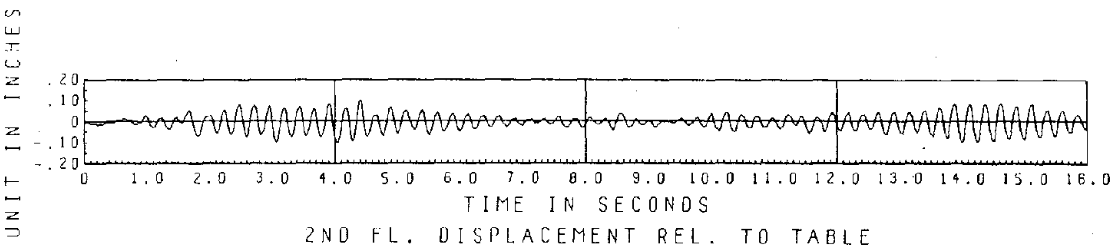

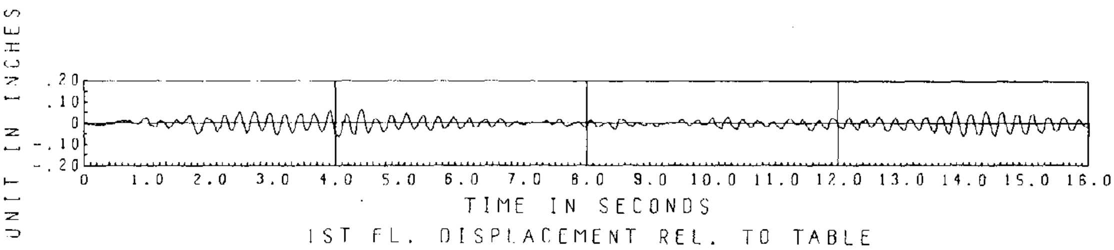

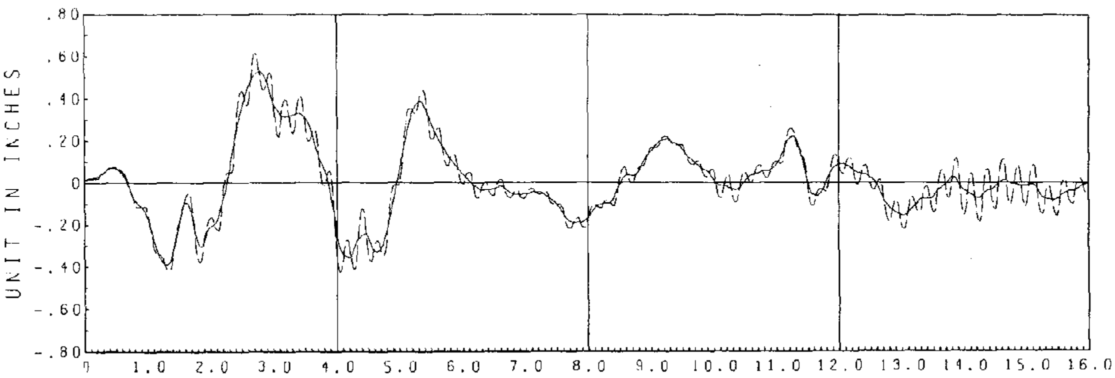

EL CENTRO SPAN 100

TEST RESULTS OF ROD BRACING

Fig. 5.1a.3 Table and Floor Displacements

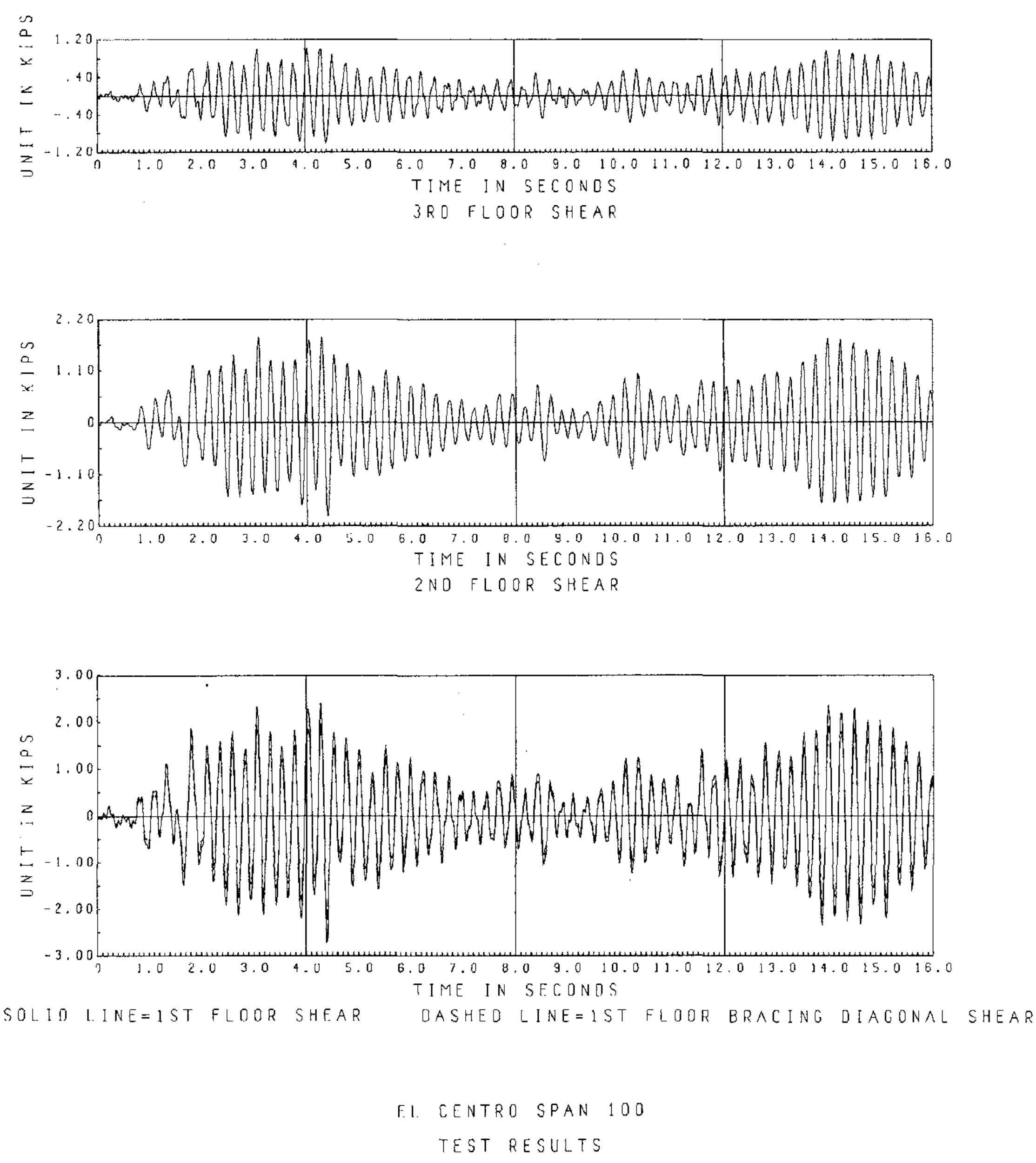

Fig. 5.1a.4 Floor Shear Forces

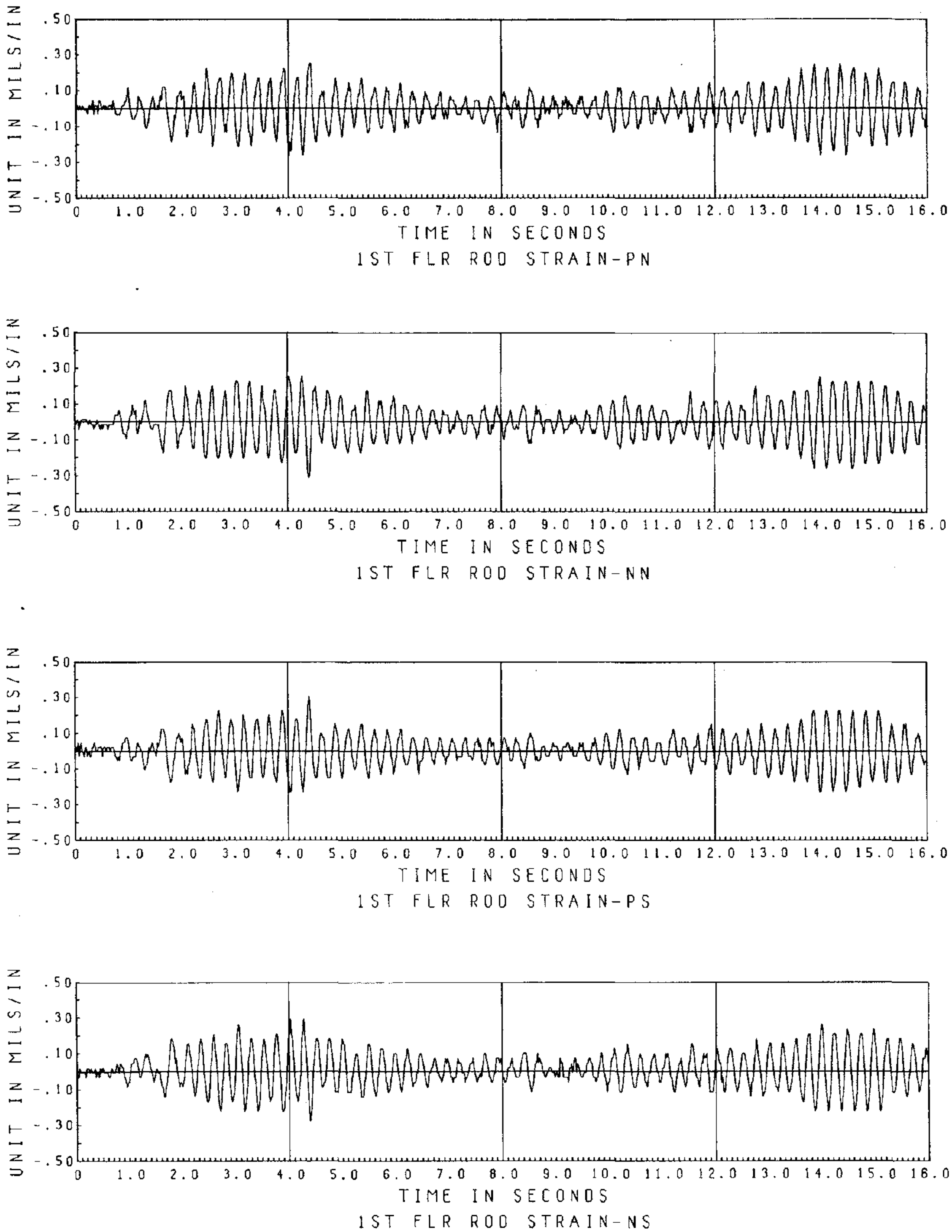

EL CENTRO SPAN 100

TEST RESULTS OF ROD BRACING

Fig. 5.1a.5 Strain Time-Histories of the 1st Floor Rod Braces

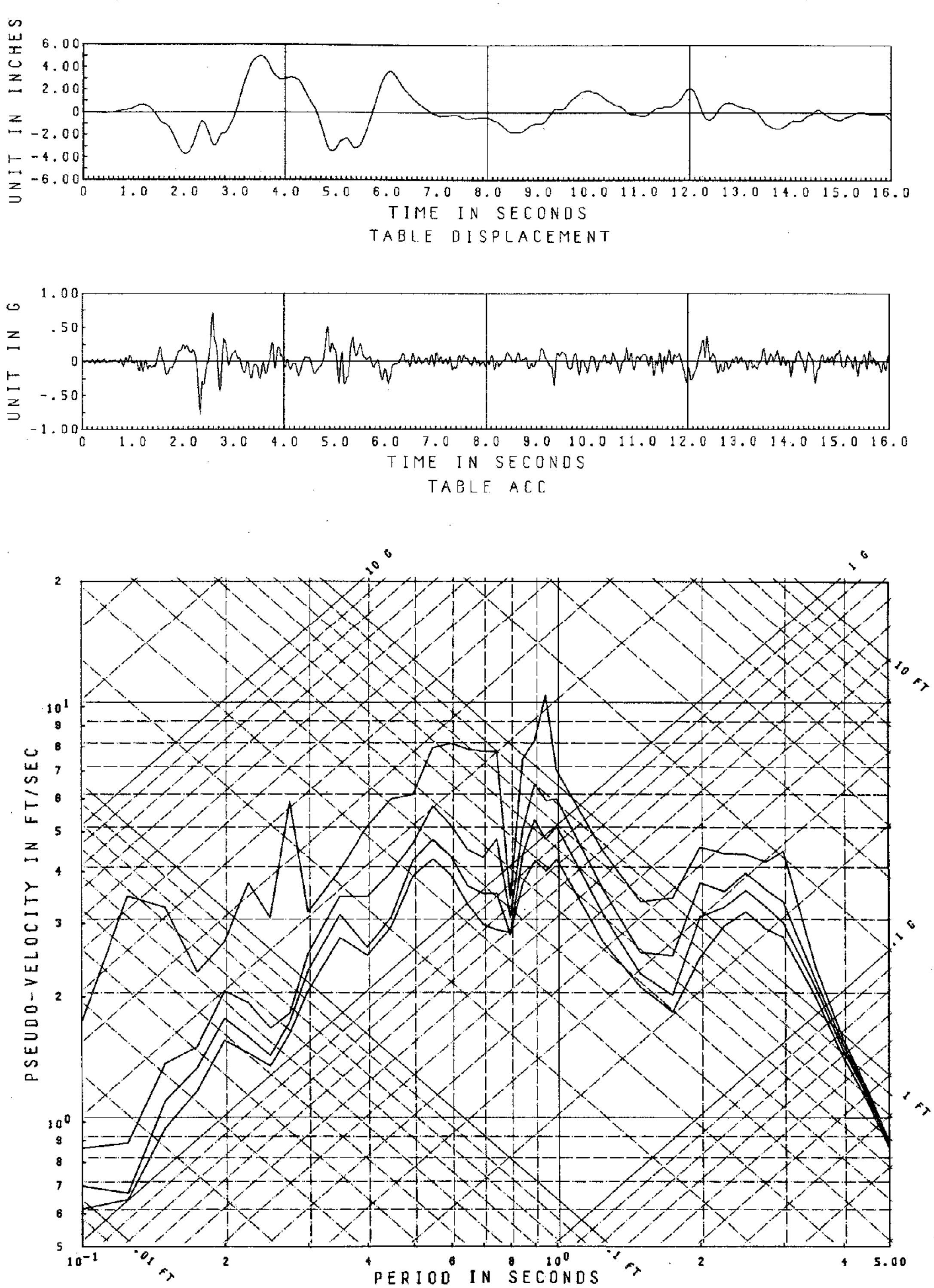

Damping = .00, .015, .03, .05 Critical

Fig. 5.1b.1 El Centro Span 1000 Horizontal Table Motion

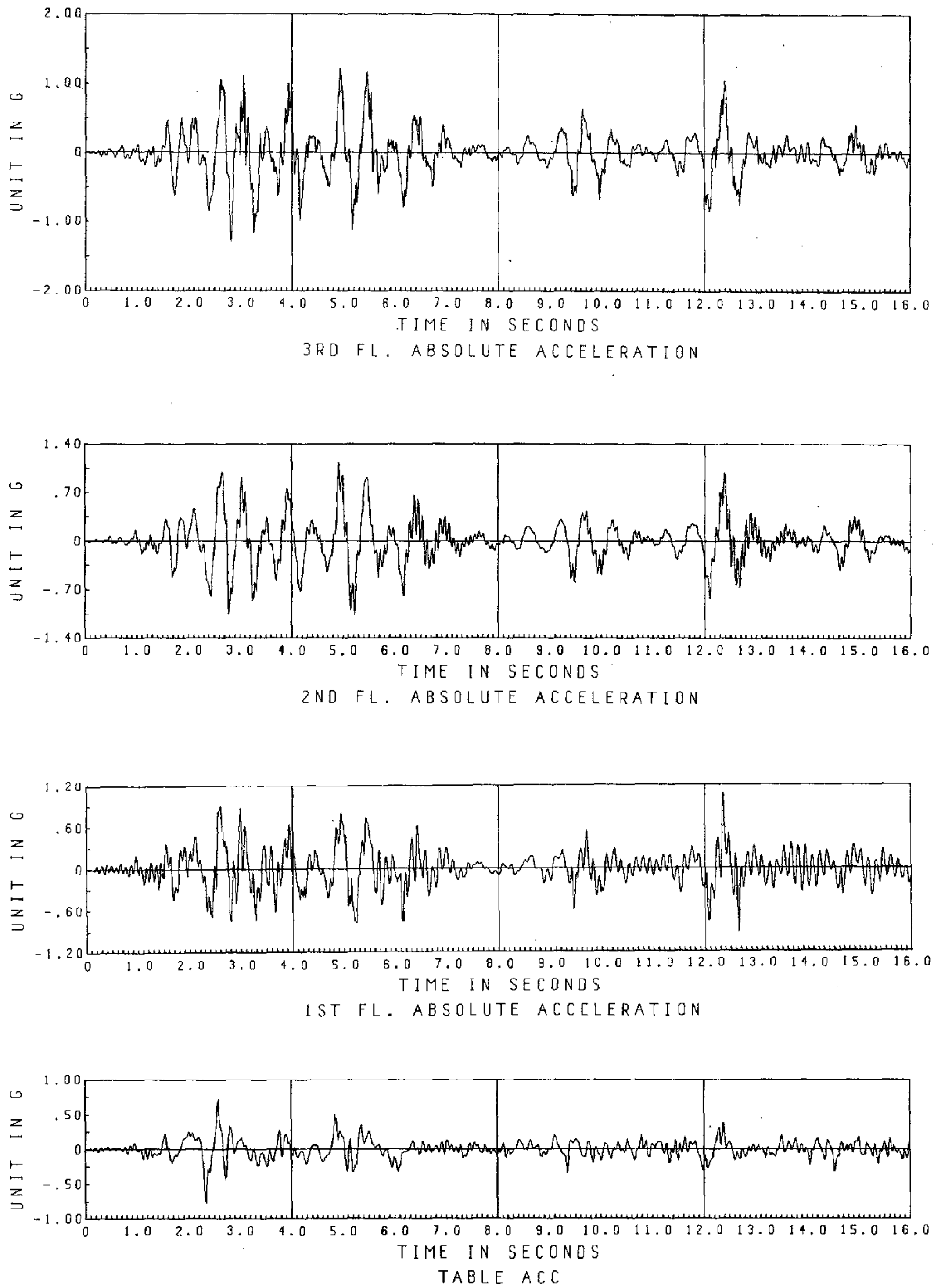

EL CENTRO SPAN 1000

TEST RESULTS OF ROD BRACING

Fig. 5.1b.2 Table and Floor Accelerations

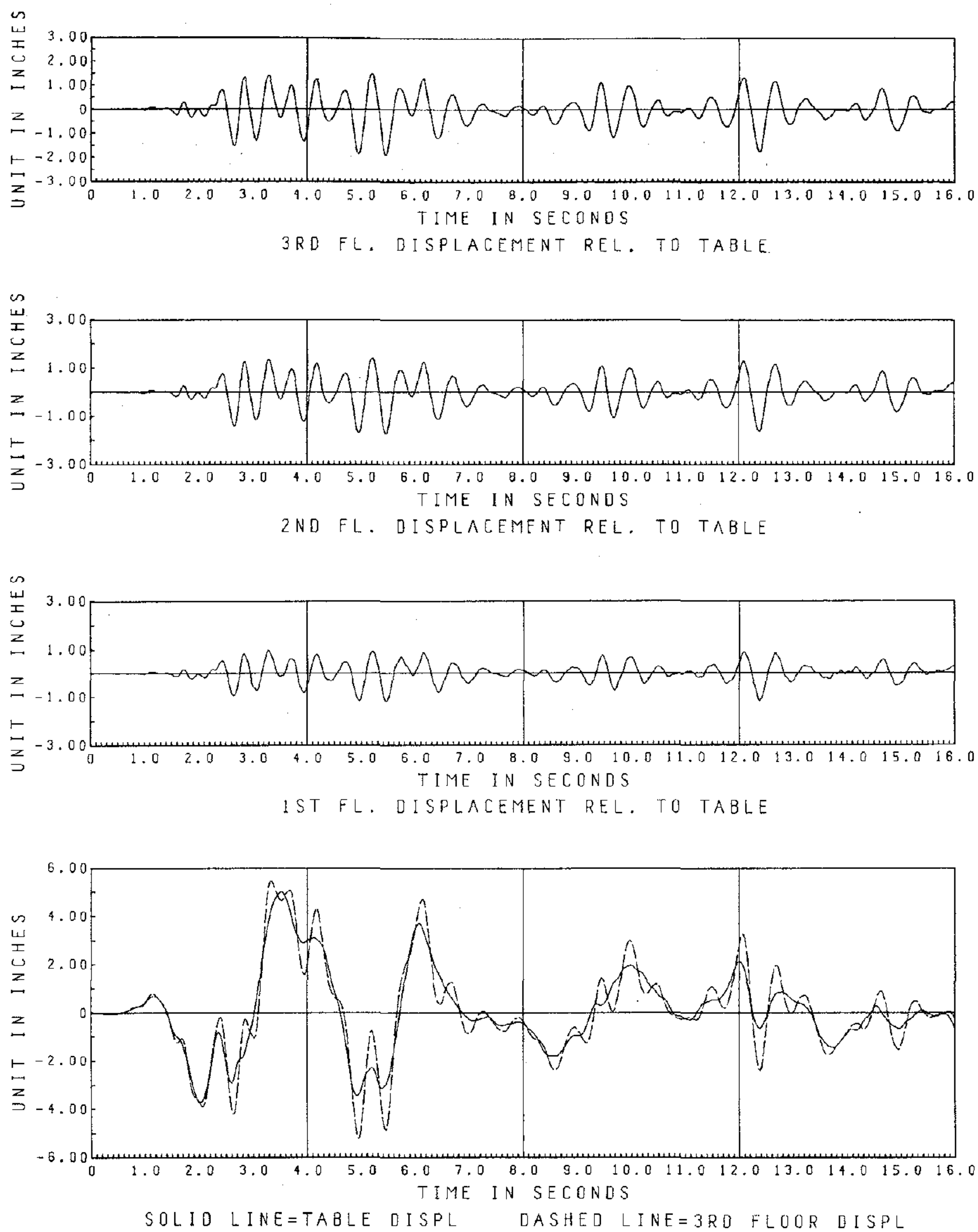

EL CENTRO SPAN 1000

TEST RESULTS OF ROD BRACING

Fig. 5.1b.3 Table and Floor Displacements

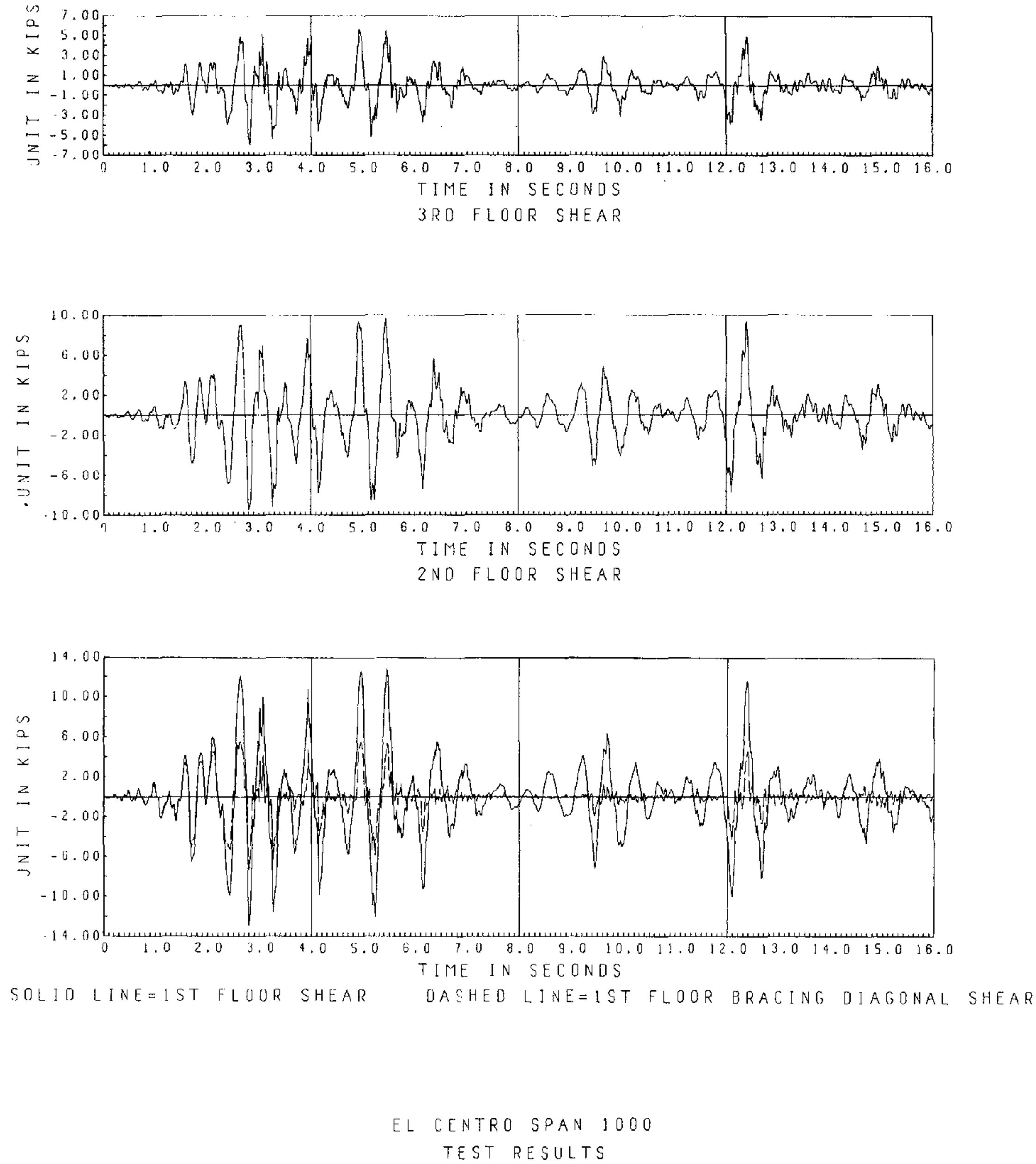

Fig. 5.1b.4 Floor Shear Forces

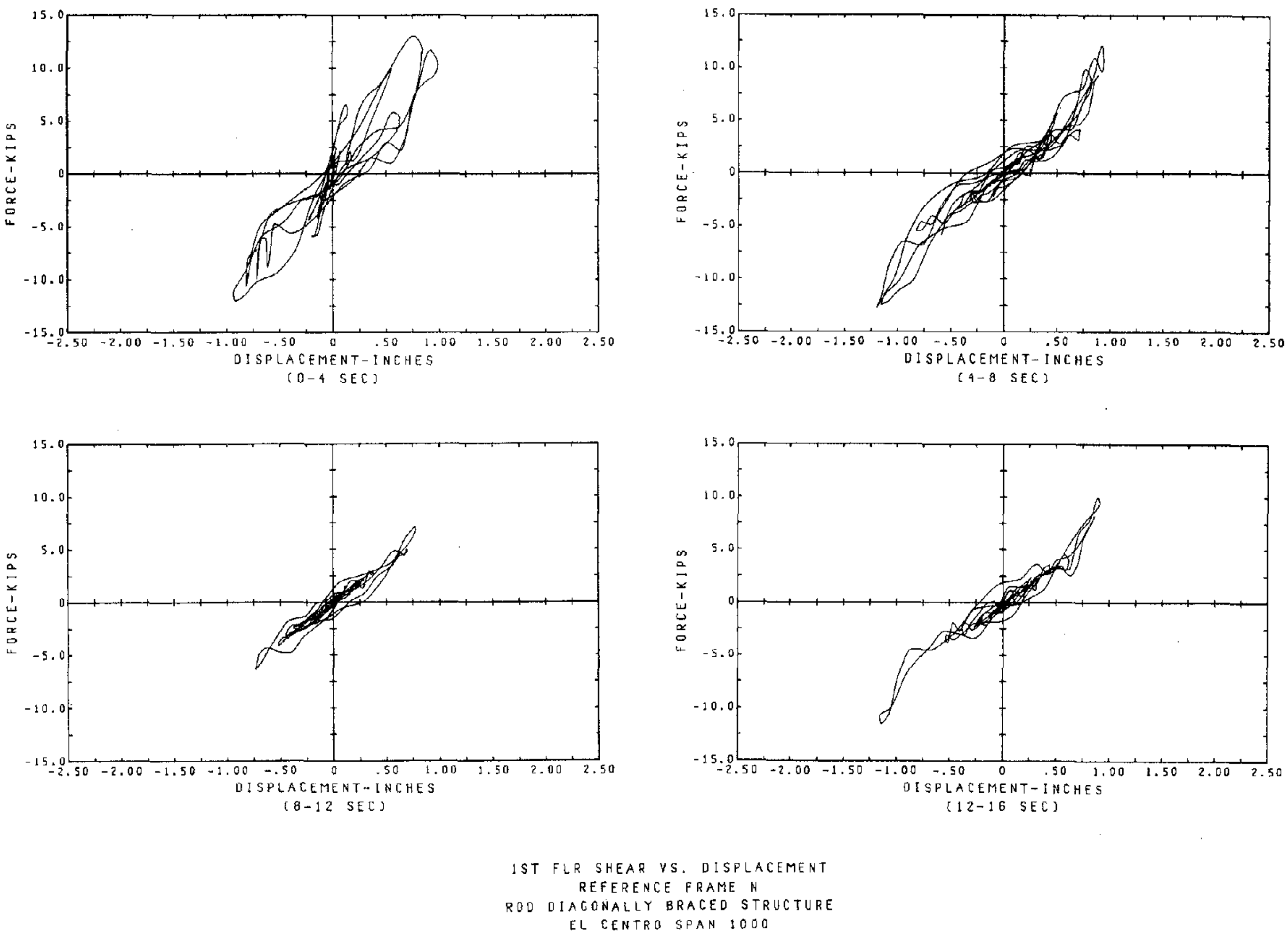

Fig. 5.1b.5 First Floor Shear-Displacement Hysteresis Loops

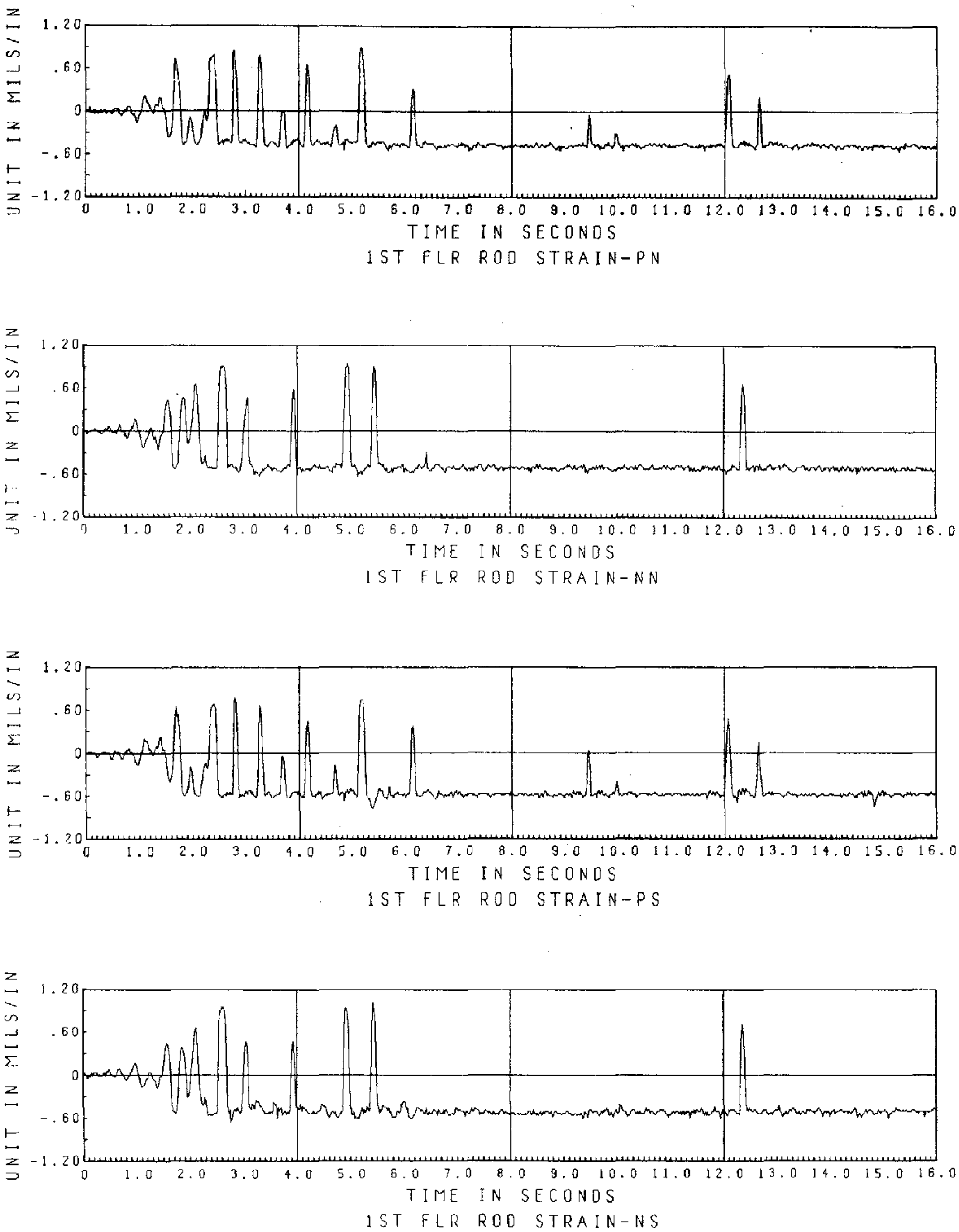

EL CENTRO SPAN 1000

TEST RESULTS

Fig. 5.1b.6 Strain Time-Histories of the 1st Floor Rod Braces

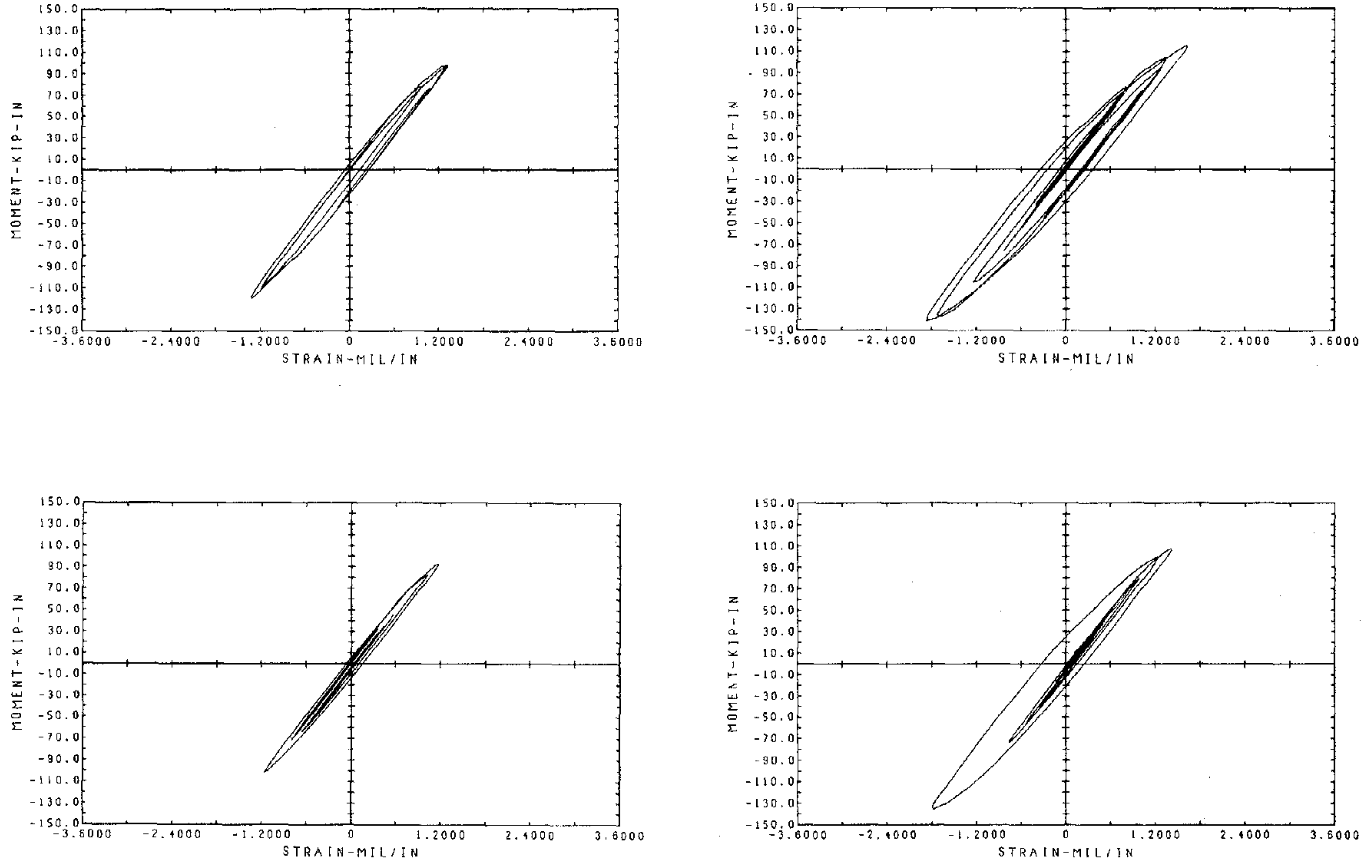

1ST FLR. COL BOTTOM END,GAGES AT 1 IN. ABOVE STIFF. PLATE
REFERENCE COLUMN LINE NB
EC 1 1000

Fig. 5.1b.7 First Floor Column Moment-Strain Hysteresis Loops

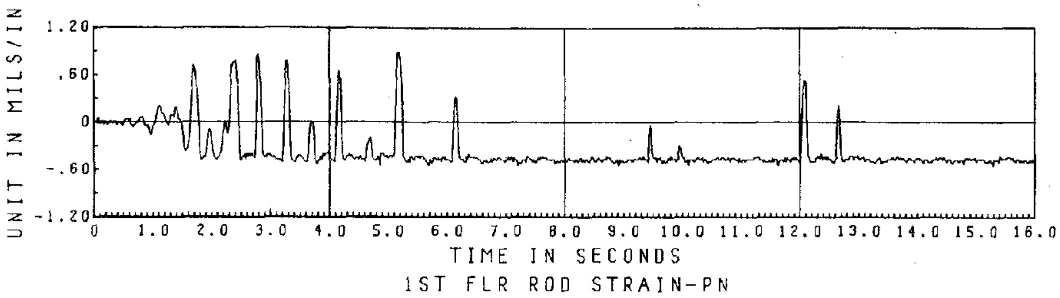

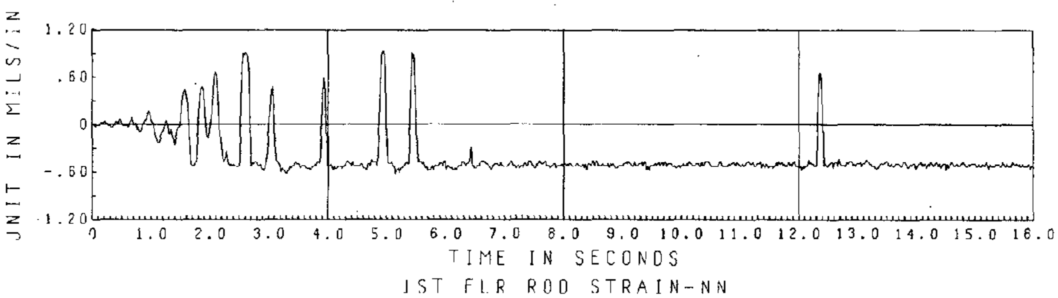

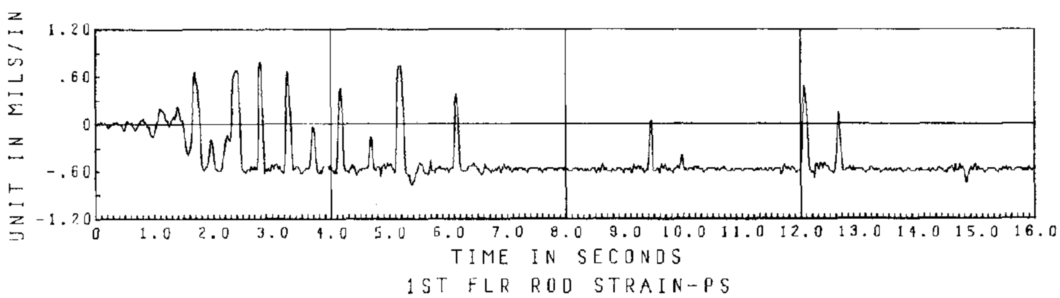

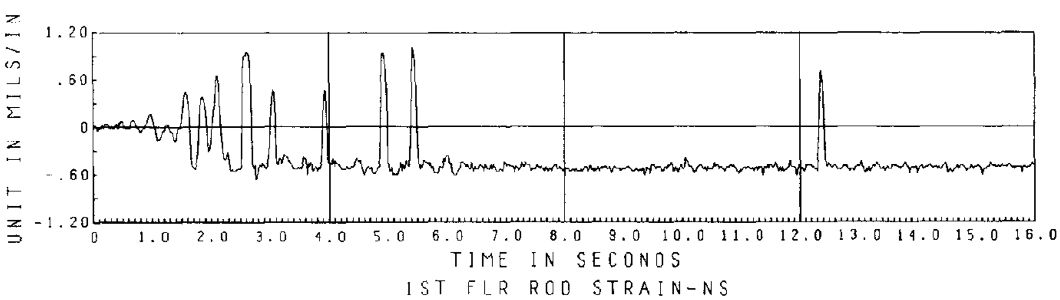

EL CENTRO SPAN 1000

TEST RESULTS

Fig. 5.1b.6 Strain Time-Histories of the 1st Floor Rod Braces

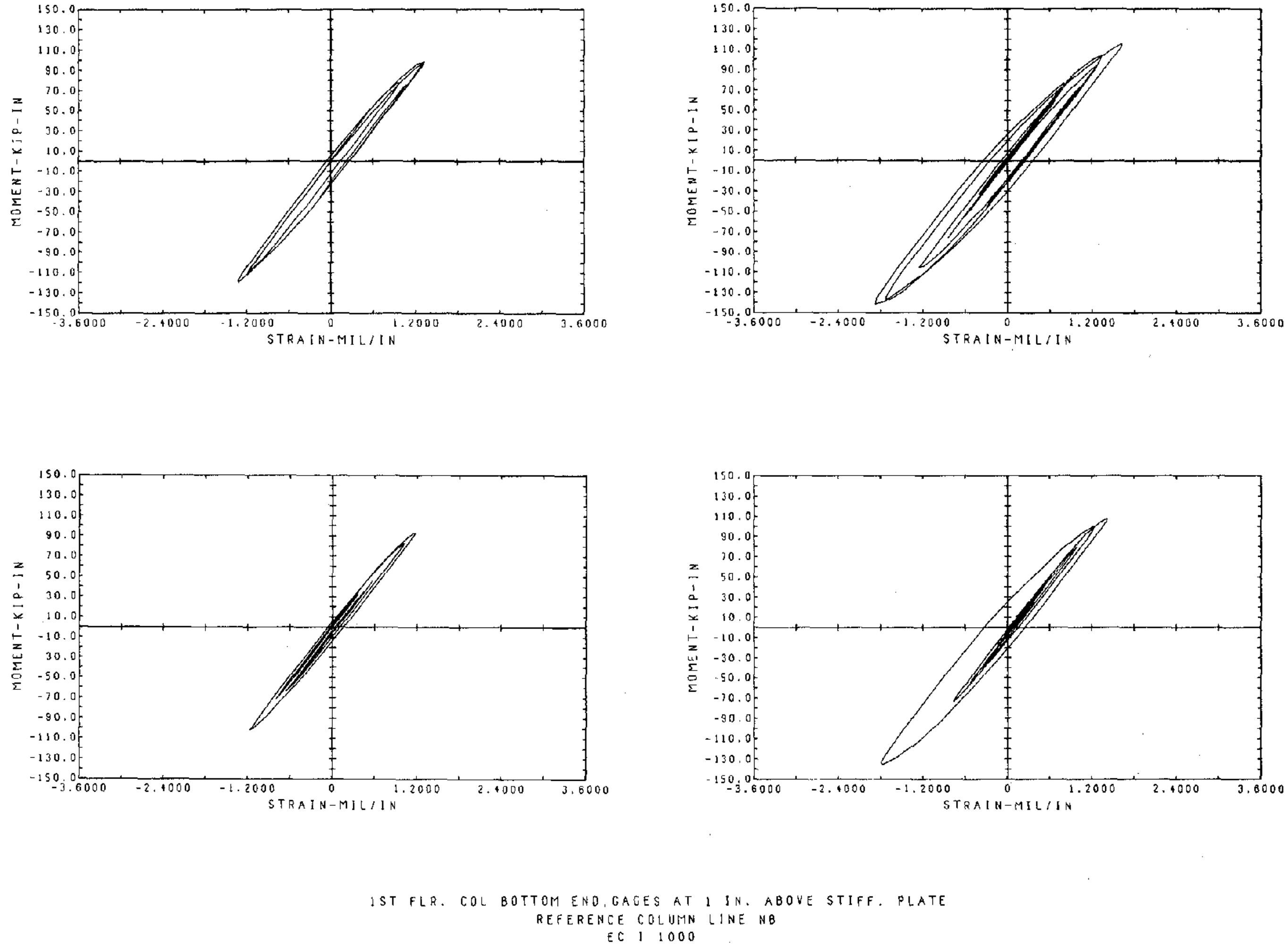

Fig. 5.1b.7 First Floor Column Moment-Strain Hysteresis Loops

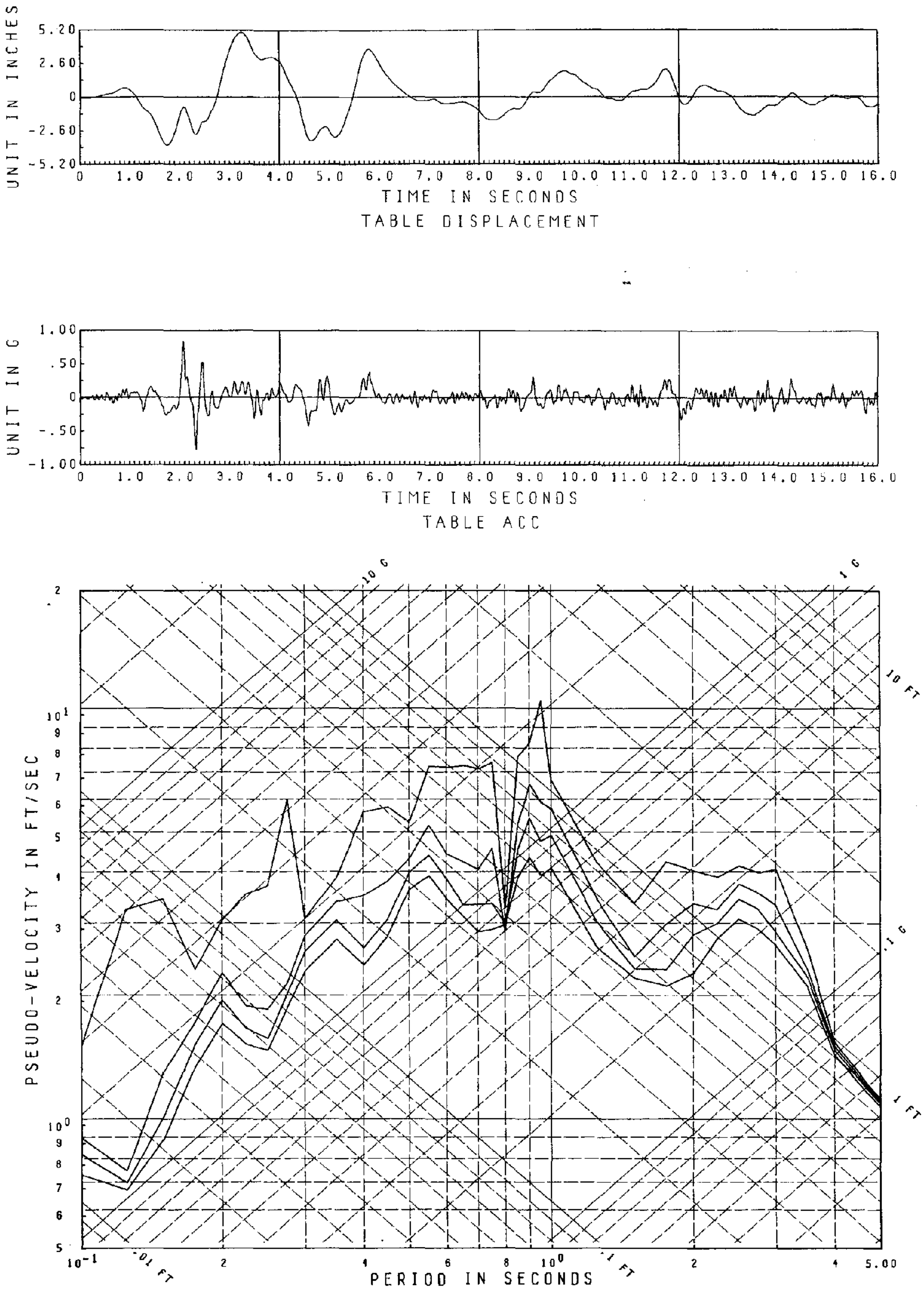

Damping = .00, .015, .03, .05 Critical

Fig. 5.1c.1 El Centro Span 950 Horizontal Table Motion

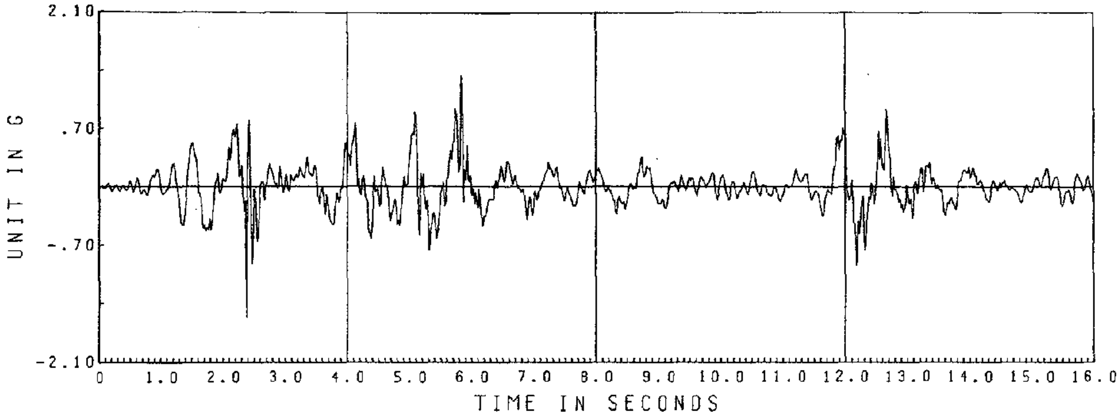

3RD FL. ABSOLUTE ACCELERATION

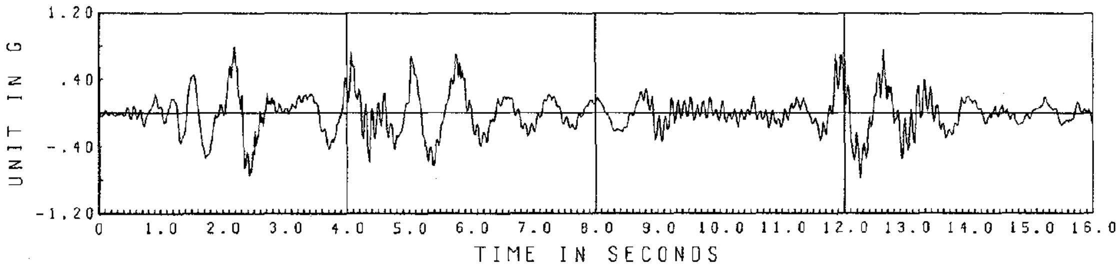

2ND FL. ABSOLUTE ACCELERATION

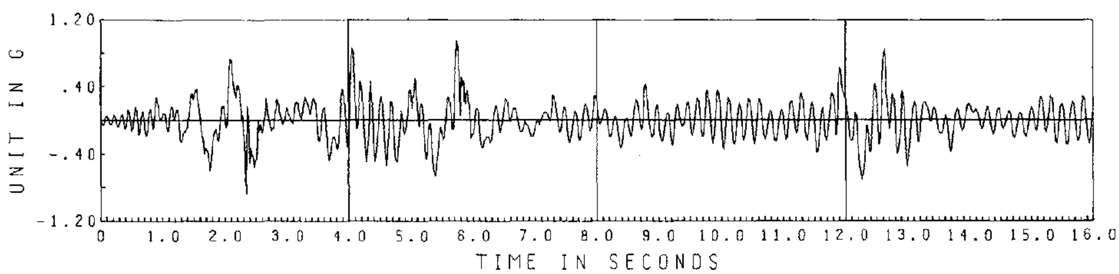

1ST FL. ABSOLUTE ACCELERATION

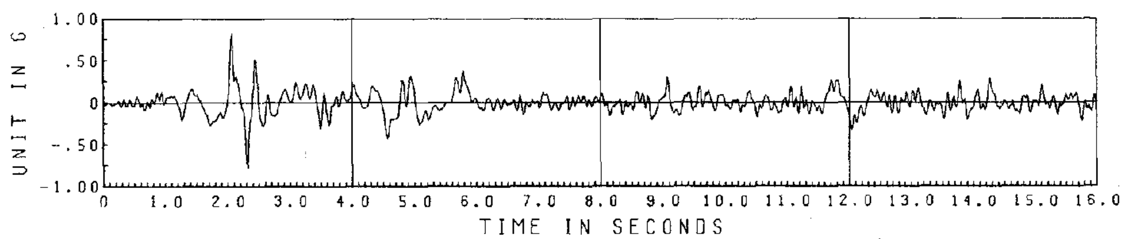

TABLE ACC

EL CENTRO SPAN 950

TEST RESULTS OF ROD BRACING

Fig. 5.1c.2 Table and Floor Accelerations

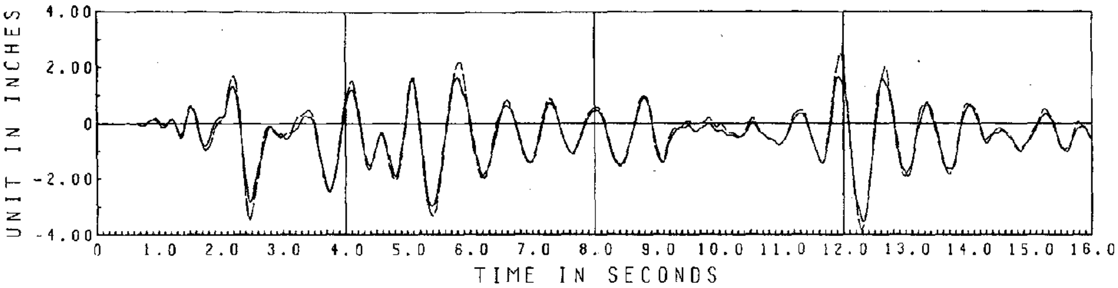

SOLID LINE=3RD FLOOR REL DISPL NA   DASHED LINE=3RD FLOOR REL DISPL SA

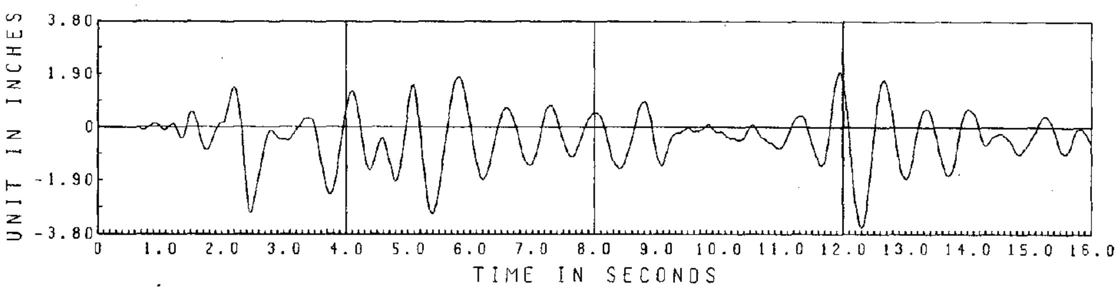

2ND FL. DISPLACEMENT REL. TO TABLE

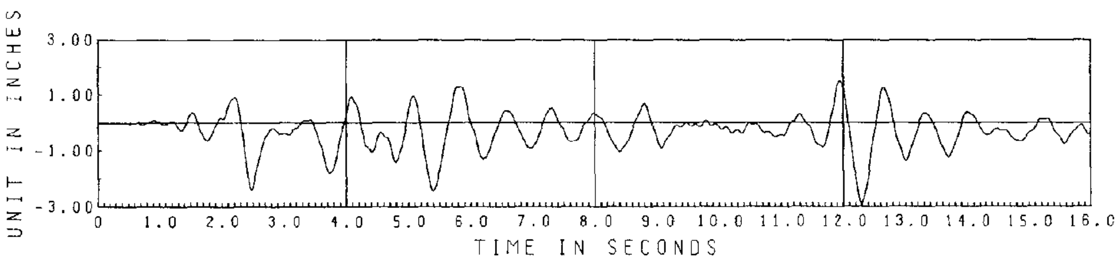

1ST FL. DISPLACEMENT REL. TO TABLE

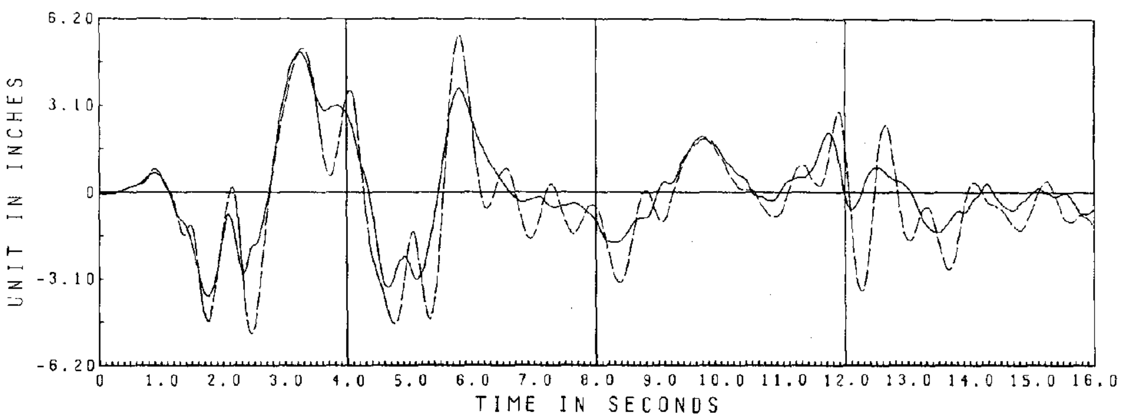

SOLID LINE=TABLE DISPL   DASHED LINE=3RD FLOOR DISPL

EL CENTRO SPAN 950

TEST RESULTS OF ROD BRACING

Fig. 5.1c.3 Table and Floor Displacements

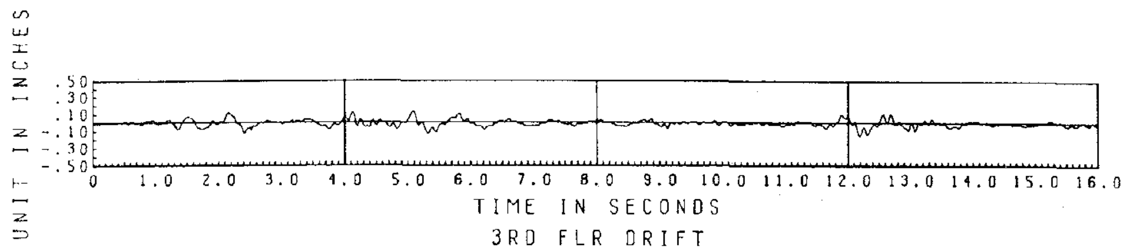

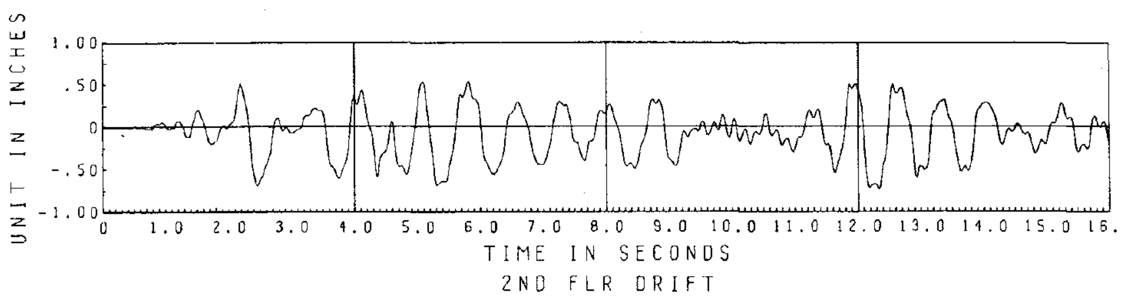

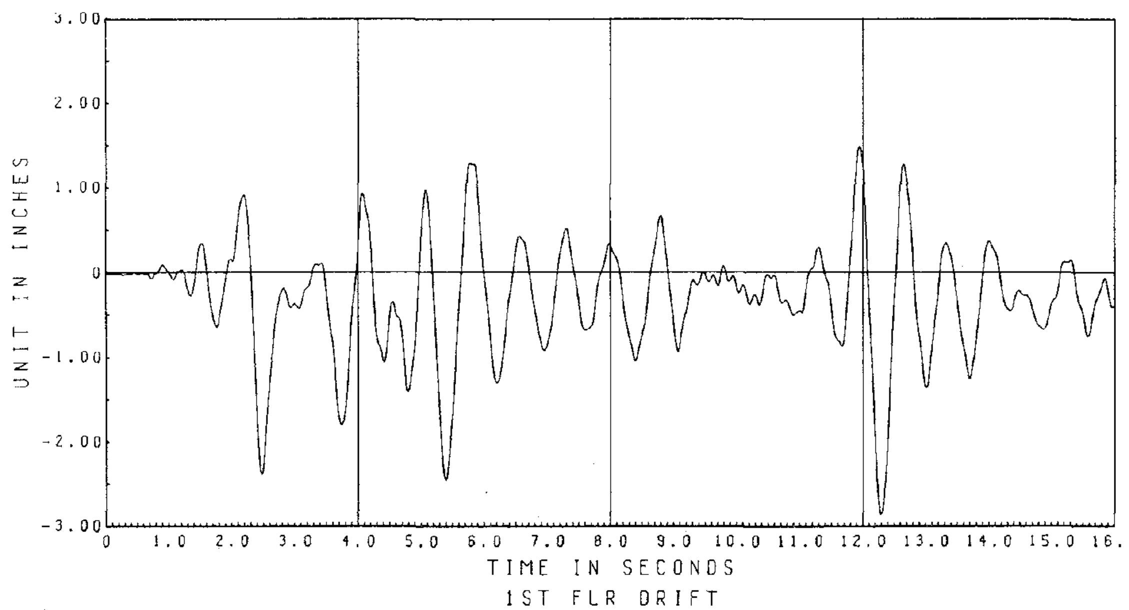

EL CENTRO SPAN 950

TEST RESULTS OF ROD BRACING

Fig. 5.1c.4 Floor Drifts

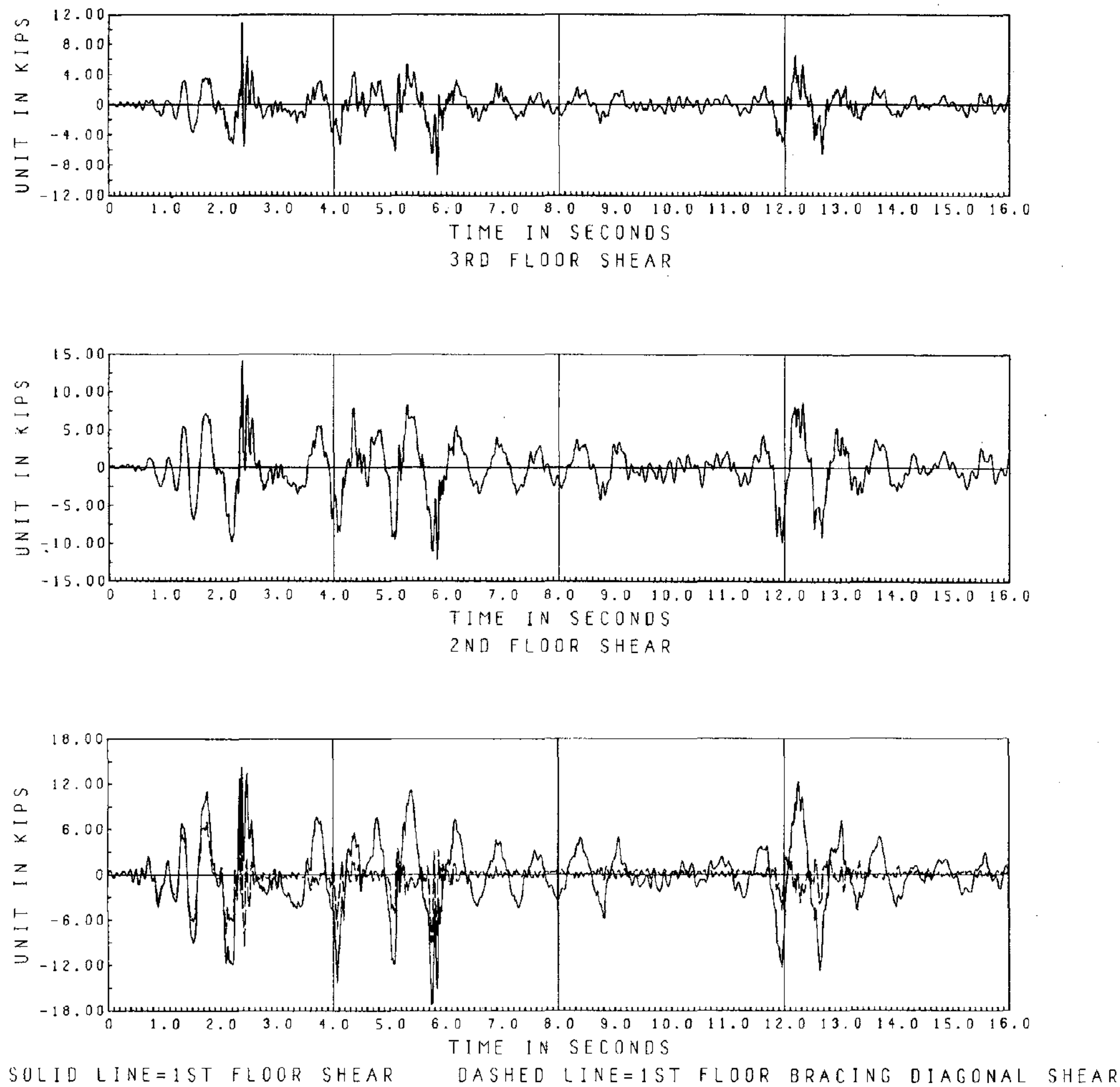

EL CENTRO SPAN 950

TEST RESULTS OF ROD BRACING

Fig. 5.1c.5 Floor Shear Forces

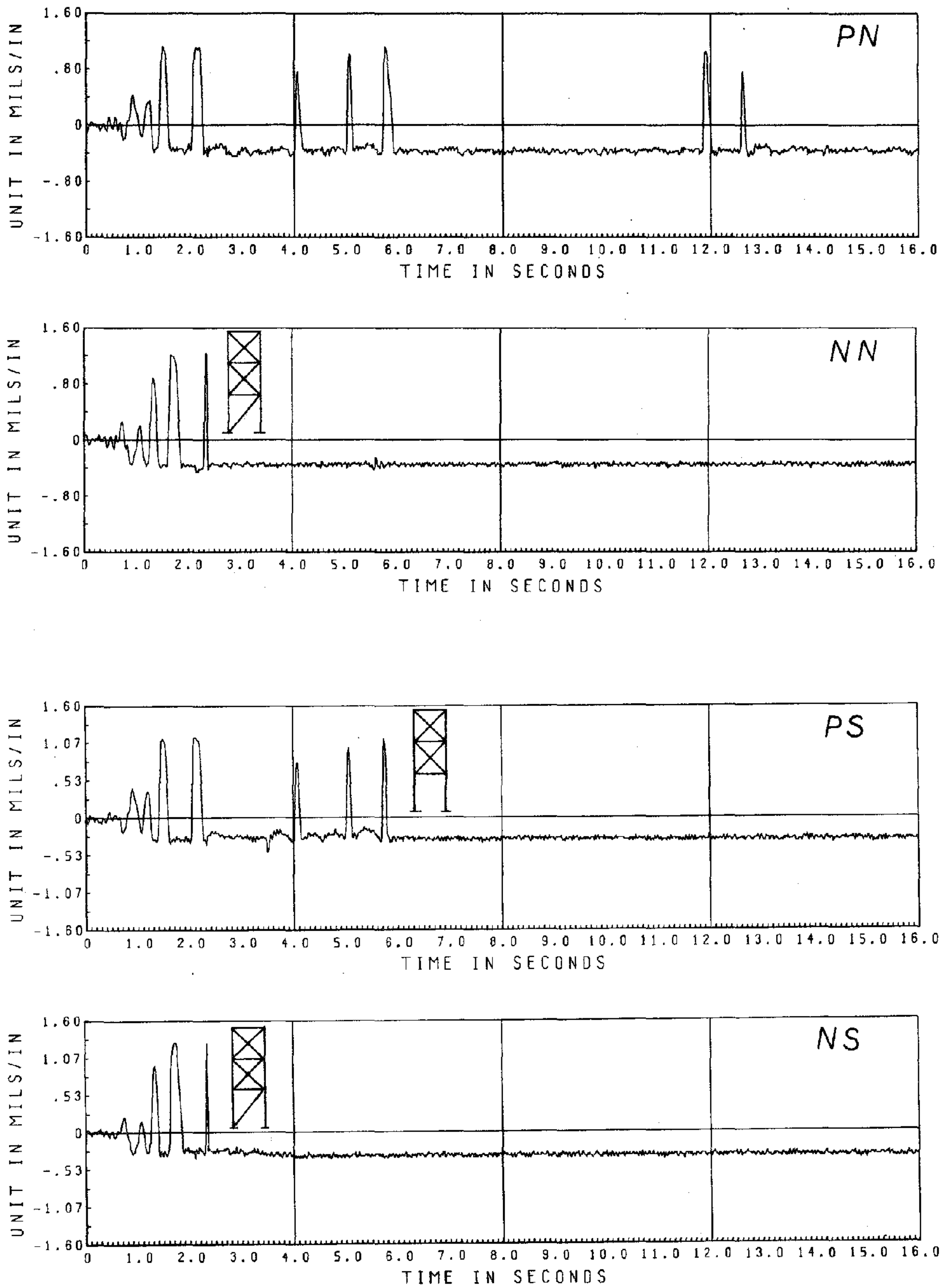

EL CENTRO SPAN 950

TEST RESULTS OF ROD BRACING

Fig. 5.1c.6 Strain Time-Histories of the 1st Floor Rod Braces

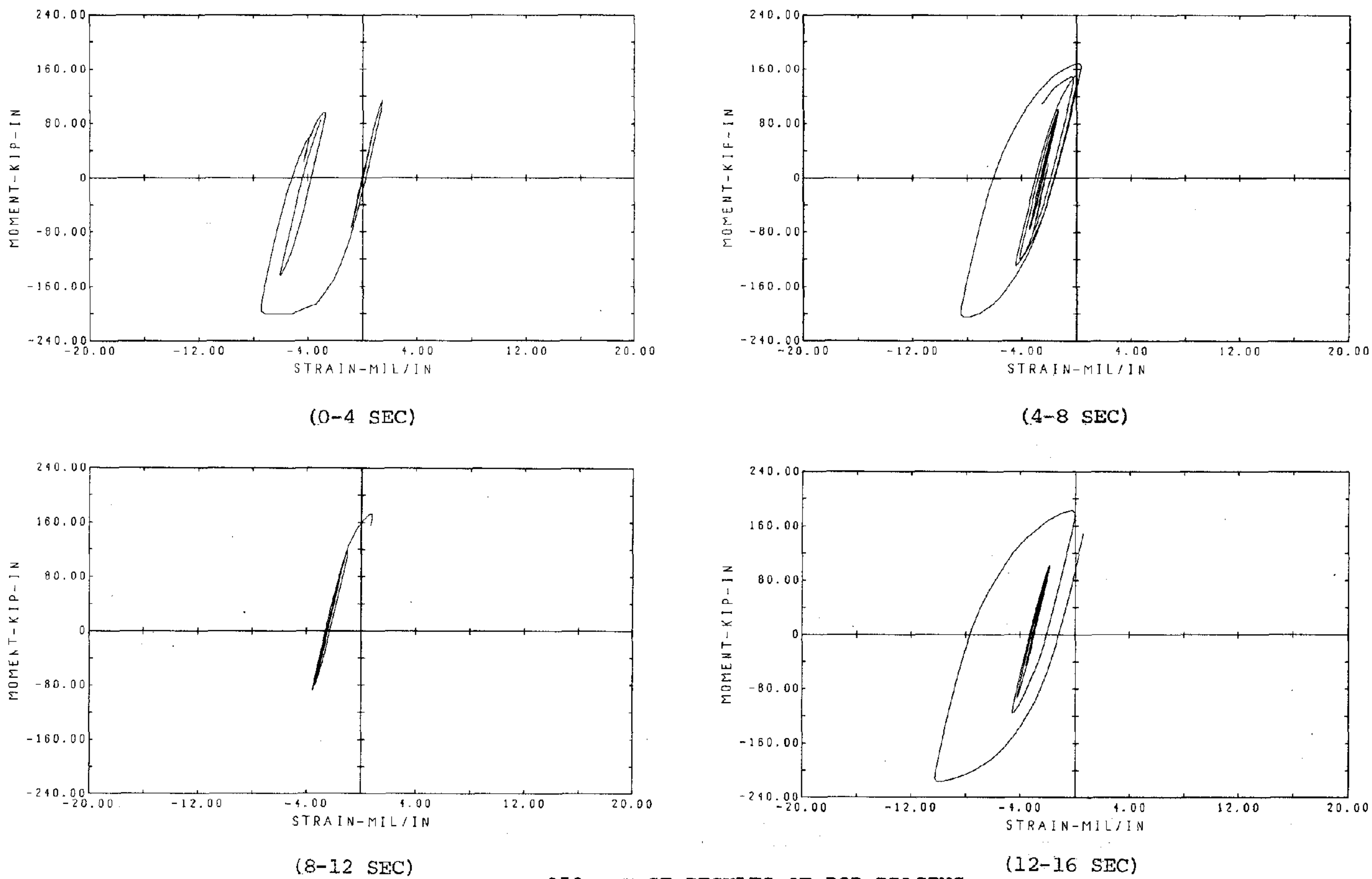

EL CENTRO SPAN 950 - TEST RESULTS OF ROD BRACING
Fig. 5.1c.7 First Floor Column Moment-Strain Hysteresis Loops

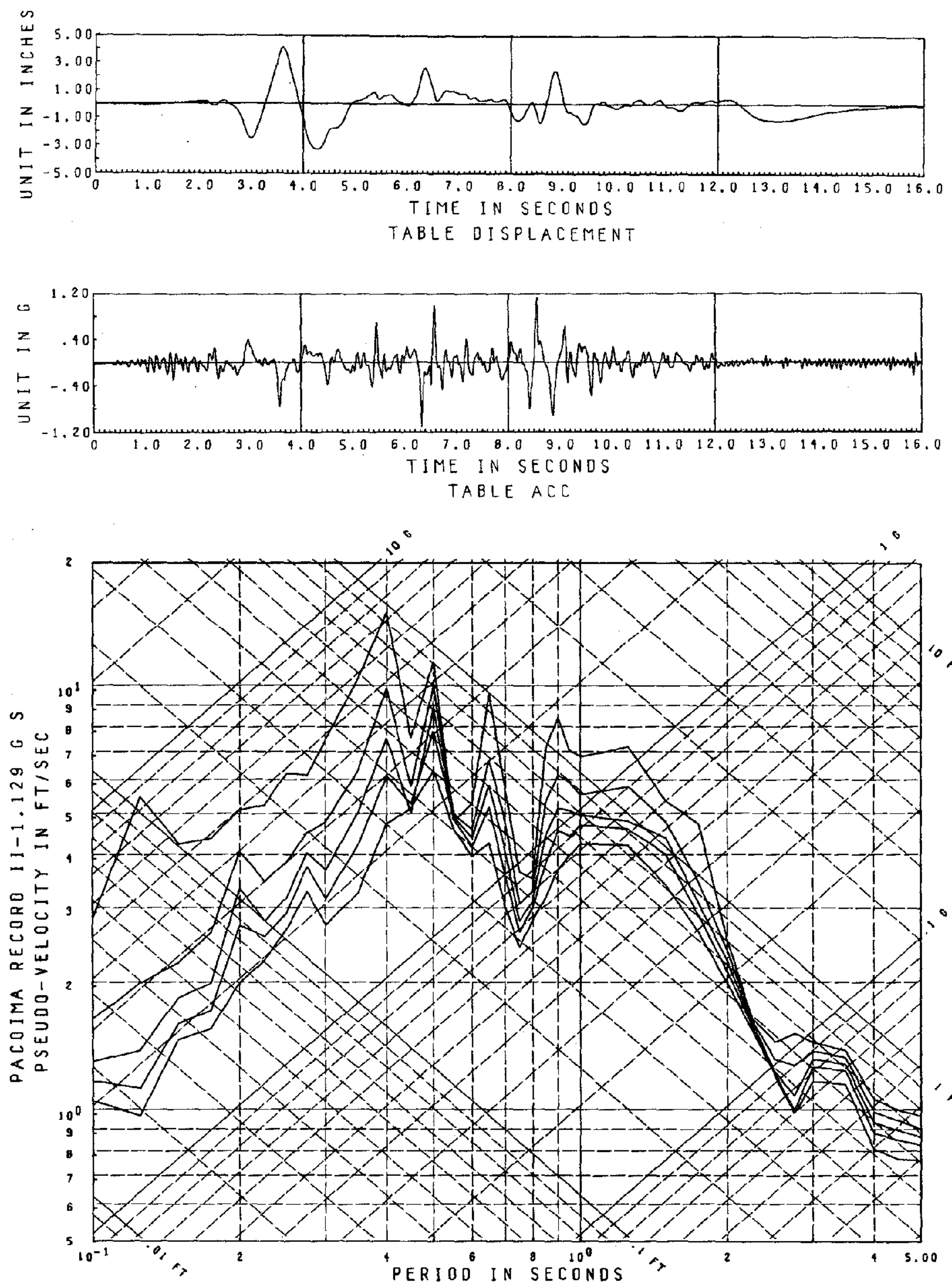

Damping = .00, .01, .02, .03, .05 Critical

Fig. 5.1d.1 Pacoima Record (1.129g) Horizontal Table Motion

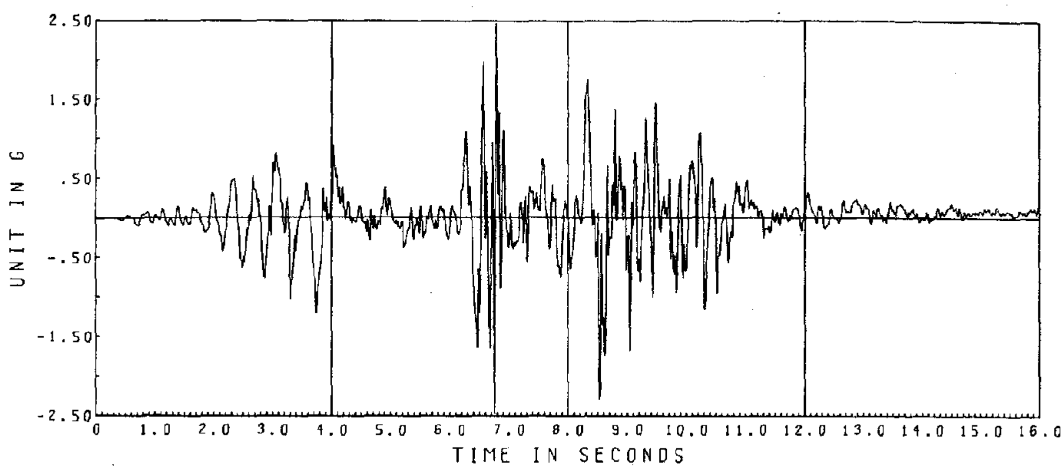

3RD FL. ABSOLUTE ACCELERATION

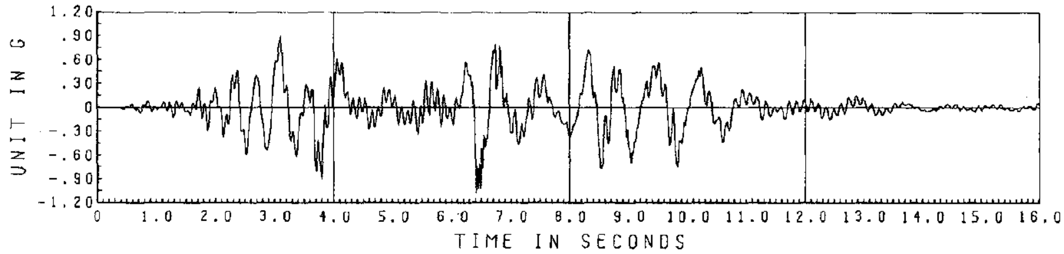

2ND FL. ABSOLUTE ACCELERATION

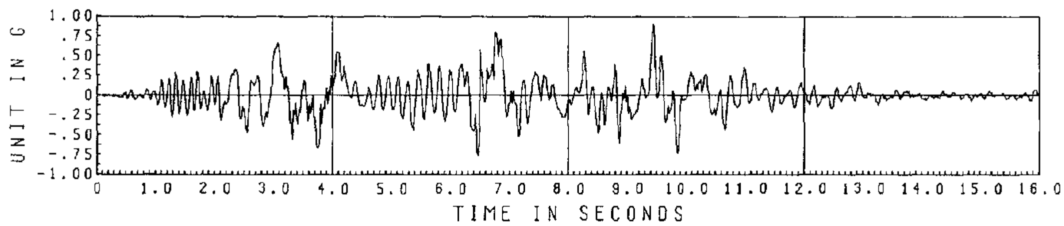

1ST FL. ABSOLUTE ACCELERATION

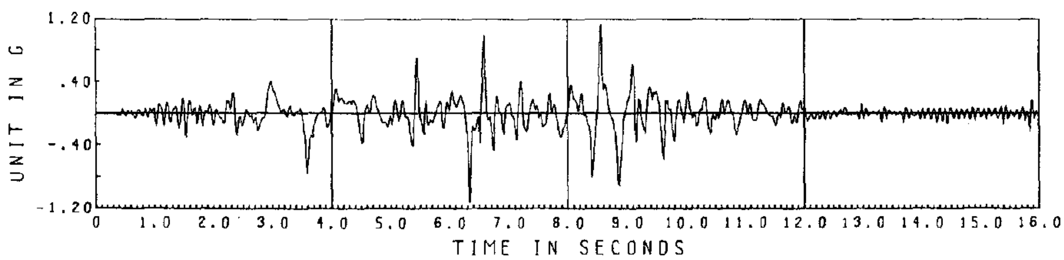

TABLE ACC

PACOIMA RECORD (1.129G)

TEST RESULTS OF ROD BRACING

Fig. 5.1d.2 Table and Floor Accelerations

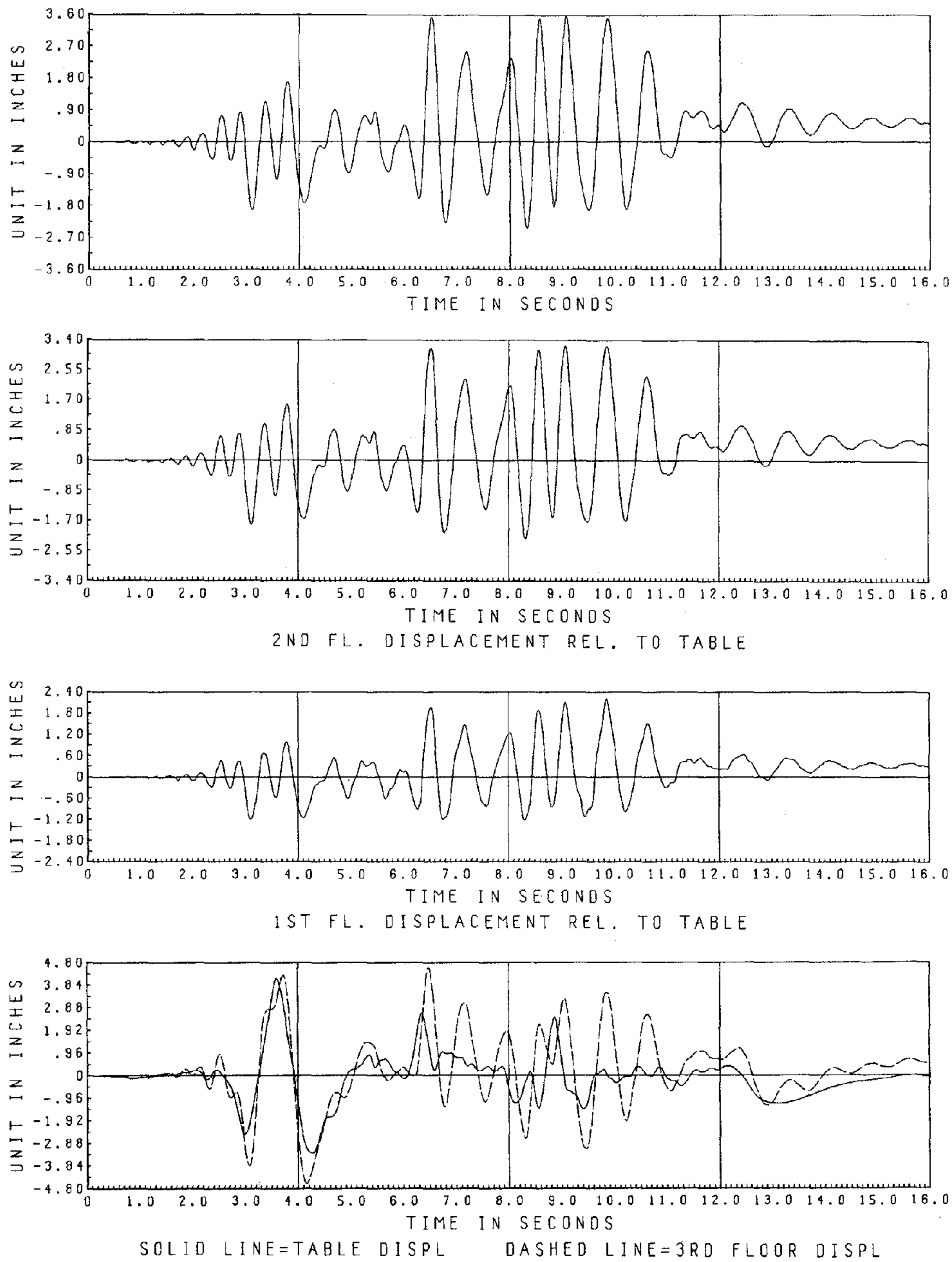

PACOIMA RECORD (1.129G)

TEST RESULTS OF ROD BRACING

Fig. 5.1d.3 Table and Floor Displacements

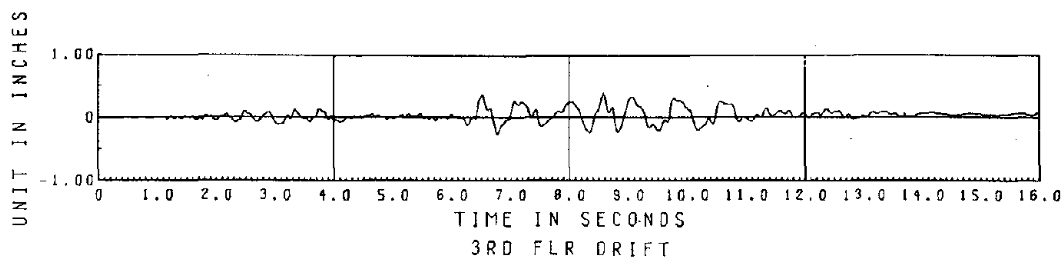

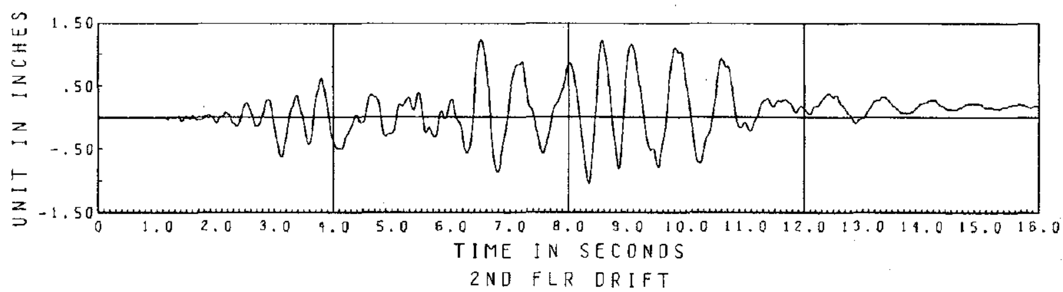

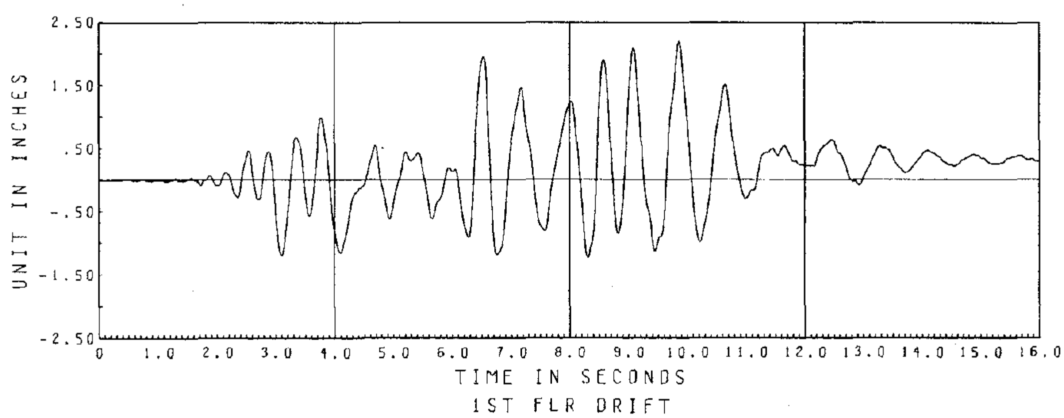

PACOIMA RECORD (1.129G)

TEST RESULTS OF ROD BRACING

Fig. 5.1d.4 Floor Drifts

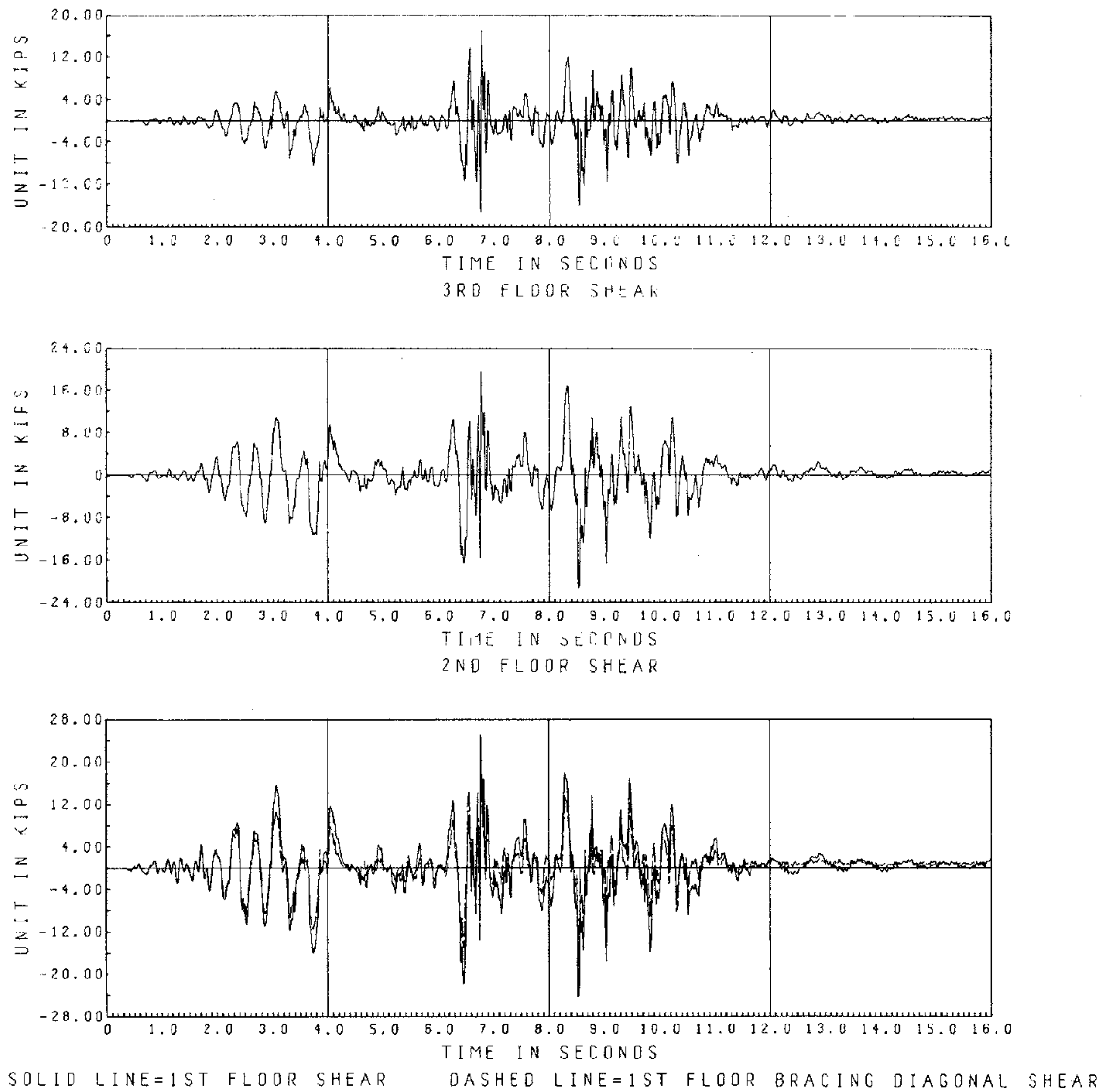

PACOIMA RECORD (1.129G)

TEST RESULTS OF ROD BRACING

Fig. 5.1d.5 Floor Shear Forces

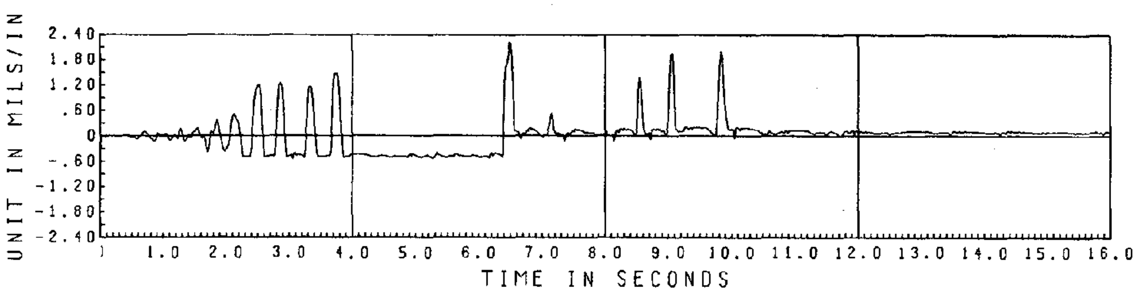

1ST FLR ROD STRAIN-PN

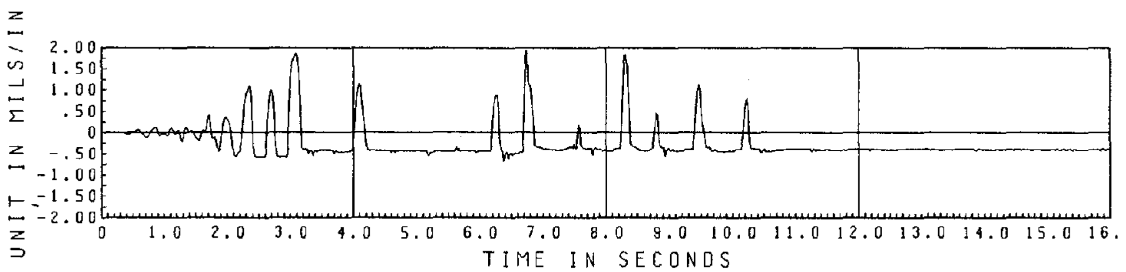

1ST FLR ROD STRAIN-NN

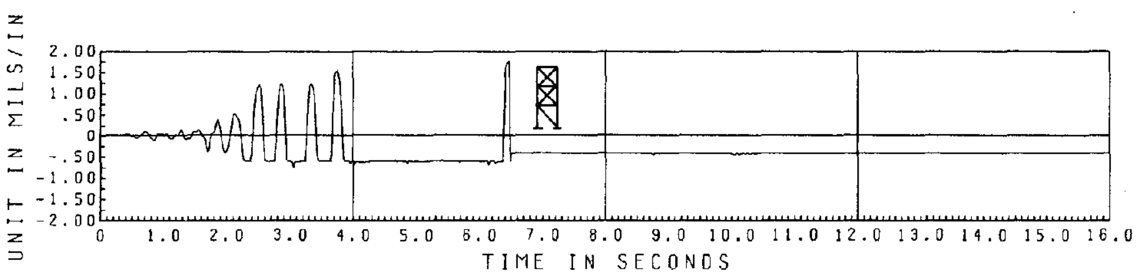

1ST FLR ROD STRAIN-PS

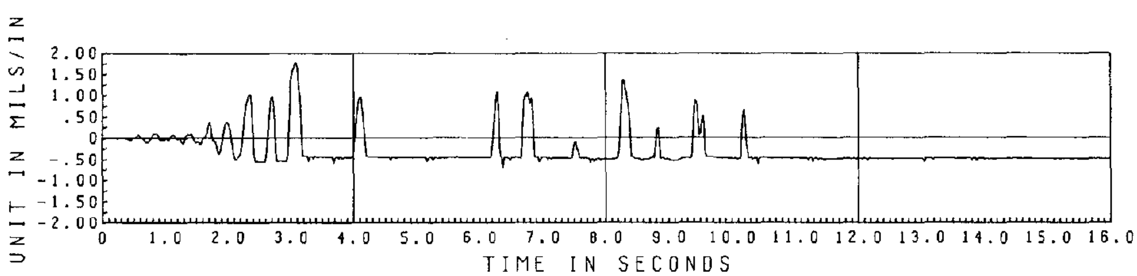

1ST FLR ROD STRAIN-NS

PACOIMA RECORD (1.129G)

TEST RESULTS OF ROD BRACING

Fig. 5.1d.6 Strain Time-Histories of the 1st Floor Rod Braces

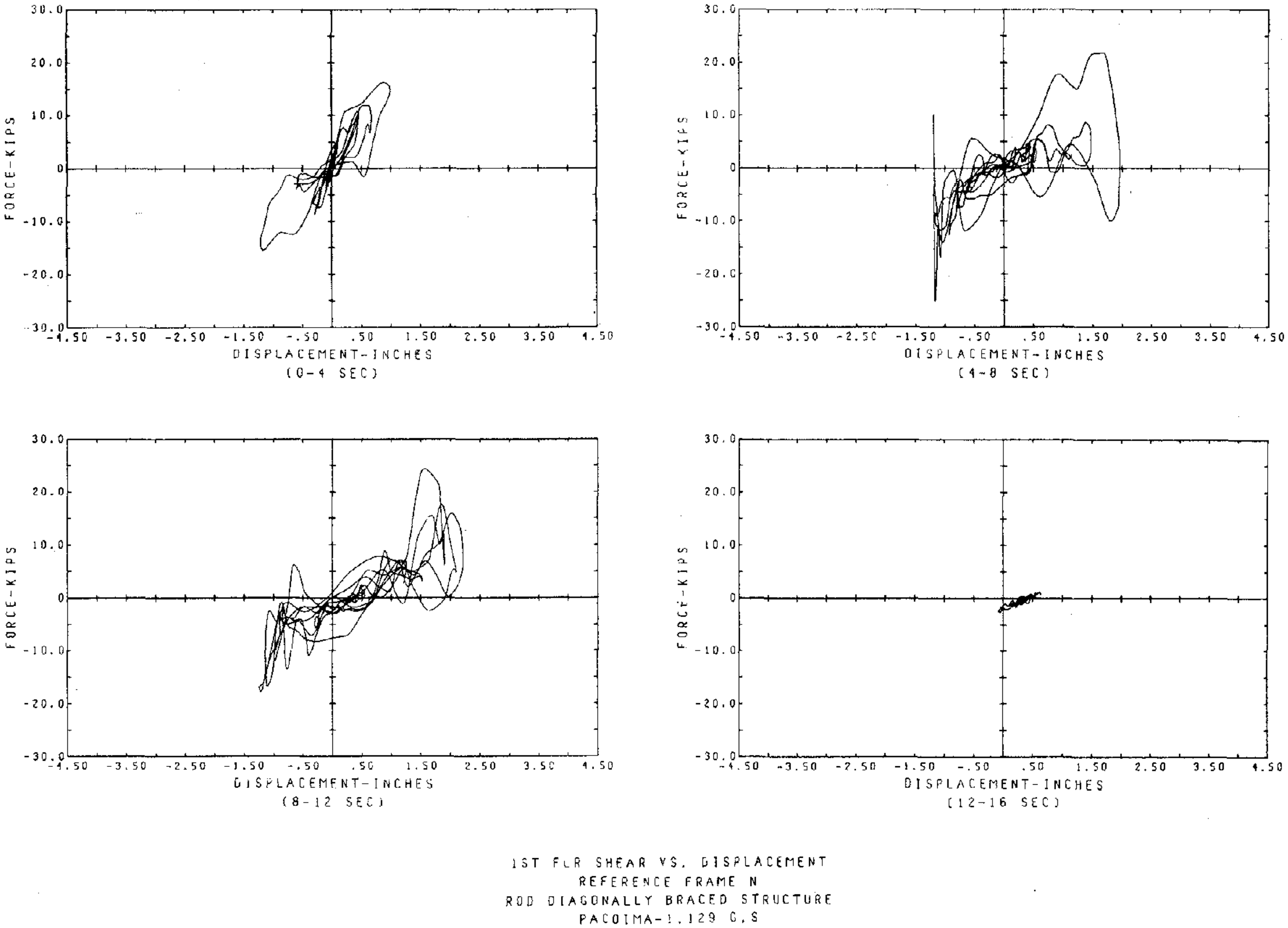

Fig. 5.1d.7 First Floor Shear-Displacement Hysteresis Loops

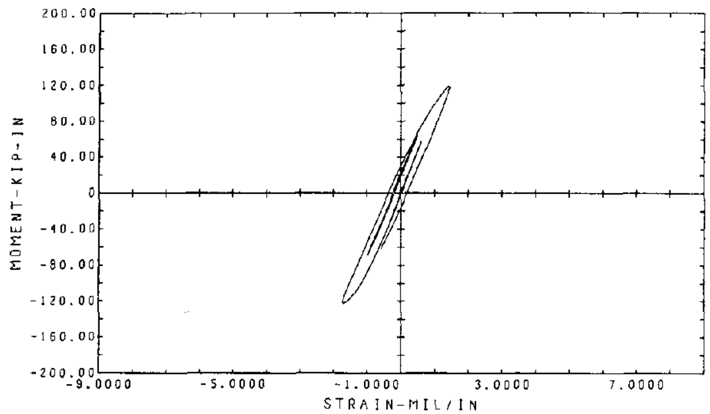

(0-4 SEC)

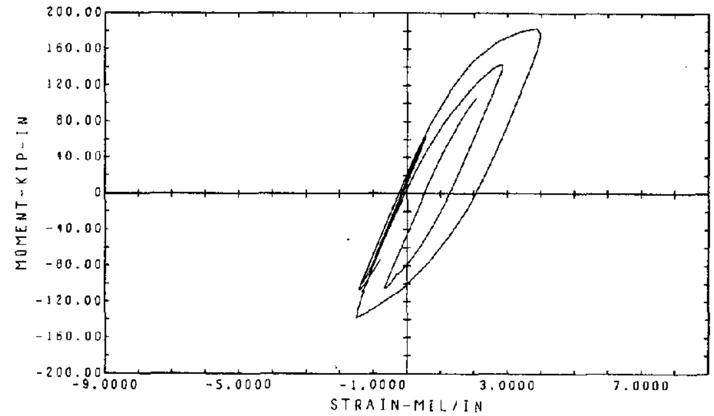

(4-8 SEC)

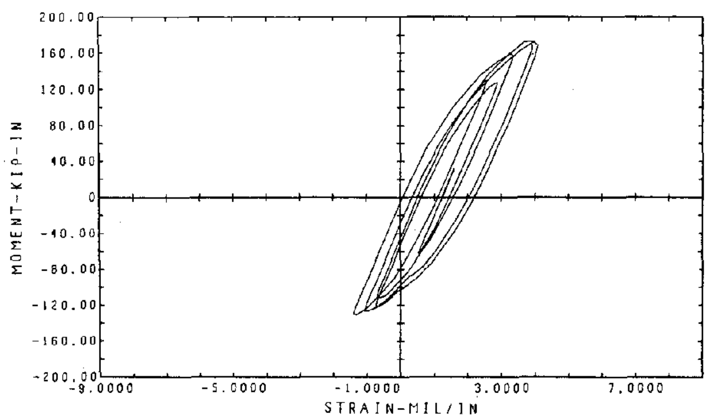

(8-12 SEC)

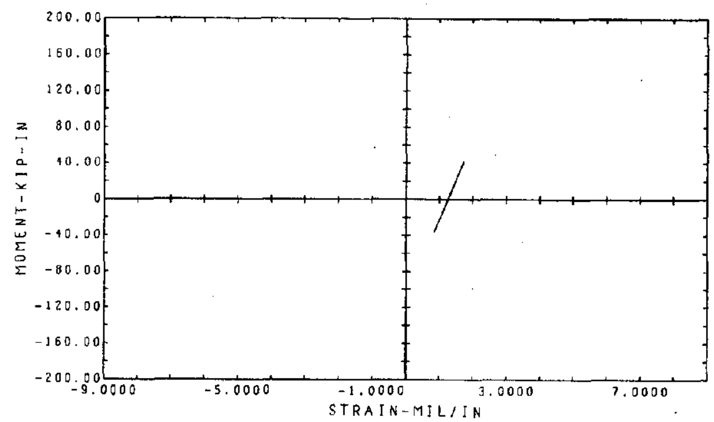

(12-16 SEC)

ROD DIAGONALLY BRACED STRUCTURE

1ST FLR. COL BOTTOM END, GAGES AT 1 IN. ABOVE STIFF. PLATE
REFERENCE COLUMN LINE NA

Fig. 5.1d.8 First Floor Column Moment-Strain Hysteresis Loops

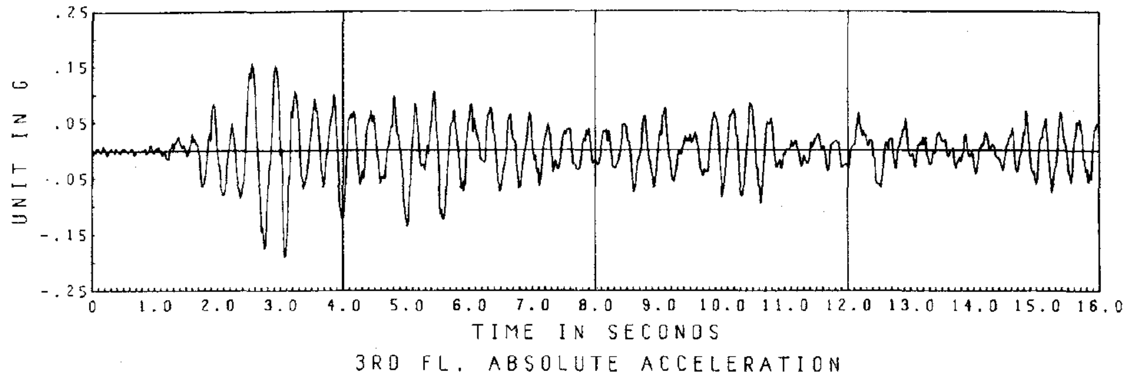

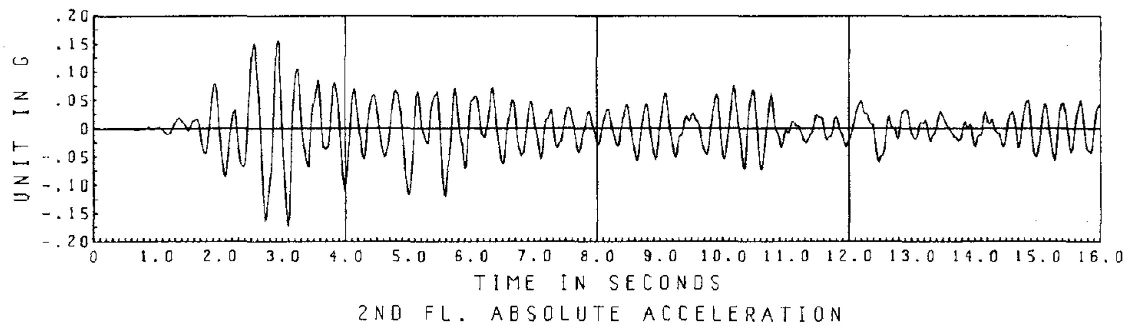

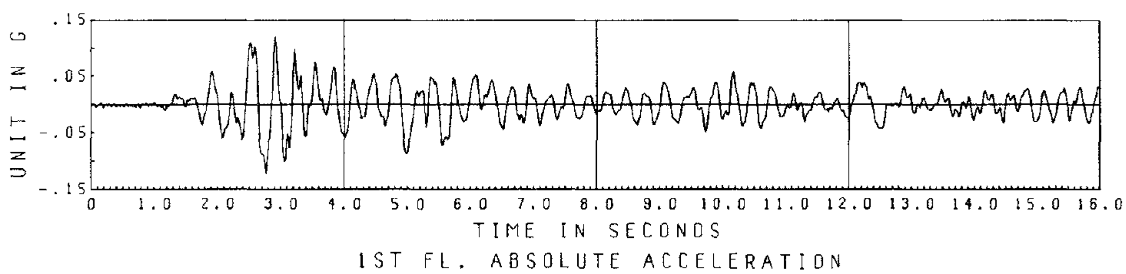

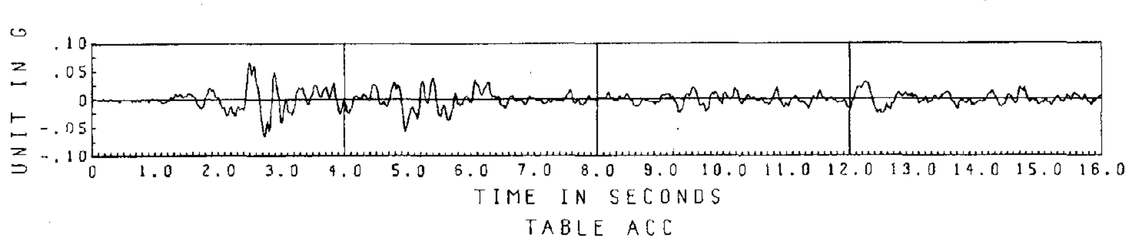

EL CENTRO SPAN 100

TEST RESULTS OF PIPE BRACING

Fig. 5.2a.1 Table and Floor Accelerations

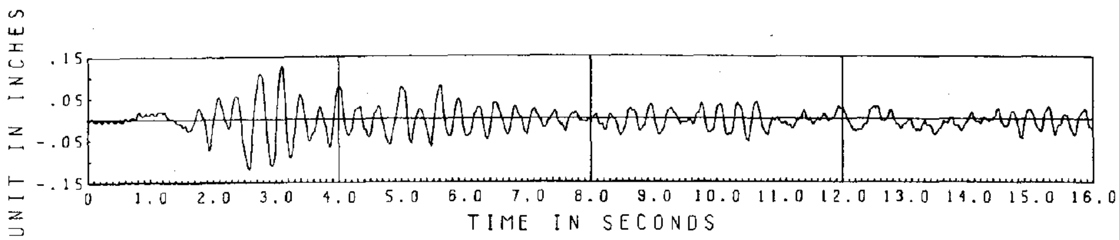

3RD FL. DISPLACEMENT REL. TO TABLE

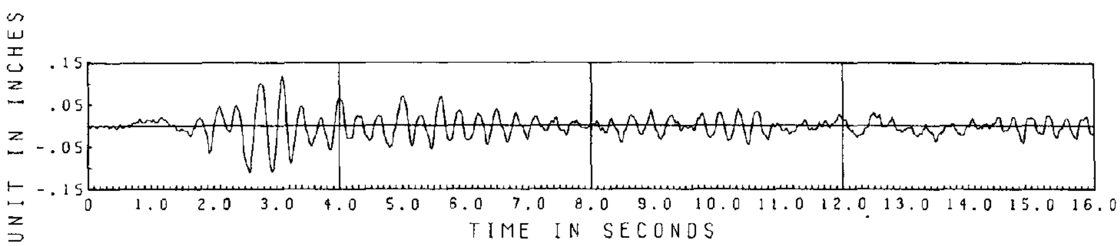

2ND FL. DISPLACEMENT REL. TO TABLE

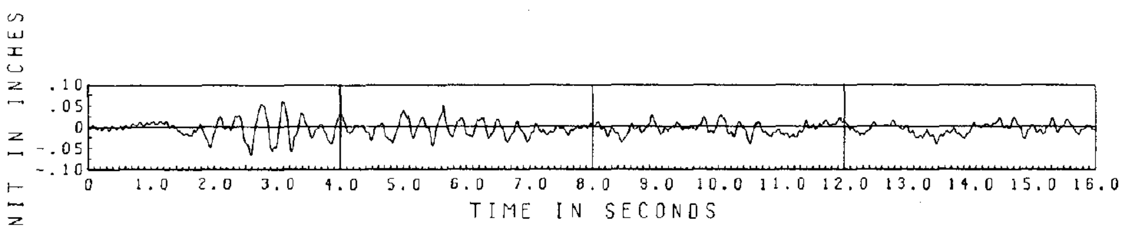

1ST FL. DISPLACEMENT REL. TO TABLE

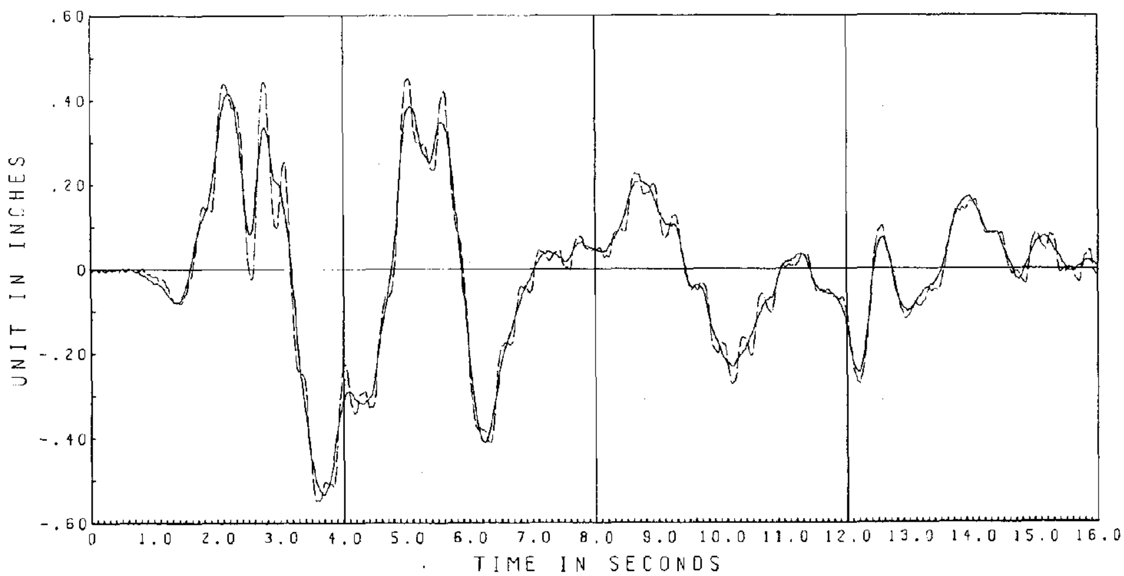

SOLID LINE=TABLE DISPL DASHED LINE=3RD FLOOR DISPL

EL CENTRO SPAN 100

TEST RESULTS OF PIPE BRACING

Fig. 5.2a.2 Table and Floor Displacements

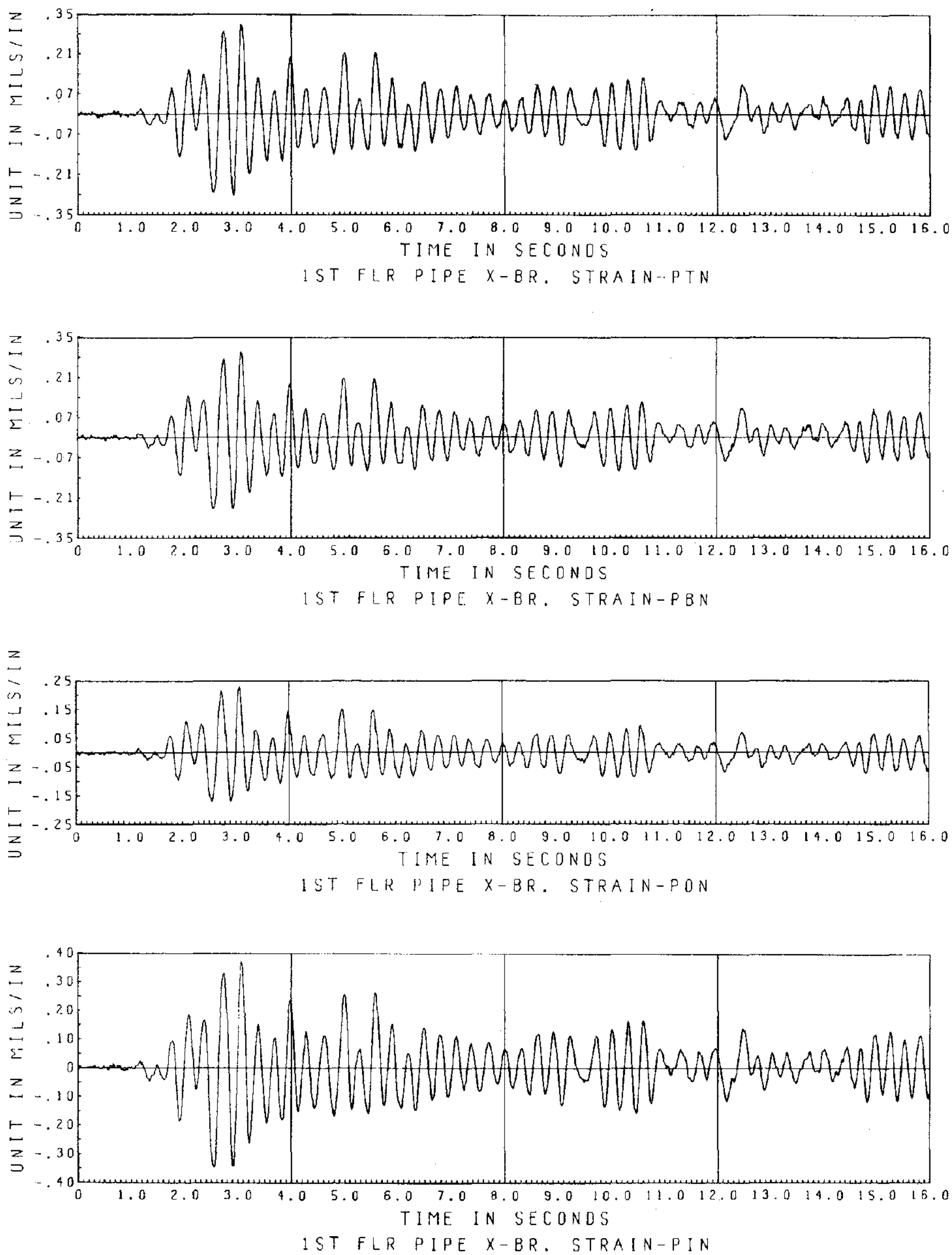

EL CENTRO SPAN 100

TEST RESULTS OF PIPE BRACING

Fig. 5.2a.3 Strain Time-Histories of the 1st Floor Pipe Braces

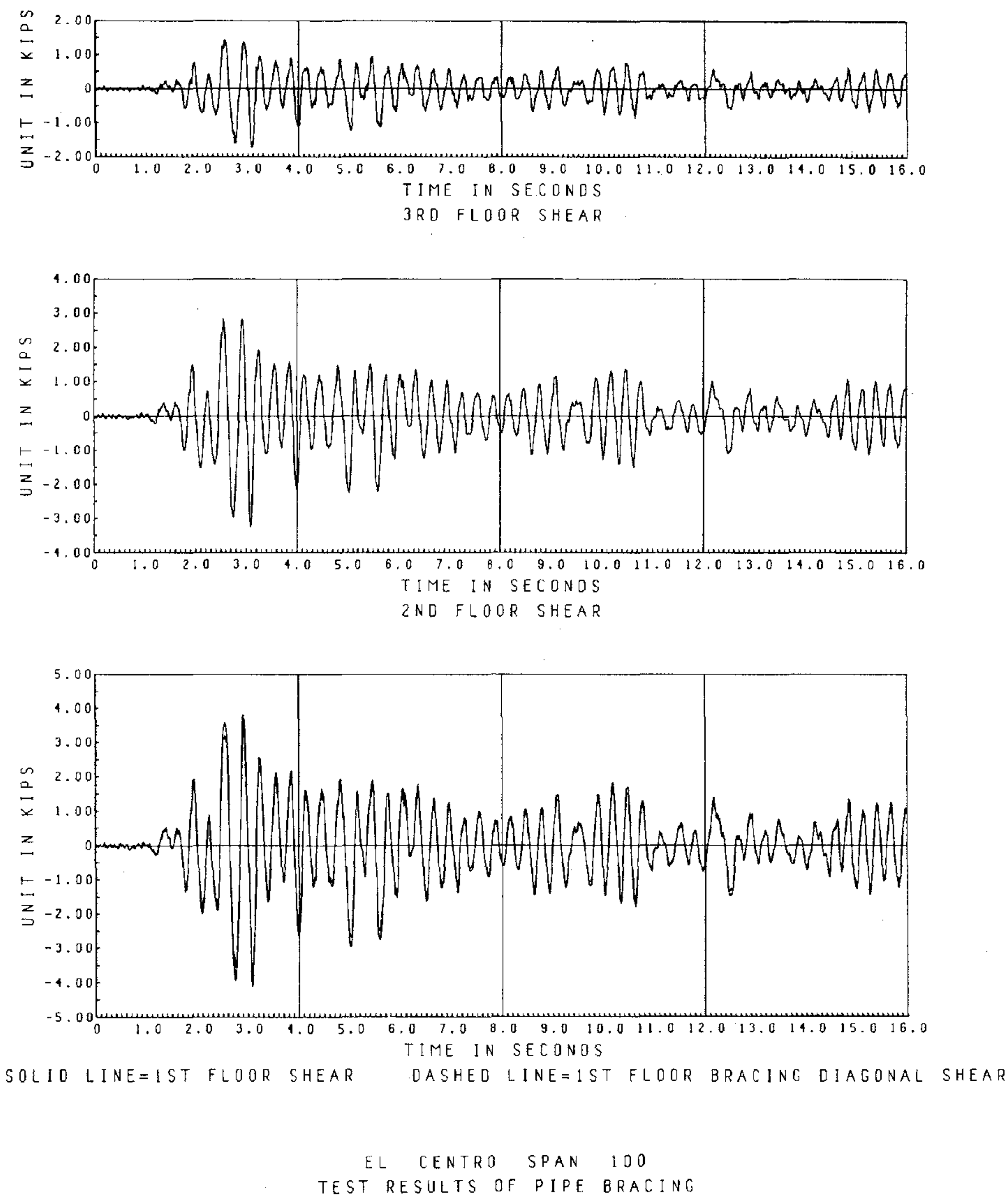

Fig. 5.2a.4 Floor Shear Forces

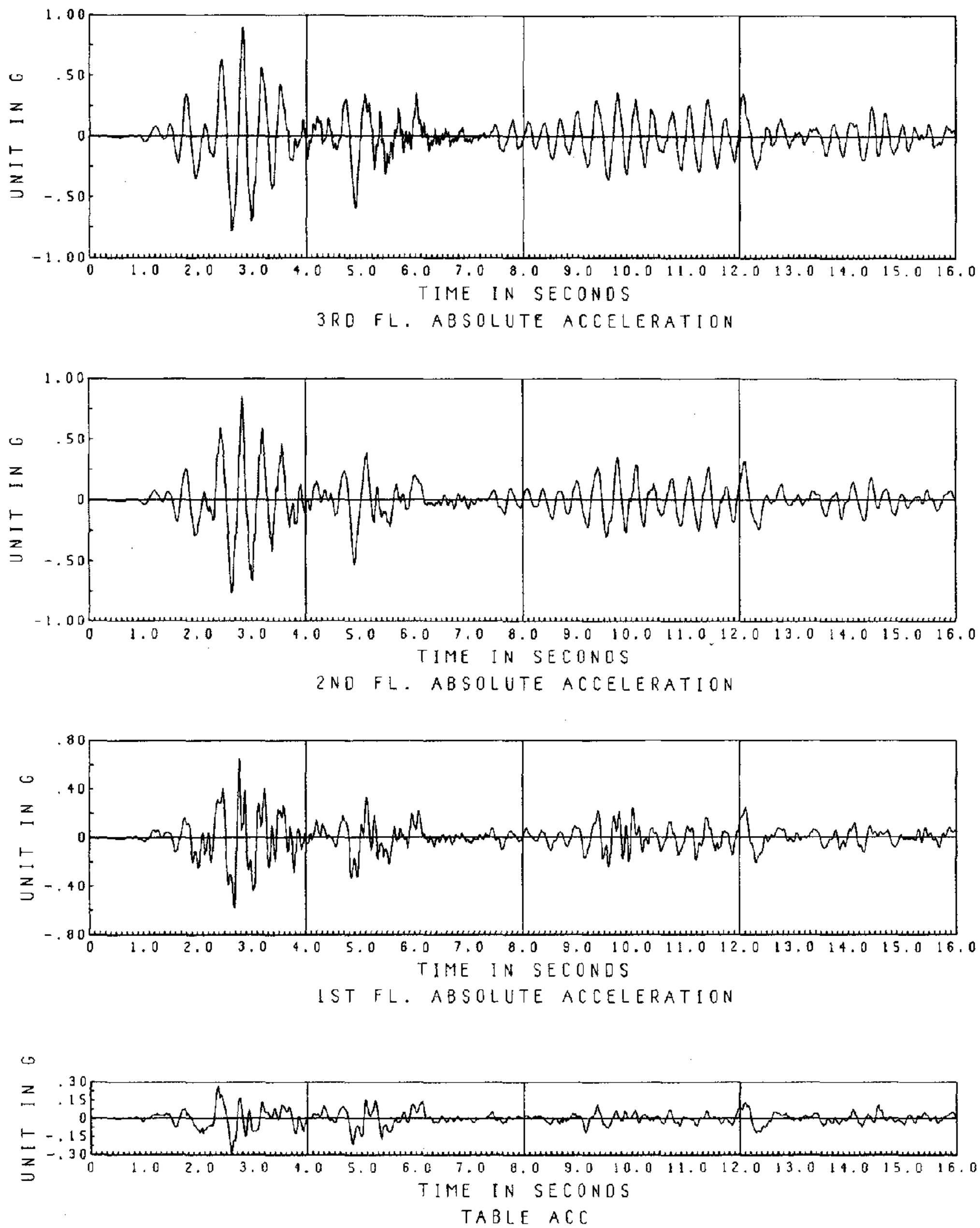

EL CENTRO SPAN 400
TEST RESULTS OF PIPE BRACING

Fig. 5.2b.1 Table and Floor Accelerations

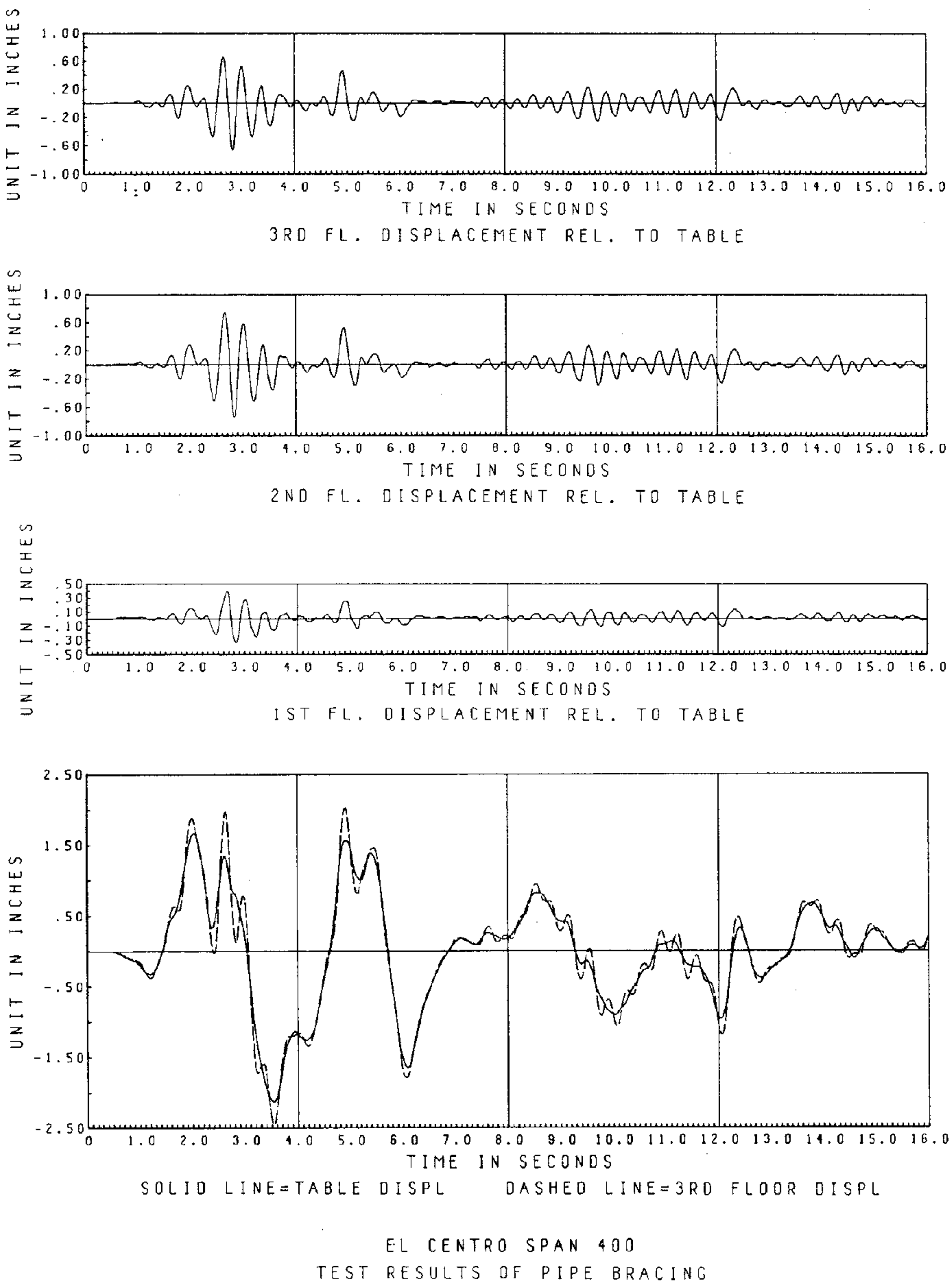

Fig. 5.2b.2 Table and Floor Displacements

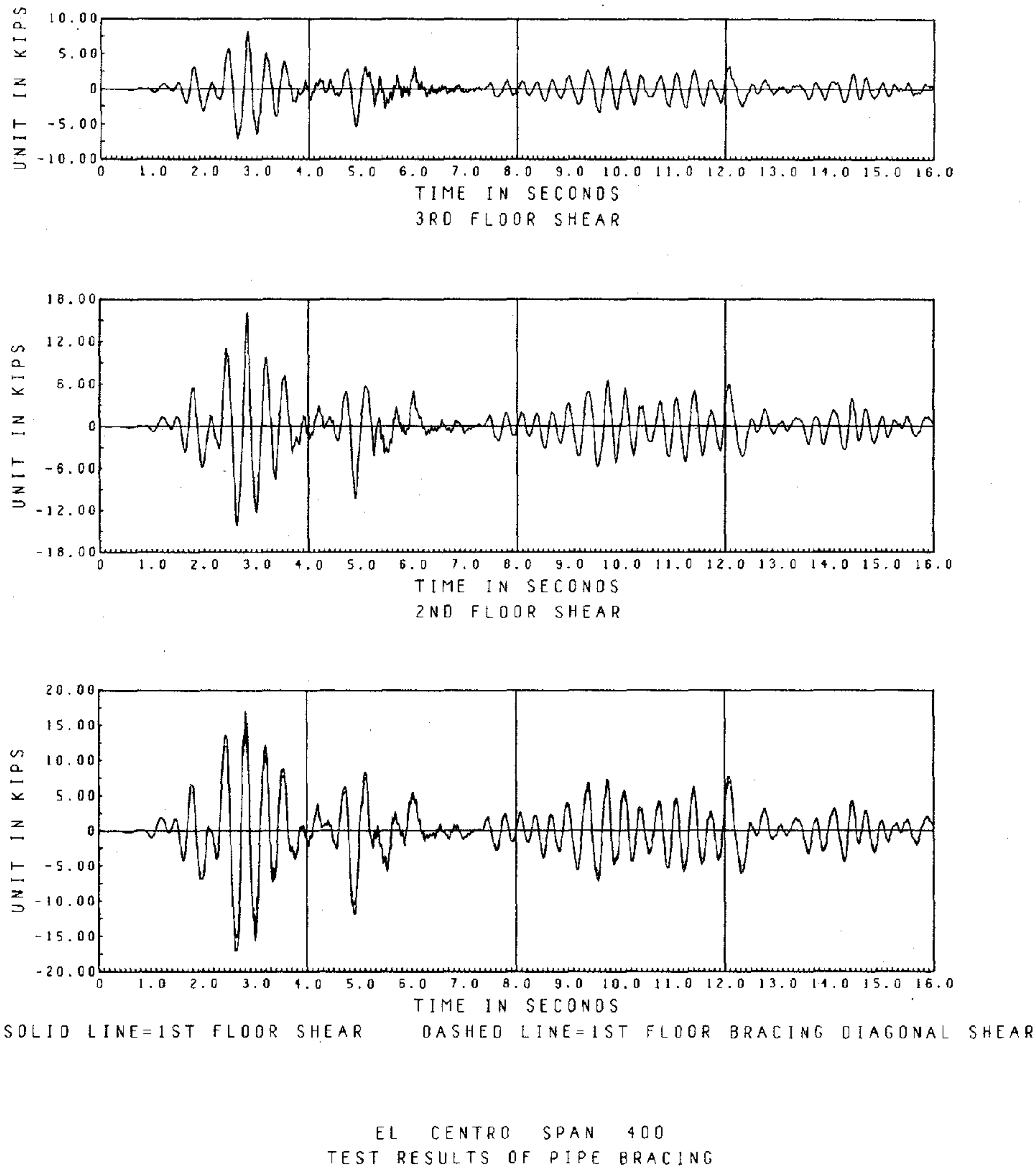

Fig. 5.2b.3 Floor Shear Forces

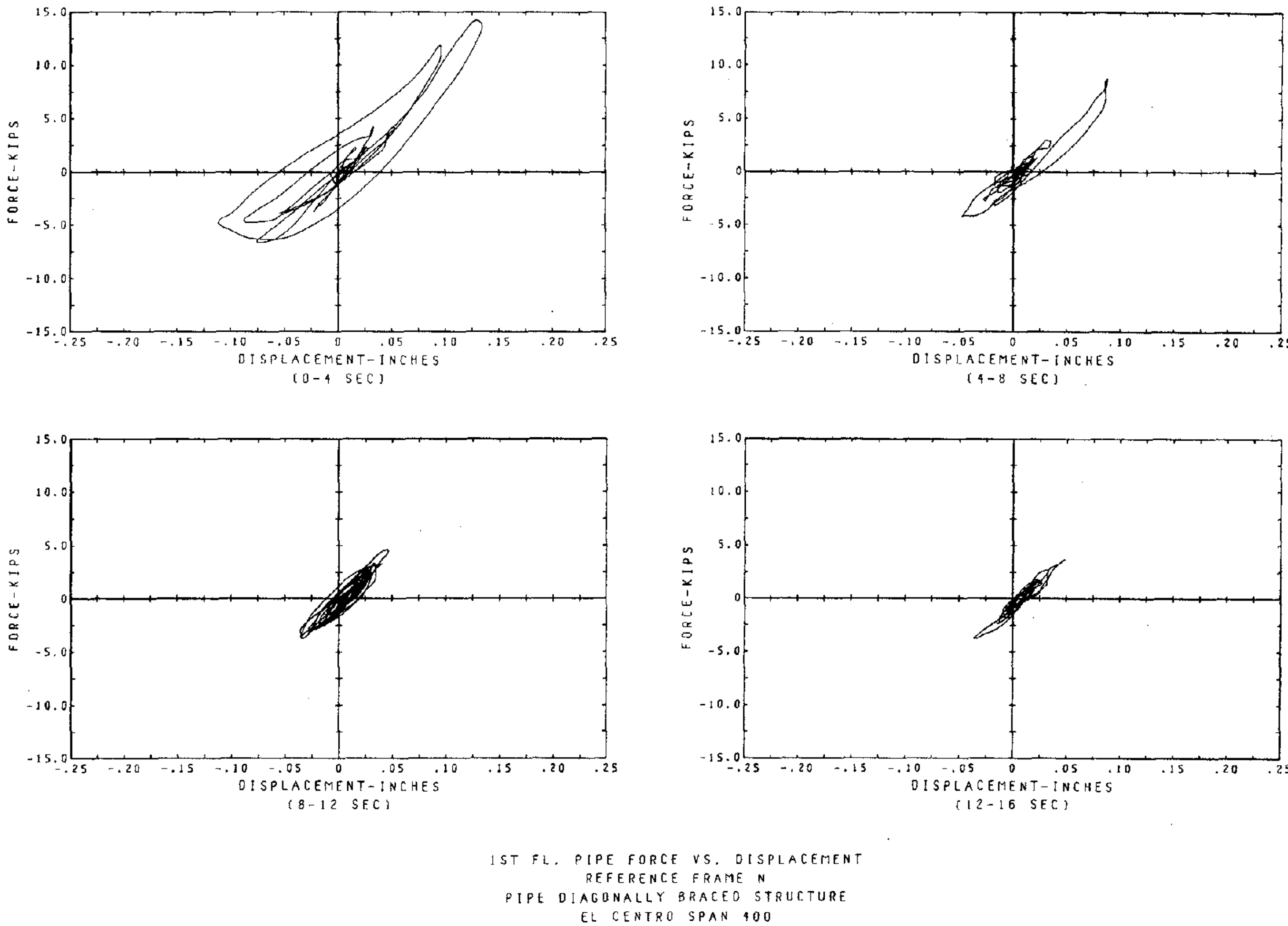

Fig. 5.2b.4 First Floor Pipe Force-Displacement Hysteresis Loops

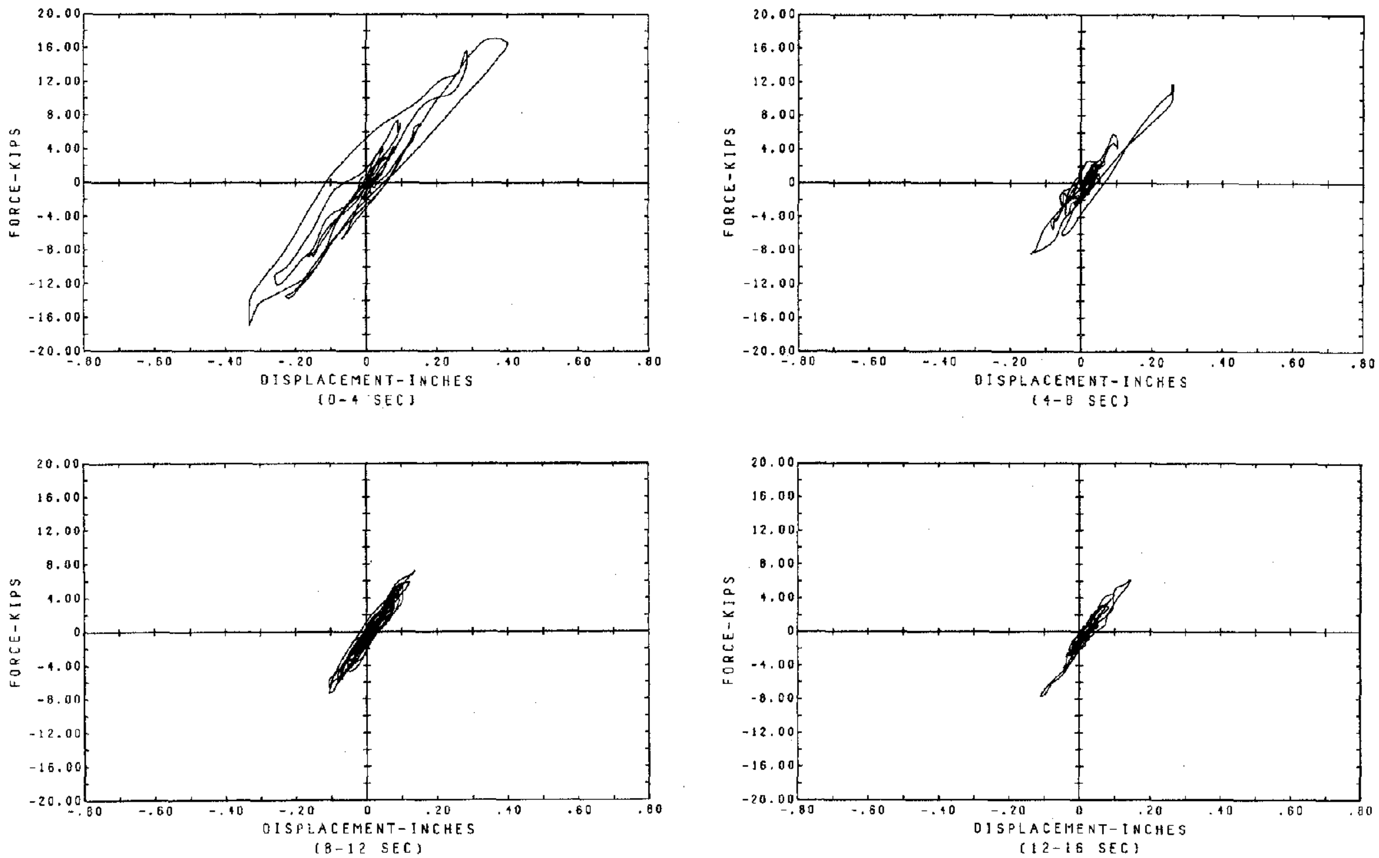

1ST FLR SHEAR VS. DISPLACEMENT
REFERENCE FRAME N
PIPE DIAGONALLY BRACED STRUCTURE
EL CENTRO SPAN 400

Fig. 5.2b.5 First Floor Shear-Displacement Hysteresis Loops

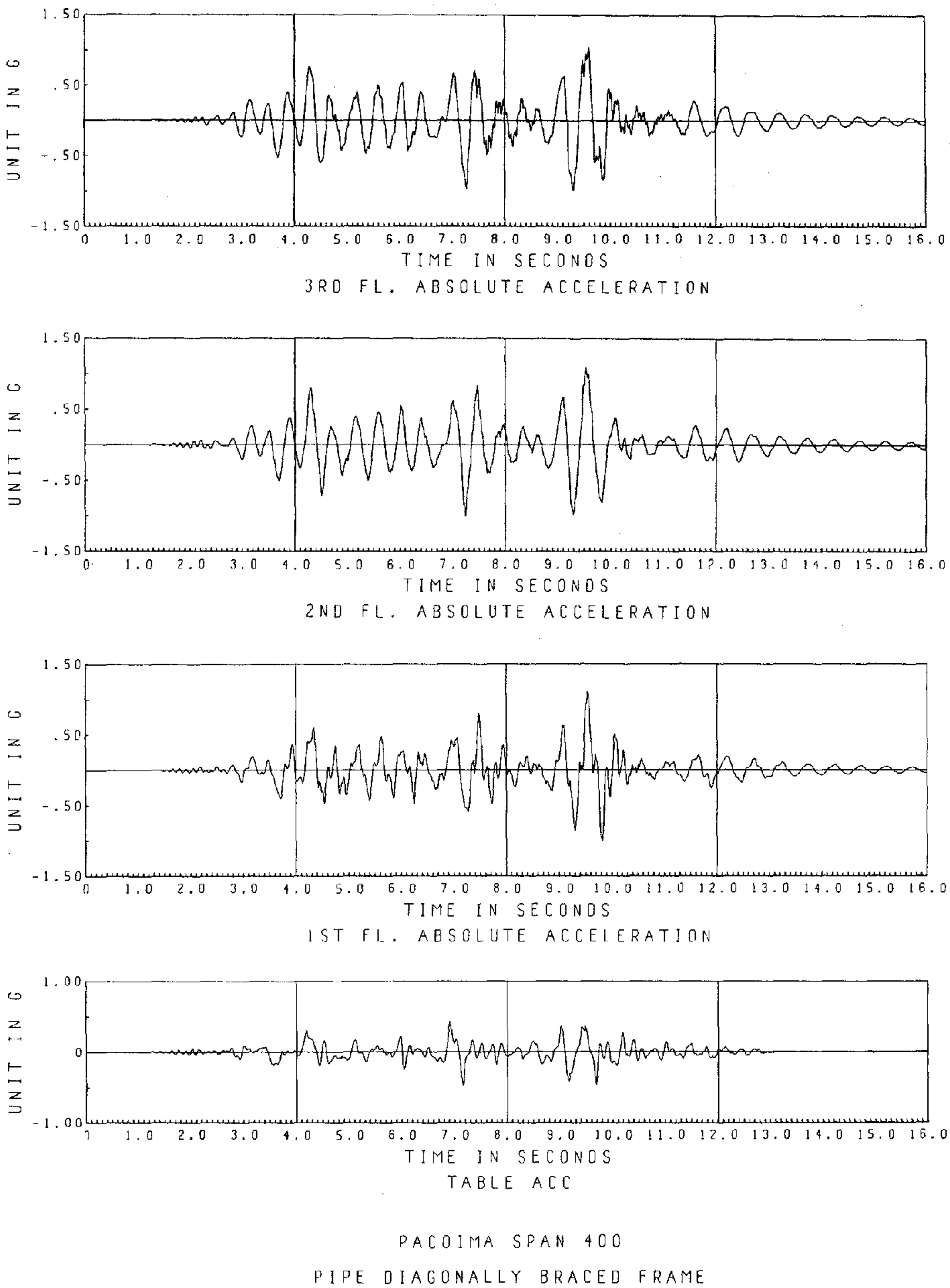

Fig. 5.2c.1 Table and Floor Accelerations

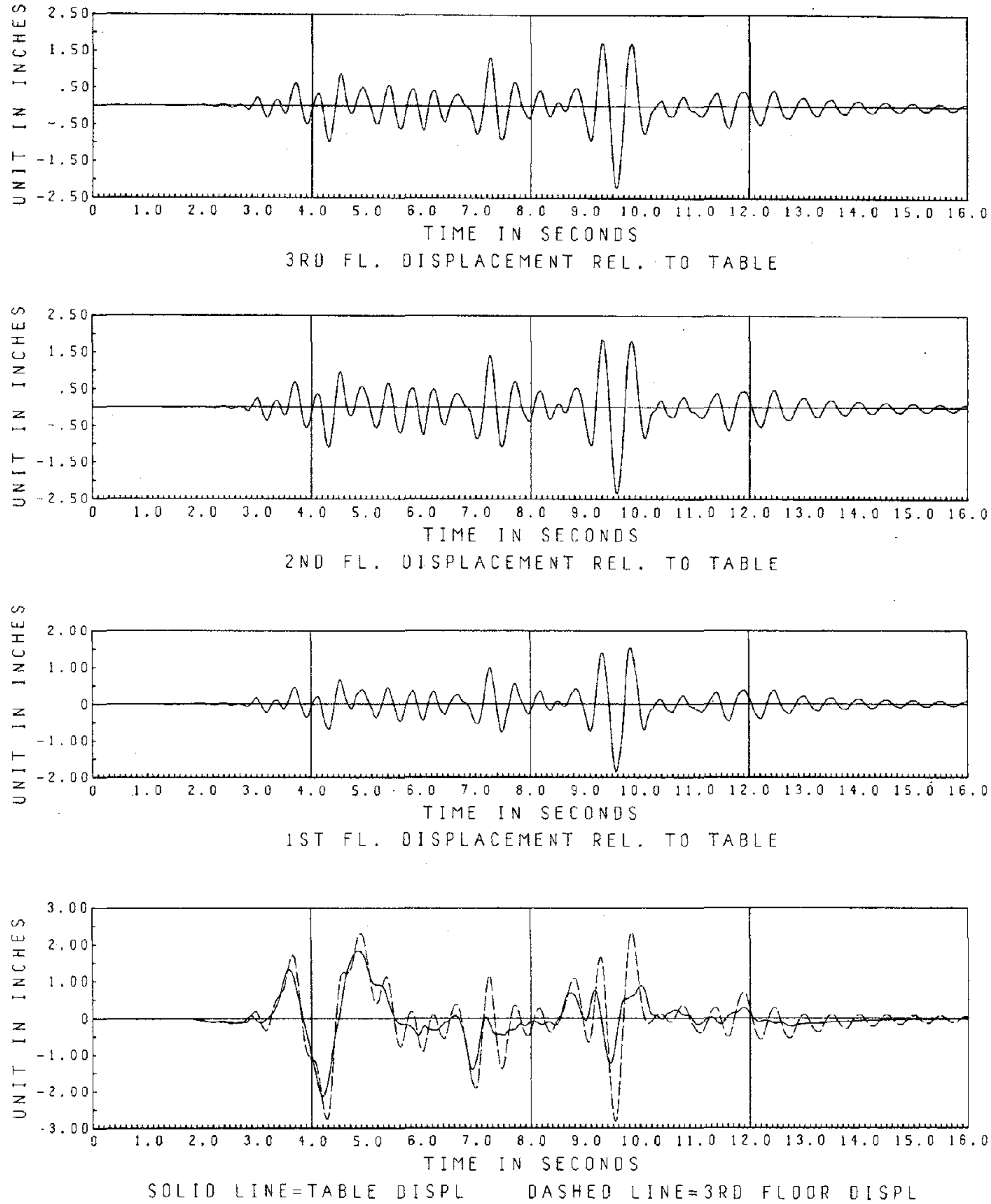

PACOIMA SPAN 400
TEST RESULTS OF PIPE BRACING

Fig. 5.2c.2 Table and Floor Displacements

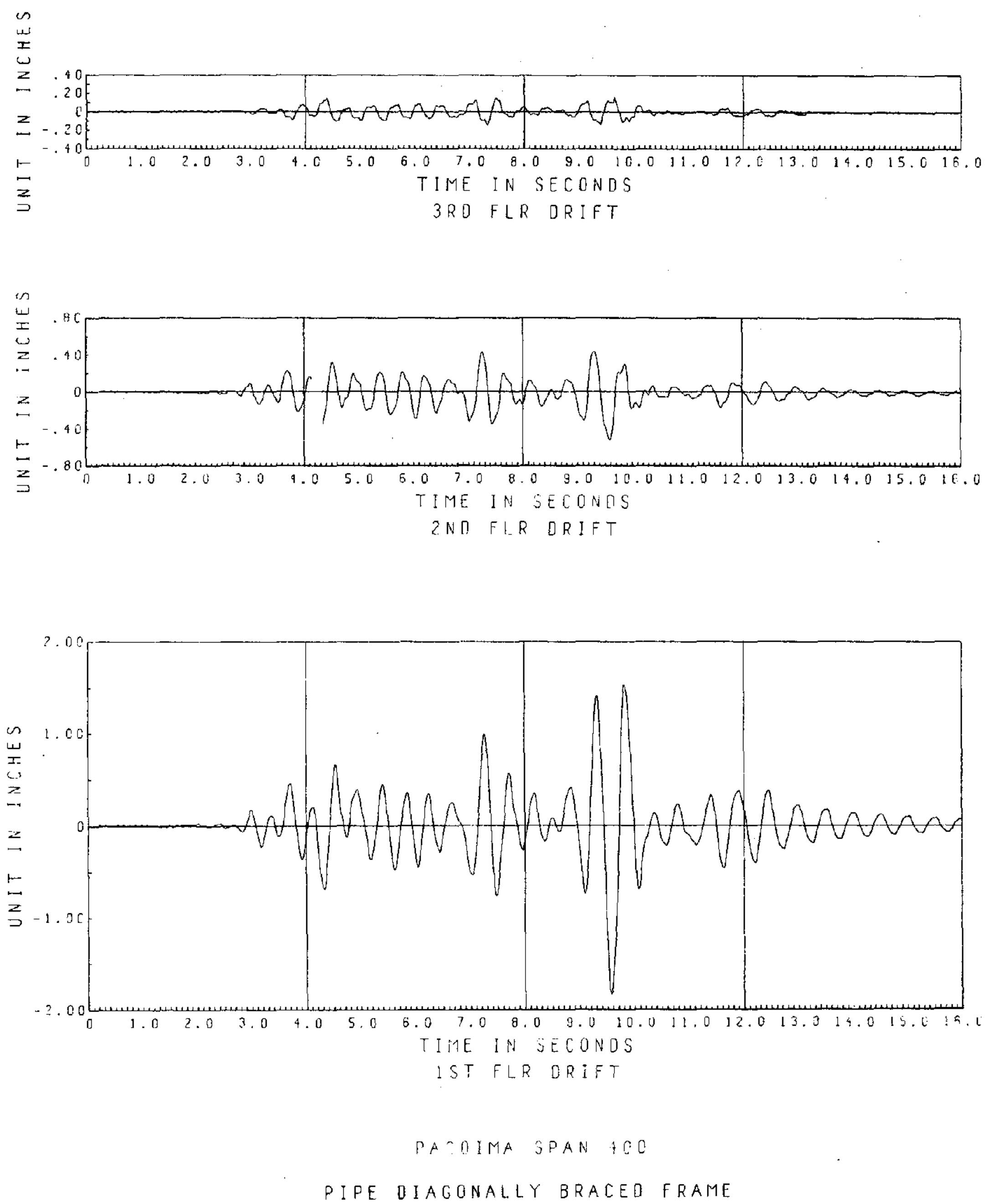

Fig. 5.2c.3 Floor Drifts

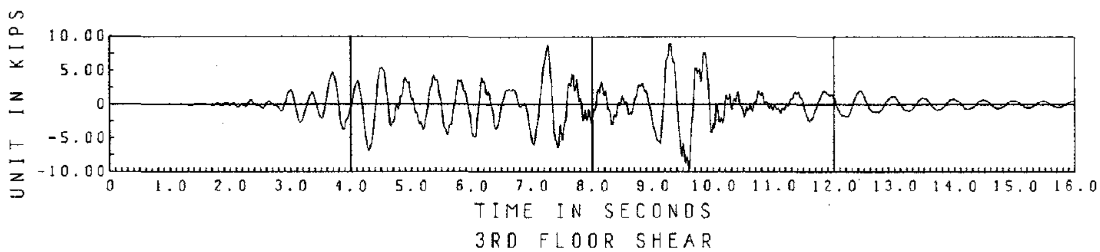

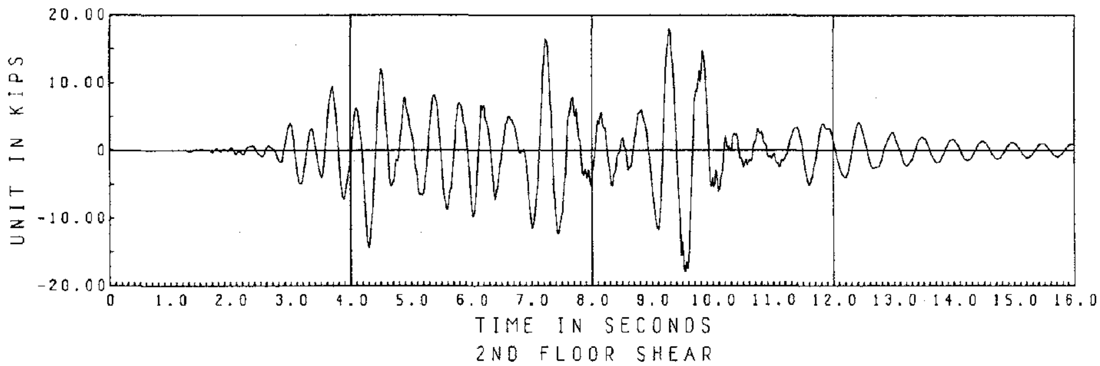

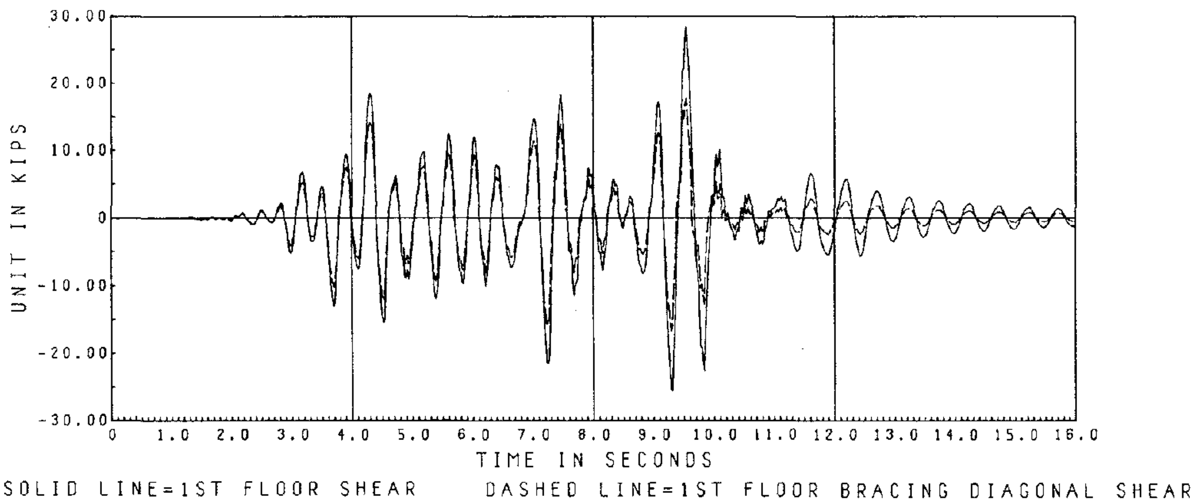

PACOIMA SPAN 400

PIPE DIAGONALLY BRACED FRAME

Fig. 5.2c.4 Floor Shear Forces

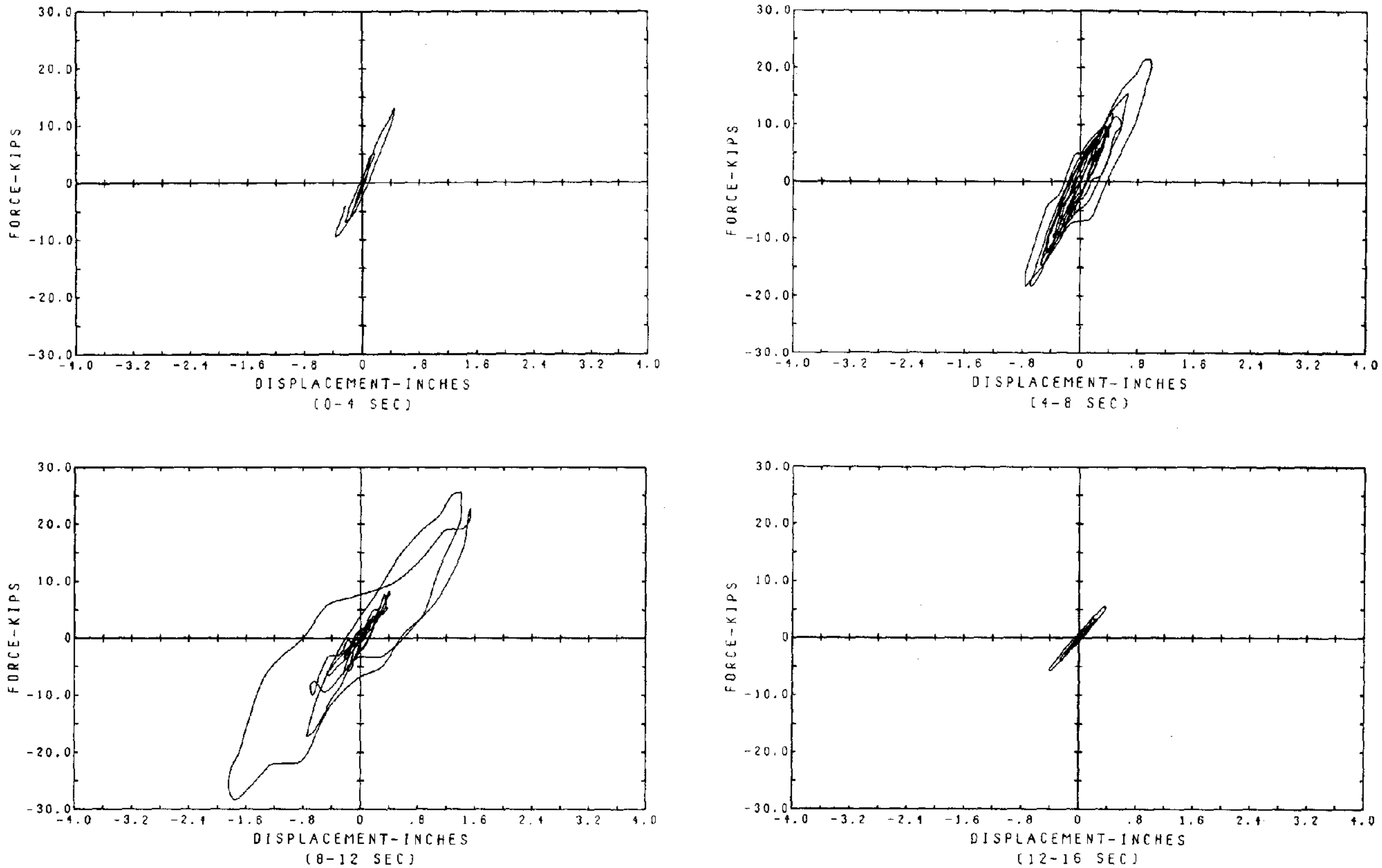

1ST FLR SHEAR VS. DISPLACEMENT
PIPE DIAGONALLY BRACED STRUCTURE
PACOIMA SPAN 400

Fig. 5.2c.5 First Floor Shear-Displacement Hysteresis Loops

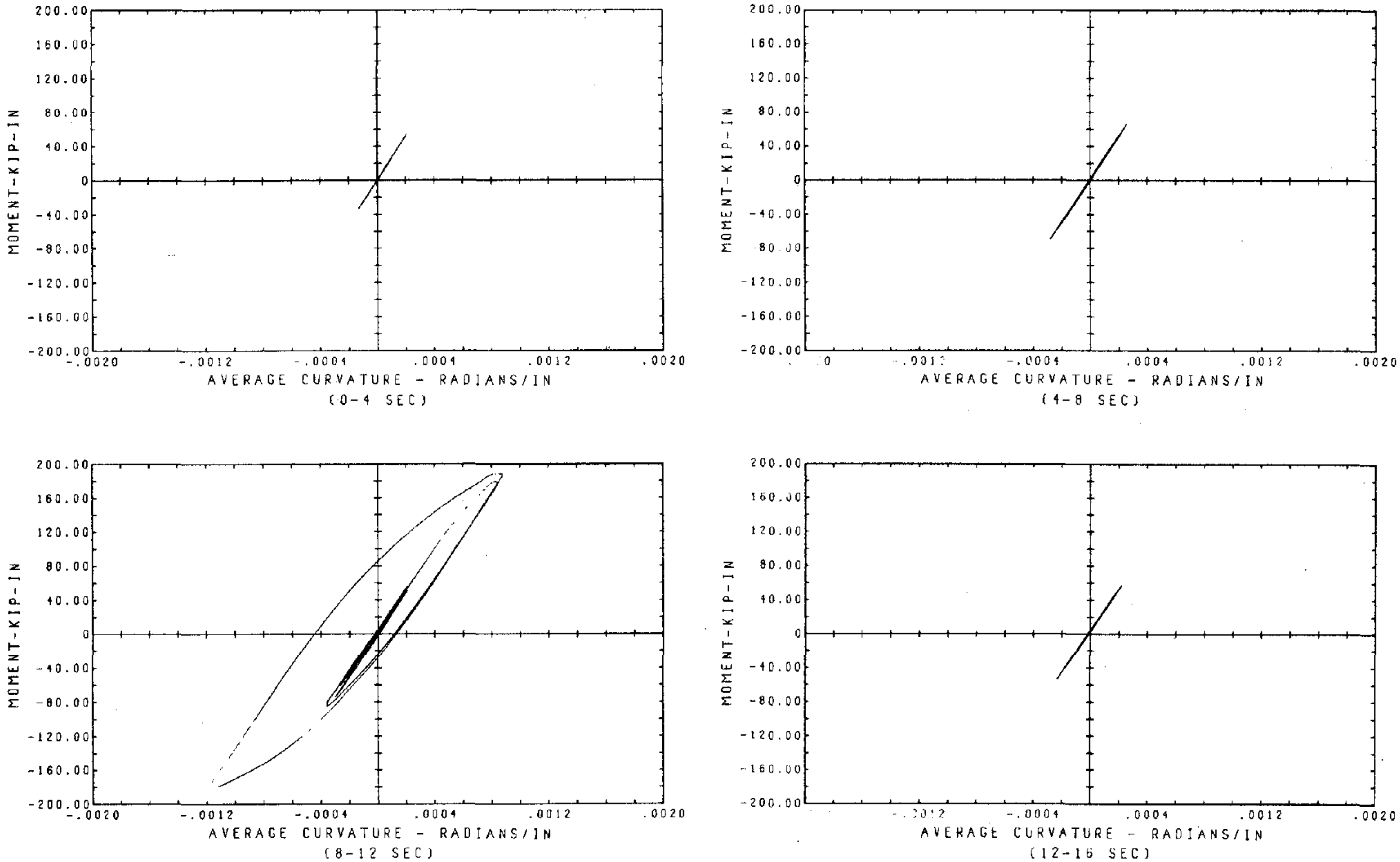

1ST FLR COL BOTTOM END , MOMENT VS. CURVATURE
REFERENCE COLUMN LINE NA
PIPE DIAGONALLY BRACED STRUCTURE
PACOIMA SPAN 400

Fig. 5.2c.6 First Floor Column Moment-Curvature Hysteresis Loops

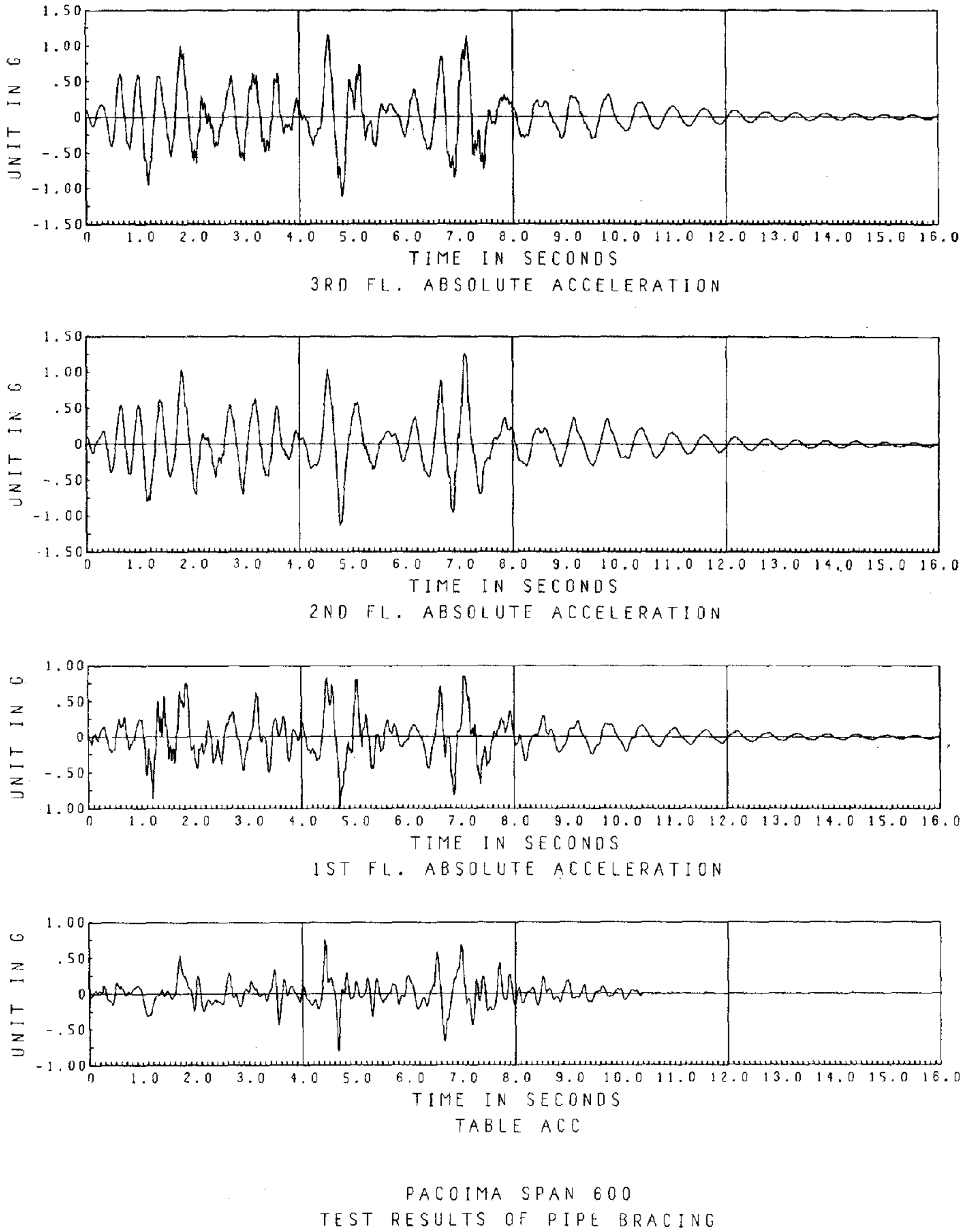

Fig. 5.2d.1 Table and Floor Accelerations

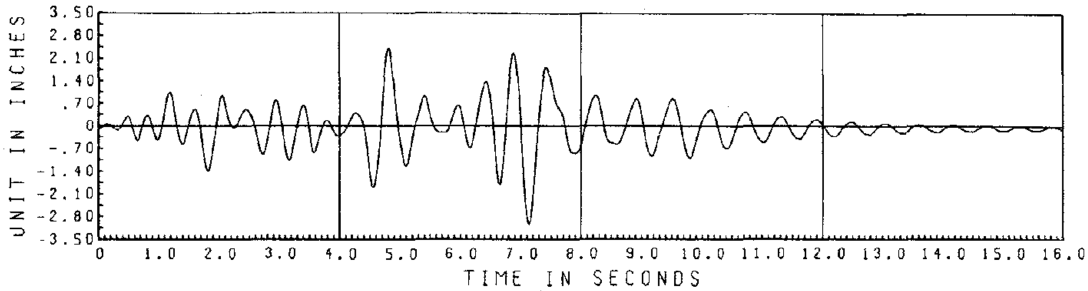

3RD FL. DISPLACEMENT REL. TO TABLE

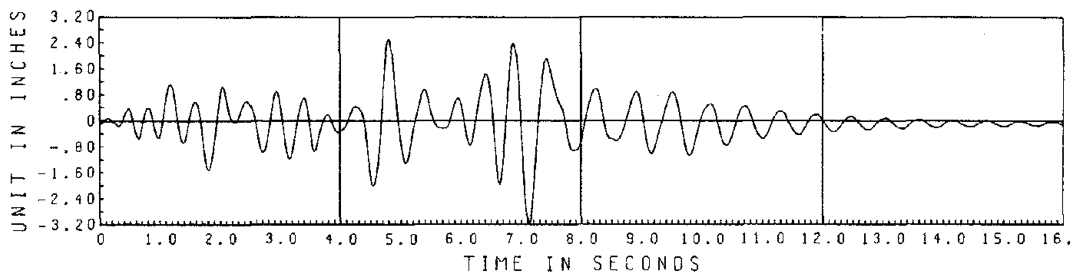

2ND FL. DISPLACEMENT REL. TO TABLE

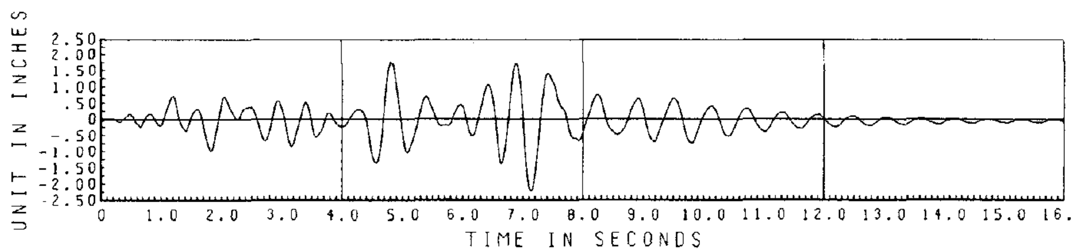

1ST FL. DISPLACEMENT REL. TO TABLE

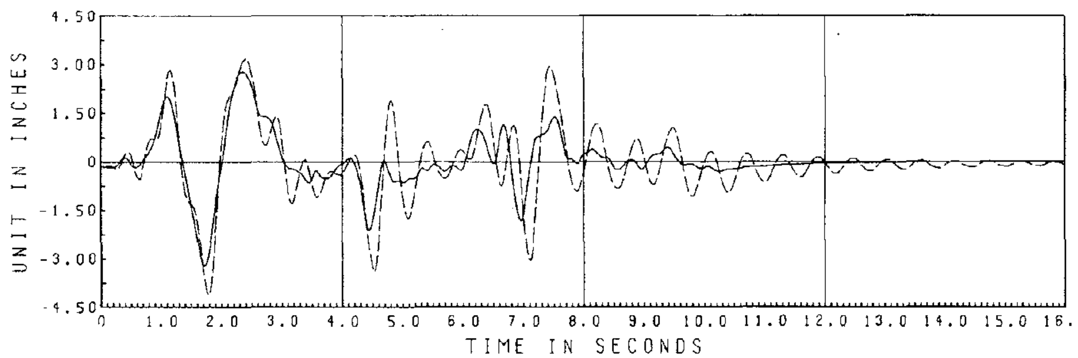

SOLID LINE=TABLE DISPL   DASHED LINE=3RD FLOOR DISPL

PACOIMA SPAN 600
TEST RESULTS OF PIPE BRACING

Fig. 5.2d.2 Table and Floor Displacements

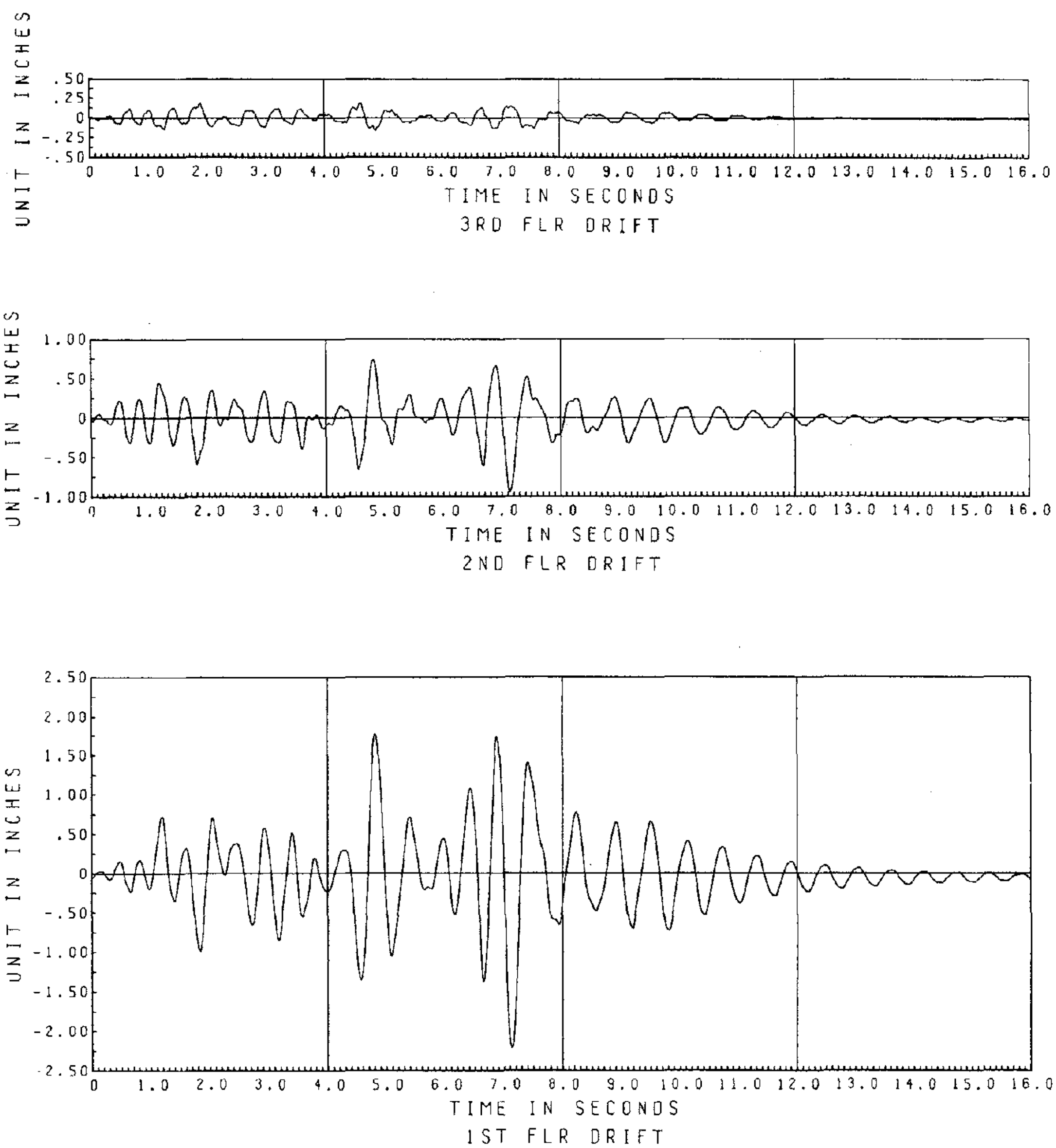

PACOIMA SPAN 600
TEST RESULTS OF PIPE BRACING

Fig. 5.2d.3 Floor Drifts

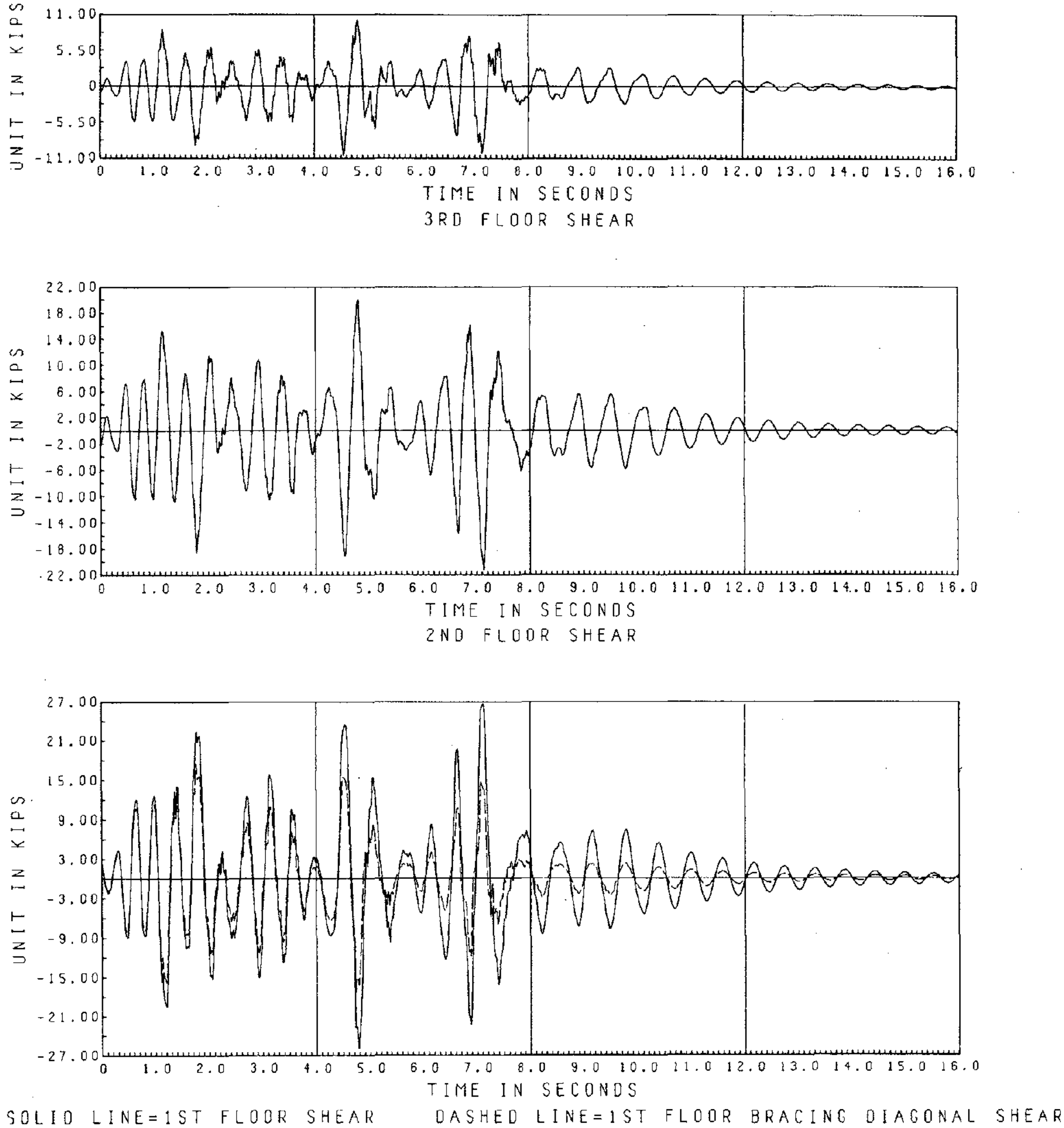

PACOIMA SPAN 600

TEST RESULTS OF PIPE BRACING

Fig. 5.2d.4 Floor Shear Forces

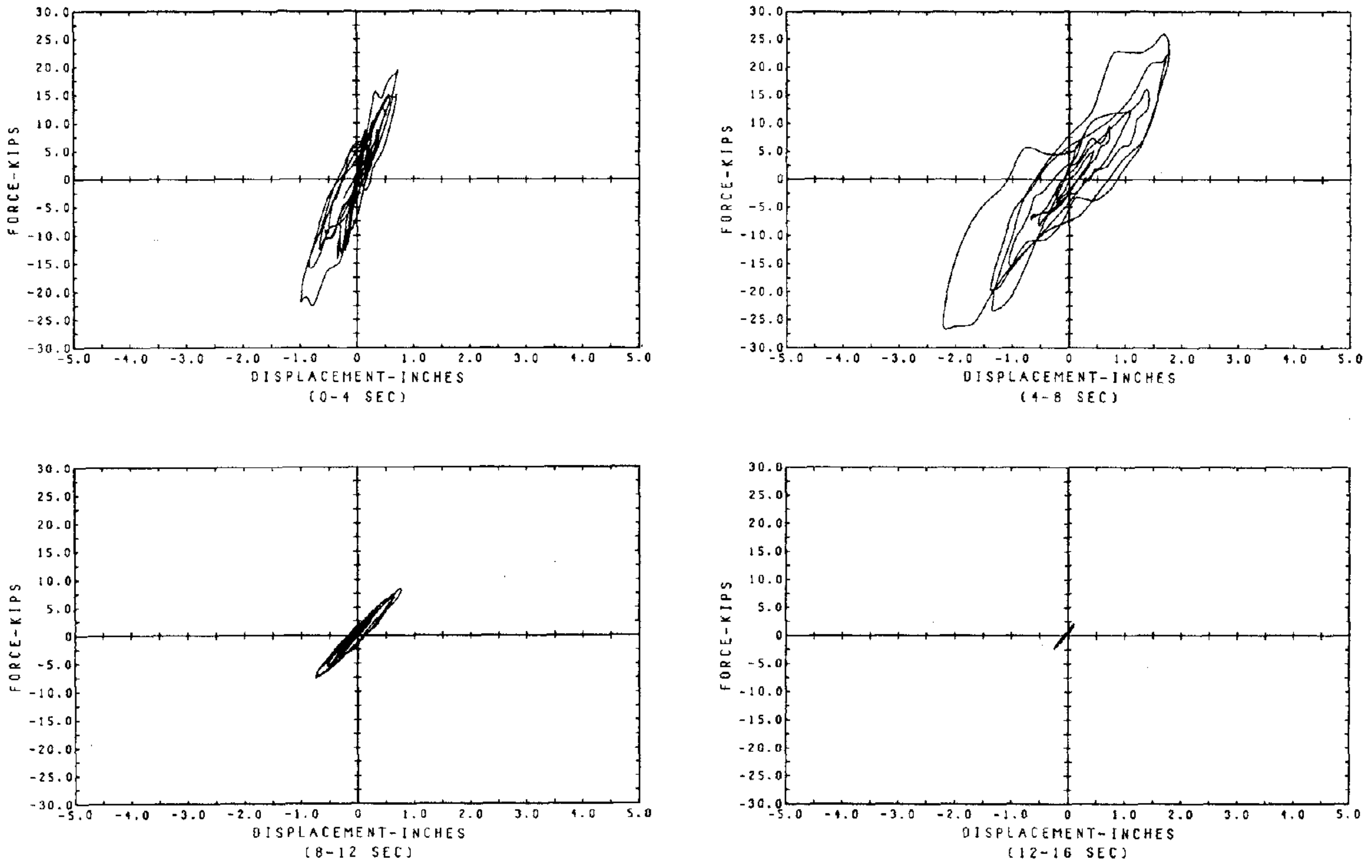

1ST FLR SHEAR VS. DISPLACEMENT
REFERENCE FRAME N
PIPE DIAGONALLY BRACED STRUCTURE
PACOIMA SPAN 600

Fig. 5.2d.5 First Floor Shear-Displacement Hysteresis Loops

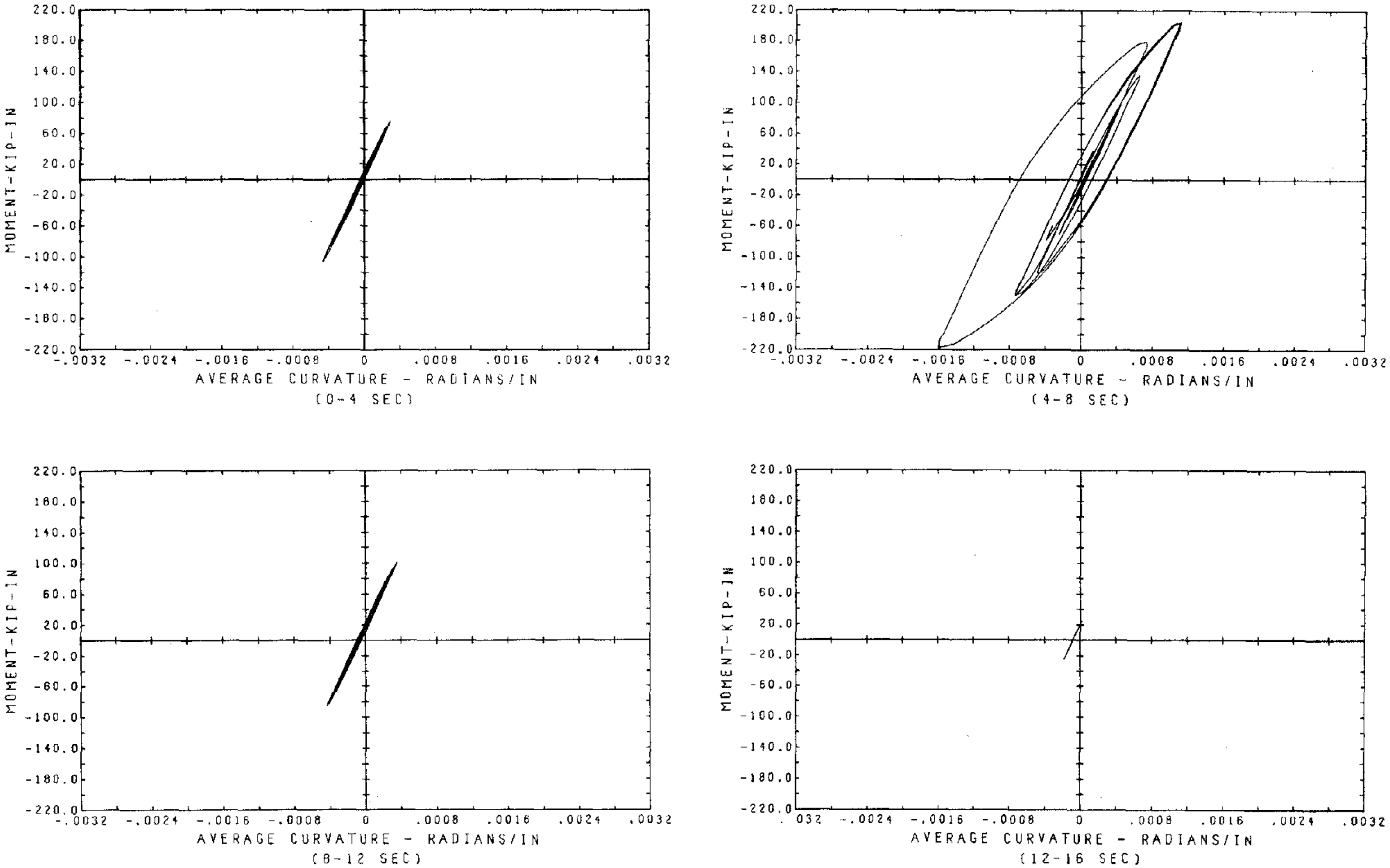

1ST FLR COL BOTTOM END , MOMENT VS. CURVATURE
REFERENCE COLUMN LINE NA
PIPE DIAGONALLY BRACED STRUCTURE
PACOIMA SPAN 600

Fig. 5.2d.6 First Floor Column Moment-Curvature Hysteresis Loops

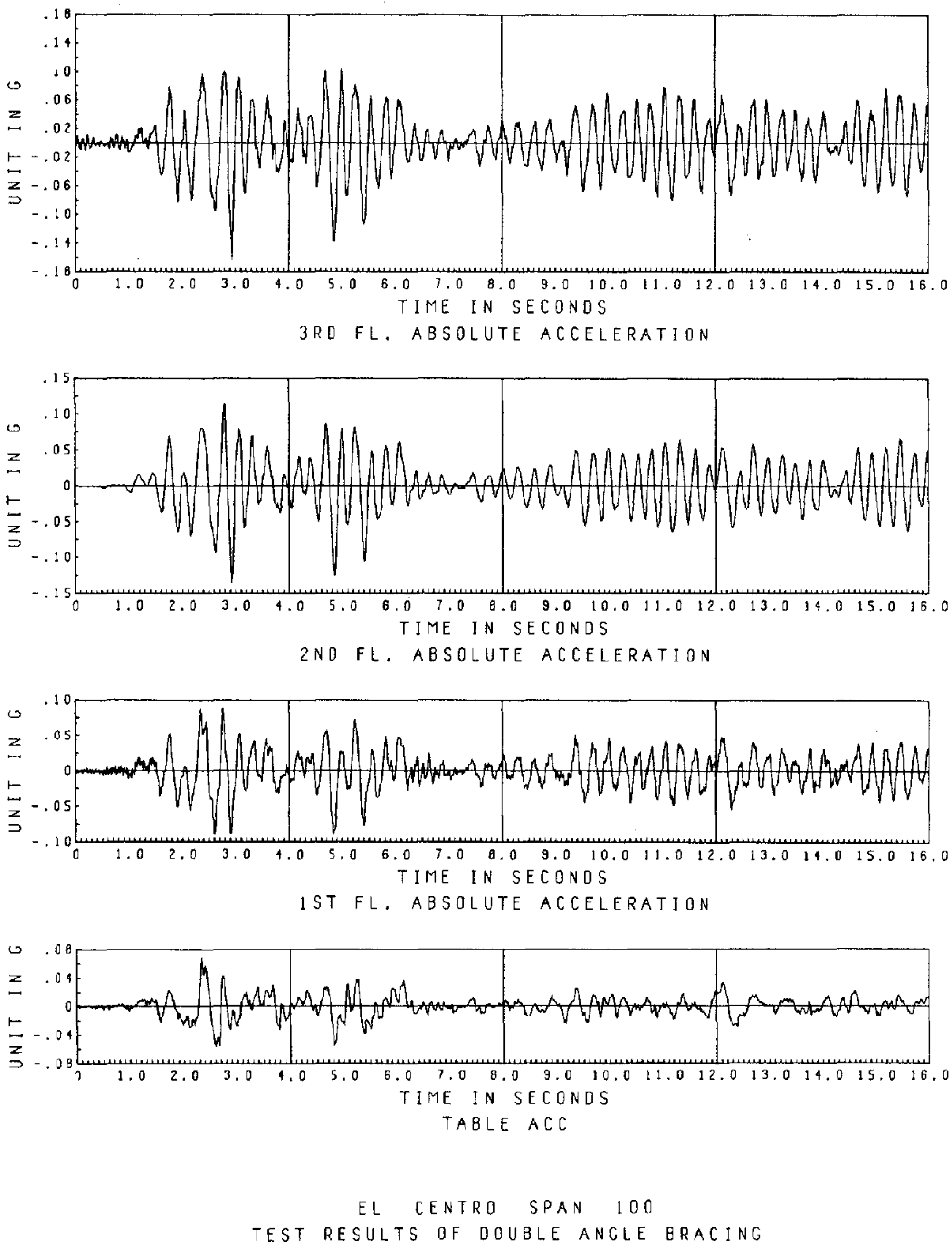

Fig. 5.3a.1 Table and Floor Accelerations

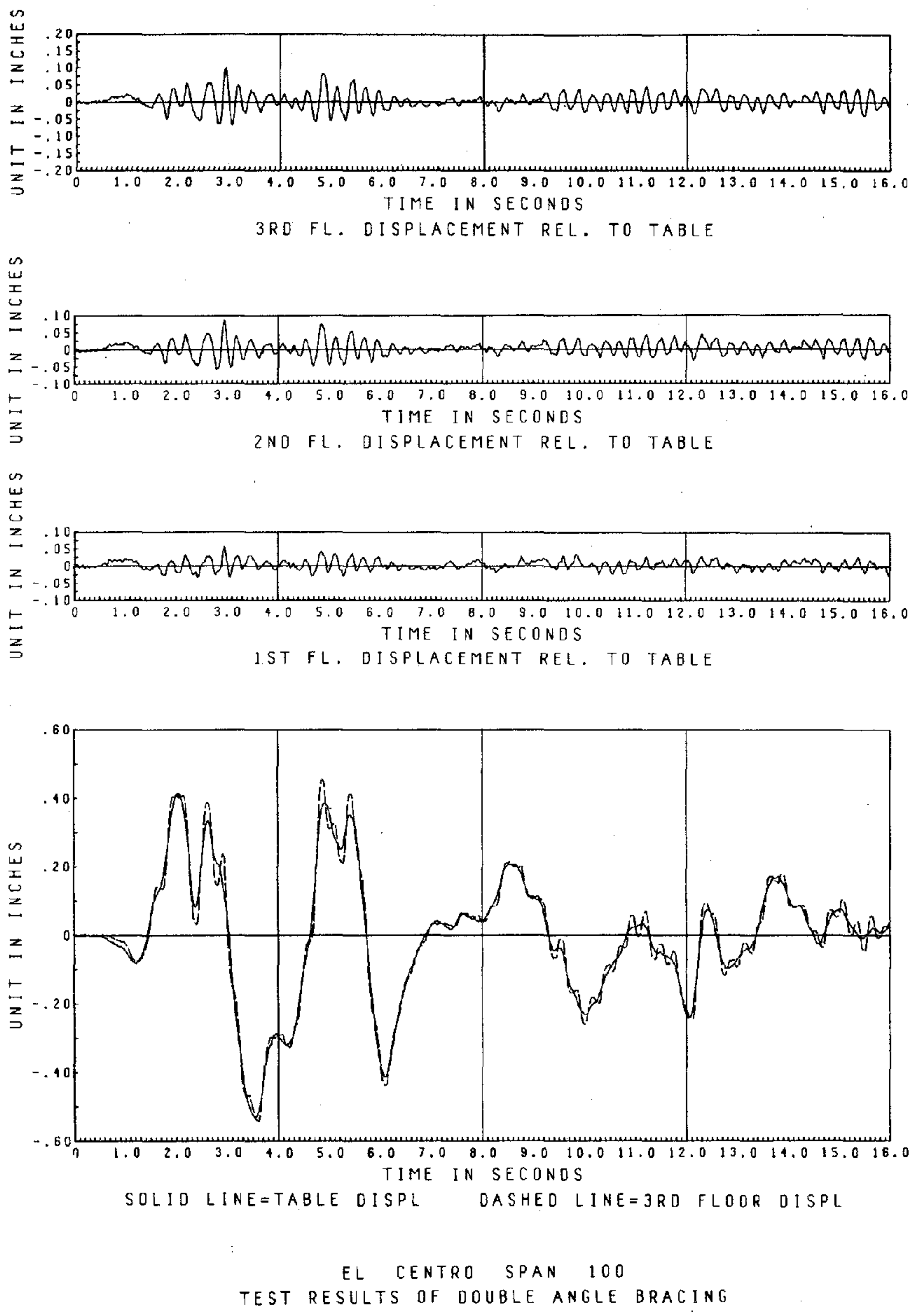

Fig. 5.3a.2 Table and Floor Displacements

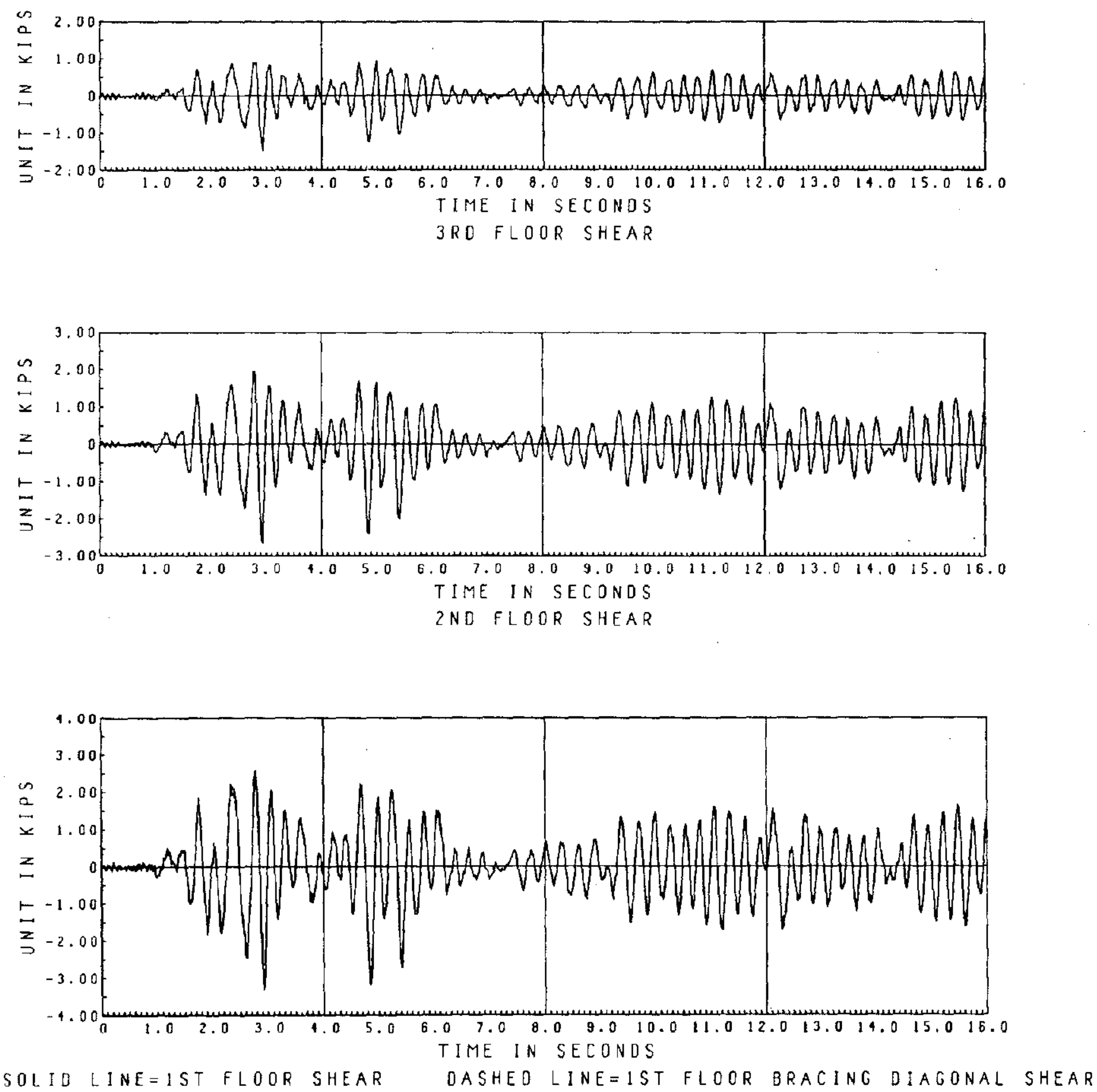

EL CENTRO SPAN 100
TEST RESULTS OF DOUBLE ANGLE BRACING

Fig. 5.3a.3 Floor Shear Forces

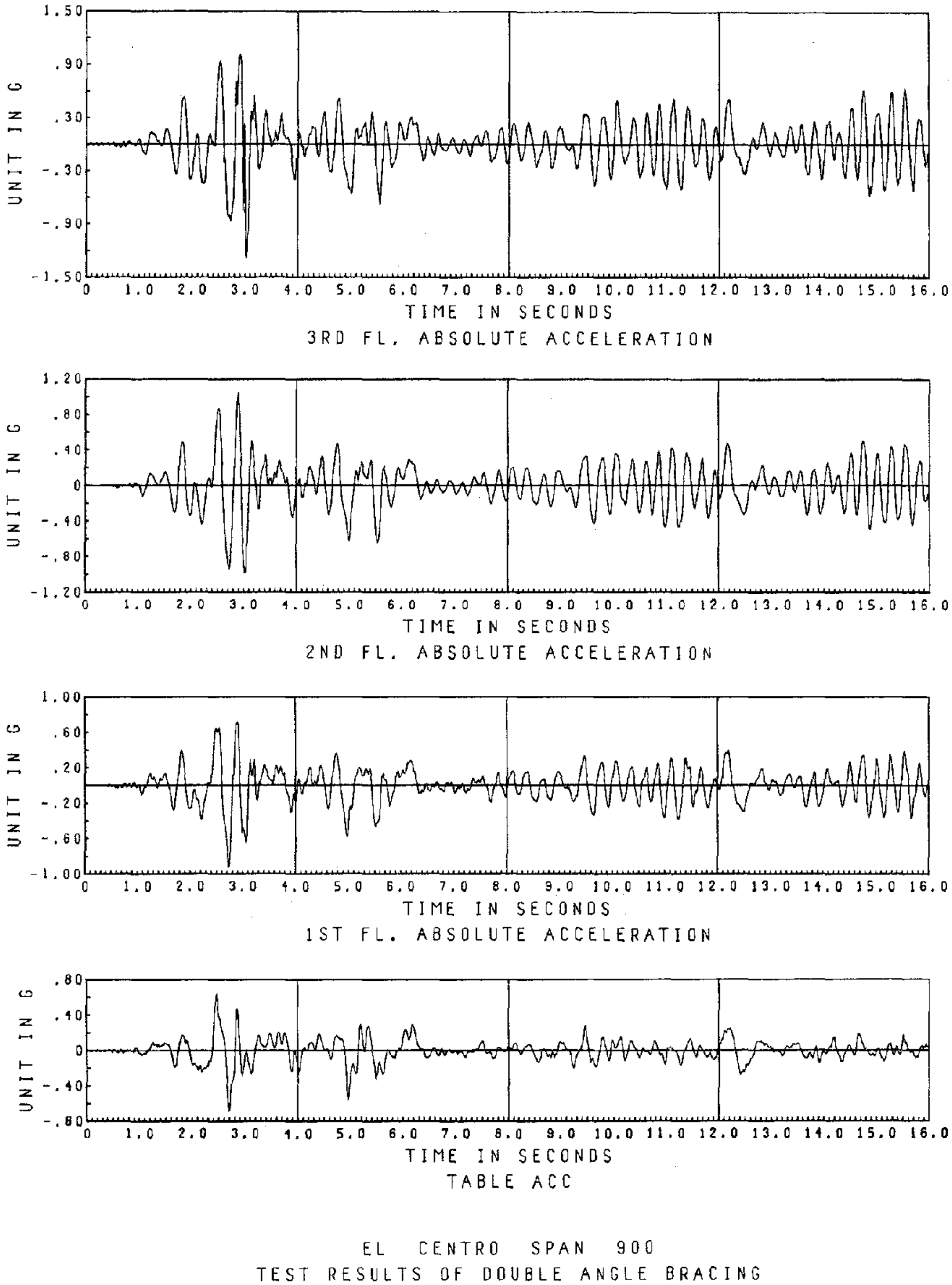

Fig. 5.3b.1 Table and Floor Accelerations

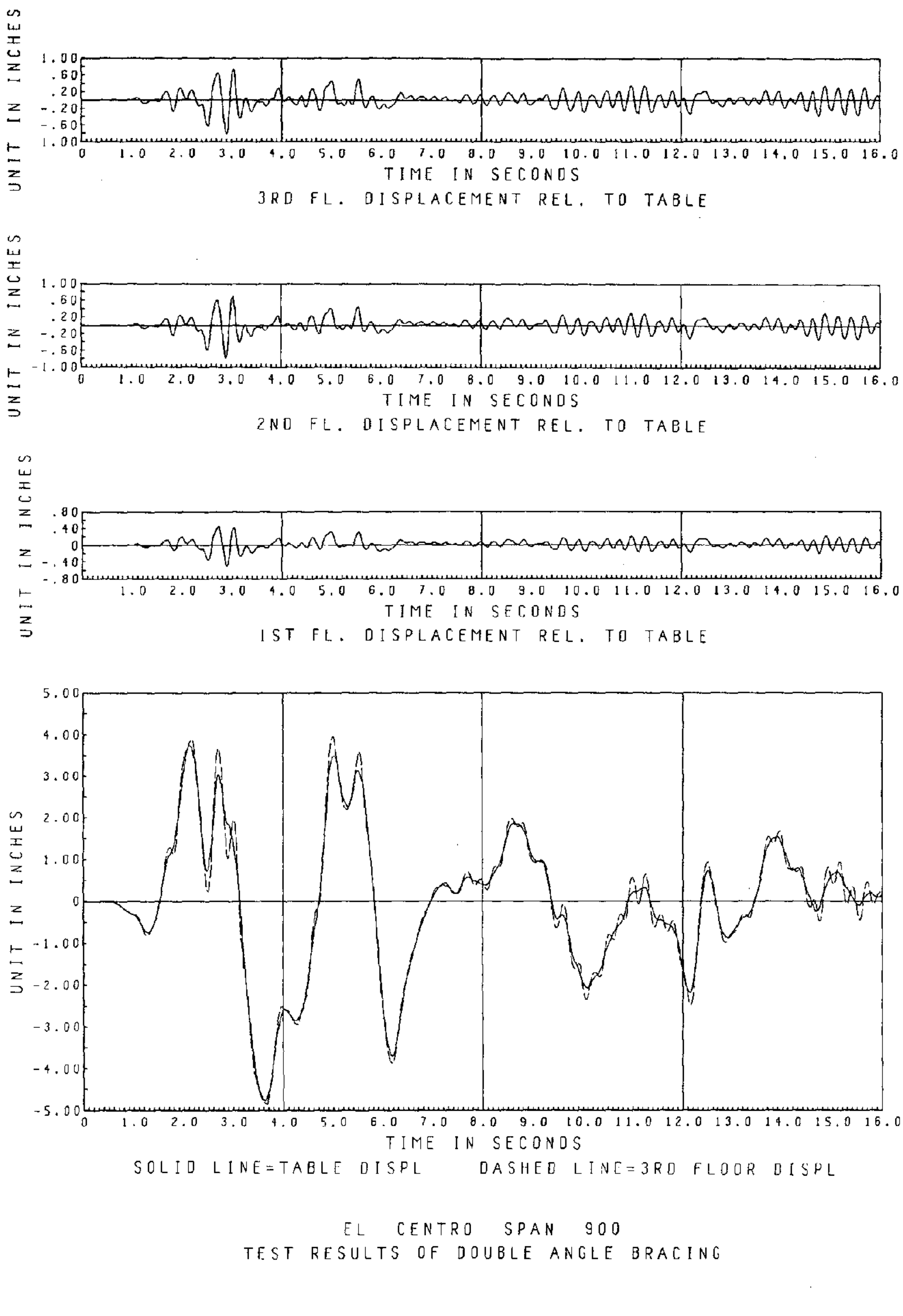

Fig. 5.3b.2 Table and Floor Displacements

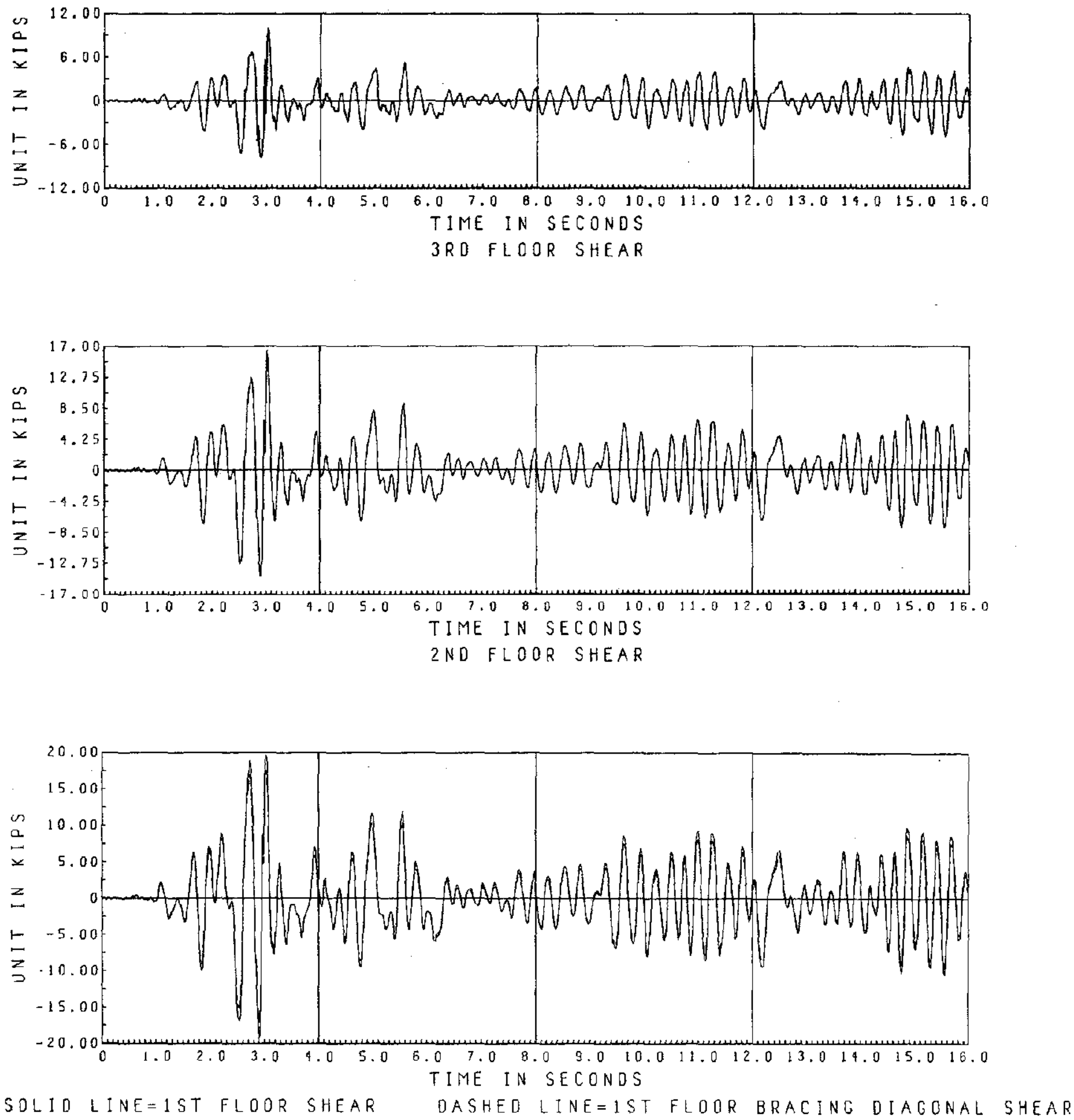

EL CENTRO SPAN 900
TEST RESULTS OF DOUBLE ANGLE BRACING

Fig. 5.3b.3 Floor Shear Forces

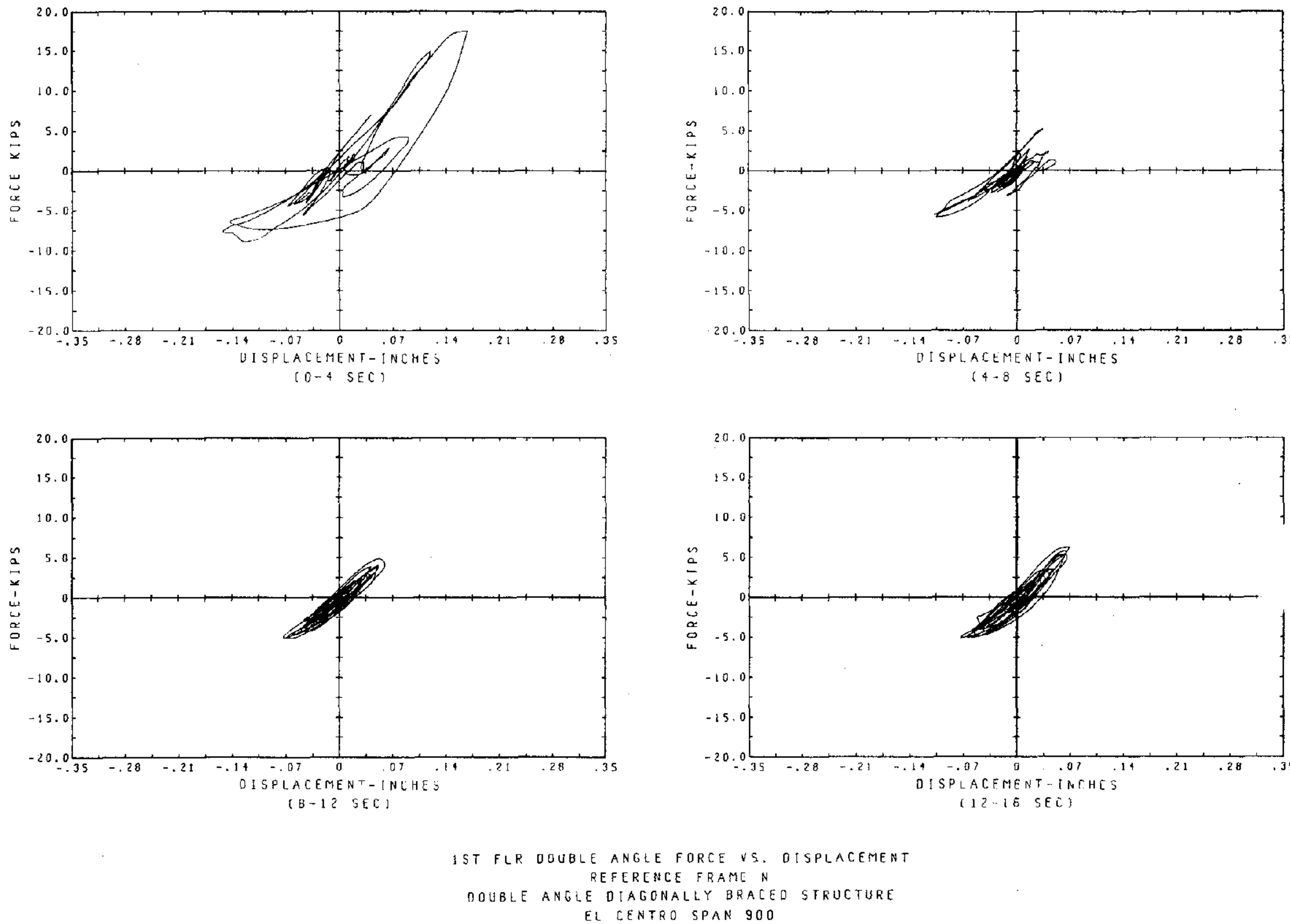

Fig. 5.3b.4 First Floor Double Angle Force-Displacement Hysteresis Loops

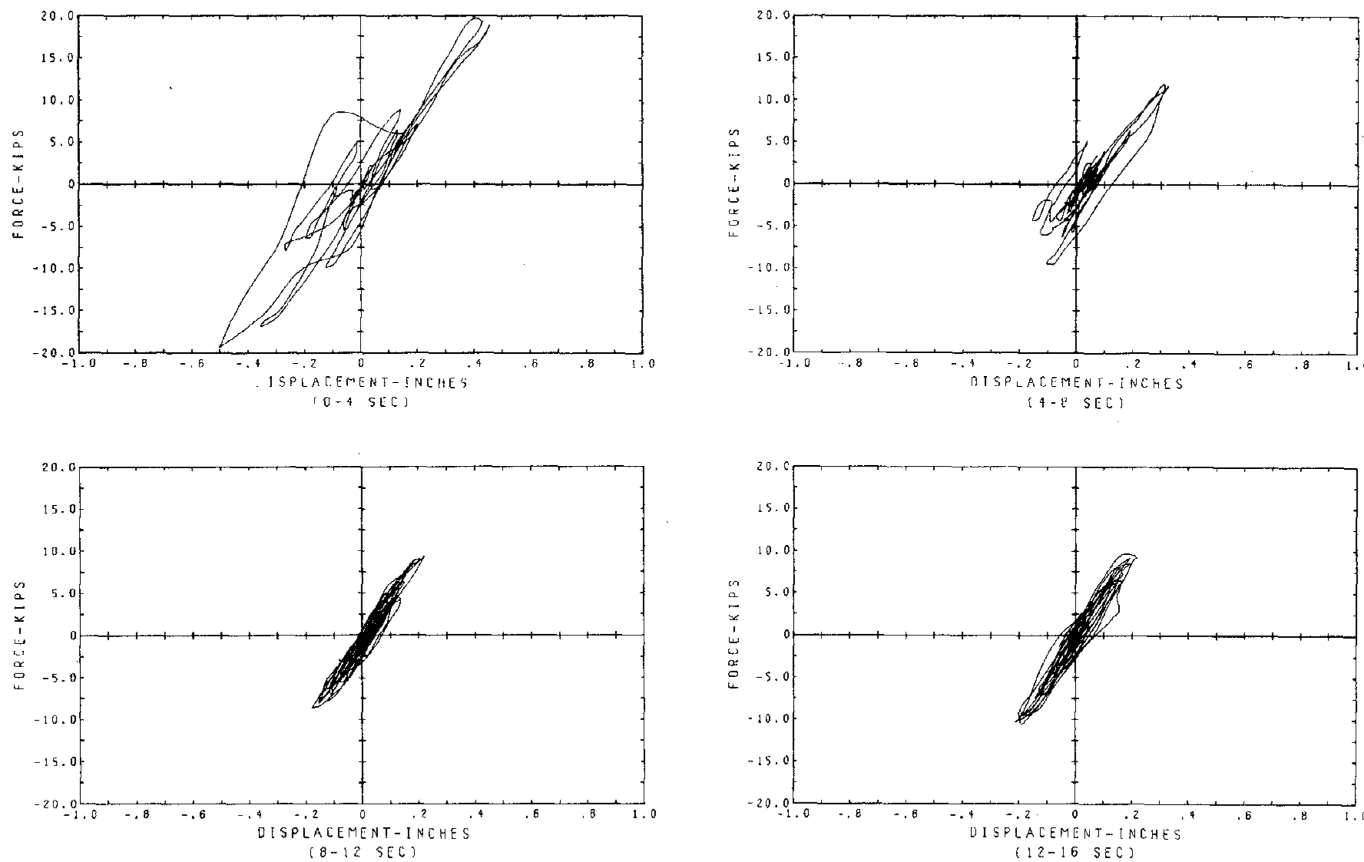

1ST FLR SHEAR VS. DISPLACEMENT
REFERENCE FRAME N
DOUBLE ANGLE DIAGONALLY BRACED STRUCTURE
EL CENTRO SPAN 900

Fig. 5.3b.5 First Floor Shear-Displacement Hysteresis Loops

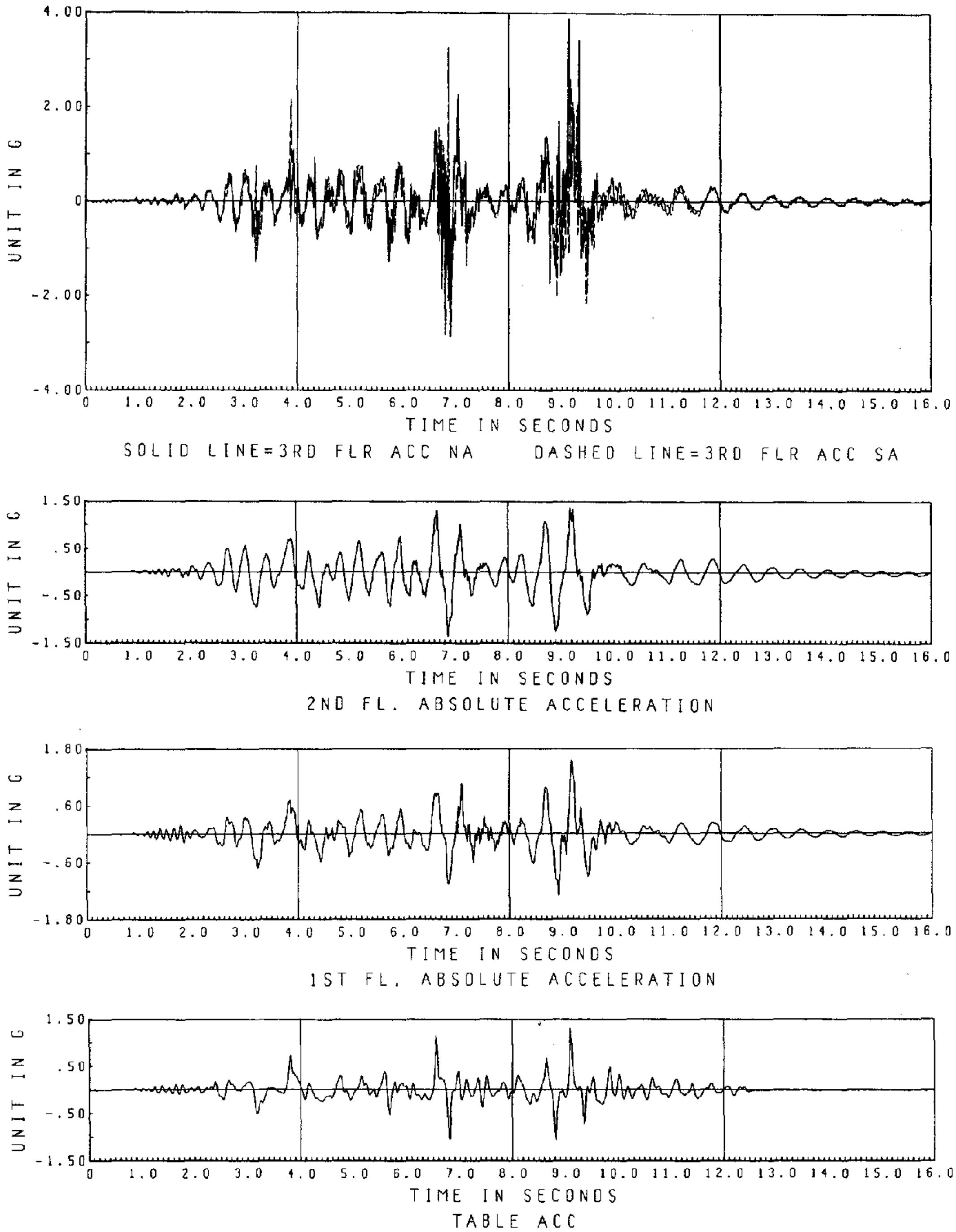

PACOIMA RECORD-1.314 G'S

TEST RESULTS OF DOUBLE ANGLE BRACING

Fig. 5.3c.1 Table and Floor Accelerations

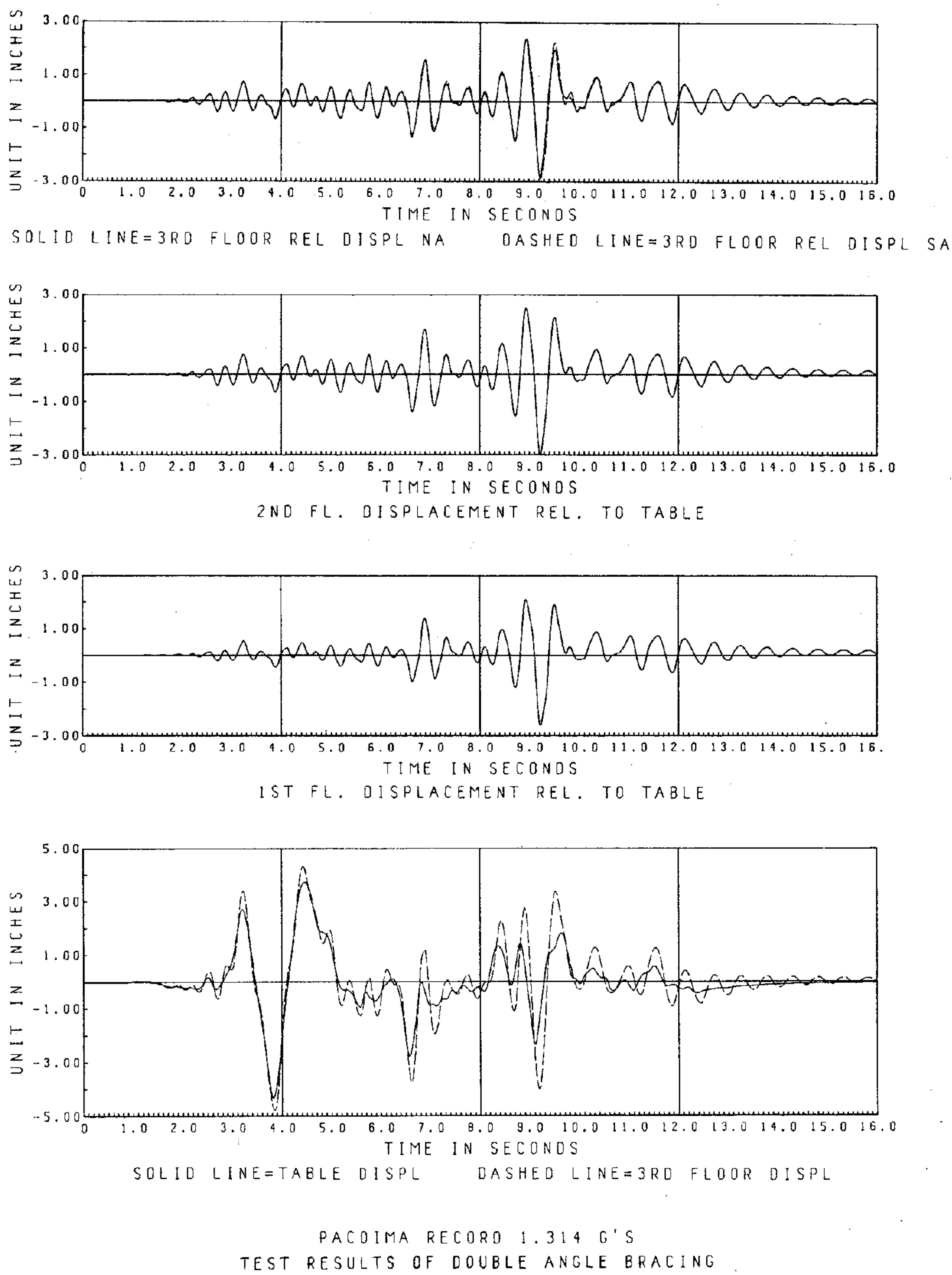

Fig. 5.3c.2 Table and Floor Displacements

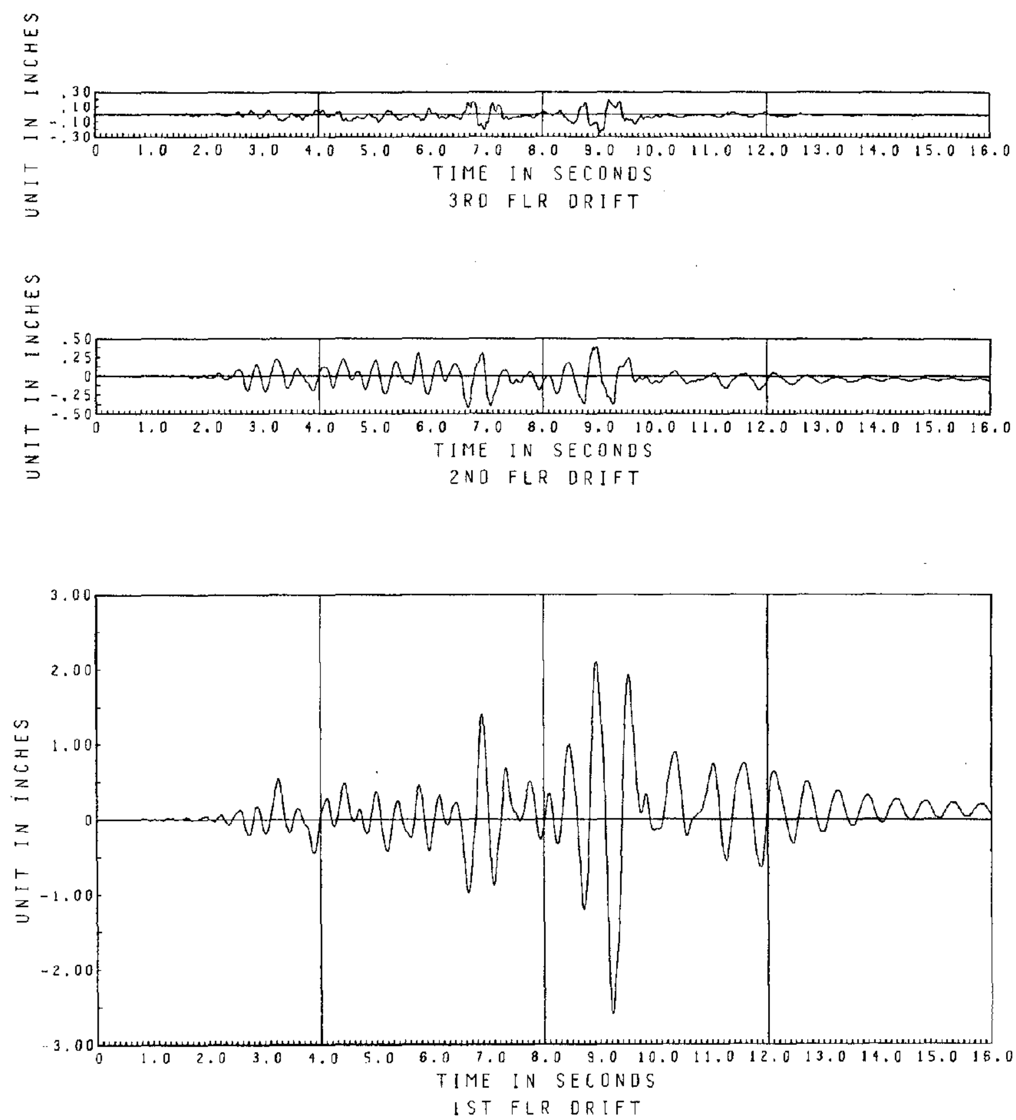

PACOIMA RECORD-1.314 G'S
TEST RESULTS OF DOUBLE ANGLE BRACING

Fig. 5.3c.3 Floor Drifts

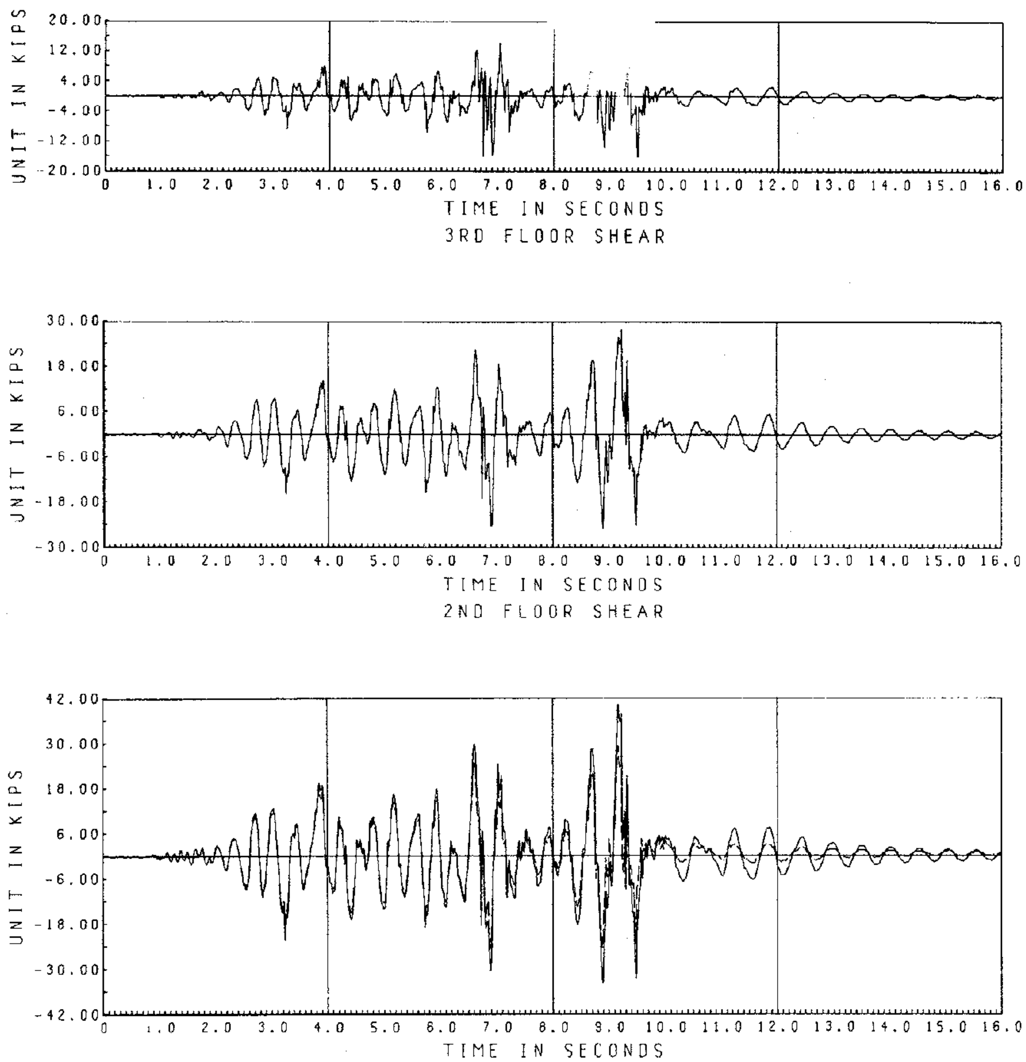

SOLID LINE=1ST FLOOR SHEAR DASHED LINE=1ST FLOOR BRACING DIAGONAL SHEAR

PACOIMA RECORD-1.314 G'S
TEST RESULTS OF DOUBLE ANGLE BRACING

Fig. 5.3c.4 Floor Shear Forces

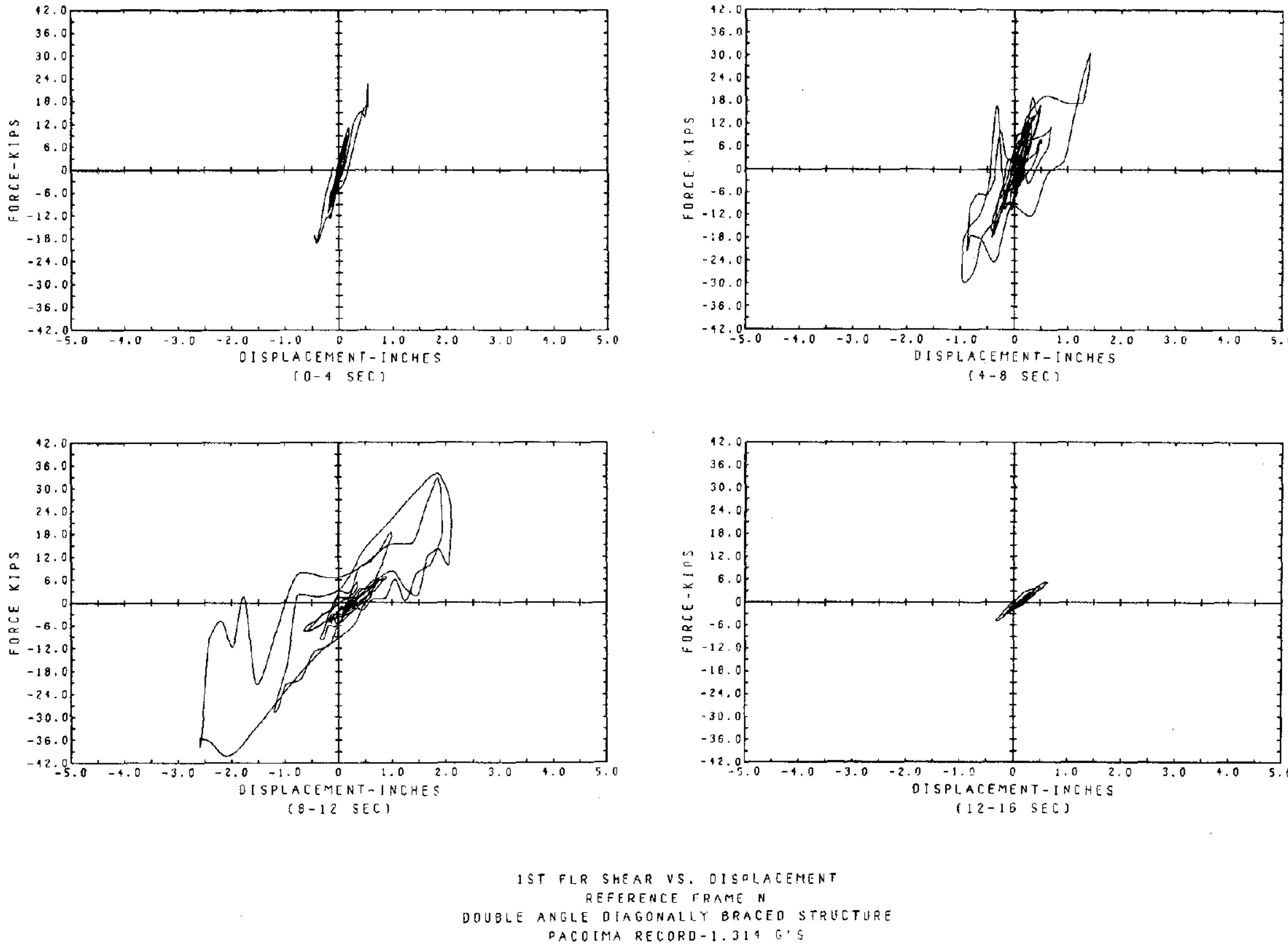

Fig. 5.3c.5 First Floor Shear-Displacement Hysteresis Loops

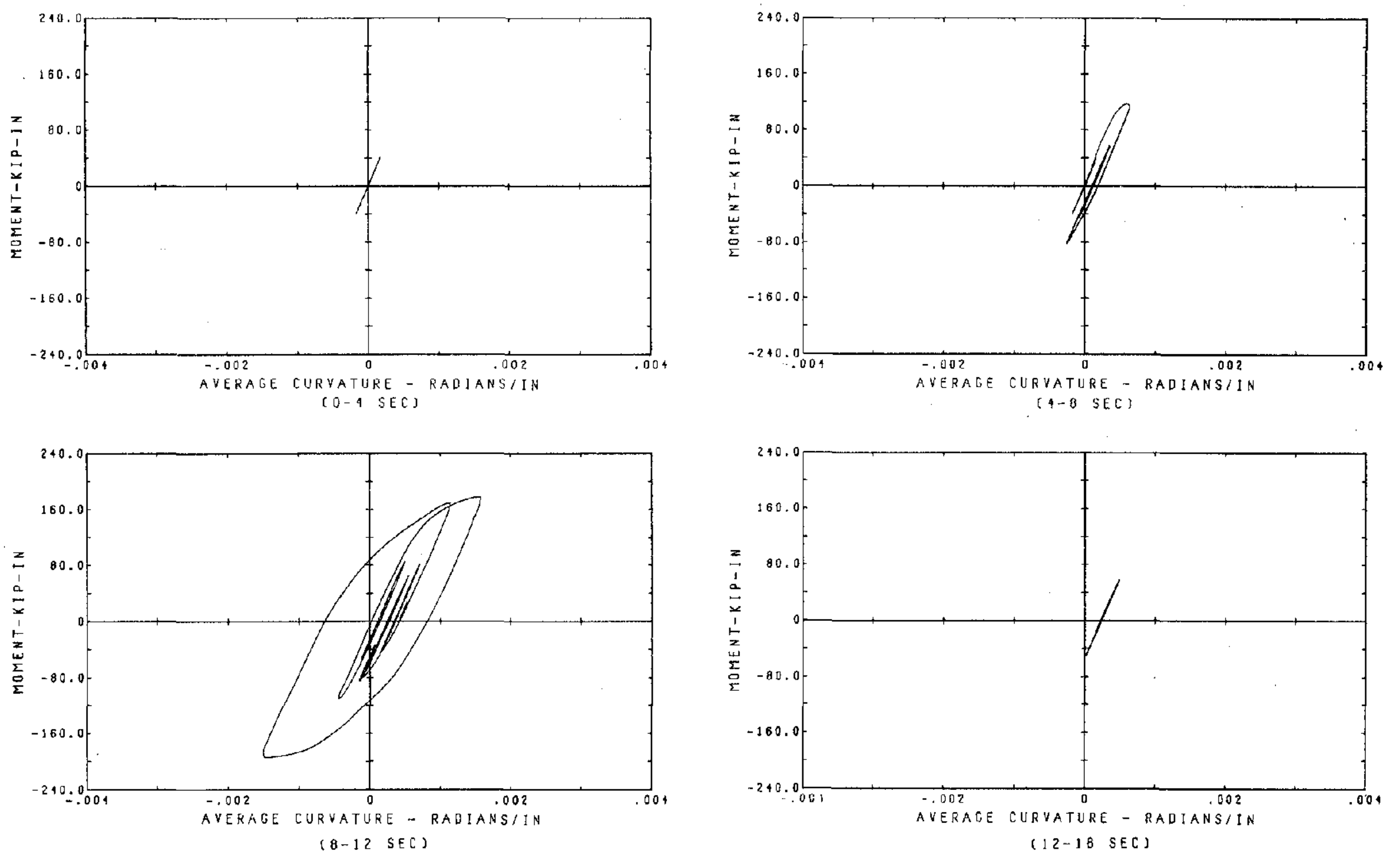

1ST FLR COL BOTTOM END , MOMENT VS. CURVATURE
REFERENCE COLUMN LINE NA
DOUBLE ANGLE DIAGONALLY BRACED STRUCTURE
PACOIMA RECORD-1.314 G'S

Fig. 5.3c.6 First Floor Column Moment-Curvature Hysteresis Loops

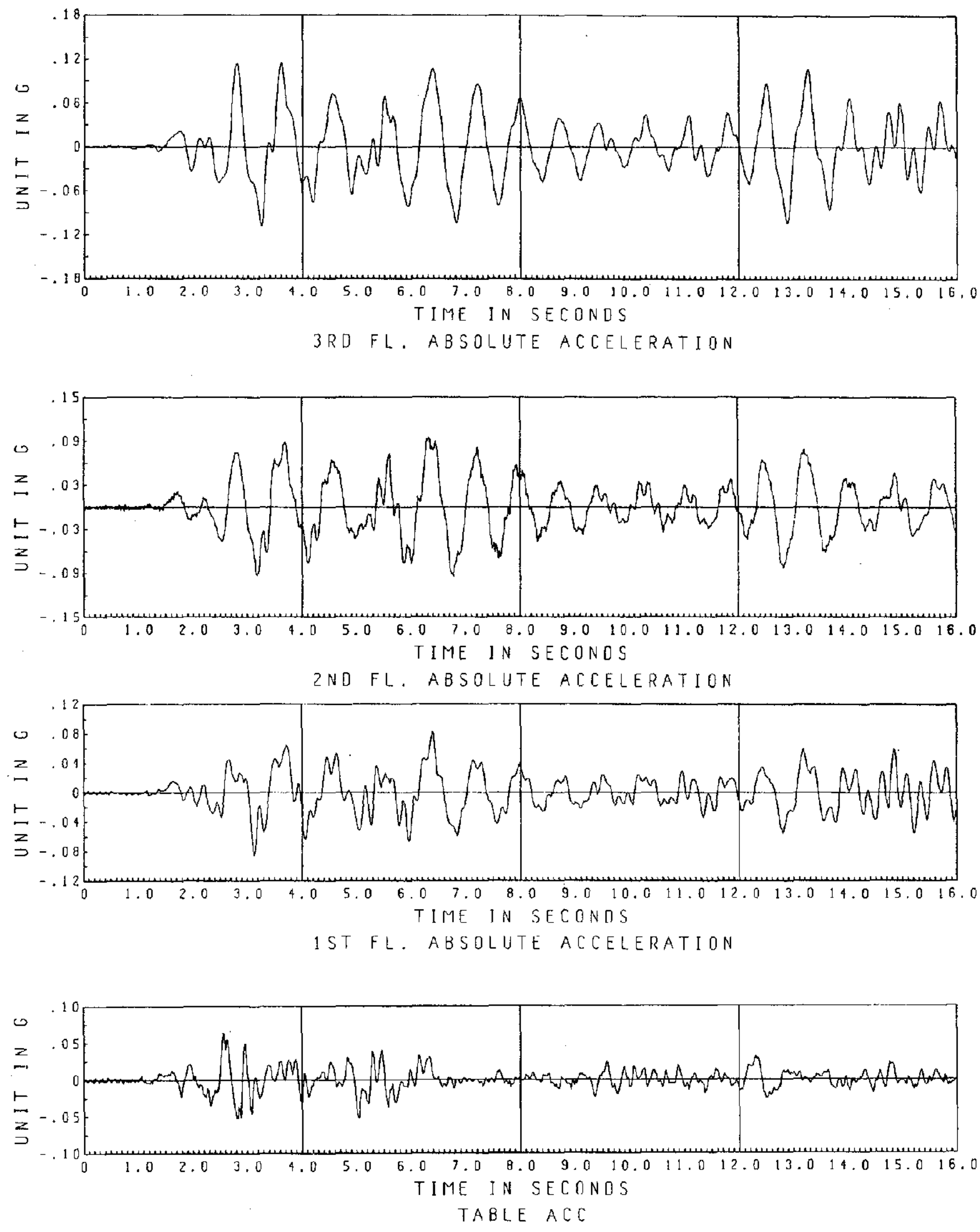

EL CENTRO SPAN 100
TEST RESULTS OF THE UNBRACED STEEL FRAME

Fig. 5.4a.1 Table and Floor Accelerations

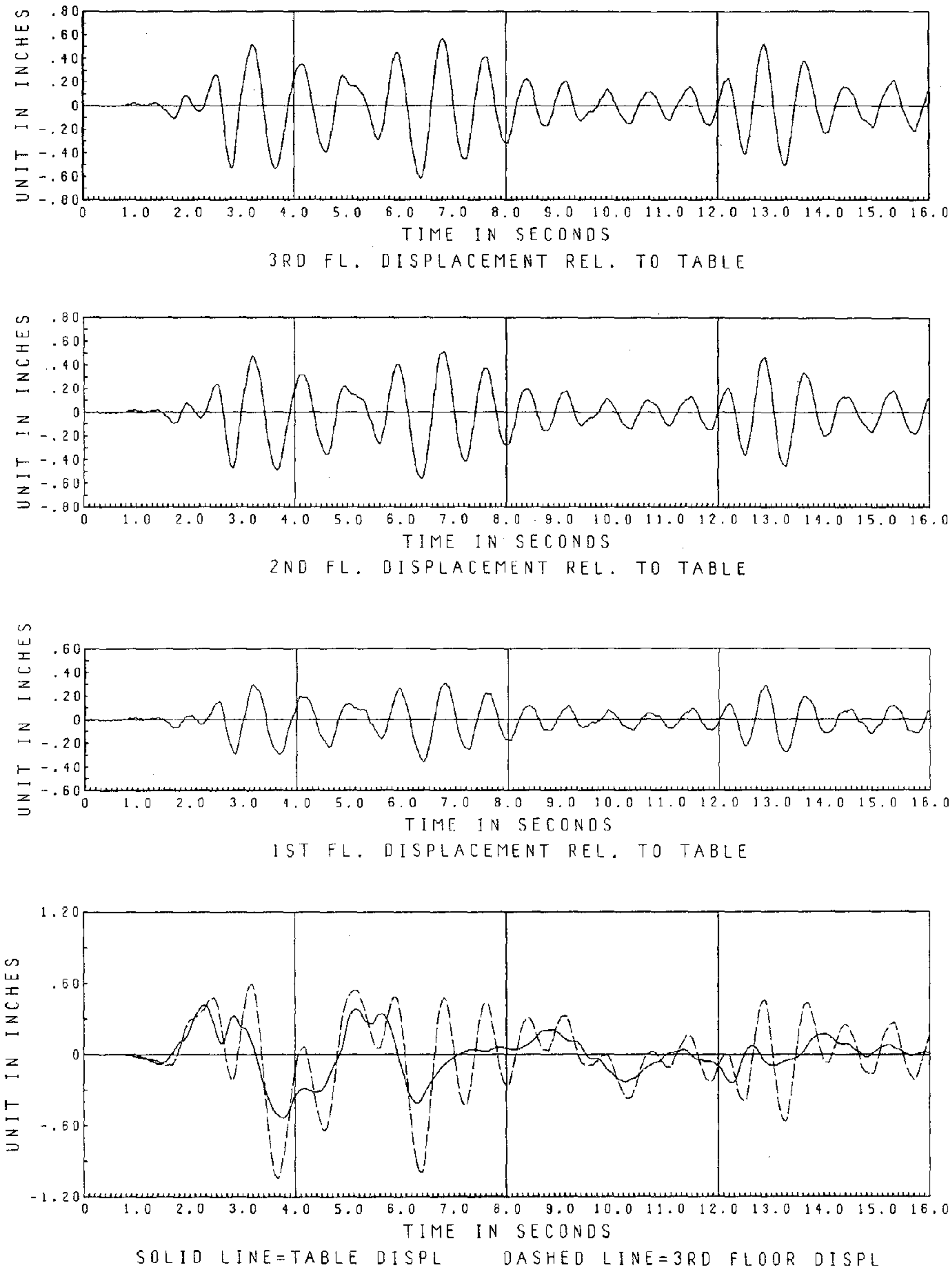

EL CENTRO SPAN 100

TEST RESULTS OF THE UNBRACED STEEL FRAME

Fig. 5.4a.2 Table and Floor Displacements

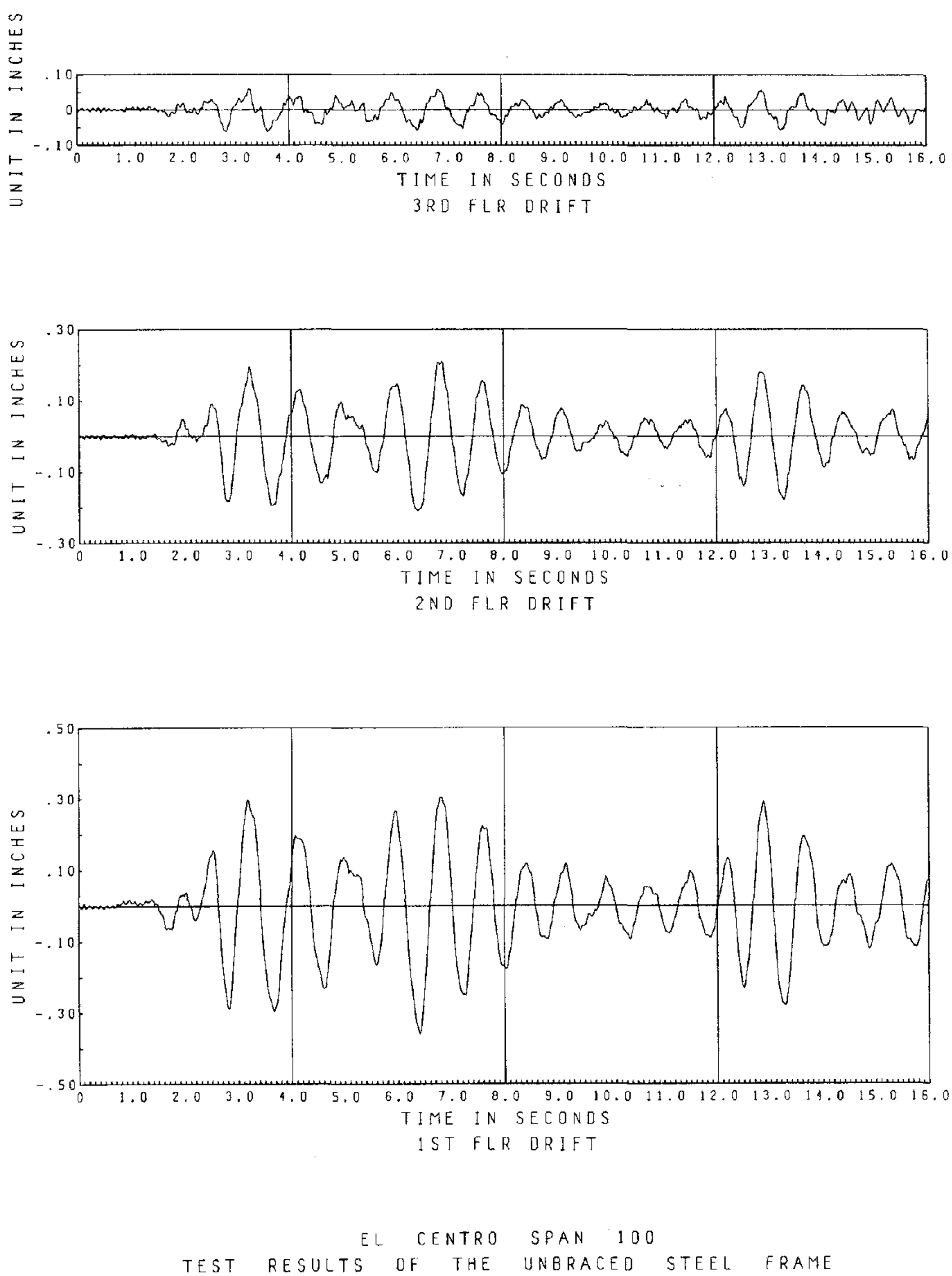

Fig. 5.4a.3 Floor Drifts

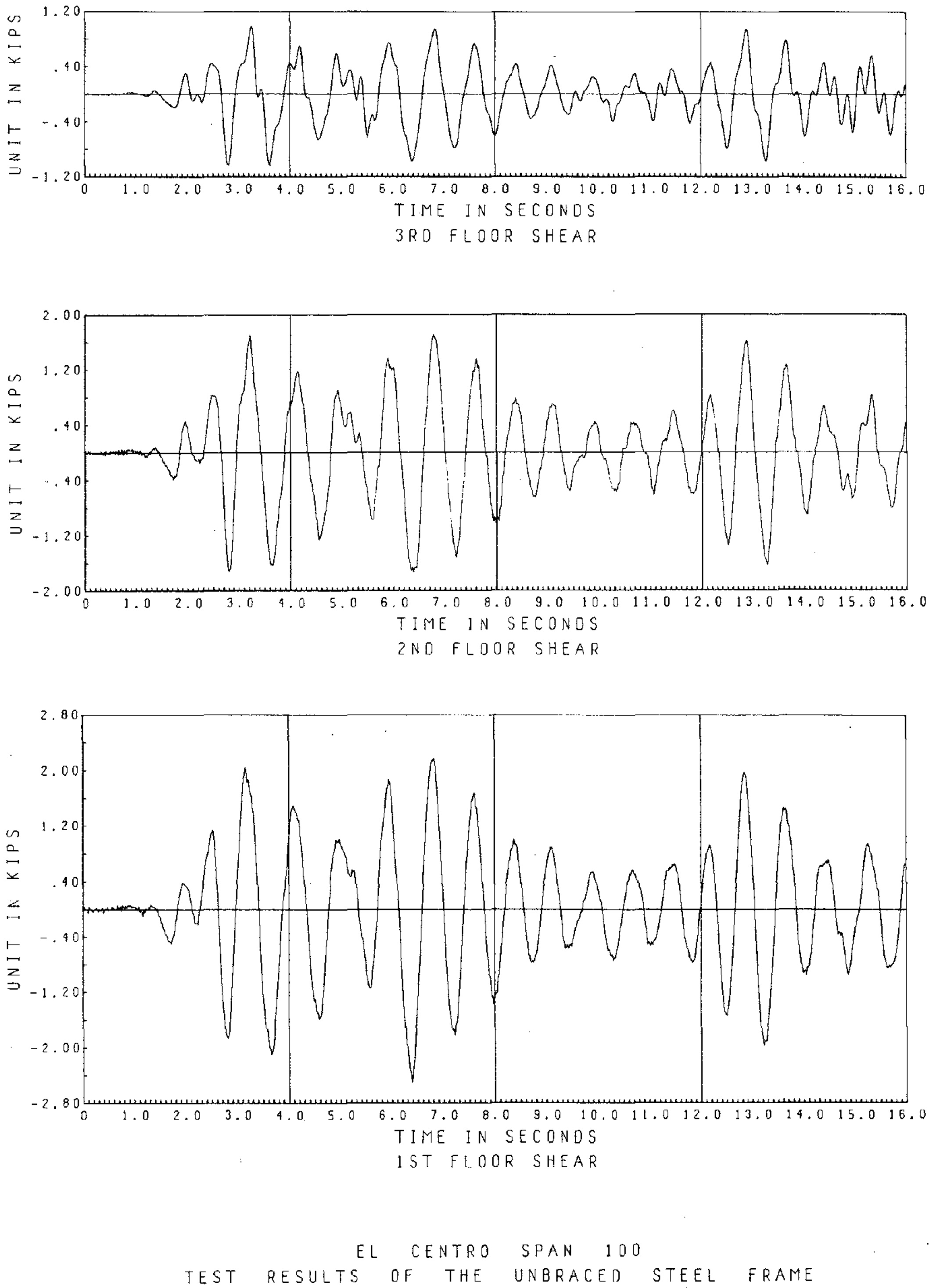

Fig. 5.4a.4 Floor Shear Forces

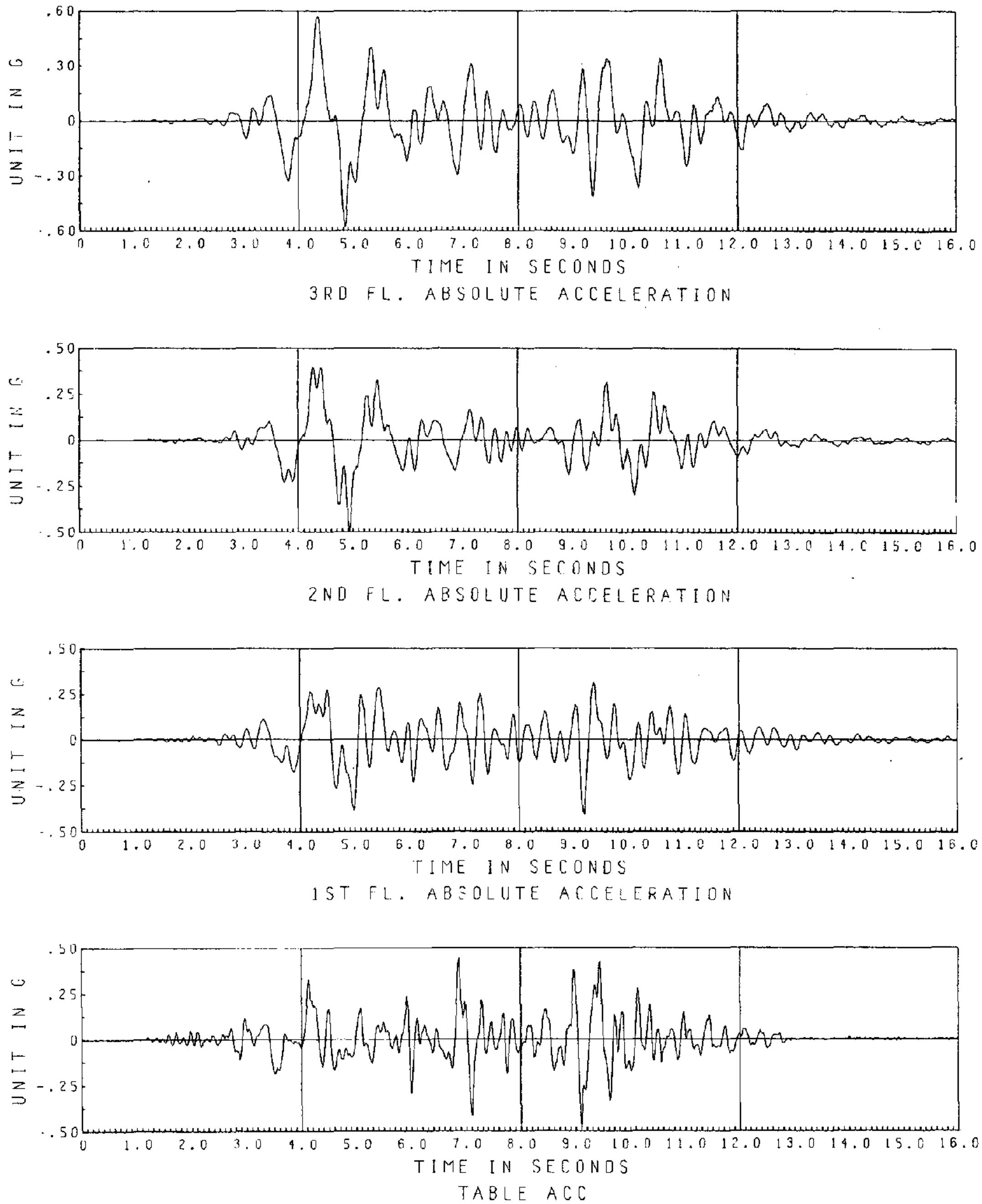

PACOIMA SPAN 400

TEST RESULTS OF THE UNBRACED STEEL FRAME

Fig. 5.4b.1 Table and Floor Accelerations

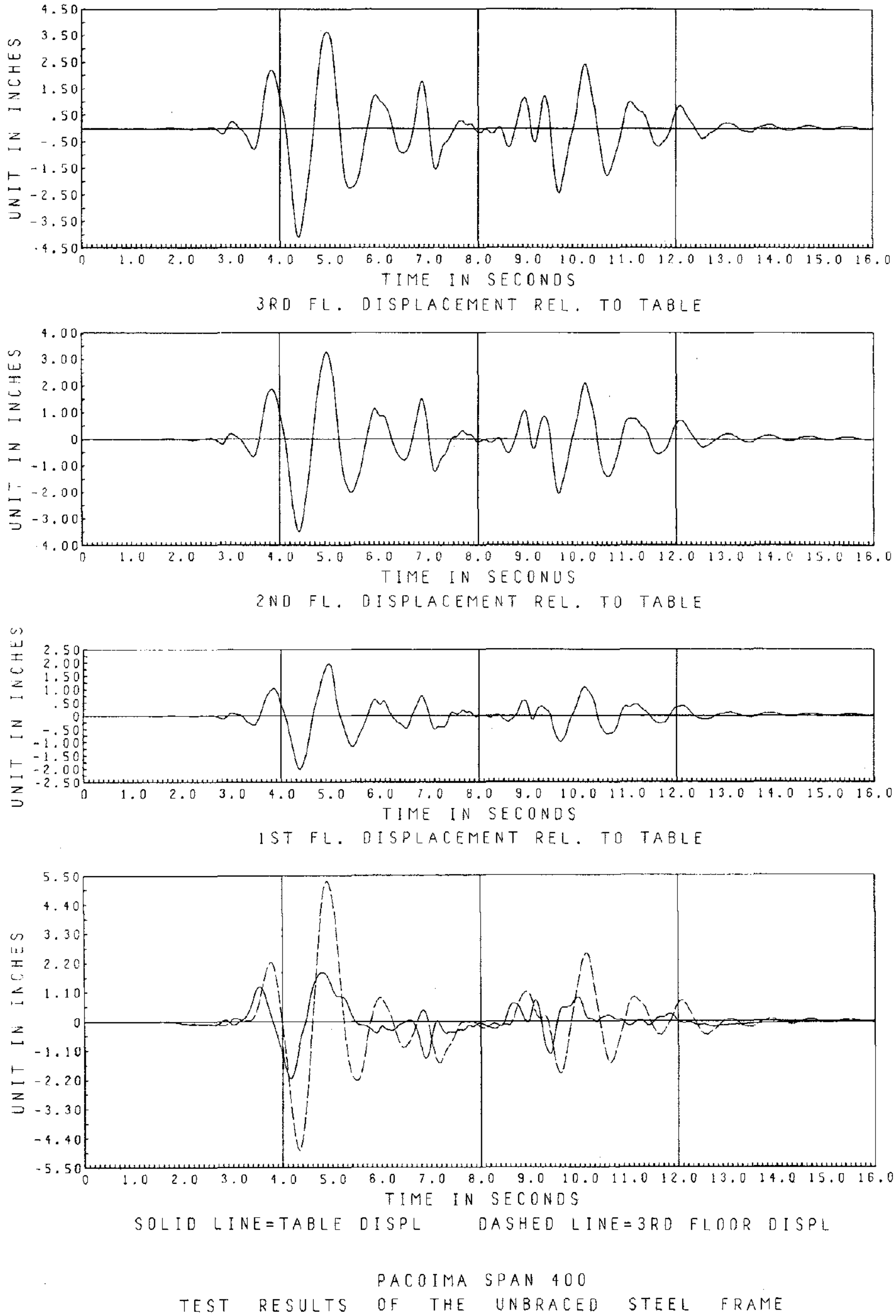

Fig. 5.4b.2 Table and Floor Displacements

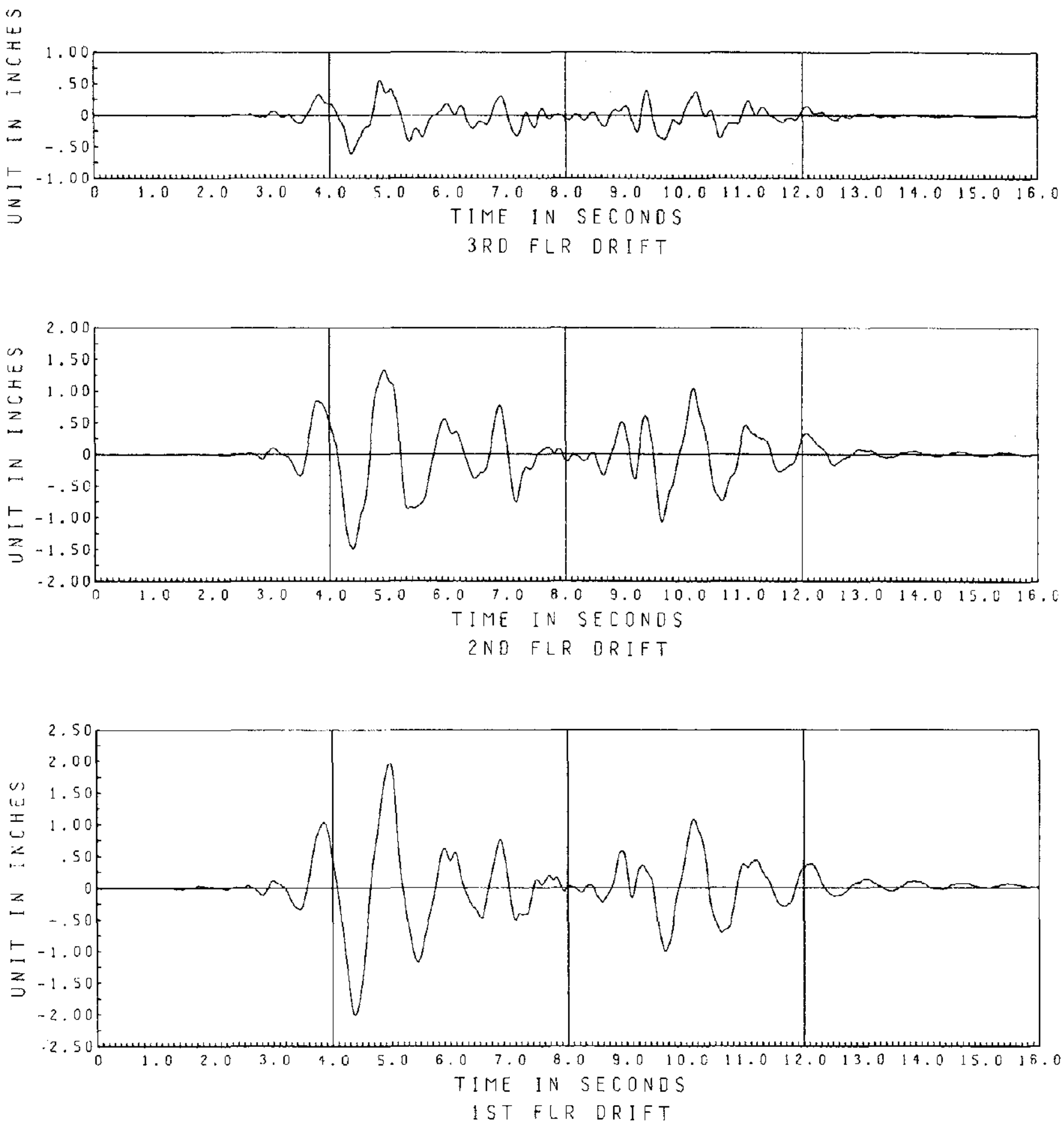

PACOIMA SPAN 400
TEST RESULTS OF THE UNBRACED STEEL FRAME

Fig. 5.4b.3 Floor Drifts

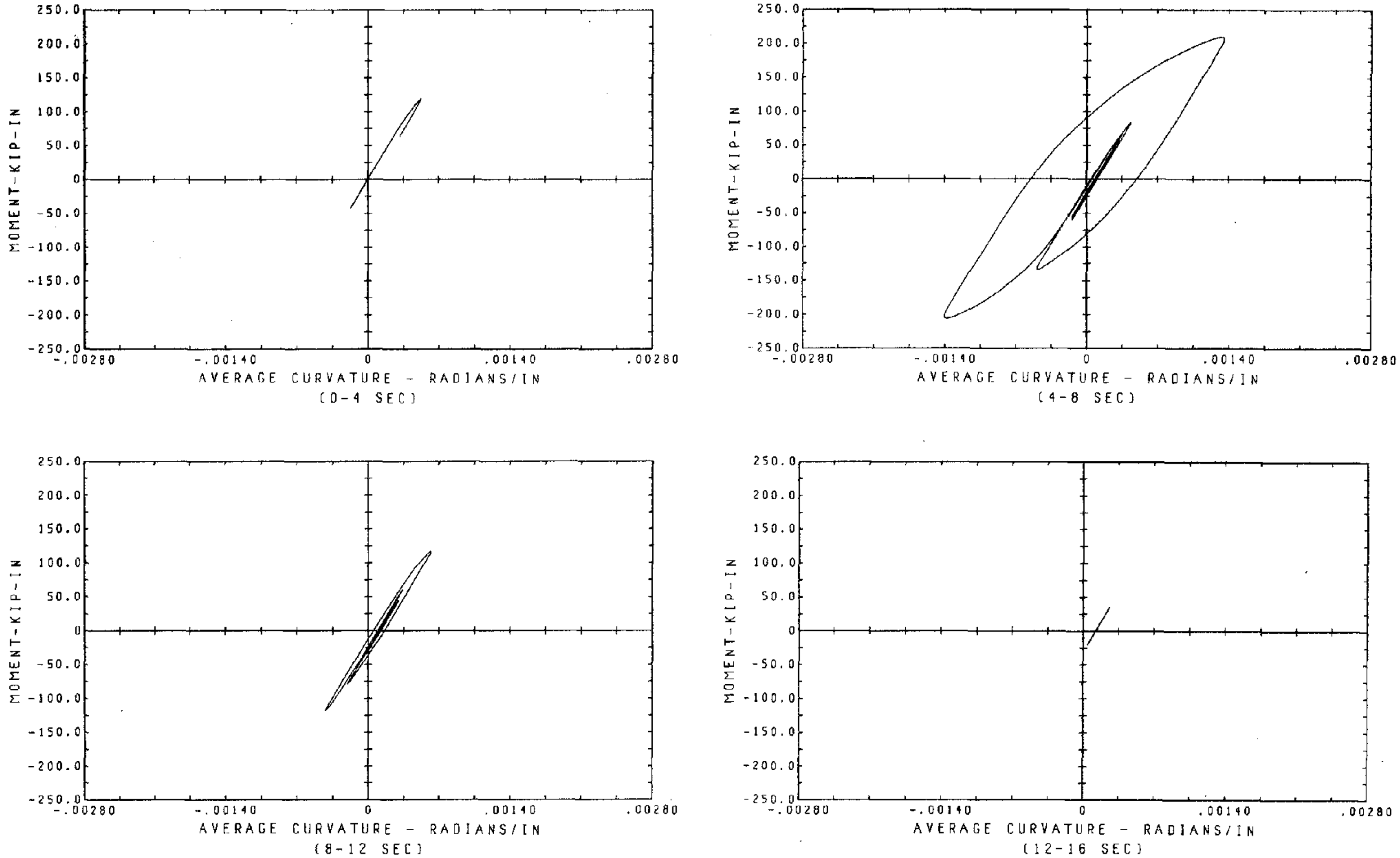

1ST FLR COL BOTTOM END , MOMENT VS. CURVATURE
REFERENCE COLUMN LINE NA
UNBRACED STRUCTURE
PACOIMA SPAN 400

Fig. 5.4b.4 First Floor Column Moment-Curvature Hysteresis Loops

6. ANALYTICAL STUDY

One of the principal purposes of this investigation was to obtain actual response results for braced frame structures which would serve to demonstrate the effectiveness of an existing nonlinear structural program, in the analysis of diagonal bracing systems. The program under consideration is DRAIN-2D[8], and of partiuclar interest was the adequacy of the tension-compression bracing element included in that program. This program was selected because it is suitable for the inelastice dynamic analysis of plane frame structures, and allows for the addition of new element routines with no modification to the basic program. Accordingly, the post-buckling truss elements of Reference 7 and Reference 10 have been developed for use in this program. Other attractive features of the program are as follows: it includes semi-rigid connection elements; various yield interaction surfaces can be assumed for beam-column elements in defining plastic hinge mechanisms at the member ends; additional nodes can be specified along a member, so that spreading of plastic hinges can be studied; and, more than one member can be connected between two nodes so that a curvilinear load-deformation behavior can be approximated by the basic bilinear yielding mechanism.

The general purpose computer program DRAIN-2D, discussed fully by Kannan and Powell[8], is for dynamic analysis of inelastic plane structures under identical in-phase motions of all support points. The analysis procedure makes use of the direct stiffness method with the nodal displacements as unknowns. The structure mass is assumed to be lumped at nodes each possessing up to three degrees of freedom. The earthquake excitations can be specified simultaneously in both horizontal and vertical directions by means of their acceleration time histories. Static loads producing elastic structural response may be applied prior to the dynamic loading. The dynamic response is calculated by step-by-step integration of the equations of motion expressed in incremental form, assuming the acceleration to be constant within each step. The tangent stiffness of the structure is employed for each step assuming linear structural behavior during the time step. Unbalanced loads resulting from error due to the assumed linearity within the step are corrected in the subsequent time step. Note that greater accuracy can be obtained by selecting fairly short time steps to avoid large overshoots at instants of significant stiffness changes. Damping capabilities include optional combinations of mass-dependent, original stiffness-dependent, and tangent stiffness-dependent viscous damping.

6.1 Rod Bracing System

The two-dimensional frame model depicted in Fig. 6.1a.1, Model 1, was the first mathematical model developed for the rod bracing system. It was assumed that the column bases were fixed rigidly to the shaking table. The structure was discretized as nine beam-columns and twelve truss members interconnected by fourteen rigid points. The mass of the structural members and of the added concrete blocks was lumped at the nodes along the columns, and was associated with motions in the X-direction only. This model has five degrees of freedom per floor level; vertical displacement and rotation of each joint, and horizontal displacement of each floor. Nominal section properties and clear span dimensions were used in modelling all members; joint panel zones were assumed rigid. Bilinear flexural behavior was assumed for beams and columns; an axial force P-Δ effect was also considered in the first floor columns. Bracing properties are described separately in the discussion of the different mathematical models used for correlation with the experimental results.

6.1a Correlation with El Centro Span 100 - Model 1

In modelling the half-inch rod braces for the El Centro span 100 test, they were treated as composite axial force members consisting of two parts in series; solid rod, and turnbuckle. Based on static tests, the turnbuckles were assumed to behave elastically, while the rods were treated as bilinear yielding elements with very low compressive capacity (see Fig. 6.1a.2(a)). This is a standard DRAIN-2D element intended to model tensile yielding and elastic compression buckling. Static pretension loads applied to these members during the experiment were considered as initial static loads prior to the dynamic analysis. The program DRAIN-2D does not consider the clear length of bracing members. Therefore, the actual flexibility of the braces was determined taking into account the rigidity of the end connections. The damping coefficient proportional to the initial stiffness was set at $\beta_o = 0.00157$ leading to first mode damping of 2 percent of critical. The floor displacements calculated for this model are shown in Fig. 6.1a.3 with the measured floor displacements. The quality of this correlation is regarded as excellent considering that no system identification study was performed to determine the member properties.

6.1b <u>Correlation with El Centro Span 1000 - Model 2</u>

The previous model is not suitable for analysis of response to the El Centro motion with a peak acceleration of 0.775 g. Because of the pitching motion of the table, there would be significant interaction between the shaking table and the structure. The interaction of the shaking table in the dynamic response analysis was accounted for by providing vertical spring supports under the table to simulate the oil column flexibility of the hydraulic actuators.

Model 2, developed for this situation, is shown in Fig. 6.1b.1. The structure was discretized as ten beam-columns and twenty truss members interconnected by twenty-two rigid points. In modelling the half-inch rod braces for this model, they were treated as composite axial force members consisting of three parts in series; solid rod, threaded portion, and turnbuckle. The addition of the threaded portion was to localize the initial yielding of braces to these members as it actually occurred during the dynamic tests. Turnbuckles were assumed to behave elastically as before while both parts of the rod were considered as bilinear yielding elements with a very low compressive capacity (see Fig. 6.1a.2(a)). All other assumptions for Model 1 are also valid in this case.

The stiffness-dependent damping coefficient was set at $\beta = 0.006$ for this analysis, leading to first mode damping of 5 percent critical. The area and length of the vertical springs under the shaking table were set arbitrarily at 10 square in. and 100 in., respectively. Thus, only the Young's modulus of the spring needed to be specified during data correlation of the model. Correlations between analytical results obtained with this model and the experimental results are presented in Fig. 6.1b.2 and Fig. 6.1b.3 for both global and local quantitites. This correlation is excellent considering that tension yielding led to an impacting type of response in the resulting slack rod system. (Note that the Young's modulus of the vertical spring was set at 1800 ksi in this analysis.)

6.1c Correlation with the Pacoima Earthquake - Model 3

To model the rod bracing behavior in the Pacoima Dam test with a peak acceleration of 1.129 g, it was necessary to revise the element properties to account for rupture. In this case, the two resisting frames were represented as a single frame, but the rod braces from the two frames were treated as independent parallel members of appropriate uniform section. The different yield levels for threaded and solid sections were simulated by parallel members having different bilinear properties, resulting in a tri-linear mechanism. Also, the standard DRAIN-2D element was modified so that the stiffness became zero when the rupture load was reached (see Fig. 6.1a.2(b)); simultaneously the element force was transferred to the end nodes as an unbalanced load. The difinition of the stiffness-dependent damping matrix for this model was the same as for Model 2, and the shaking table-structure interaction was also included; the modulus of the vertical spring was set at 1500 ksi. Correlation between results obtained with this model and the experimental results described in Chapter 5.1d are shown for both global and local response quantities in Figs. 6.1c.1 and 6.1c.2, respectively. The model successfully predicts the rupture of the first and second floor braces and the time at which they occurred, but it is evident that the correlation is not as good as was obtained with Model 2 for the El Centro test. However, the analytical estimates of story displacements and column moments and shears are considered adequate; the high frequency "noise" in the experimental shear values is due to damage to the accelerometer attachments. Also, there is good reason to believe that the main source of discrepancy in the analysis is associated with inadequacy of the mathematical model for the bracing members in representing the impacting type response that developed in the slack-rod system during the more intense tests.

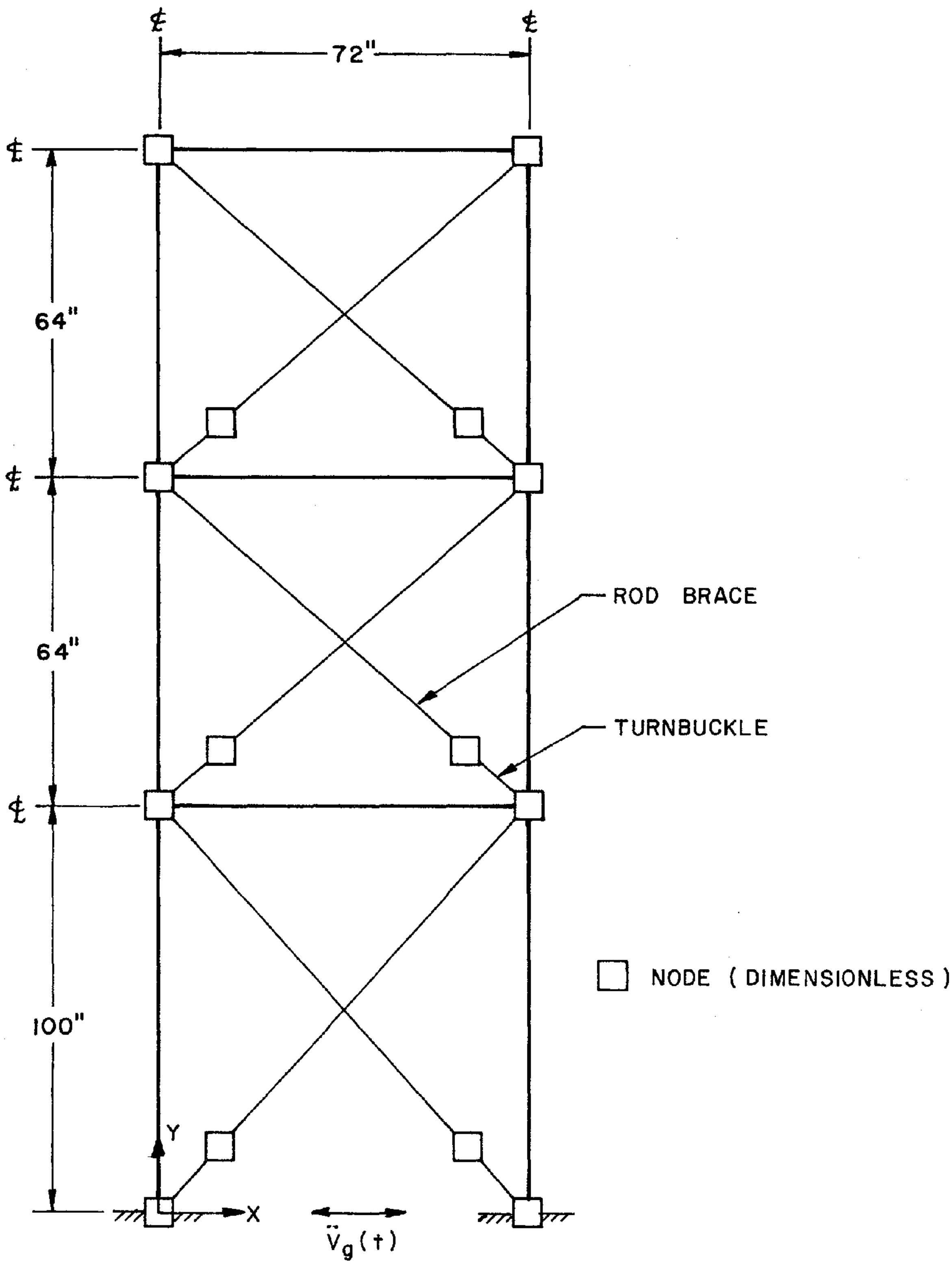

Fig. 6.1a.1 Mathematical Model 1 With Rod Diagonal Braces

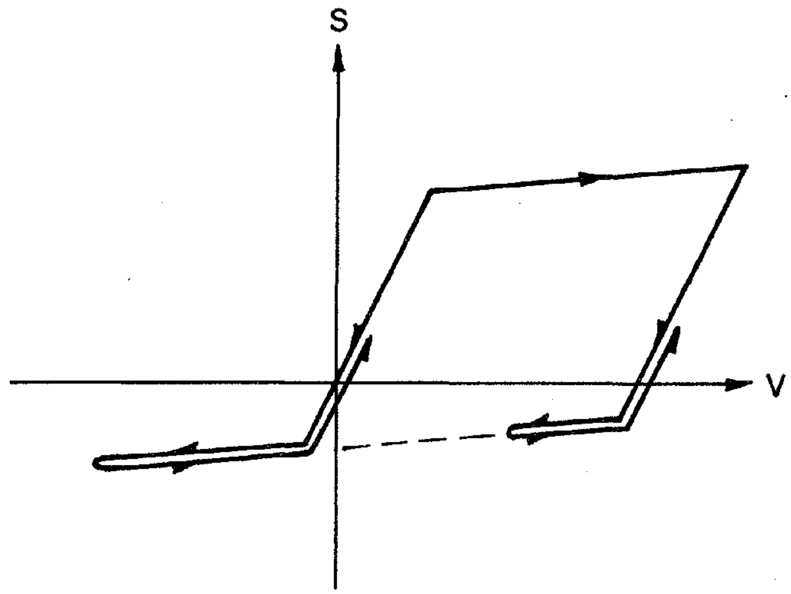

(a) Yield in Tension, Buckling in Compression

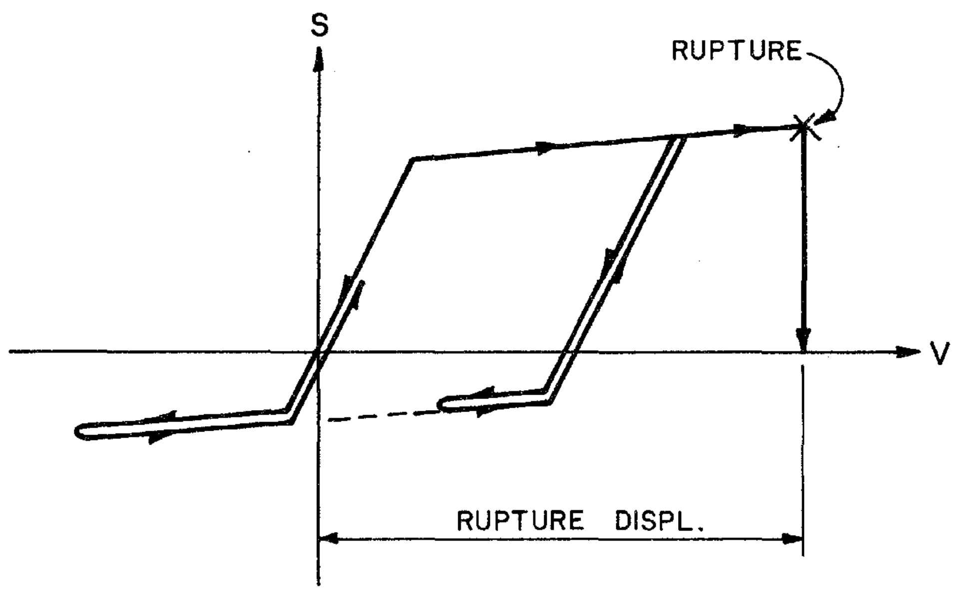

(b) Yield and Rupture in Tension, Buckling in Compression

Fig. 6.1a.2 Force-Displacement for Rod Bracing Members

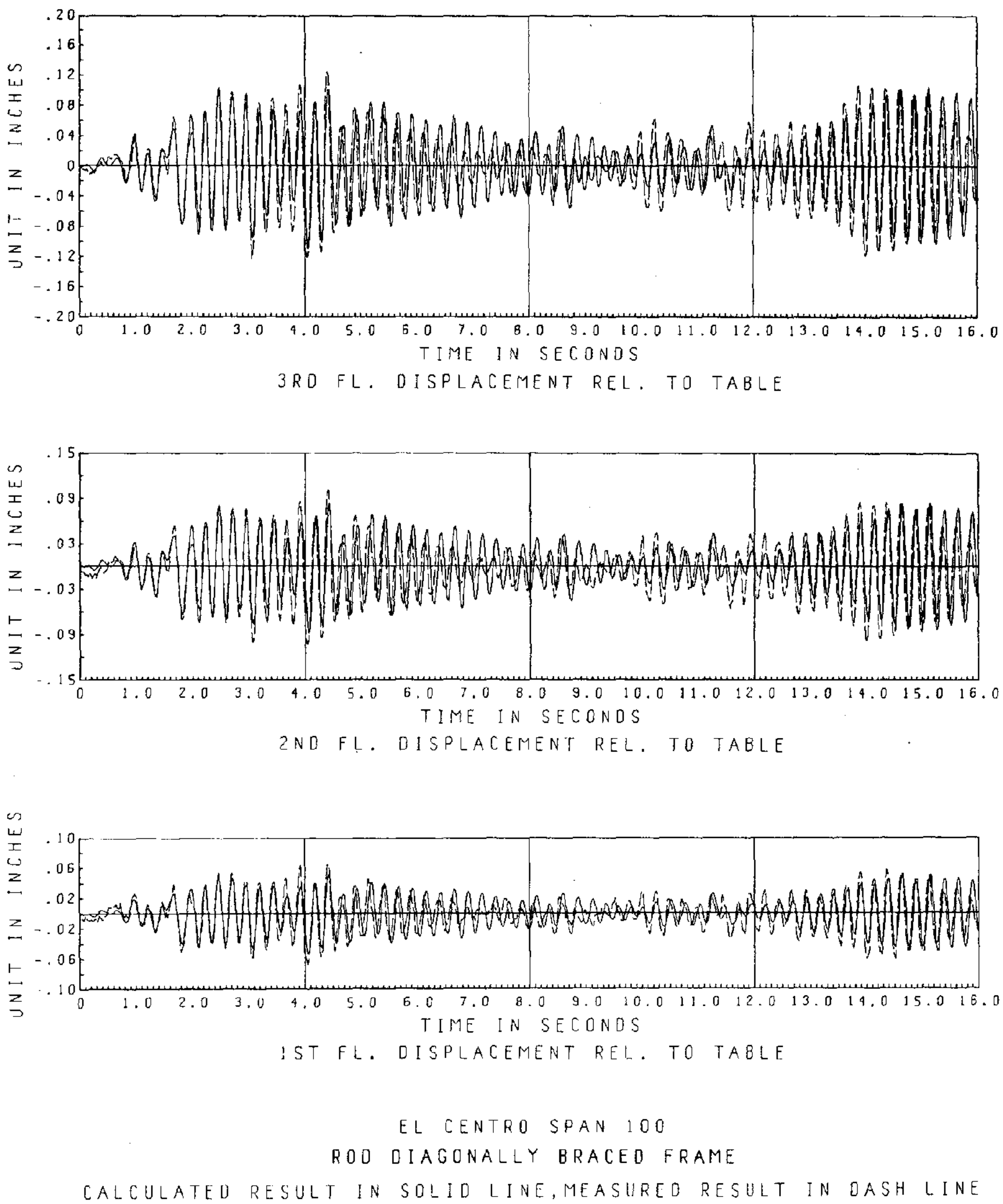

Fig. 6.1a.3 Correlation of the Floor Displacements - Model 1

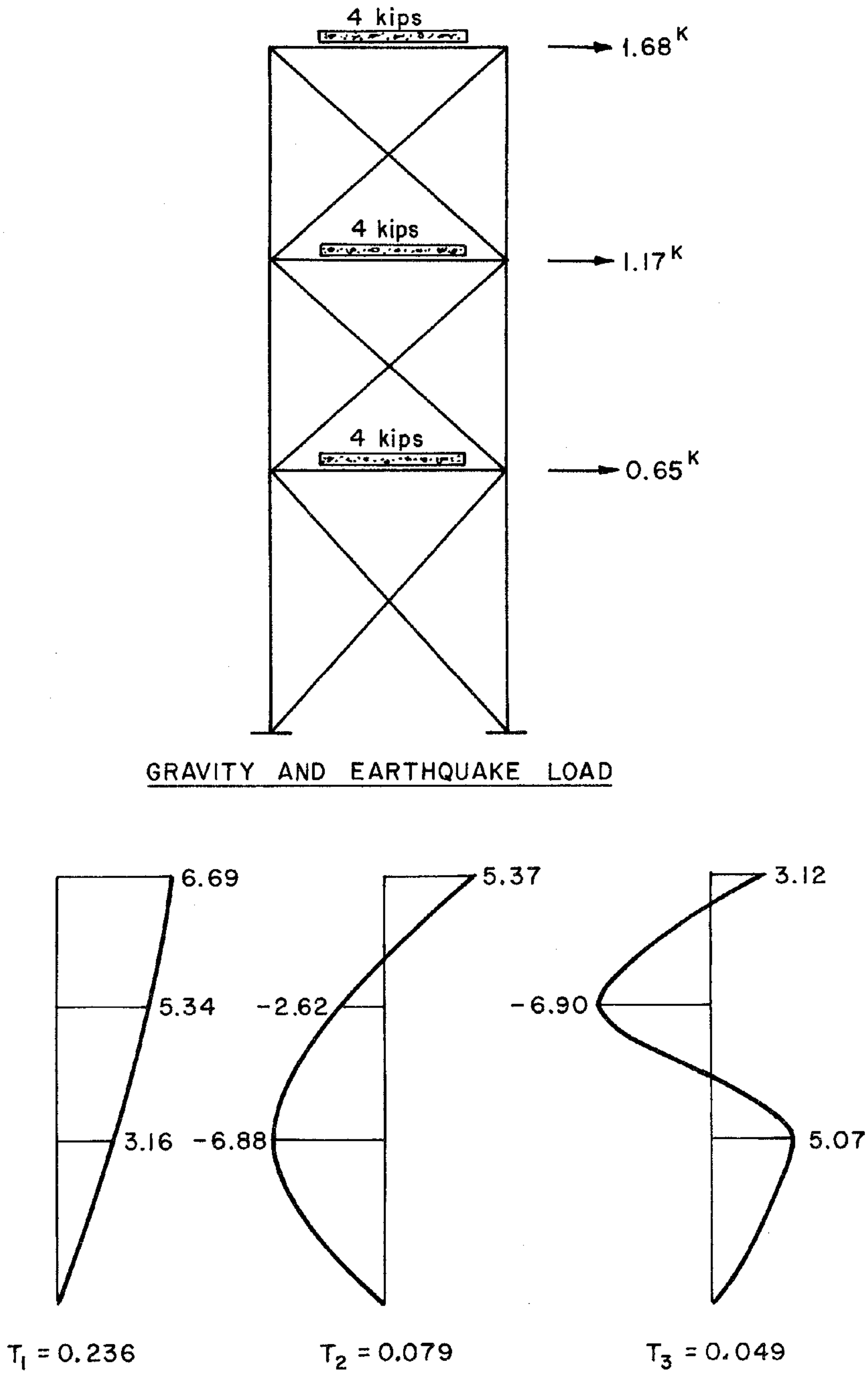

Fig. 6.1a.4 Calculated Periods and Mode Shapes

(Rod Braced Structure)

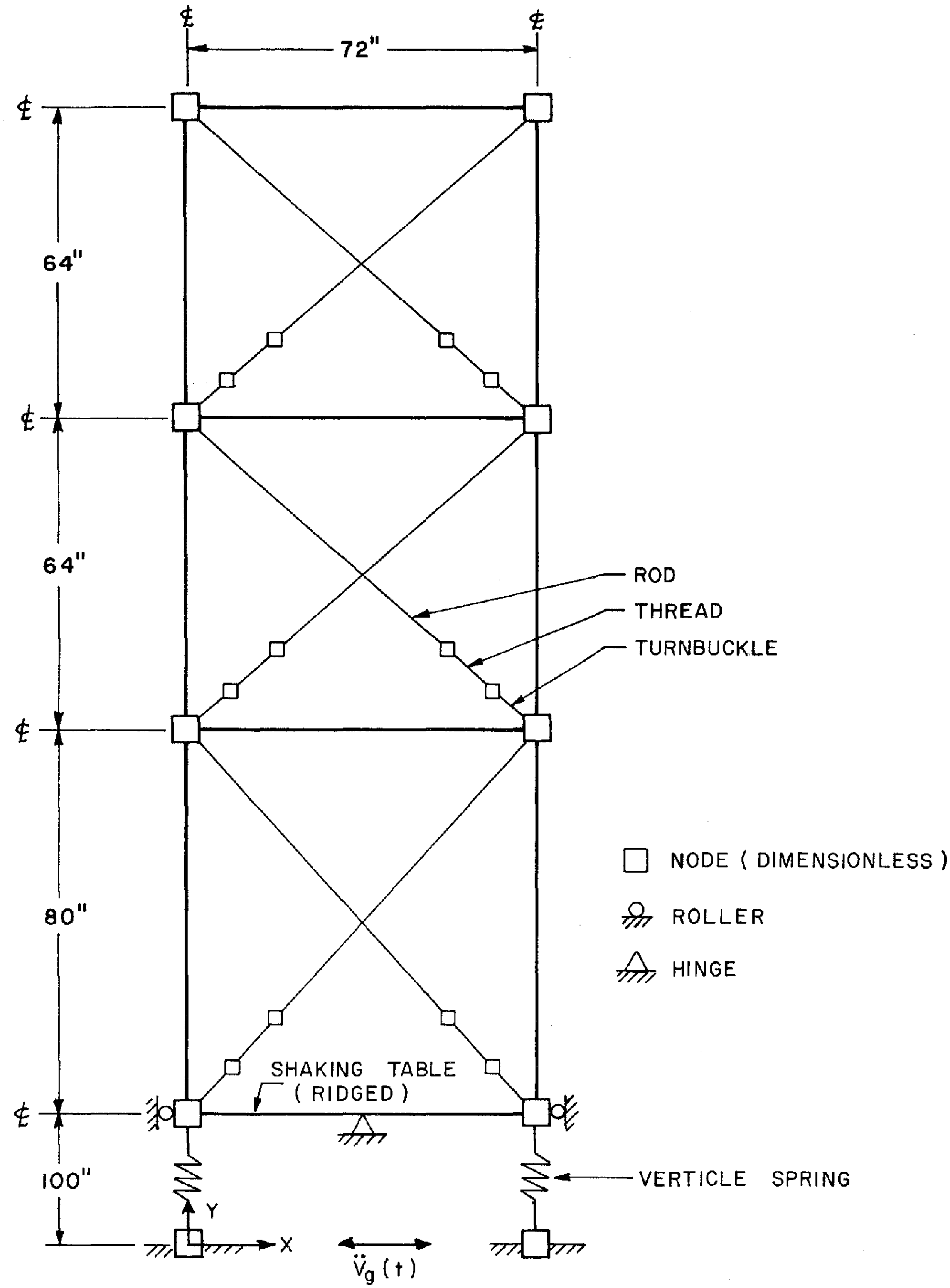

Fig. 6.1b.1 Mathematical Model 2
(shaking table-structure
interaction included)

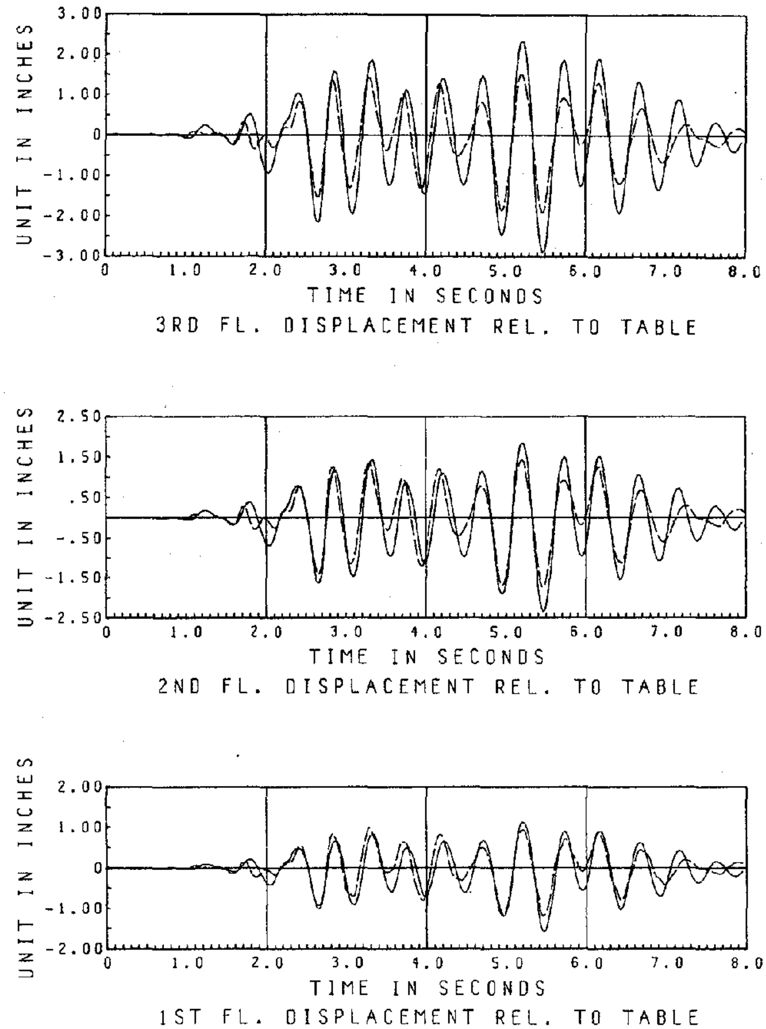

ROD DIAGONALLY BRACED FRAME

EL CENTRO SPAN 1000

CALCULATED RESULT IN SOLID LINE, MEASURED RESULT IN DASH LINE

Fig. 6.1b.2 Correlation of Floor Displacements - Model 2

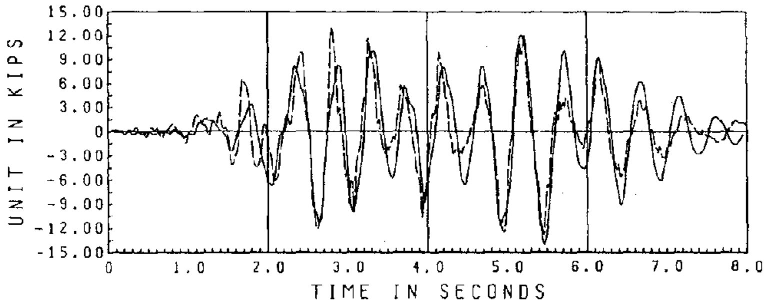

1ST FLR SHEAR FORCE

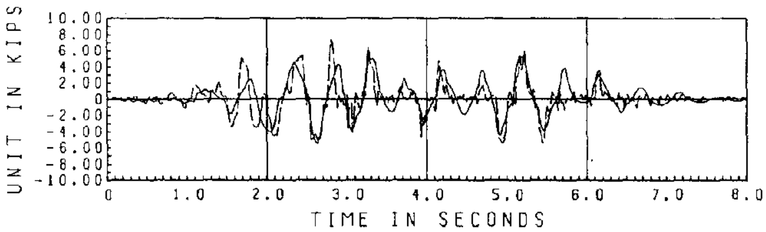

1ST FLR BRACES SHEAR FORCE

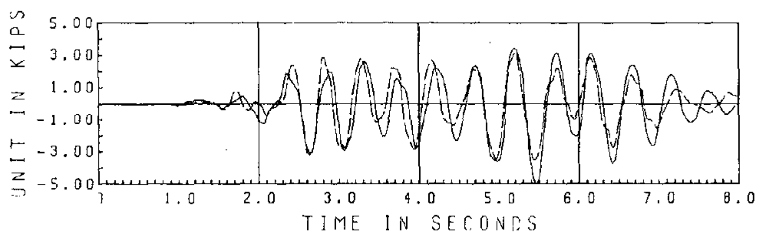

1ST FLR COLUMN SHEAR FORCE-NA

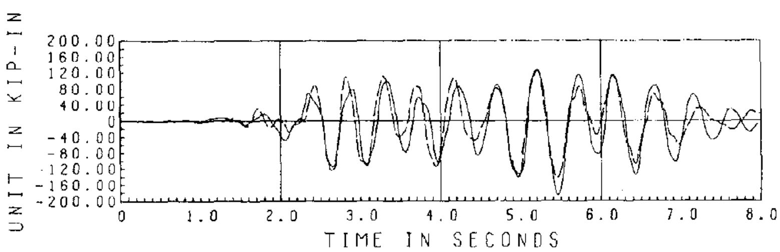

1ST FLR COLUMN BOTTOM END MOMENT-NA

ROD DIAGONALLY BRACED FRAME

EL CENTRO SPAN 1000

CALCULATED RESULT IN SOLID LINE, MEASURED RESULT IN DASH LINE

Fig. 6.1b.3 Correlation of Global and Local Forces - Model 2

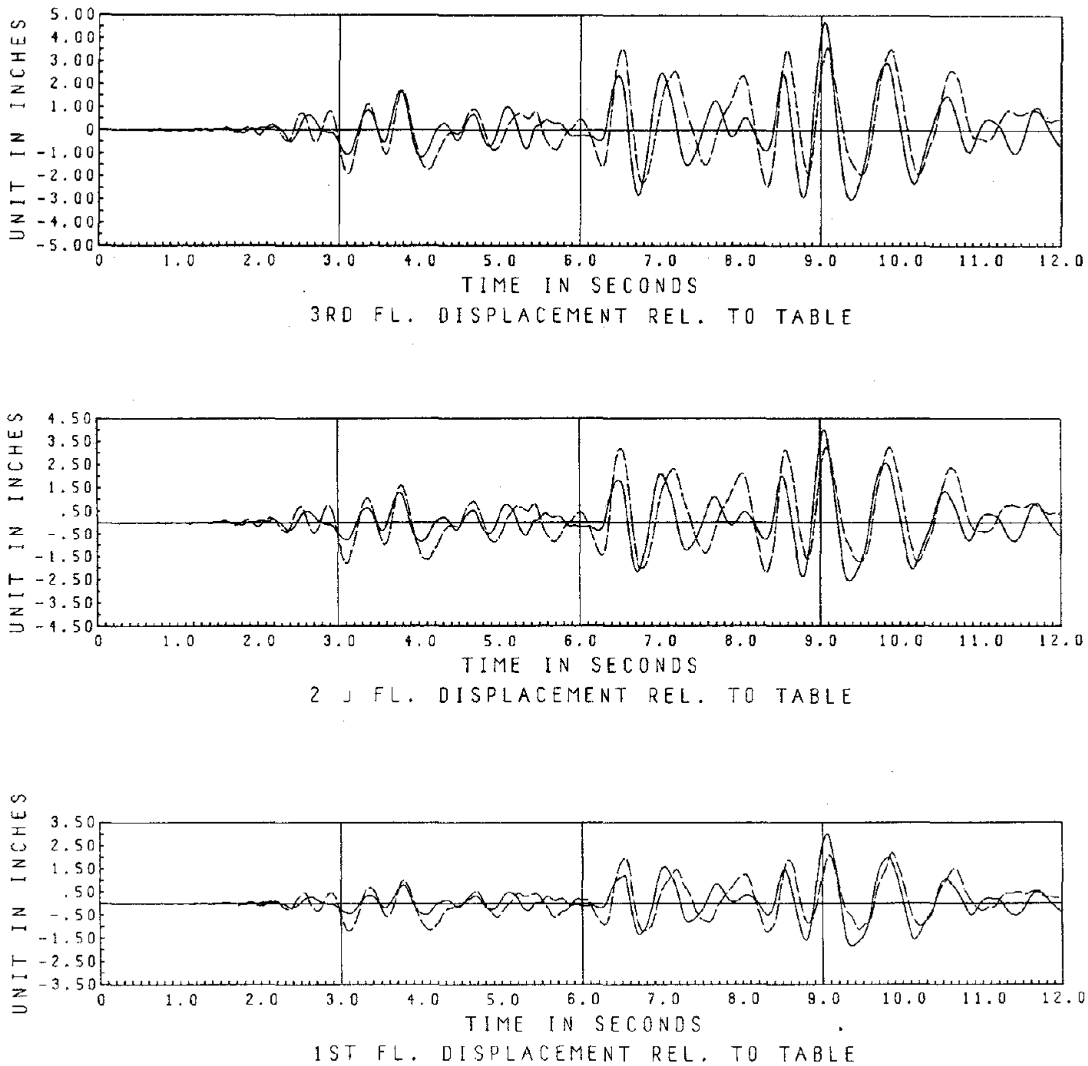

PACOIMA RECORD-1..129 G S , ROD DIAGONALLY BRACED FRAME
CALCULATED RESULT IN SOLID LINE,MEASURED RESULT IN DASH LINE

Fig. 6.1c.1 Correlation of Floor Displacements - Model 3

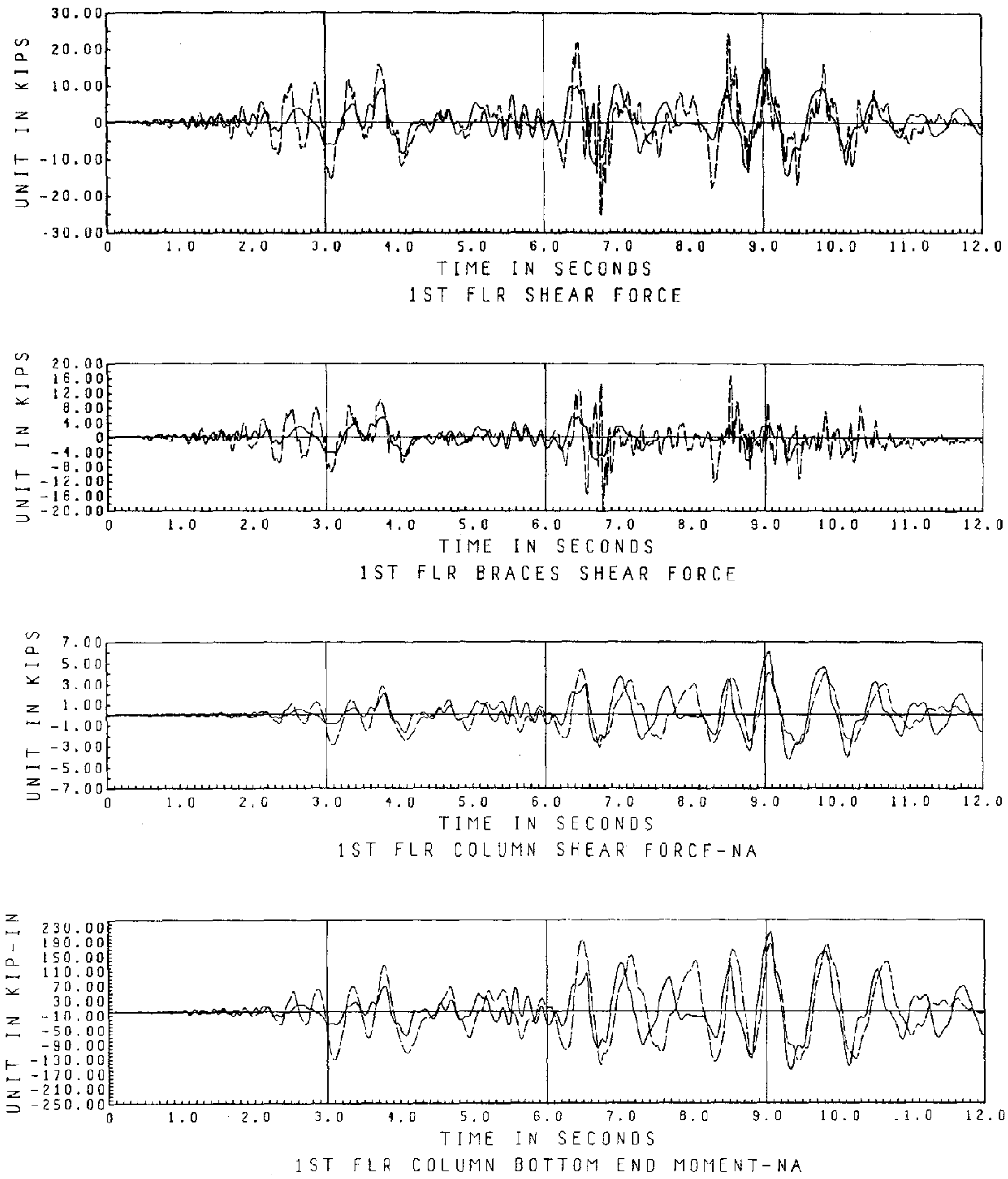

PACOIMA RECORD-1.129 G S , ROD DIAGONALLY BRACED FRAME
CALCULATED RESULT IN SOLID LINE, MEASURED RESULT IN DASH LINE

Fig. 6.1c.2 Correlation of Global and Local Forces - Model 3

6.2 Pipe Bracing System

The experimentally determined force-displacement relationship of the pipe bracing members, obtained in the El Centro test, is given in Fig. 5.2b.4. These hysteresis plots indicate that pipe braces with intermediate slenderness ratios have a significant compression strength and can dissipate energy in their post-buckling region. The model used in the analysis of rod braces does not reflect the actual behavior of pipe braces after they have buckled, thus it cannot be used in the inelastic analysis of these elements. Similarly, a brace mechanism which yields in compression, as assumed by the DRAIN-2D truss element, greatly overestimates the ability of a brace to dissipate energy and is not suitable for the pipe braces.

An accurate brace mechanism should include the post-buckling displacement behavior of pipe braces; such an element was developed originally by Nilforoushan(6) and then modified by Roeder and Popov(7). The brace model of Reference 7 is a linear approximation of the true behavior of bracing members as shown in Fig. 6.2.1, and has been adapted for use in the program DRAIN-2D. In this model, nine linear zones which are defined by the strain history and other critical parameters, are used in the approximation. The critical parameters are input values and they are specified by experimental results, by theoretical derivation or by other acceptable means. Although this general model can be used in the modelling of pipe braces, it was felt that a simplified version is more useful for practical purposes. Therefore, using this general model, a model with a smaller number of linear zones, shown in Fig. 6.2.2, was developed. The results of analytical studies based on this model are presented in the following subsections.

6.2a Correlation with El Centro Span 400 - Model 4

The mathematical model used to represent the pipe braces (Fig. 6.2.2) includes the hystersis effects of both tension yielding and compression buckling. The critical input parameters were determined from experimental results. The model of the structure with pipe braces, depicted in Fig. 6.2.3, is similar to the previous models except for the braces, but with the addition of dynamic axial force P-Δ effects which were included in the second floor columns. This addition was made because of the larger axial forces induced in these columns by the bracing members.

In this analysis, the damping coefficient proportional to the initial stiffness was set at $\beta_o = 0.007$ to obtain the desired first mode damping ratio of 6 percent. Also, a stiffness of 400 kips/in. was selected for the vertical shaking table spring supports to obtain a proper frequency match. Correlation between the analytical results obtained with this model and experimental data of the El Centro span 400 test is shown in Figs. 6.2.4 and 6.2.5. Agreement between analysis and experiment is considered to be good, especially considering that significant buckling occurred in the braces, as shown in Fig. 5.2b.4. Thus the modified bracing member hysteresis mechanism proved to be fairly good.

6.2b Correlation with Pacoima Span 400

To predict response to the Pacoima test with span 400, the previous model (Model 4) was employed with minor adjustments. The main change was associated with the buckling capacity of the first floor pipe braces. Because the braces had suffered buckling and yielding in earlier tests, it was determined that the residual buckling strength of the damaged first floor braces was only 3 kips.

In this analysis, the damping coefficient proportional to the initial stiffness was set at $\beta_o = 0.004$ corresponding to a first mode damping ratio of 3 percent and the stiffness of the shaking table compliance springs was estimated to be about 300 kips/in. Correlation between the results computed with this model and the experimental data of the Pacoima test are shown in Figs. 6.2.6 and 6.2.7. Agreement between analysis and experiment is considered excellent, particularly considering that the first floor braces buckled repeatedly and consequently induced a significant pinching effect, as shown in Fig. 5.2c.5. In addition, significant yielding occurred in the first floor columns. The greatest discrepancy in the analytical results is in the shear forces; this deviation resulted from assuming the bracing stiffness to vanish after tensile yielding occurred.

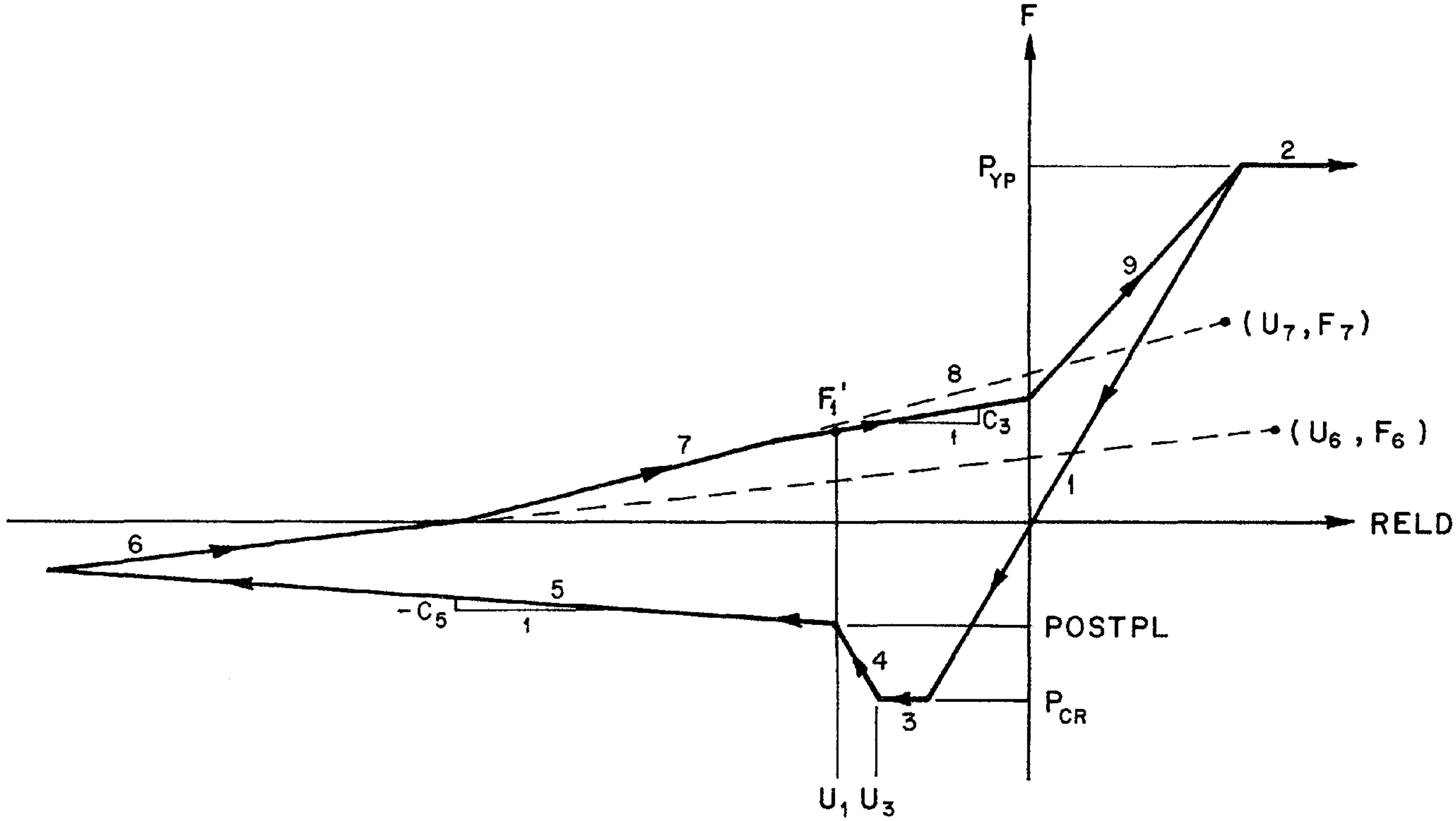

Fig. 6.2.1 Force-Displacement of Post-Buckling Brace Element (after Roeder and Popov)

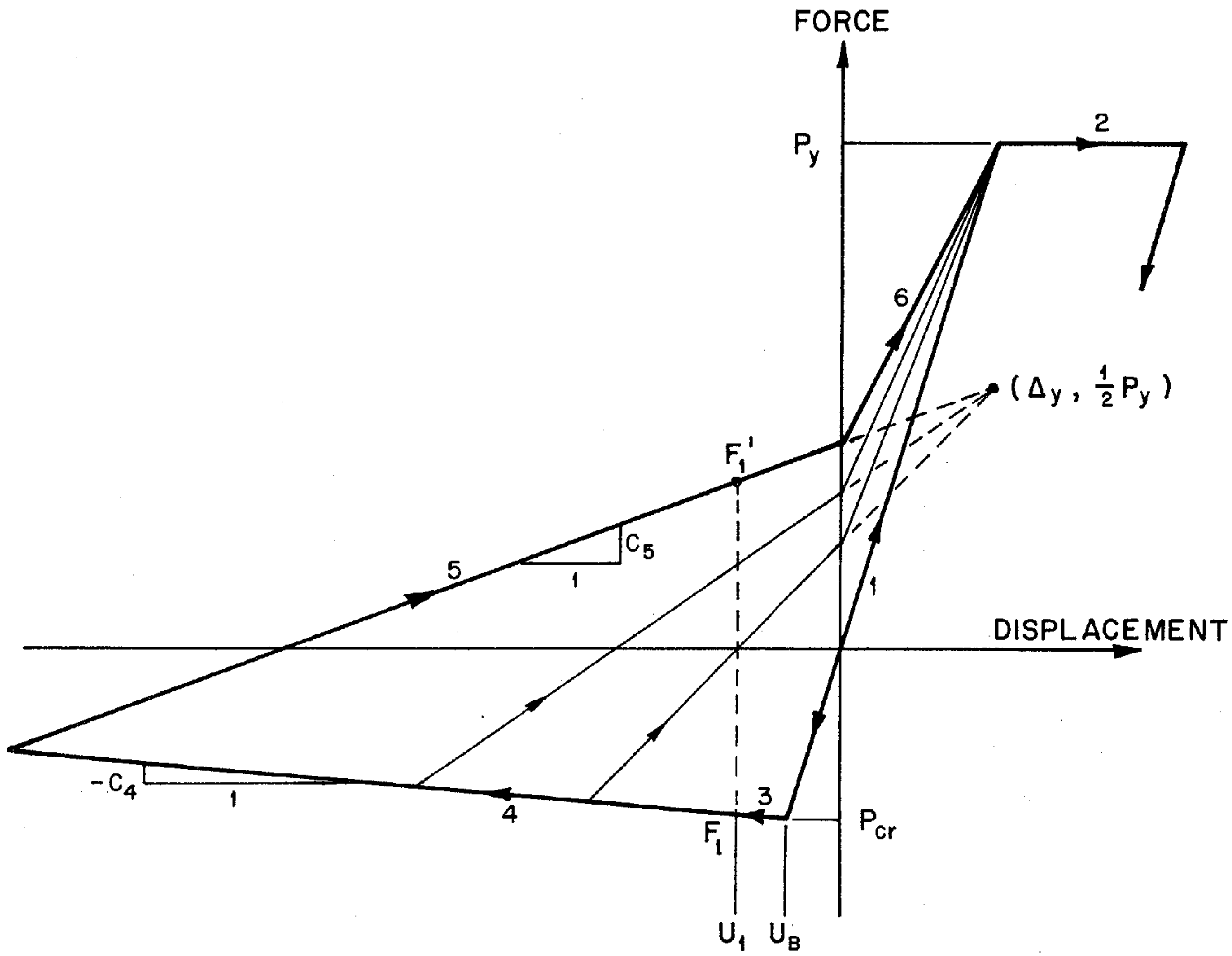

Fig. 6.2.2 Proposed Force-Displacement Model for Pipe Bracing Members

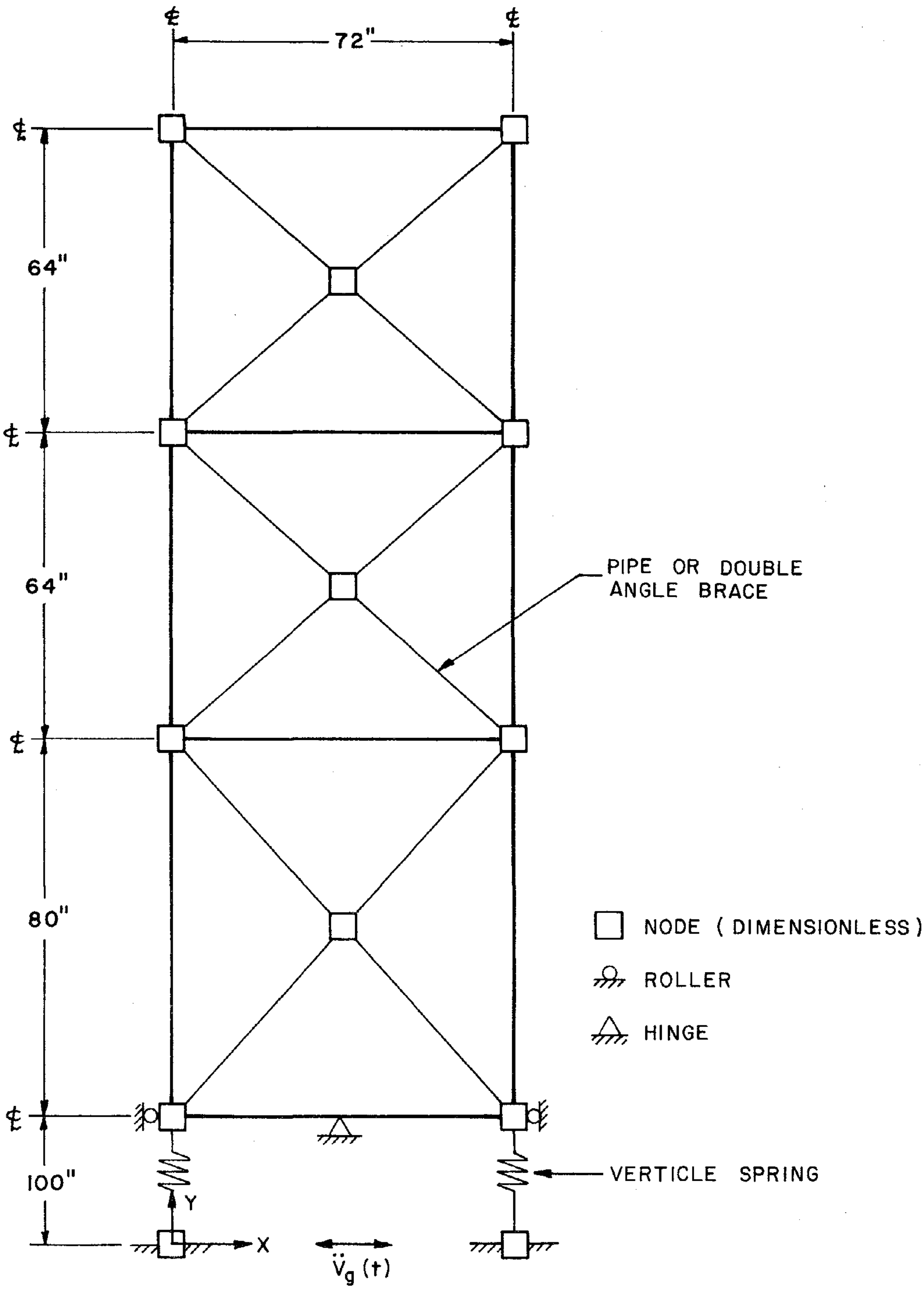

Fig. 6.2.3 Mathematical Model for Pipe and Double Angle Braced Structures

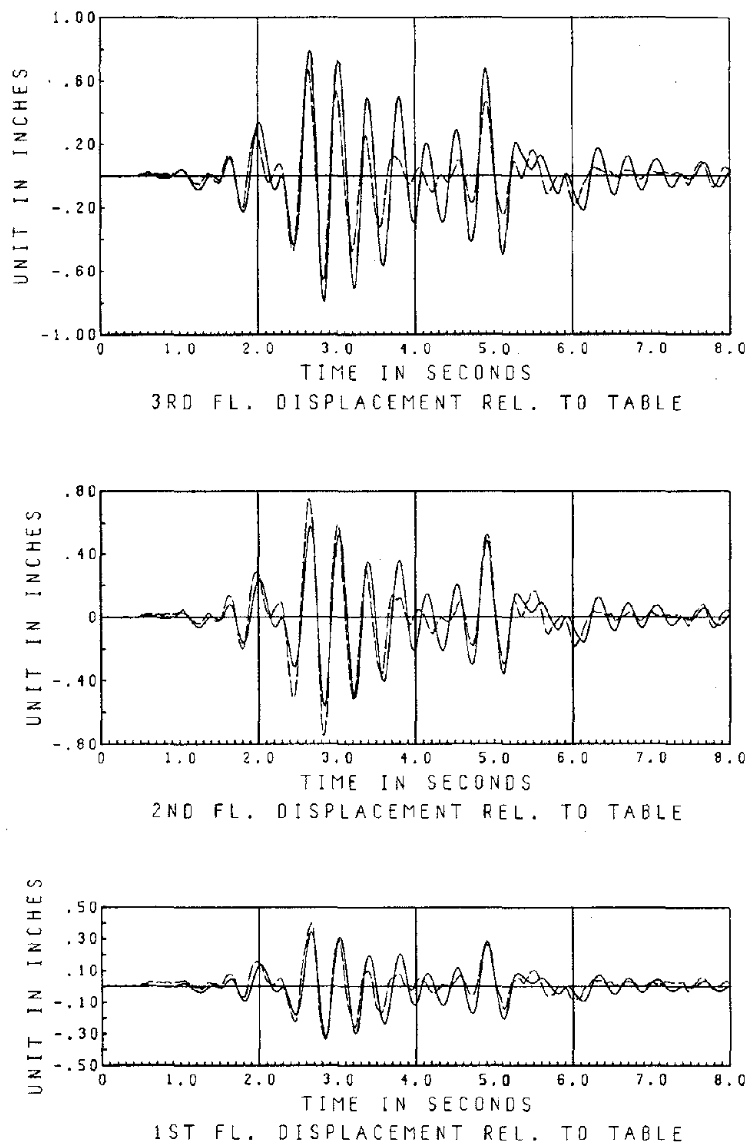

EC SPAN 400 , PIPE DIAGONALLY BRACED FRAME
CALCULATED RESULT IN SOLID LINE,MEASURED RESULT IN DASH LINE

Fig. 6.2.4 Correlation of Floor Displacements

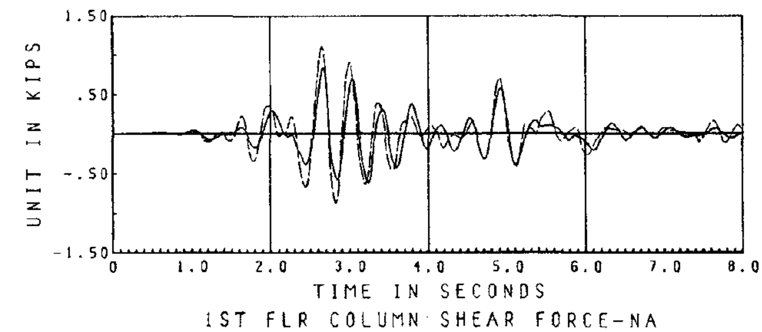

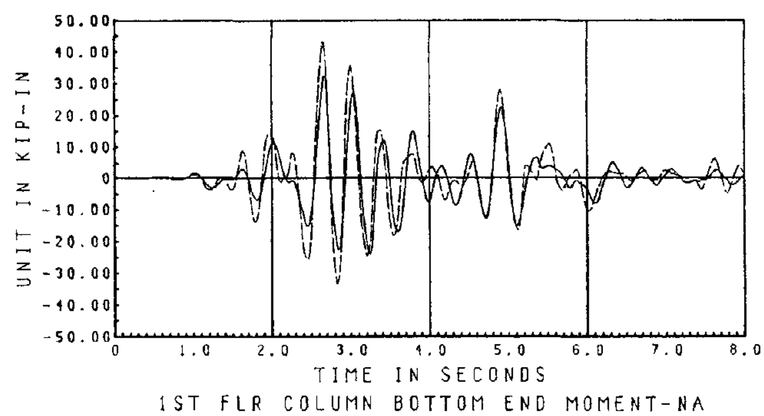

EC SPAN 400 , PIPE DIAGONALLY BRACED FRAME
CALCULATED RESULT IN SOLID LINE,MEASURED RESULT IN DASH LINE

Fig. 6.2.5 Correlation of Column Forces

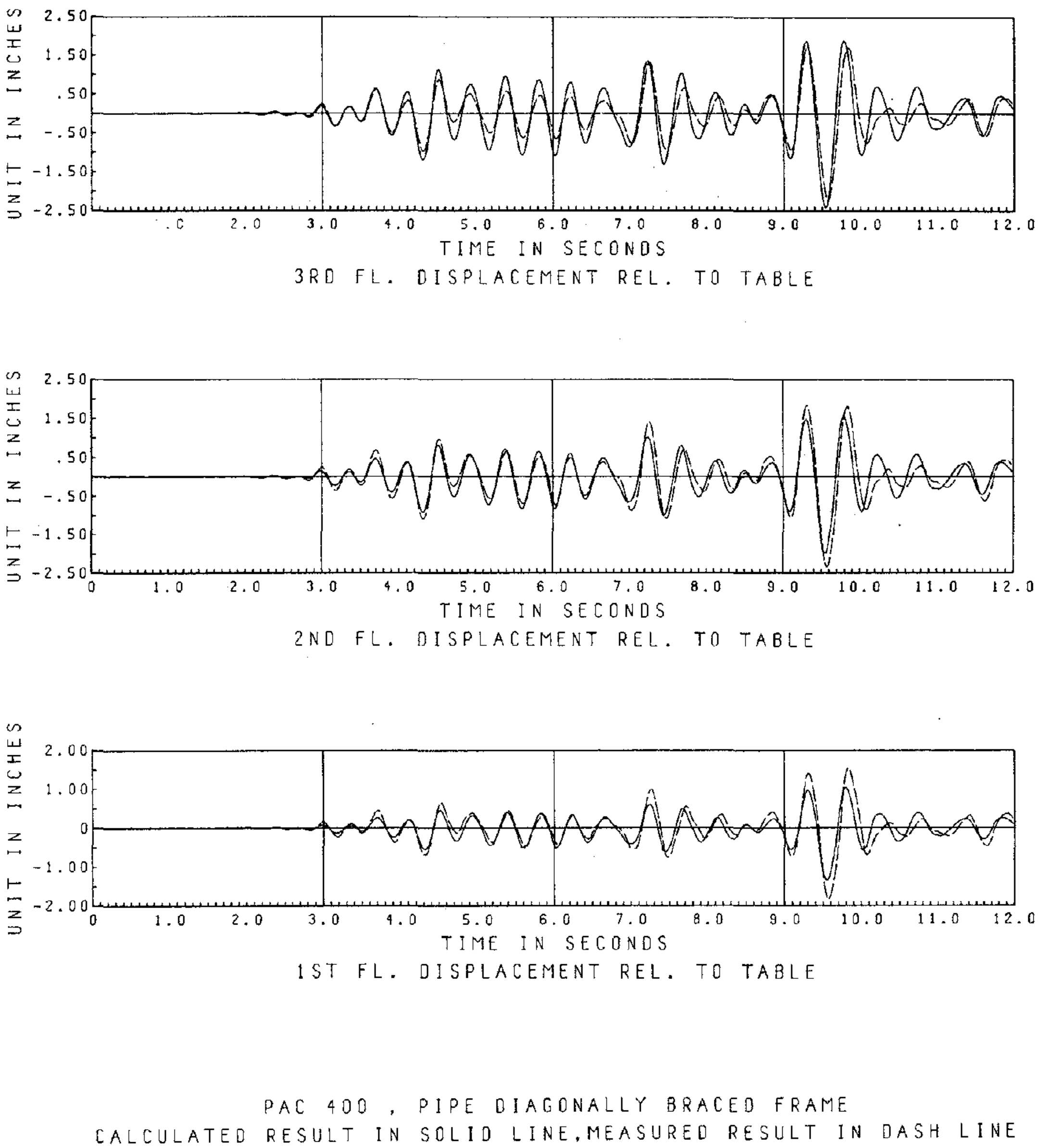

Fig. 6.2.6 Correlation of Floor Displacements

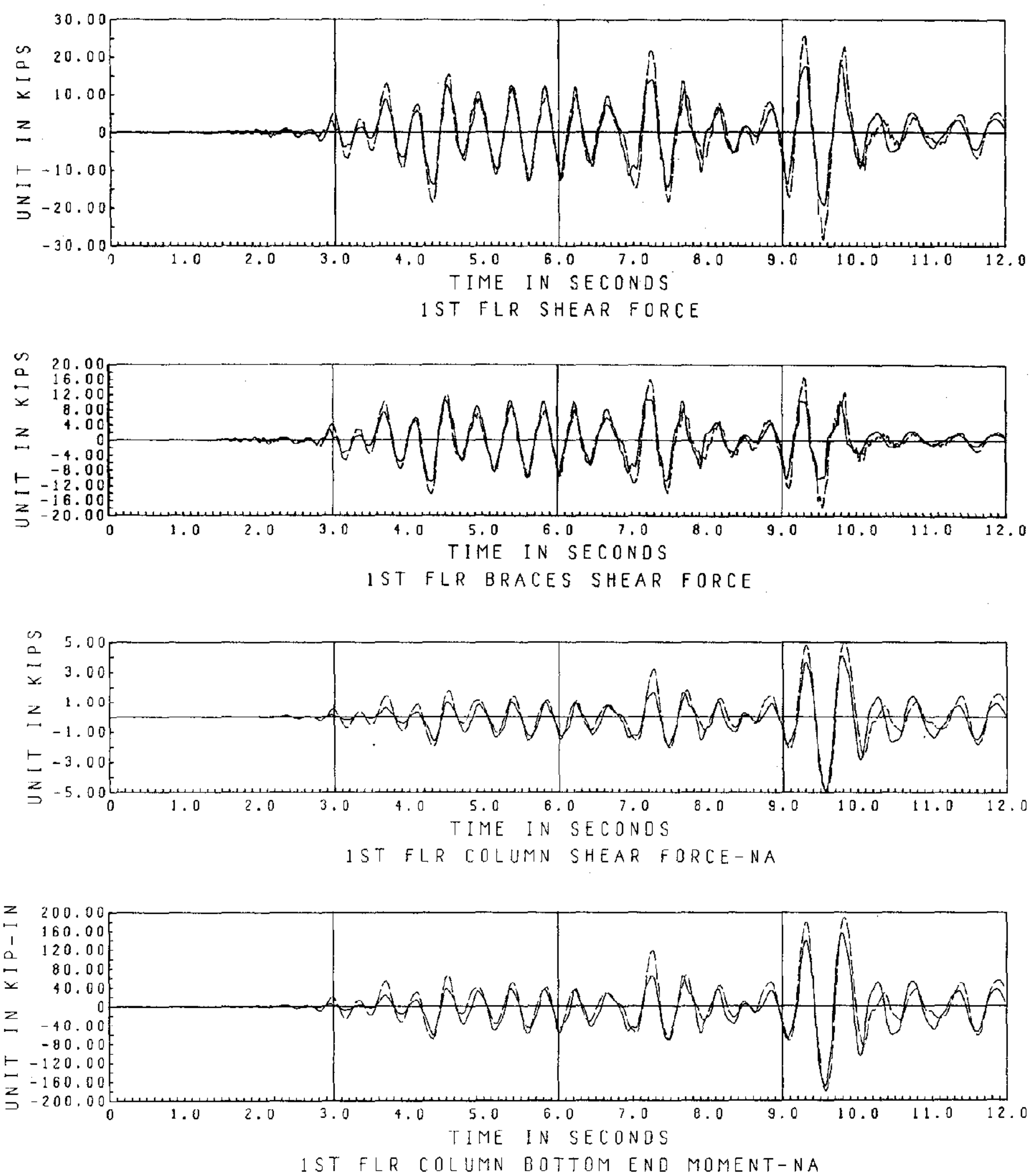

PAC 400 , PIPE DIAGONALLY BRACED FRAME
CALCULATED RESULT IN SOLID LINE,MEASURED RESULT IN DASH LINE

Fig. 6.2.7 Correlation of Global and Local Forces

6.3 Double Angle Bracing System

The mathematical model developed for the structure with double angle braces was similar to the pipe brace model (Model 4) except for the hysteresis mechanism of the bracing members. A preliminary analysis indicated that the hysteresis model used in the pipe bracing system was not suitable for the double angle braces, and buckling element of Reference 10 shown in Fig. 6.3.1 was selected. This hysteresis model is described fully by Jain and Goel[10]. It includes two significant characteristics of a brace; residual elongation, and reduction in compressive strength with number of cycles. These parameters are especially important in braces with small slenderness ratios. The input parameters of this model are fewer and were directly determined from the experimental results of the El Centro span 900 test described in Section 5.3b.

In this analysis, the damping coefficient proportional to the initial stiffness was set at $\beta_o = 0.0044$ to obtain the desired first mode damping ratio of 5 percent. Also, the stiffness of the shaking table spring support was set at 600 kips/in. to account for the shaking table-structure interaction. Correlation between the results calculated with this model and measured results of the El Centro span 900 test described earlier are shown in Figs. 6.3.2 and 6.3.3. Both global and local quantities of the analytical model are in good general agreement with the experimental values, and the peak values have been predicted fairly well. This correlation is considered excellent, especially considering that the first floor angles had been distorted slightly during earlier tests; therefore, the selected buckling element is regarded as satisfactory.

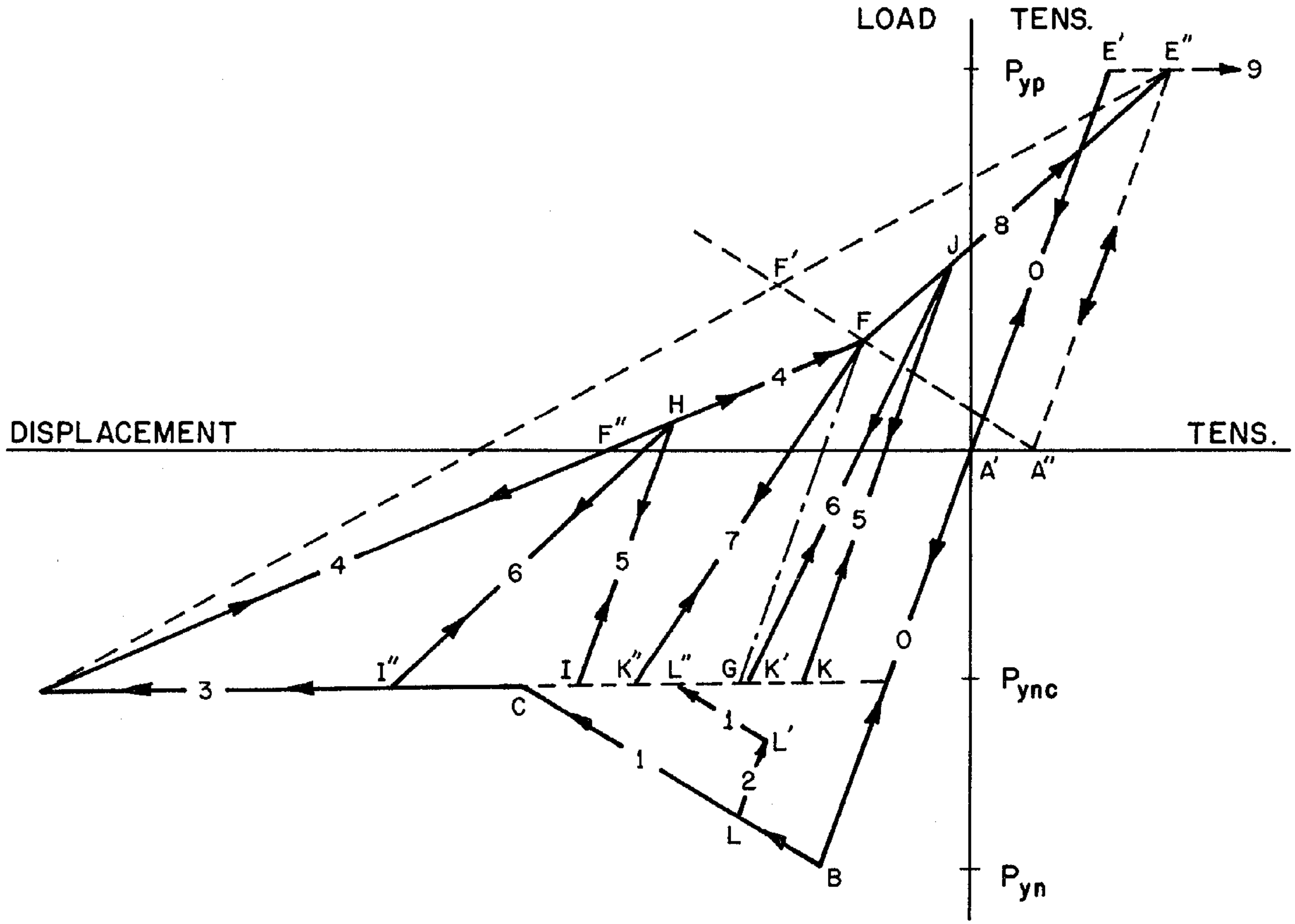

Fig. 6.3.1 Axial Hysteresis Behavior of Double Angle Braces
(after Jain and Goel)

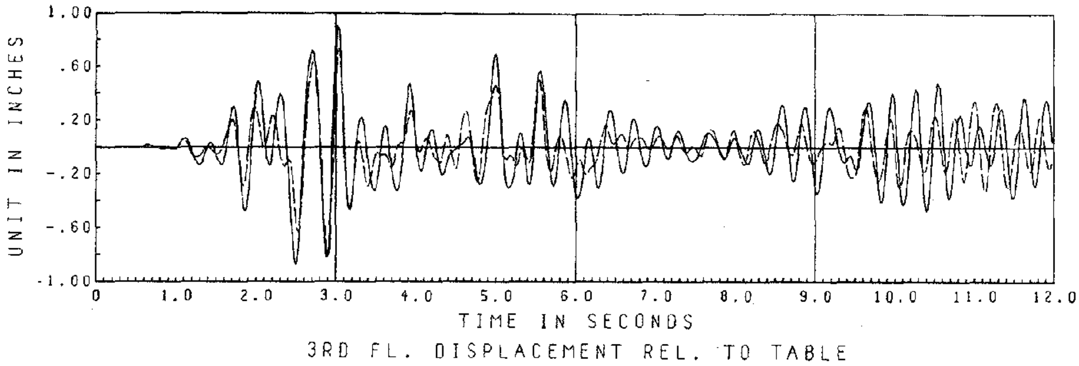

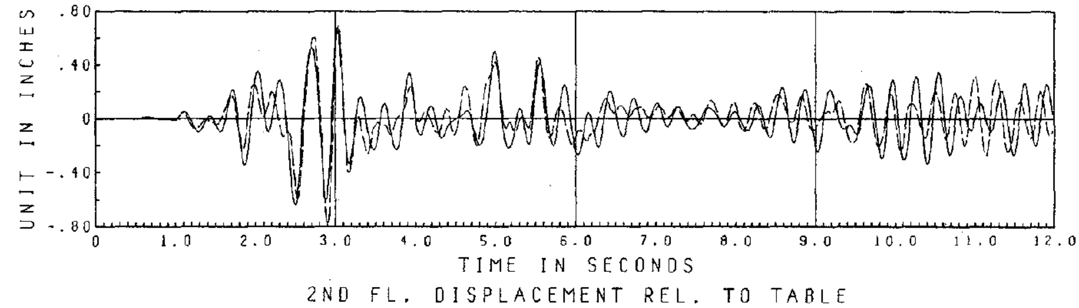

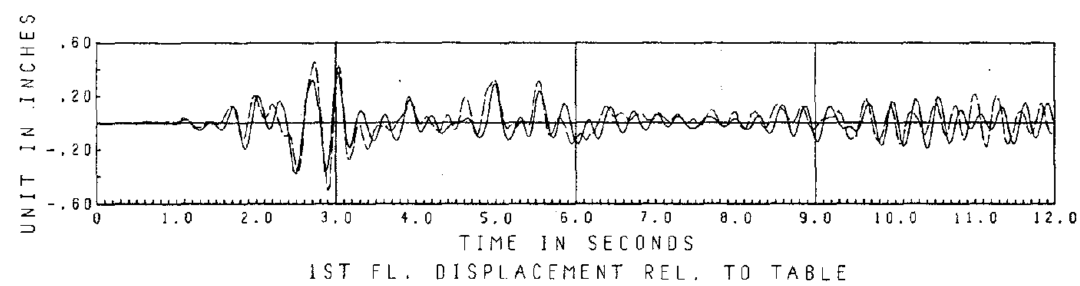

EL CENTRO SPAN 900 , ANGLE DIAGONALLY BRACED FRAME
CALCULATED RESULT IN SOLID LINE,MEASURED RESULT IN DASH LINE

Fig. 6.3.2 Correlation of Floor Displacements

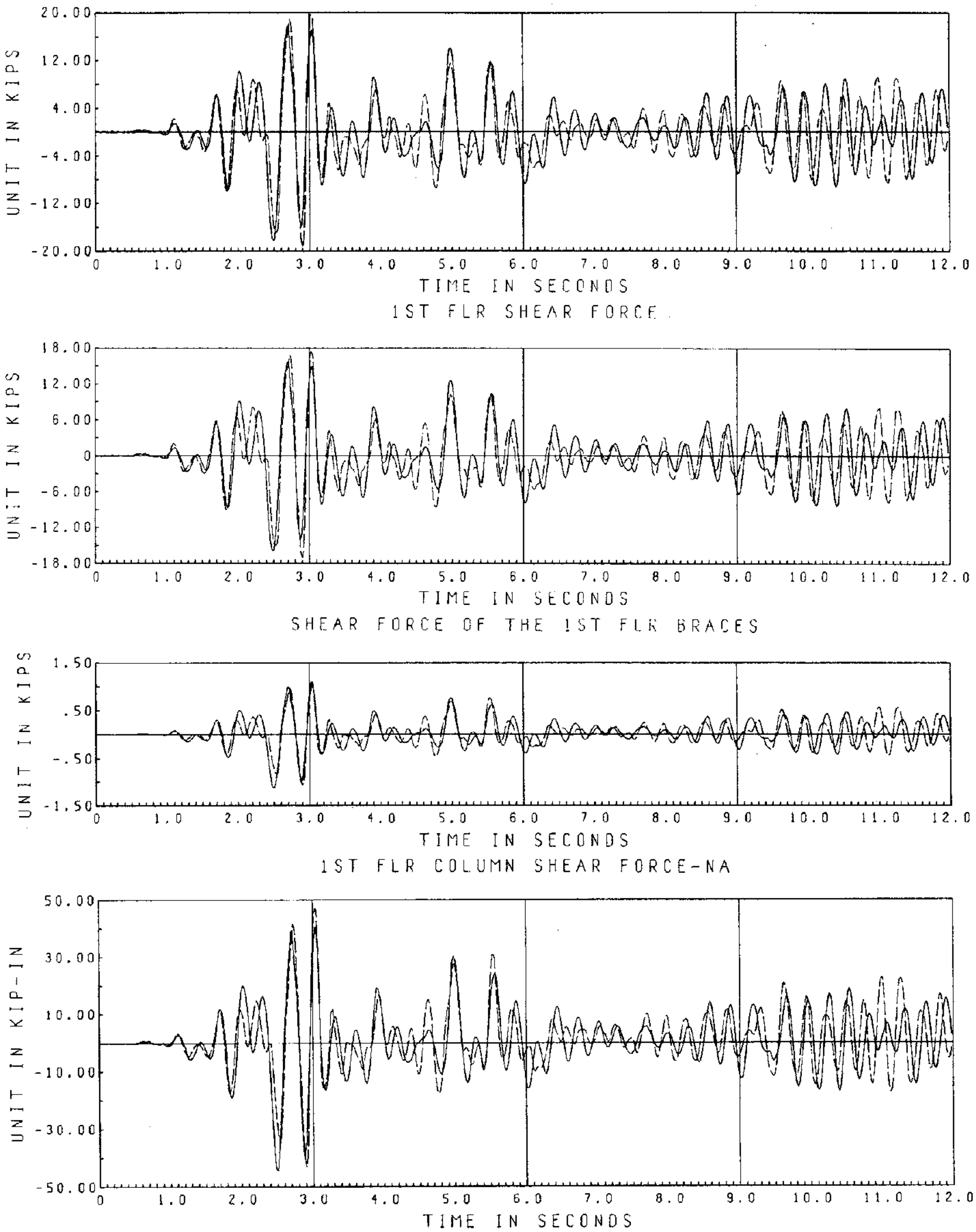

EL CENTRO SPAN 900 , ANGLE DIAGONALLY BRACED FRAME
CALCULATED RESULT IN SOLID LINE, MEASURED RESULT IN DASH LINE

Fig. 6.3.3 Correlation of Global and Local Forces

6.4 Unbraced Frame

The mathematical model developed for the unbraced moment-resistant frame is shown in Fig. 6.4.1. Note that eight semi-rigid connection elements have been introduced at the beam-to-column connections, and at the column ends in this model. These elements were used to model the type of joint connection shown in Fig. 3.2.3, to account for the significant angle change which occurred between the connected beams and columns. Each semi-rigid connection is connected to two nodes, and is influenced only by the relative rotational displacement between the nodes. The rotational stiffnesses of these connections were determined by frequency analysis of the mathematical model, treating them as the unknown parameters. To perform this frequency analysis, an explicit stiffness matrix formulation corresponding to the mathematical model was derived. All matrix operations were performed by the Symbolic Matrix Interpretive System (SMIS), a computer program described in Reference 17. In this process, the stiffness properties of all structural components except those of the semi-rigid connections were kept unchanged. Then, by varying the stiffness of the connections, a trial and error procedure was used until a close match was obtained between the frequency of the analytical model and that of the actual structure. The resulting rotational stiffness of the connections was then utilized in the dynamic response analysis of the unbraced frame model.

6.4a Correlation with El Centro Span 400

The model depicted in Fig. 6.4.1 was used to predict the results of the El Centro span 400 test. In this analysis, an initial stiffness-dependent damping coefficient of $\beta_o = 0.018$ was selected to provide the desired first mode damping ratio of 6 percent. The stiffness properties of the various members used in the frequency analysis were 400 kips/in. for the vertical spring supports, 15,900 kip-in./rad for the beam-to-column connection joint, and 30,000 kip-in./rad for the connection joint of the column ends. Bilinear hysteresis behavior was assumed for all members except for the vertical supports which were treated as elastic axial members. Figure 6.4.2 shows that the predicted floor displacements obtained with this model appear to correlate adequately with the observed floor displacements of the El Centro test. These results are considered to be fairly good; more accurate matching is only possible using a mathematically optimized system identification method, which is beyond the scope of this study.

6.4b Correlation with Pacoima Span 400

The response of the unbraced structure to the Pacoima span 400 earthquake, as described in Section 4.5b, was nonlinear and induced significant column yielding. These results were used to examine the applicability of the model discussed above for predicting the response of severely nonlinear cases. In this analysis, the same initial stiffness-dependent damping coefficient of $\beta_o = 0.018$ provided the first mode damping ratio of 6 percent. The stiffness values of the various structural components were kept the same except that of the vertical spring supports. This stiffness was reduced to 300 kips/in. to represent the more intense response behavior. Figures 6.4.3 and 6.4.4 show the correlation between the calculated and the measured results. Both global and local quantities are in excellent agreement. Note that the column moments were predicted quite accurately despite the assumed bilinear behavior instead of a more relistic curvilinear mechanism. Thus, based on the assumptions made, this correlation is regarded as excellent and the model is adequate.

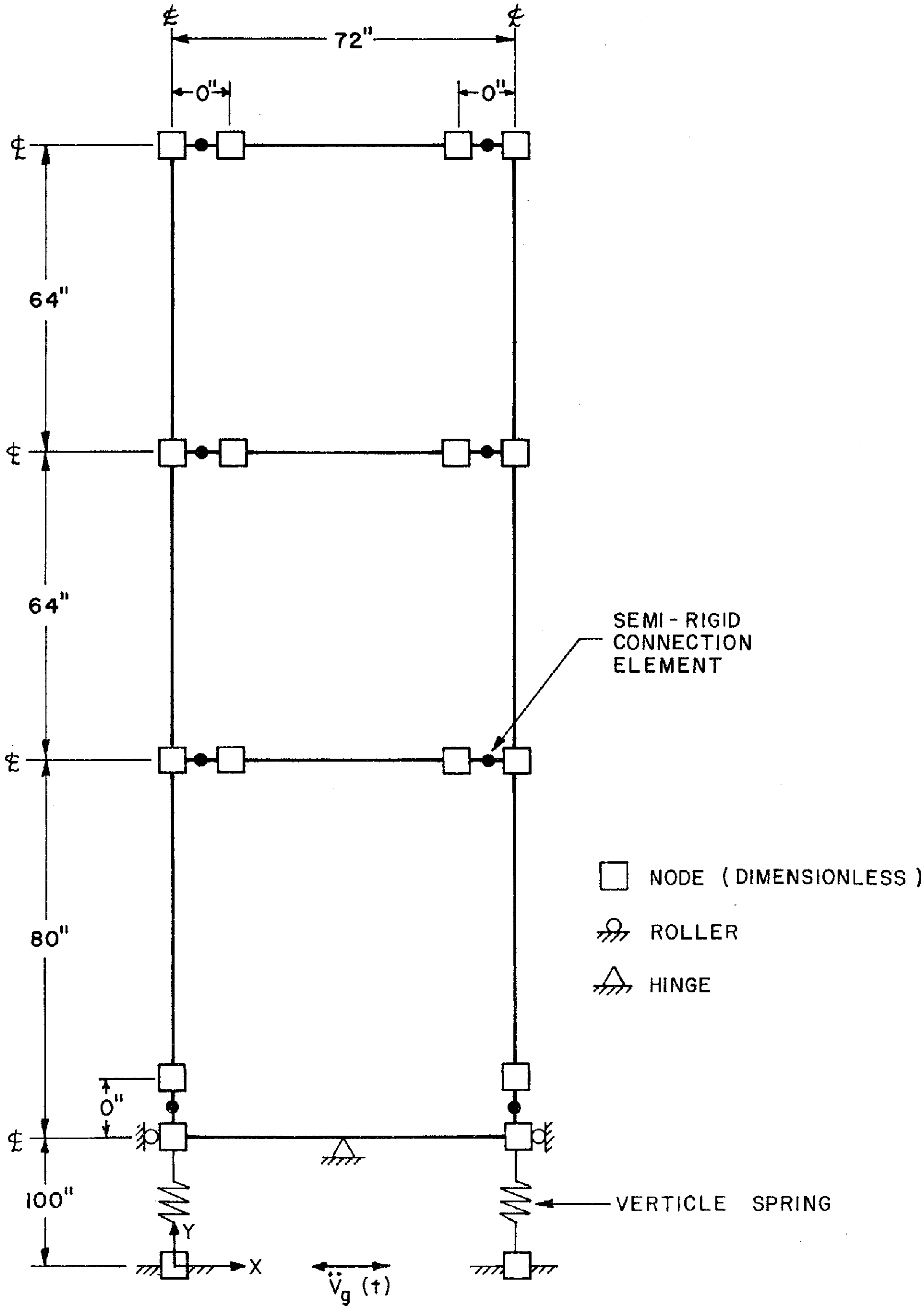

Fig. 6.4.1 Mathematical Model for Unbraced Frame

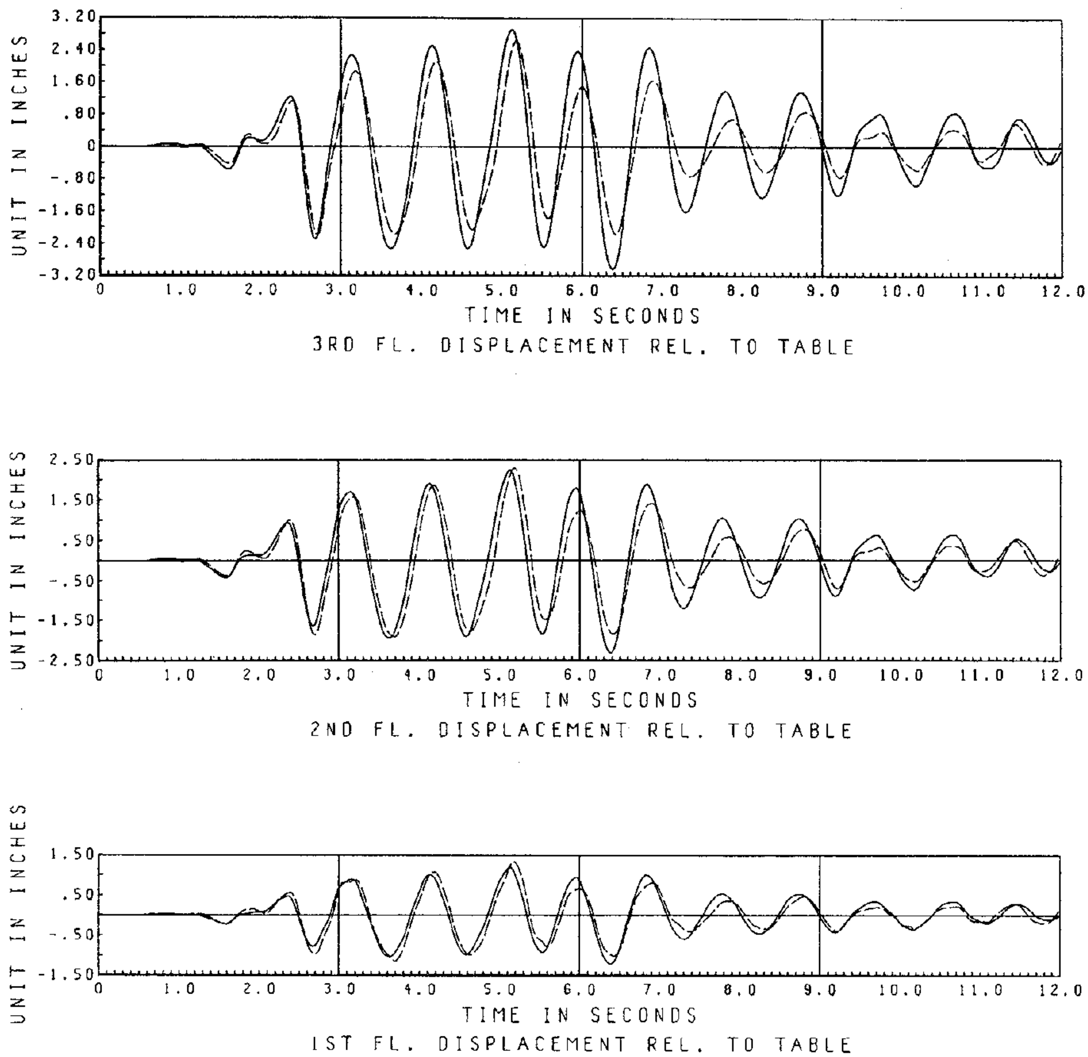

EL CENTRO SPAN 400 , UNBRACED FRAME
CALCULATED RESULT IN SOLID LINE,MEASURED RESULT IN DASH LINE

Fig. 6.4.2 Correlation of Floor Displacements

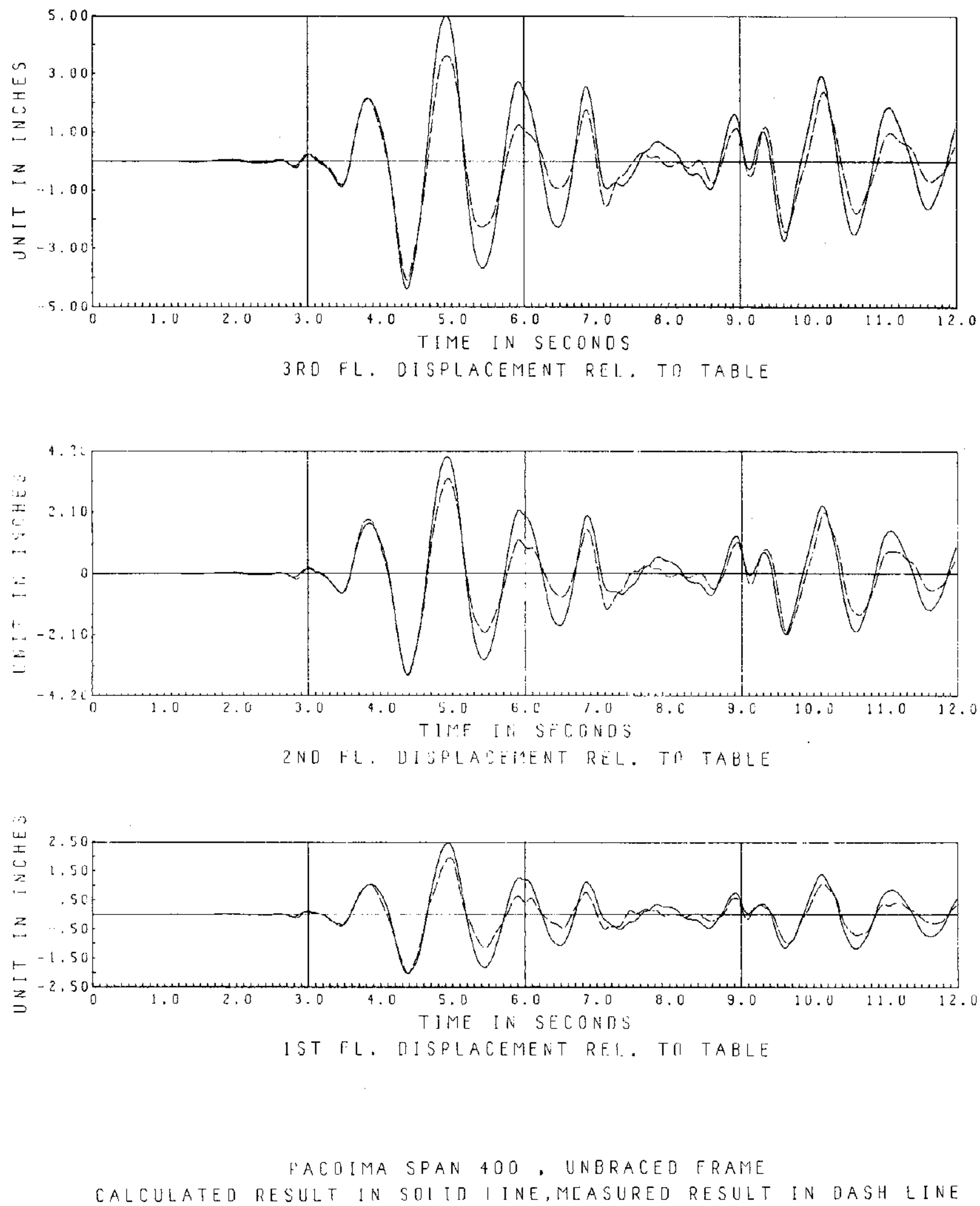

Fig. 6.4.3 Correlation of Floor Displacements

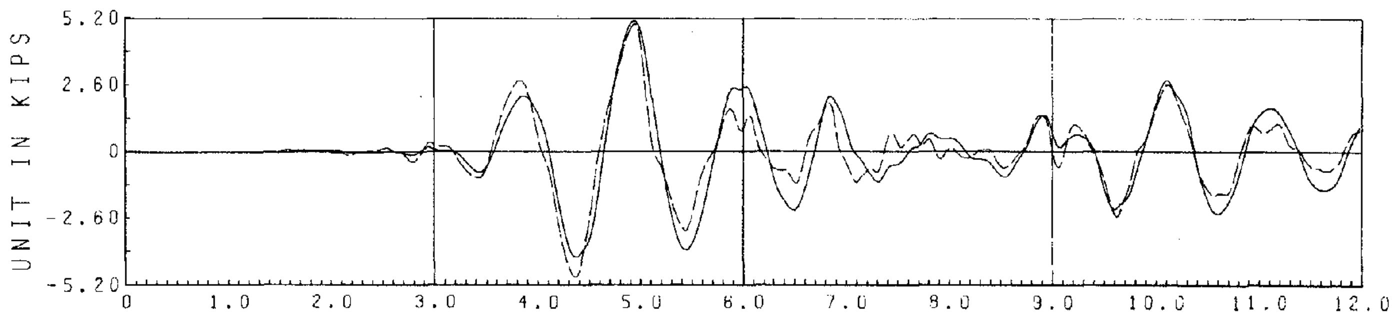

TIME IN SECONDS
1ST FLR COLUMN SHEAR FORCE-NA

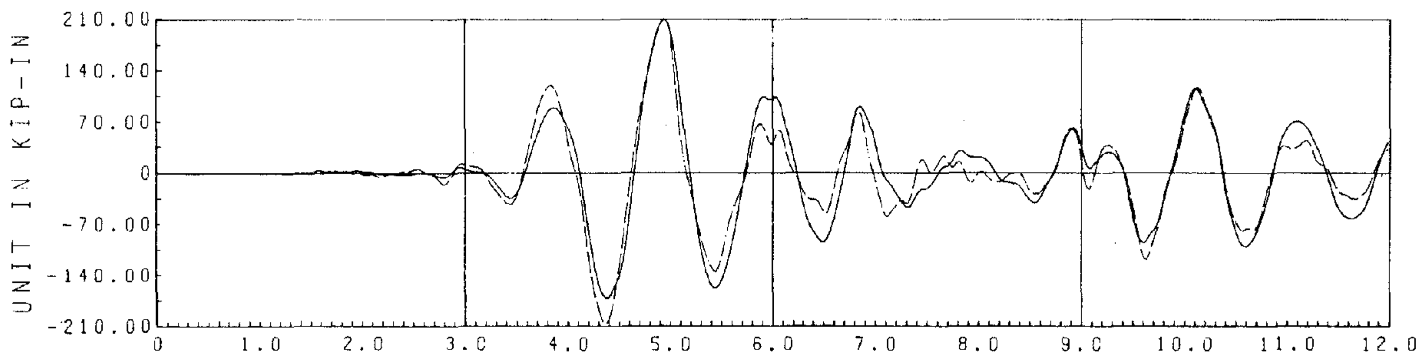

TIME IN SECONDS
1ST FLR COLUMN BOTTOM END MOMENT-NA

PACOIMA SPAN 400 , UNBRACED FRAME
CALCULATED RESULT IN SOLID LINE,MEASURED RESULT IN DASH LINE

Fig. 6.4.4 Correlation of Column Forces

7. COMPARISON OF DIFFERENT BRACING SYSTEMS

The experimental results presented in Chapter 5 cannot be directly used in a comparison of the seismic efficiency of the bracing systems considered in this study, because each structure was tested under different load conditions and/or was subjected to the earthquake motions in a different sequence and with different intensities. However, the mathematical models developed in Chapter 6 satisfactorily predicted the experimental response of each structure. Thus, it was decided to apply the same analytical procedures to predict the seismic response of unbraced frame, rod, pipe, and double angle braced structures under identical dead loads and identical earthquake motions. In these analyses, all four structures were loaded with 17 kips dead load per floor and were subjected to motions patterned after the El Centro earthquake record. These anlaytical results were then used to compare the seismic behavior and efficiency of each structure.

The maximum calculated floor drifts and lateral forces were selected for purposes of comparison, and they are displayed versus the peak acceleration of the input motions in Figs. 7.1 to 7.6. In general, the largest floor drifts and largest floor shear forces were associated with the unbraced (the softest) and the double angle braced (the stiffest) structures, respectively. The first floor drifts of the rod braced structure were the largest among the bracing systems and became relatively close to those of the unbraced structure as the slacking mechanism developed in rod members during moderate earthquake motions (about 0.3 g peak acceleration). Rupture of the rod braces started during motions with a peak acceleration of about 0.5 g (see Fig. 7.1). At the second floor level, the drifts of the rod bracing system were also relatively large due to the same type of behavior, but the slacking and rupture occurred at the second floor during higher input intensities (see Fig. 7.2). Yielding of the third floor rods was minor and no rupture occurred at this level, so drifts were relatively smaller than those of the unbraced frame.

The floor drifts of the pipe and double angle bracing systems were the smallest despite their frequent buckling and/or yielding during the moderate and strong input motions. In fact, the pipe and particularly the double angle braces were very effective in limiting the floor drifts even at an input peak acceleration of 0.8 g, and their strength loss was not significant at this level.

Although the pipe and double angle braces were efficient in reducing the floor drifts, as shown in Figs. 7.4 to 7.6, they provided larger floor shear forces. However, this behavior is tolerable considering that the major portion of these lateral forces were resisted by the bracing members, and the plastic deformations in the main structural components such as the columns were correspondingly reduced. The lowest floor shear forces were associated with the unbraced frame, but they were resisted only by the columns. In this case the shear resisting capacity of the first floor was estimated to be about 11 kips per frame, with plastic hinges formed at the column ends during a peak acceleration of 0.775 g. At this same input intensity, plastic hinges were not formed at the column ends of the pipe and double angle braced structures. Thus, even though the lateral forces of the unbraced frame were not as large as those of the braced structures, the columns suffered significant plastic deformations and the resulting lateral drifts were larger than what can be considered tolerable. Damage of the non-structural components such as the partitions as well as of the major structural members would be greatest in this type of construction.

The shear forces of the rod braced structure were about the same magnitude as those of the pipe and double angle braced structures for low intensity motions (up to 0.2 g) even though the rod bracing provided a softer system. This was due to the fact that the participation of the columns in the shear resistance was more significant in a system with lighter braces having low compressive capacity. As was mentioned earlier, the efficiency of the rod braces diminished as their slacking behavior developed during moderate earthquake motions, and they ruptured in response to stronger excitations. Accordingly, the resisting force capacity of the rod braced structure decreased and was limited to about 14 kips per frame even with complete participation of the columns, this behavior resembled the response of the unbraced structure.

To provide a more useful comparison and to evaluate the efficiency of the bracing systems, the floor drifts of the different systems were also compared with the drift limits allowed by the Uniform Building Code[13] and the Applied Technology Council (ATC) regulations[18]. The UBC requires that the lateral deflections or drifts of a story relative to its adjacent stories shall not exceed 0.005 times the story height, and the allowable drifts according to the seismic design regulations provided by the ATC shall not exceed 0.015 times the story height. The limits for both codes are shown in Figs. 7.1 to 7.3.

According to the UBC requirements, the unbraced structure should not be subjected to motions with peak accelerations greater than 0.07 g. This limits the applicability of this type of structure to very low intensity earthquake regions where only elastic response is expected. The newly developed ATC seismic design regulation, which considers the modern concept of ductility, modifies the UBC demand and allows the unbraced structure to be subjected to earthquakes with peak accelerations up to 0.2 g (see Fig. 7.1).

The rod bracing system, according to the UBC is limited to earthquakes with peak accelerations less than 0.12 g corresponding to the elastic behavior of the rod braces. On the other hand, under ATC regulations, rod bracing is beneficial up to a peak acceleration of 0.3 g. The pipe and double angle bracing systems satisfy the UBC requirements with great efficiency up to peak accelerations of 0.28 g and 0.34 g, respectively. At moderate to relatively strong motions they buckle and yield frequently, but their drifts do not exceed the ATC drift limits up to a peak acceleration of 0.68 g in the pipe system and 0.8 g in the double angle system. According to these results, the pipe brace and particularly the angle brace are very efficient and effective in controlling lateral displacements of the steel frame structure. But their efficiencies diminish during very strong earthquake motions as the braces undergo severe yeidling and buckling. For instance, the maximum first floor drift of the double angle braced structure was 2.22 in. in the Pacoima test described in Section 5.3c.

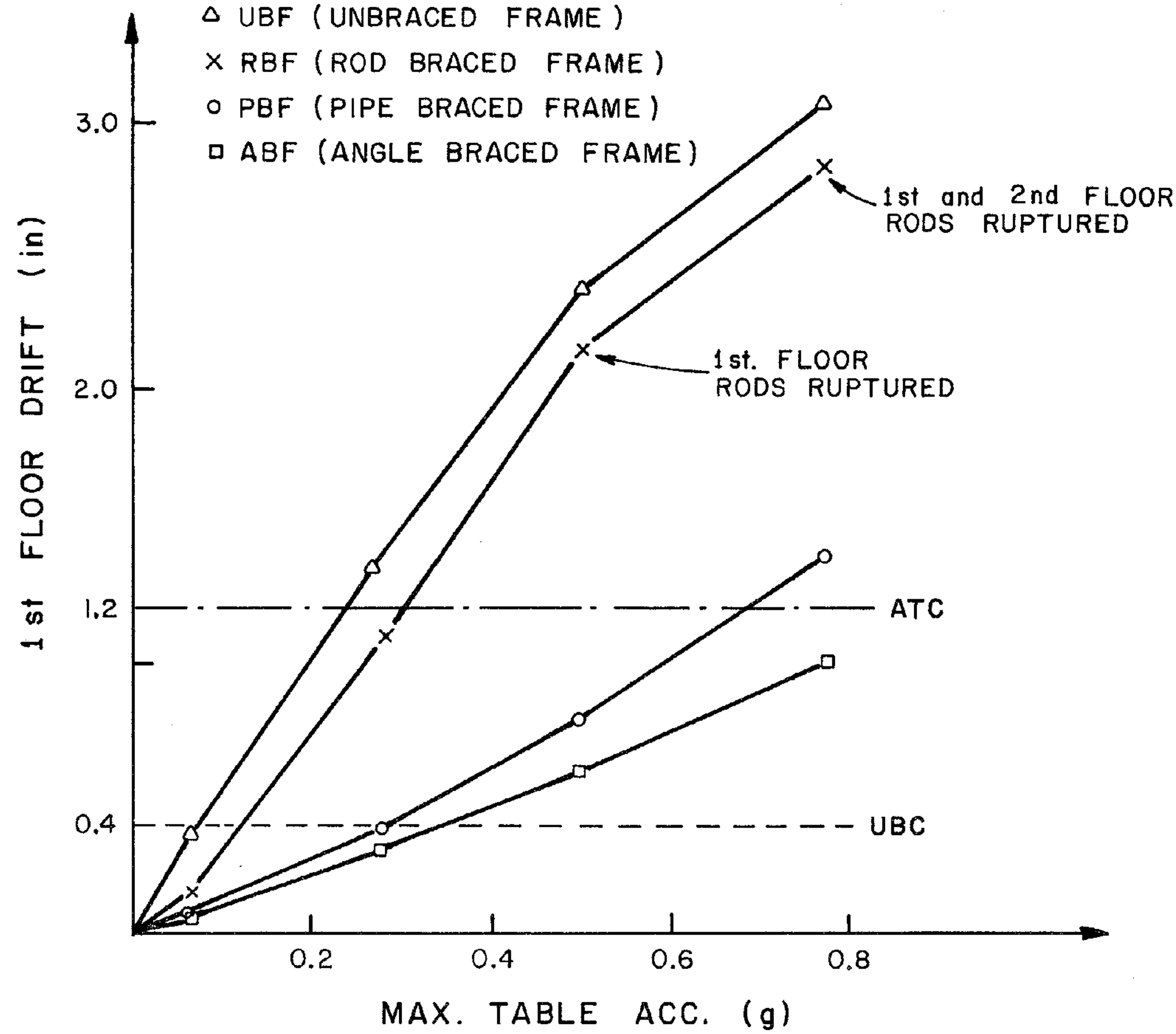

Fig. 7.1 Maximum 1st Floor Drift vs. Peak Table Acc.

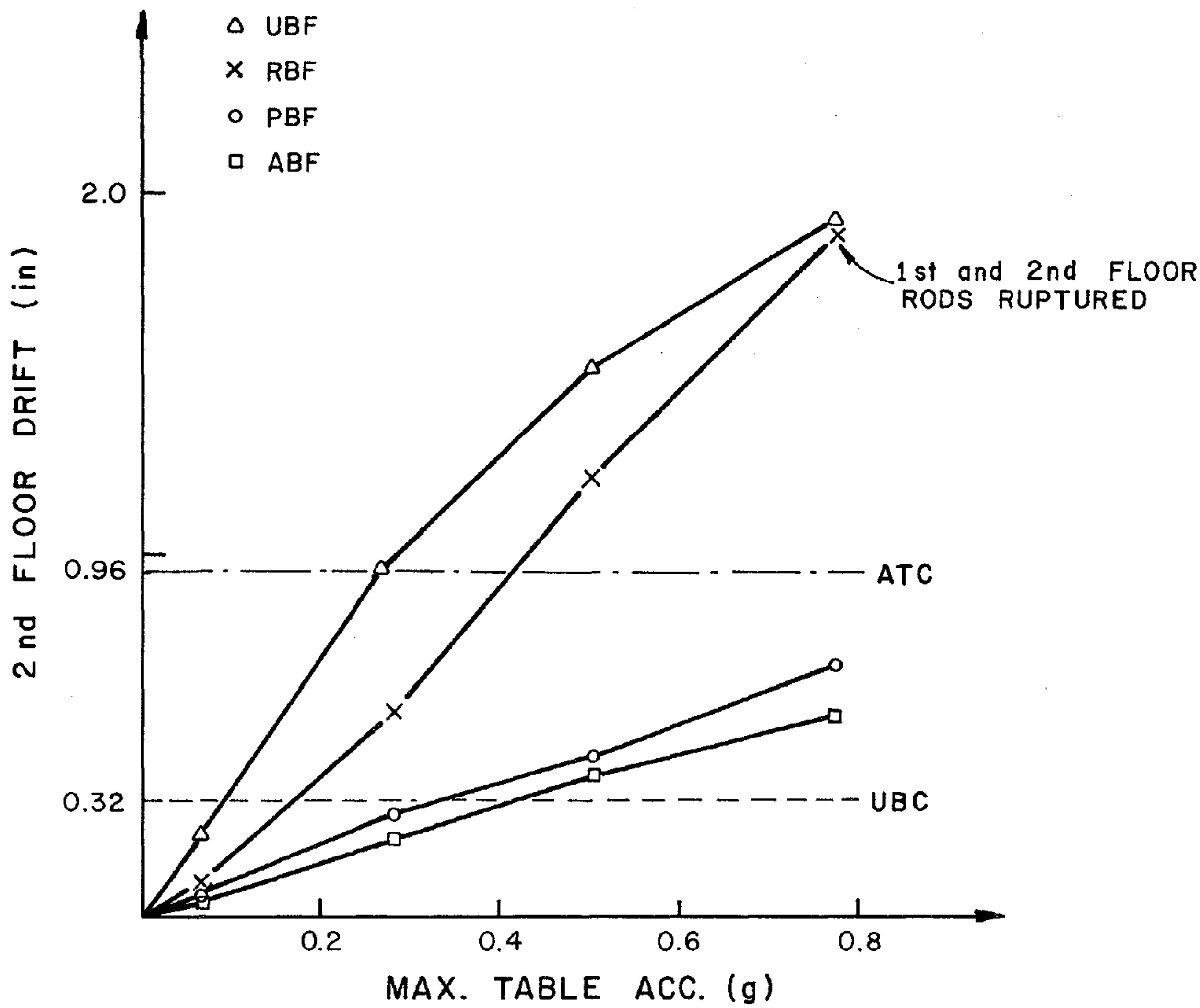

Fig. 7.2 Maximum 2nd Floor Drift vs. Peak Table Acceleration

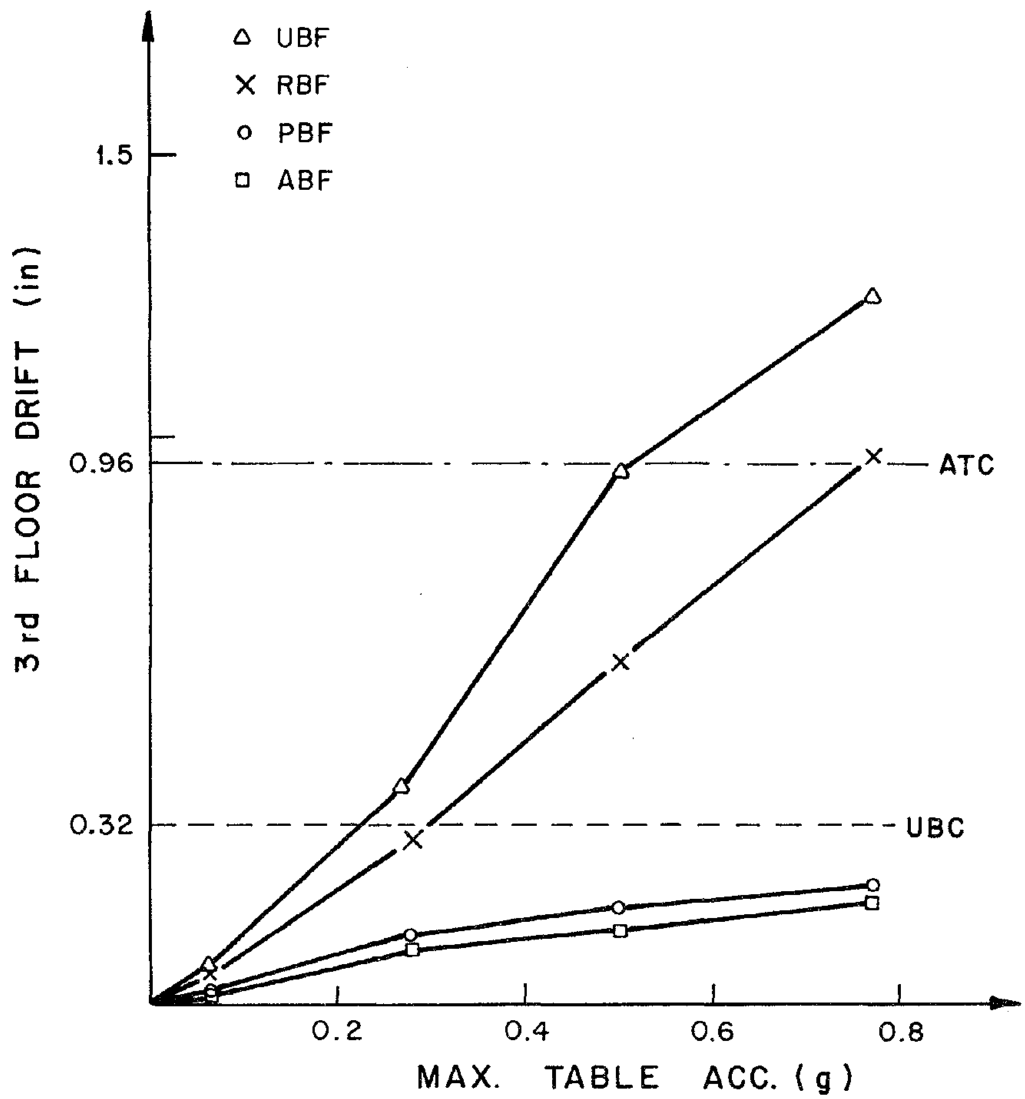

Fig. 7.3 Maximum 3rd Drift vs. Peak Table Acceleration

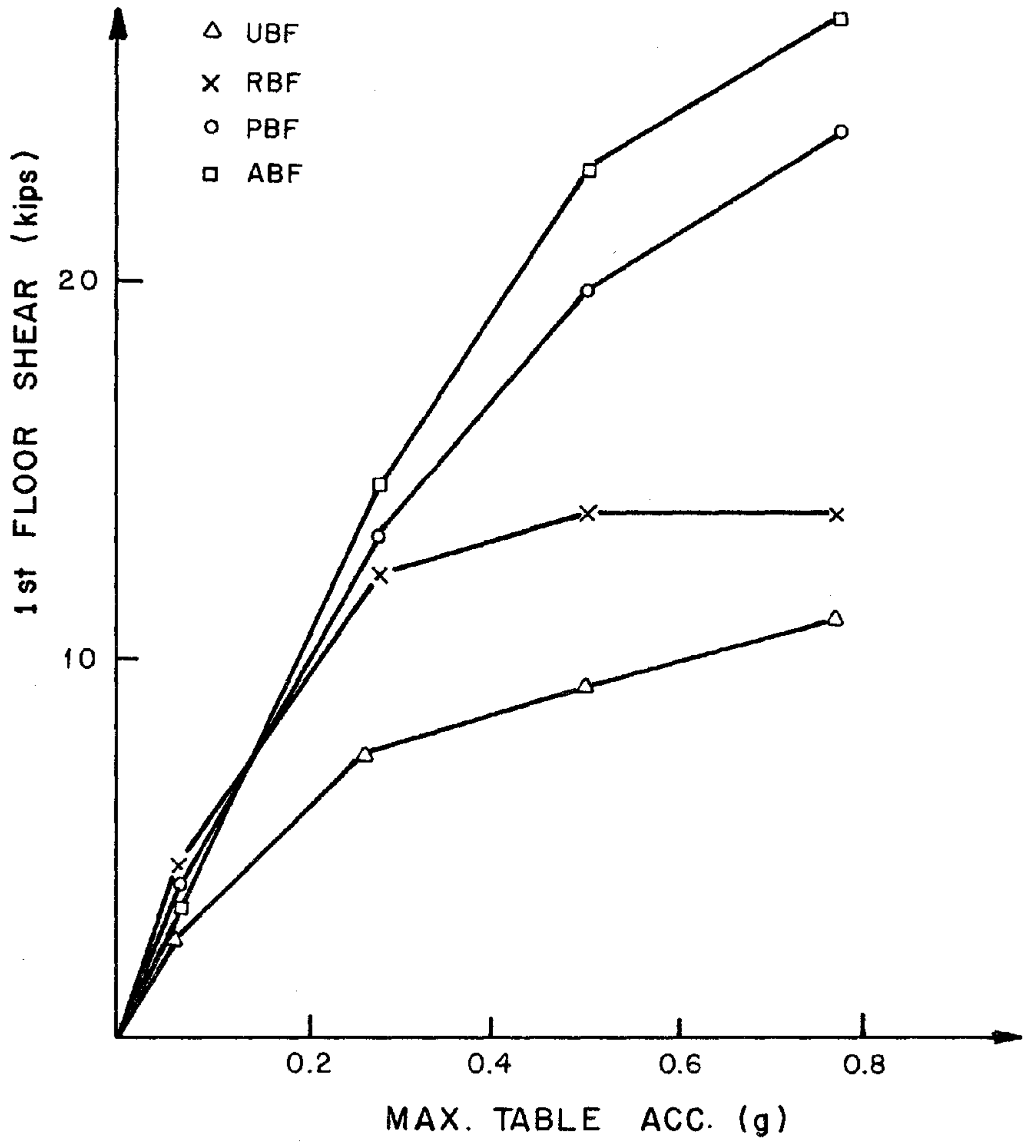

Fig. 7.4 Maximum 1st Floor Shear vs. Peak Table Acceleration

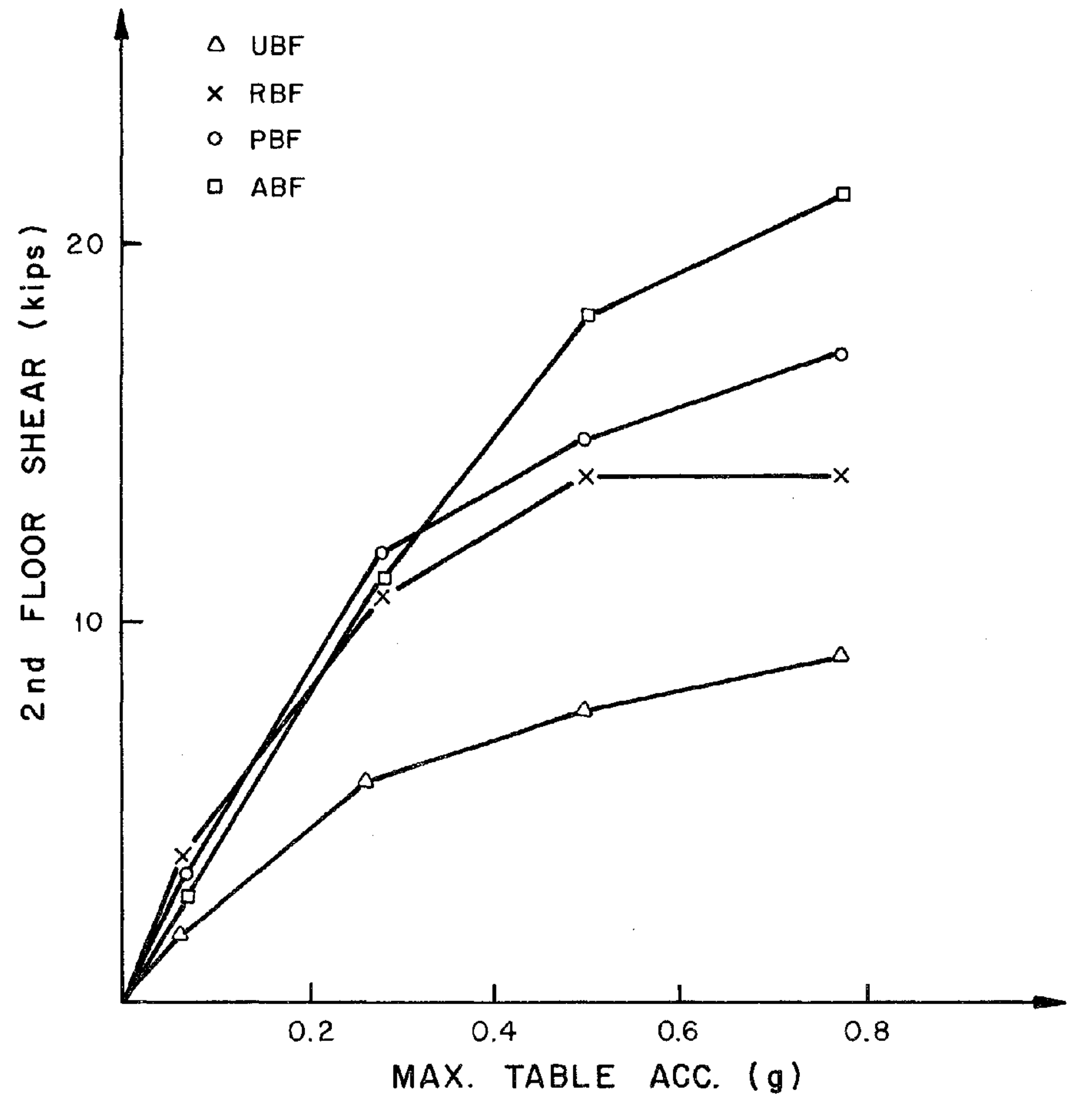

Fig. 7.5 Maximum 2nd Floor Shear vs. Peak Table Acceleration

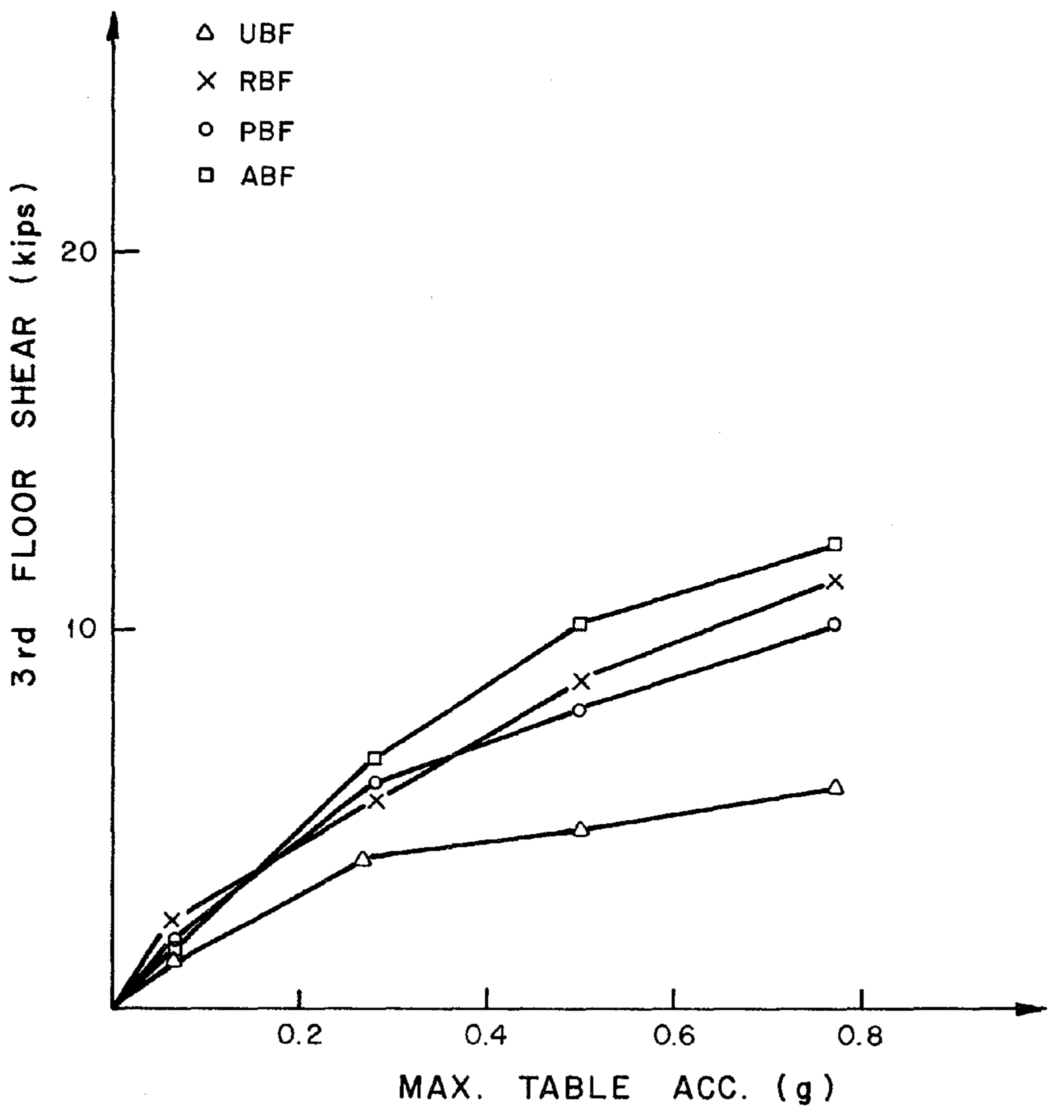

Fig. 7.6 Maximum 3rd Floor Shear vs. Peak Table Acceleration

8. CONCLUSIONS

This investigation demonstrated the seismic response behavior of steel frames with and without wind bracing and the feasibility of predicting the response by existing nonlinear frame analysis programs. The most important feature of the response behavior with rod braces is that pre-tension is lost during moderate earthquakes, leading to an impacting type response in the resulting slack rod system. As a result, the efficiency of rod braces diminishes and the story drifts of the structure become relatively large. For larger earthquakes, the rods may be expected to break during the successive impacts; but it is significant that the structure without braces may still survive the earthquake motions, if it is stable under the action of the static gravity loads.

The structures with pipe and double angle braces behave better because the pipes and double angles retain some significant compressive capacity after buckling. Thus, there is no slack response mechanism with associated impacting, and significant energy is absorbed by the braces in post-buckling displacement cycles. The pipe braces and the double angle braces each are quite effective in limiting story drifts during moderate and moderate-to-strong earthquakes, respectively. Their efficiencies reduce only for rather strong earthquakes as a "pinching" effect develops in the force-displacement hysteresis loops because of accumulated tensile yield deformations.

The lateral stiffness of the unbraced structure is very small so its story drifts are very large even for moderate earthquakes. The structure is not expected to collapse under strong earthquakes because the P-Δ effect for such a low rise structure is not large enough.

But, damage of the non-structural members such as partitions and also residual distortion of the columns may be very significant.

The results of this study show that supplemental diagonal wind bracing has a beneficial effect on the earthquake resistance of the steel frame structure because it tends to limit the story drifts and thus to reduce damage of both structural and non-structural components. However, each bracing type has its own limitations and specific recommendations can be made as follows:

1. Tension type wind braces with large slenderness ratios (greater than 200) and correspondingly low compressive capacity are only beneficial for wind loading and very low intensity earthquakes.

2. Compression type wind braces with intermediate slenderness ratios (less than 200) and compressive strength not less than 50 percent of the tension strength provide a bracing system which can also resist moderate earthquakes with great efficiency.

3. Compression type wind braces with slenderness ratios less than 100 and compressive strength not less than 50 percent of tension strength are very effective and beneficial for moderate-to-strong earthquakes.

Analyses made with the DRAIN-2D program showed generally good agreement with the experimental results. Rod bracing models simulated both tension yielding and elastic buckling behavior satisfactorily; the tension rod rupture mechanism was modelled least satisfactorily, but such ruptures also were found to be quite random in the experiments.

Hysteresis models of pipe and double angle bracing members included both tension yielding and post-buckling deflection behavior; the hysteresis model of the double angle braces also considered residual elongation and reduction in compressive capacity with number of cycles. Both the pipe and the double angle mathematical models proved to be satisfactory.

The analytical response prediction of the unbraced frame showed that angle changes in the joints between connected beams and column are significant in this type of construction, and should be included in the analysis.

This study indicated that diagonal cross bracing systems, such as pipe and double angle braces, are very efficient for moderate earthquakes and their energy dissipation will be significant if their compressive capacity is not less than 50 percent of their tension capacity. However, the energy dissipation characteristics of these diagonals may be less satisfactory during major earthquakes due to the pinching effect in the bracing hysteresis loops.

A braced frame suitable for resisting major ground motion may be achieved by using a split K-bracing system whose diagonal members have significant eccentricities. In such a system, the benefits of bracing elements to minimize drift (with consequent damage control and increased stability) are combined with the ductility of the moment-resistant frame. In addition, the split K-bracing system can be adapted to accommodate architectural requirements such as windows, doors, or utilities in the walls. The principles of the eccentric K-bracing system discussed here have not been verified by dynamic tests; but, it is believed that dynamic testing of a steel frame with split K-bracing members can provide significant information regarding the applicability of the concept.

REFERENCES

1. Clough, R. W., and Jenschke, V. A., "The Effect of Diagonal Bracing on the Earthquake Performance of a Steel Frame Building," Bulletin Seismological of America, Vol. 53, No. 2, Feb. 1963.

2. Hanson, R. D., and Fan, W.R.S., "The Effect of Minimum Cross Bracing on the Inelastic Response of Multistory Buildings, " Proceeding, IV World Conference on Earthquake Engineering, Santiago, Chile, Jan., 1969.

3. Workman, G. W., "The Inelastic Behavior of Multistory Braced Frame Structures Subjected to Earthquake Excitation," thesis presented to the University of Michigan, at Ann Arbor, Mich., in 1969, in partial fulfillment of the requirements for the degree of doctor of philosophy.

4. Goel, S. C., and Hanson, R. D., "Seismic Behavior of Multistory Braced Steel Frames," Journal of the Structural Division, ASCE, Vol. 100, No. ST1, January, 1974, pp. 79-95.

5. Popov, E. P., Takanashi, K., and Roeder, C. W., "Structural Steel Systems: Behavior Under Cyclic Loading," EERC Report 76-17, Earthquake Engineering Research Center, University of California, Berkeley, Calif., 1976.

6. Nilforoushan, R., "Seismic Behavior of Multistory K-Braced Frame Structures," Report No. UMEE 73R9, Department of Civil Engineering, The University of Michigan, Ann Arbor, Mich. Nov., 1973.

7. Roeder, C. W., and Popov, E. P., "Inelastic Behavior of Eccentrically Braced Steel Frame Under Cyclic Loading," EERC Report No. 77-18, Earthquake Engineering Research Center, University of California, Berkeley, Calif., August, 1977.

8. Kannan, A. E., and Powell, G. H., "DRAIN-2D...A General Purpose Computer Program for the Dynamic Analysis of Inelastic Plane Structures," EERC Report, Earthquake Engineering Research Center, University of California, Berkeley, Calif., Apr., 1973.

9. Singh, P., "Seismic Behavior of Braces and Braced Steel Frames," Report No. UMEE 77R1, Department of Civil Engineering, The University of Michigan, Ann Arbor, Mich., July, 1977.

10. Jain, A. K., and Goel, S. C., " Hysteresis Model for Steel Member Subjected to Cyclic Buckling or Cycling End Moment and Buckling," Report No. UMEE 78R6, Department of Civil Engineering, The University of Michigan, Ann Arbor, Mich., Dec., 1978.

11. Rea, D., and Penzien, J., "Dynamic Response of a 20' x 20' Shaking Table," Proceeding of the 5th World Conference on Earthquake Engineering , Rome, 1973.

12. Clough, R. W., and Tang, D., "Earthquake Simulator Study of a Steel Frame Structure Vol. I - Experimental Results," EERC Report No. 73-5, University of California, Berkeley, 1973.

13. Uniform Building Code, International Conference of Building Officials, Whittier, California, 1979 edition.

14. Specification for the Design Fabrication and Erection of Structural Steel for Buildings, American Institute of Steel Construction, New York, 1969.

15. Tentative Criteria for Structural Application of Steel Tubing and Pipe, D. R. Sherman, American Iron and Steel Institute, Washington, D. C., August, 1976.

16. Wilson, E. L., "FRMSTC-Static Load Analysis of Multistory Buildings," Computer Programming Series, SESM, University of California, Berkeley, Calif., 1967.

17. Wilson, E. L., "SMIS-Symbolic Matrix Interpretive System," SESM Report No. 73-3, University of California, Berkeley, Calif., Original April 1963, Modified January 1973.

18. Tentative Provisions for the Development of Seismic Regulations for Buildings, ATC Publication ATC 3-06, Applied Technology Council, June, 1978.

APPENDIX A

List of Data Channels

Channel No.	Name	Description
0	T/R ACC-1	Command Horizontal Acceleration Signal
1	T/R ACC-2	Command Vertical Acceleration Signal
2	CMD H DISP	Command Horizontal Displacement Signal
3	CMD V DISP	Command Vertical Displacement Signal
4	AV H T DISP	Average Horizontal Table Displacement
5	AV V T DISP	Average Vertical Table Displacement
6	AV H T ACC	Average Horizontal Table Acceleration
7	AV V T ACC	Average Vertical Table Acceleration
8	PITCH	Angular Acceleration in Pitching Mode
9	ROLL	Angular Acceleration in Rolling Mode
10	TWIST	Angular Acceleration in Twisting Mode
11	FORCE H1	Force in Horizontal Actuator
12	FORCE H2	Force in Horizontal Actuator
13	FORCE H3	Force in Horizontal Actuator
14	ACC H1	Horizontal Table Acceleration at Actuator H1
15	ACC H2	Horizontal Table Acceleration at Actuator H2
16	ACC V1	Vertical Table Acceleration at Actuator V1
17	ACC V2	Vertical Table Acceleration at Actuator V2
18	ACC V3	Vertical Table Acceleration at Actuator V3
19	ACC V4	Vertical Table Acceleration at Actuator V4
20	FORCE V1	Force in Vertical Actuator V1
21	FORCE V2	Force in Vertical Actuator V2

Table A-1 Data channel listing for diagonal rod bracing

Channel No.	Name	Description
22	FORCE V3	Force in Vertical Actuator V3
23	FORCE V4	Force in Vertical Actuator V4
24	DISP V1	Vertical Table Displacement at Actuator V1
25	DISP V2	Vertical Table Displacement at Actuator V2
26	DISP V3	Vertical Table Displacement at Actuator V3
27	DISP V4	Vertical Table Displacement at Actuator V4
28	DISP H1	Horizontal Table Displacement at Actuator H1
29	DISP H2	Horizontal Table Displacement at Actuator H2
30	DISP H3	Horizontal Table Displacement at Actuator H3
31	BLANK	
32	PS FORCE-1	Force in Passive Stabilizer
33	PS FORCE-2	Force in Passive Stabilizer
34	PS FORCE-3	Force in Passive Stabilizer
35	PS FORCE-4	Force in Passive Stabilizer
36	CLELG-NAOF	Column NA DCDT, Outside Face
37	CLELG-NAIF	Column NA DCDT, Inside Face
38	CLELG-NBOF	Column NB DCDT, Outside Face
39	CLELG-NBIF	Column NB DCDT, Inside Face
40	CLELG-SAOF	Column SA DCDT, Outside Face
41	CLELG-SAIF	Column SA DCDT, Inside Face
42	CLELG-SBOF	Column SB DCDT, Outside Face
43	CLELG-SBIF	Column SB DCDT, Inside Face

Channel No.	Name	Description
44	FLR DSP-NA3	3rd Floor Absolute Displacement at Column NA
45	FLR DSP-SA3	3rd Floor Absolute Displacement at Column SA
46	FLR DSP-NA2	2nd Floor Absolute Displacement
47	FLR DSP-NA1	1st Floor Absolute Displacement
48	ROD DFM-N1	1st Floor Rod Brace Displacement, Frame N
49	ROD DFM-S1	1st Floor Rod Brace Displacement, Frame S
50	BLANK	
51	BLANK	
52	FLR ACC-1	1st Floor Absolute Acceleration
53	FLR ACC-2	2nd Floor Absolute Acceleration
54	FLR ACC-3N	3rd Floor Absolute Acceleration, Frame N
55	FLR ACC-3S	3rd Floor Absolute Acceleration, Frame S
56	CLPYSTR-NAB	1st Floor Column NA Post-Yield Flexural Strain, Bottom End
57	CLPYSTR-NAT	1st Floor Column NA Post-Yield Flexural Strain, Top End
58	CLPYSTR-NBB	1st Floor Column NB Post-Yield Flexural Strain, Bottom End
59	CLPYSTR-NBT	1st Floor Column NB Post-Yield Flexural Strain, Top End
60	CLSTRG-NAB1	1st Floor Column NA Elastic Flexural Strain, Bottom End
61	CLSTRG-NAT1	1st Floor Column NA Elastic Flexural Strain, Top End
62	CLSTRG-NBB1	1st Floor Column NB Elastic Flexural Strain, Bottom End
63	CLSTRG-NBT1	1st Floor Column NB Elastic Flexural Strain, Top End
64	CLSTRG-SAB1	1st Floor Column SA Elastic Flexural Strain, Bottom End
65	CLSTRG-SAT1	1st Floor Column SA Elastic Flexural Strain, Top End
66	CLSTRG-SBB1	1st Floor Column SB Elastic Flexural Strain, Bottom End

Channel No.	Name	Description
67	CLSTRG-SBT1	1st Floor Column SB Elastic Flexural Strain, Top End
68	CLSTRG-NAB2	2nd Floor Column NA Elastic Flexural Strain, Bottom End
69	CLSTRG-NAT2	2nd Floor Column NA Elastic Flexural Strain, Top End
70	CLSTRG-NBB2	2nd Floor Column NB Elastic Flexural Strain, Bottom End
71	CLSTRG-NBT2	2nd Floor Column NB Elastic Flexural Strain, Top End
72	CLSTRG-SAB2	2nd Floor Column SA Elastic Flexural Strain, Bottom End
73	CLSTRG-SAT2	2nd Floor Column SA Elastic Flexural Strain, Top End
74	CLSTRG-SBB2	2nd Floor Column SB Elastic Flexural Strain, Bottom End
75	CLSTRG-SBT2	2nd Floor Column SB Elastic Flexural Strain, Top End
76	RPYSTR-PN1	1st Floor Rod Post-Yield Axial Strain, North Frame Positive Direction
77	RPYSTR-NN1	1st Floor Rod Post-Yield Axial Strain, North Frame Negative Direction
78	RPYSTR-PS1	1st Floor Rod Post-Yield Axial Strain, South Frame Positive Direction
79	RPYSTR-NS1	1st Floor Rod Post-Yield Axial Strain, South Frame Negative Direction
80	RPYSTR-PN2	2nd Floor Rod Post-Yield Axial Strain, North Frame Positive Direction
81	RPYSTR-NN2	2nd Floor Rod Post-Yield Axial Strain, North Frame Negative Direction
82	RPYSTR-PS2	2nd Floor Rod Post-Yield Axial Strain, South Frame Positive Direction
83	RPYSTR-NS2	2nd Floor Rod Post-Yield Axial Strain, South Frame Negative Direction
84	RPYSTR-PN3	3rd Floor Rod Post-Yield Axial Strain, North Frame Positive Direction
85	RPYSTR-NN3	3rd Floor Rod Post-Yield Axial Strain, North Frame Negative Direction
86	RPYSTR-PS3	3rd Floor Rod Post-Yield Axial Strain, South Frame Positive Direction
87	RPYSTR-NS3	3rd Floor Rod Post-Yield Axial Strain, South Frame Negative Direction
88	CLFRC-NAO	1st Floor Column NA Elastic Axial Strain, Outside Face
89	CLFRC-NAI	1st Floor Column NA Elastic Axial Strain, Inside Face

Channel No.	Name	Description
90	CLFRC-NBO	1st Floor Column NB Elastic Axial Strain, Outside Face
91	CLFRC-NBI	1st Floor Column NB Elastic Axial Strain, Inside Face
92	CLFRC-SAO	1st Floor Column SA Elastic Axial Strain, Outside Face
93	CLFRC-SAI	1st Floor Column SA Elastic Axial Strain, Inside Face
94	CLFRC-SBO	1st Floor Column SB Elastic Axial Strain, Outside Face
95	CLFRC-SBI	1st Floor Column SB Elastic Axial Strain, Inside Face

Channel No.	Name	Description
0	T/R ACC-1	Command Horizontal Acceleration Signal
1	T/R ACC-2	Command Vertical Acceleration Signal
2	CMD H DISP	Command Horizontal Displacement Signal
3	CMD V DISP	Command Vertical Displacement Signal
4	AV H T DISP	Average Horizontal Table Displacement
5	AV V T DISP	Average Vertical Table Displacement
6	AV H T ACC	Average Horizontal Table Acceleration
7	AV V T ACC	Average Vertical Table Acceleration
8	PITCH	Angular Acceleration in Pitching Mode
9	ROLL	Angular Acceleration in Rolling Mode
10	TWIST	Angular Acceleration in Twisting Mode
11	FORCE H1	Force in Horizontal Actuator H1
12	FORCE H2	Force in Horizontal Actuator H2
13	FORCE H3	Force in Horizontal Actuator H3
14	ACC H1	Horizontal Table Acceleration at Actuator H1
15	ACC H2	Horizontal Table Acceleration at Actuator H2
16	ACC V1	Vertical Table Acceleration at Actuator V1
17	ACC V2	Vertical Table Acceleration at Actuator V2
18	ACC V3	Vertical Table Acceleration at Actuator V3
19	ACC V4	Vertical Table Acceleration at Actuator V4
20	FORCE V1	Force in Vertical Actuator V1

Table A-2 Data channel listing for diagonal pipe bracing

Channel No.	Name	Description
21	FORCE V2	Force in Vertical Actuator V2
22	FORCE V3	Force in Vertical Actuator V3
23	FORCE V4	Force in Vertical Actuator V4
24	DISP V1	Vertical Table Displacement at Actuator V1
25	DISP V2	Vertical Table Displacement at Actuator V2
26	DISP V3	Vertical Table Displacement at Actuator V3
27	DISP V4	Vertical Table Displacement at Actuator V4
28	DISP H1	Horizontal Table Displacement at Actuator H1
29	DISP H2	Horizontal Table Displacement at Actuator H2
30	DISP H3	Horizontal Table Displacement at Actuator H3
31	BLANK	
32	PPYS-PTS	1st Floor Pipe Post-Yield Strain, Positive Direction, Top Face, Frame S
33	PPYS-PBS	1st Flr Pipe Post-Yield Strain, Positive Direction, Bottom Face, Frame S
34	PPYS-POS	1st Flr Pipe Post-Yield Strain, Positive Direction, Outside Face, Frame S
35	PPYS-PIS	1st Flr Pipe Post-Yield Strain, Positive Direction, Inside Face, Frame S
36	CLELG-NAOF	Column NA DCDT, Outside Face
37	CLELG-NAIF	Column NA DCDT, Inside Face
38	CLELG-NBOF	Column NB DCDT, Outside Face
39	CLELG-NBIF	Column NB DCDT, Inside Face
40	CLELG-SAOF	Column SA DCDT, Outside Face
41	CLELG-SAIF	Column SA DCDT, Inside Face
42	CLELG-SBOF	Column SB DCDT, Outside Face

Channel No.	Name	Description
43	CLELG-SBIF	Column SB DCDT, Inside Face
44	FLR DSP-MA1	1st Floor Absolute Displacement
45	FLR DSP-MA2	2nd Floor Absolute Displacement
46	FLR DSP-NA3	3rd Floor Absolute Displacement at Column NA
47	FLR DSP-SA3	3rd Floor Absolute Displacement at Column SA
48	FLR ACC-1	1st Floor Absolute Acceleration
49	FLR ACC-2	2nd Floor Absolute Acceleration
50	FLR ACC-N3	3rd Floor Absolute Acceleration, Frame N
51	FLR ACC-S3	3rd Floor Absolute Acceleration, Frame S
52	CPYS-NABO	1st Floor Column NA Post-Yield Flexural Strain, Bottom End, Outside Face
53	CPYS-NABI	1st Floor Column NA Post-Yield Flexural Strain, Bottom End, Inside Face
54	CPYS-NBBO	1st Floor Column NB Post-Yield Flexural Strain, Bottom End, Outside Face
55	CPYS-NBBI	1st Floor Column NB Post-Yield Flexural Strain, Bottom End, Inside Face
56	CESTR-NAB1	1st Floor Column NA Elastic Flexural Strain, Bottom End
57	CESTR-NAT1	1st Floor Column NA Elastic Flexural Strain, Top End
58	CESTR-NBB1	1st Floor Column NB Elastic Flexural Strain, Bottom End
59	CESTR-NBT1	1st Floor Column NB Elastic Flexural Strain, Top End
60	CESTR-SAB1	1st Floor Column SA Elastic Flexural Strain, Bottom End
61	CESTR-SAT1	1st Floor Column SA Elastic Flexural Strain, Top End
62	CESTR-SBB1	1st Floor Column SB Elastic Flexural Strain, Bottom End
63	CESTR-SBT1	1st Floor Column SB Elastic Flexural Strain, Top End
64	CESTR-NAB2	2nd Floor Column NA Elastic Flexural Strain, Bottom End
65	CESTR-NAT2	2nd Floor Column NA Elastic Flexural Strain, Top End

Channel No.	Name	Description
66	CESTR-NBB2	2nd Floor Column NB Elastic Flexural Strain, Bottom End
67	CESTR-NBT2	2nd Floor Column NB Elastic Flexural Strain, Top End
68	CESTR-SAB2	2nd Floor Column SA Elastic Flexural Strain, Bottom End
69	CESTR-SAT2	2nd Floor Column SA Elastic Flexural Strain, Top End
70	CESTR-SBB2	2nd Floor Column SB Elastic Flexural Strain, Bottom End
71	CESTR-SBT2	2nd Floor Column SB Elastic Flexural Strain, Top End
72	BESTR-LN1	1st Floor Beam Elastic Flexural Strain, Left End, Frame N
73	BESTR-RN1	1st Floor Beam Elastic Flexural Strain, Right End, Frame N
74	PPYS-NN1	1st Floor Pipe Post-Yield Axial Strain, Negative Direction, Frame N
75	PPYS-PN1	1st Floor Pipe Post-Yield Axial Strain, Positive Direction, Frame N
76	PPYS-NS1	1st Floor Pipe Post-Yield Axial Strain, Negative Direction, Frame S
77	PPYS-PS1	1st Floor Pipe Post-Yield Axial Strain, Positive Direction, Frame S
78	PPYS-PN2	2nd Floor Pipe Post-Yield Axial Strain, Positive Direction, Frame N
79	PPYS-NN2	2nd Floor Pipe Post-Yield Axial Strain, Negative Direction, Frame N
80	PPYS-PS2	2nd Floor Pipe Post-Yield Axial Strain, Positive Direction, Frame S
81	PPYS-NS2	2nd Floor Pipe Post-Yield Axial Strain, Negative Direction, Frame S
82	PPYS-PN3	3rd Floor Pipe Post-Yield Axial Strain, Positive Direction, Frame N
83	PPYS-NN3	3rd Floor Pipe Post-Yield Axial Strain, Negative Direction, Frame N
84	PPYS-PS3	3rd Floor Pipe Post-Yield Axial Strain, Positive Direction, Frame S
85	PPYS-NS3	3rd Floor Pipe Post-Yield Axial Strain, Negative Direction, Frame S
86	PPYS-NTS	1st Flr Pipe Post-Yield Strain, Negative Direction, Top Face, Frame S
87	PPYS-NBS	1st Flr Pipe Post-Yield Strain, Negative Direction, Bottom Face, Frame S
88	PPYS-NOS	1st Flr Pipe Post-Yield Strain, Negative Direction, Outside Face, Frame S

Channel No.	Name	Description
89	PPYS-NIS	1st Flr Pipe Post-Yield Strain, Negative Direction, Inside Face, Frame S
90	PPYS-NTN	1st Flr Pipe Post-Yield Strain, Negative Direction, Top Face, Frame N
91	PPYS-NBN	1st Flr Pipe Post-Yield Strain, Negative Direction, Bottom Face, Frame N
92	PPYS-NON	1st Flr Pipe Post-Yield Strain, Negative Direction, Outside Face, Frame N
93	PPYS-NIN	1st Flr Pipe Post-Yield Strain, Negative Direction, Inside Face, Frame N
94	CLFRC-NA	1st Floor Column NA Elastic Axial Strain
95	CLFRC-NB	1st Floor Column NB Elastic Axial Strain
96	CLFRC-SA	1st Floor Column SA Elastic Axial Strain
97	CLFRC-SB	1st Floor Column SB Elastic Axial Strain
98	CPYS-NAT	1st Floor Column NA Post-Yield Flexural Strain, Top End
99	CPYS-NBT	1st Floor Column NB Post-Yield Flexural Strain, Top End
100	PPYS-PTN	1st Flr Pipe Post-Yield Strain, Positive Direction, Top Face, Frame N
101	PPYS-PBN	1st Flr Pipe Post-Yield Strain, Positive Direction, Bottom Face, Frame N
102	PPYS-PON	1st Flr Pipe Post-Yield Strain, Positive Direction, Outside Face, Frame N
103	PPYS-PIN	1st Flr Pipe Post-Yield Strain, Positive Direction, Inside Face, Frame N

Channel No.	Name	Description
0	T/R ACC-1	Command Horizontal Table Acceleration Signal
1	T/R ACC-2	Command Vertical Table Acceleration Signal
2	CMD H DISP	Command Horizontal Table Displacement Signal
3	CMD V DISP	Command Vertical Table Displacement Signal
4	AV H T DISP	Average Horizontal Table Displacement
5	AV V T DISP	Average Vertical Table Displacement
6	AV H T ACC	Average Horizontal Table Acceleration
7	AV V T ACC	Average Vertical Table Acceleration
8	PITCH	Angular Table Acceleration in Pitching Mode
9	ROLL	Angular Table Acceleration in Rolling Mode
10	TWIST	Angular Table Acceleration in Twisting Mode
11	FORCE H1	Force in Horizontal Actuator H1
12	FORCE H2	Force in Horizontal Actuator H2
13	FORCE H3	Force in Horizontal Actuator H3
14	ACC H1	Horizontal Table Acceleration at Actuator H1
15	ACC H2	Horizontal Table Acceleration at Actuator H2
16	ACC V1	Vertical Table Acceleration at Actuator V1
17	ACC V2	Vertical Table Acceleration at Actuator V2
18	ACC V3	Vertical Table Acceleration at Actuator V3
19	ACC V4	Vertical Table Acceleration at Actuator V4
20	FORCE V1	Force in Vertical Actuator V1
21	FORCE V2	Force in Vertical Actuator V2

Table A-3 Data channel listing for diagonal double angle bracing

Channel No.	Name	Description
22	FORCE V3	Force in Vertical Actuator V3
23	FORCE V4	Force in Vertical Actuator V4
24	DISP V1	Vertical Displacement at Actuator V1
25	DISP V2	Vertical Displacement at Actuator V2
26	DISP V3	Vertical Displacement at Actuator V3
27	DISP V4	Vertical Displacement at Actuator V4
28	DISP H1	Horizontal Table Displacement at Actuator H1
29	DISP H2	Horizontal Table Displacement at Actuator H2
30	DISP H3	Horizontal Table Displacement at Actuator H3
31	BLANK	
32	PS FORCE-1	Force in Passive Stabilizer 1
33	PS FORCE-2	Force in Passive Stabilizer 2
34	PS FORCE-3	Force in Passive Stabilizer 3
35	PS FORCE-4	Force in Passive Stabilizer 4
36	CLELG-NAOF	1st Floor Column NA DCDT, Outside Face
37	CLELG-NAIF	1st Floor Column NA DCDT, Inside Face
38	CLELG-NBOF	1st Floor Column NB DCDT, Outside Face
39	CLELG-NBIF	1st Floor Column NB DCDT, Inside Face
40	CLELG-SAOF	1st Floor Column SA DCDT, Outside Face
41	CLELG-SAIF	1st Floor Column SA DCDT, Inside Face
42	CLELG-SBOF	1st Floor Column SB DCDT, Outside Face
43	CLELG-SBIF	1st Floor Column SB DCDT, Inside Face

Channel No.	Name	Description
44	FLR DSP-MA1	1st Floor Absolute Displacement
45	FLR DSP-MA2	2nd Floor Absolute Displacement
46	FLR DSP-NA3	3rd Floor Absolute Displacement at Column NA
47	FLR DSP-SA3	3rd Floor Absolute Displacement at Column SA
48	FLR ACC-1	1st Floor Absolute Acceleration
49	FLR ACC-2	2nd Floor Absolute Acceleration
50	FLR ACC-N3	3rd Floor Absolute Acceleration, Frame N
51	FLR ACC-S3	3rd Floor Absolute Acceleration, Frame S
52	CPYS-NABO	1st Floor Column NA Post-Yield Flexural Strain, Bottom End, Outside Face
53	CPYS-NABI	1st Floor Column NA Post-Yield Flexural Strain, Bottom End, Inside Face
54	CPYS-NBBO	1st Floor Column NB Post-Yield Flexural Strain, Bottom End, Outside Face
55	CPYS-NBBI	1st Floor Column NB Post-Yield Flexural Strain, Bottom End, Inside Face
56	CESTR-NAB1	1st Floor Column NA Elastic Flexural Strain, Bottom End
57	CESTR-NAT1	1st Floor Column NA Elastic Flexural Strain, Top End
58	CESTR-NBB1	1st Floor Column NB Elastic Flexural Strain, Bottom End
59	CESTR-NBT1	1st Floor Column NB Elastic Flexural Strain, Top End
60	CESTR-SAB1	1st Floor Column SA Elastic Flexural Strain, Bottom End
61	CESTR-SAT1	1st Floor Column SA Elastic Flexural Strain, Top End
62	CESTR-SBB1	1st Floor Column SB Elastic Flexural Strain, Bottom End
63	CESTR-SBT1	1st Floor Column SB Elastic Flexural Strain, Top End
64	CESTR-NAB2	2nd Floor Column NA Elastic Flexural Strain, Bottom End
65	CESTR-NAT2	2nd Floor Column NA Elastic Flexural Strain, Top End
66	CESTR-NBB2	2nd Floor Column NB Elastic Flexural Strain, Bottom End

Channel No.	Name	Description
67	CESTR-NBT2	2nd Floor Column NB Elastic Flexural Strain, Top End
68	CESTR-SAB2	2nd Floor Column SA Elastic Flexural Strain, Bottom End
69	CESTR-SAT2	2nd Floor Column SA Elastic Flexural Strain, Top End
70	CESTR-SBB2	2nd Floor Column SB Elastic Flexural Strain, Bottom End
71	CESTR-SBT2	2nd Floor Column SB Elastic Flexural Strain, Top End
72	BESTR-LN1	1st Floor Beam Elastic Flexural Strain, Left End, Frame N
73	BESTR-RN1	1st Floor Beam Elastic Flexural Strain, Right End, Frame N
74	DAPYS-PN1	1st Flr Angle Post-Yield Axial Strain, Positive Direction, Frame N
75	DAPYS-NN1	1st Flr Angle Post-Yield Axial Strain, Negative Direction, Frame N
76	DAPYS-PS1	1st Flr Angle Post-Yield Axial Strain, Positive Direction, Frame S
77	DAPYS-NS1	1st Flr Angle Post-Yield Axial Strain, Negative Direction, Frame S
78	DAPYS-PN2	2nd Flr Angle Post-Yield Axial Strain, Positive Direction, Frame N
79	DAPYS-NN2	2nd Flr Angle Post-Yield Axial Strain, Negative Direction, Frame N
80	DAPYS-PS2	2nd Flr Angle Post-Yield Axial Strain, Positive Direction, Frame S
81	DAPYS-NS2	2nd Flr Angle Post-Yield Axial Strain, Negative Direction, Frame S
82	DAPYS-PN3	3rd Flr Angle Post-Yield Axial Strain, Positive Direction, Frame N
83	DAPYS-NN3	3rd Flr Angle Post-Yield Axial Strain, Negative Direction, Frame N
84	DAPYS-PS3	3rd Flr Angle Post-Yield Axial Strain, Positive Direction, Frame S
85	DAPYS-NS3	3rd Flr Angle Post-Yield Axial Strain, Negative Direction, Frame S
86	DAPYS-PBIF	1st Flr Angle Post-Yield Strain, Positive Direction, Bottom Inside Face
87	DAPYS-PBOF	1st Flr Angle Post-Yield Strain, Positive Direction, Bottom Outside Face
88	DAPYS-PTIF	1st Flr Angle Post-Yield Strain, Positive Direction, Top Inside Face
89	DAPYS-PTOF	1st Flr Angle Post-Yield Strain, Positive Direction, Top Outside Face

Channel No.	Name	Description
90	DAPYS-NBOF	1st Flr Angle Post-Yield Strain, Negative Direction, Bottom Outside Face
91	DAPYS-NBIF	1st Flr Angle Post-Yield Strain, Negative Direction, Bottom Inside Face
92	DAPYS-NTOF	1st Flr Angle Post-Yield Strain, Negative Direction, Top Outside Face
93	DAPYS-NTIF	1st Flr Angle Post-Yield Strain, Negative Direction, Top Inside Face
94	CLFRC-NA	1st Floor Column NA Elastic Axial Strain
95	CLFRC-NB	1st Floor Column NB Elastic Axial Strain
96	CLFRC-SA	1st Floor Column SA Elastic Axial Strain
97	CLFRC-SB	1st Floor Column SB Elastic Axial Strain
98	CPYS-NAT	1st Floor Column NA Post-Yield Flexural Strain, Top End
99	CPYS-NBT	1st Floor Column NB Post-Yield Flexural Strain, Top End
100	DAPYS-PMBO	1st Flr Angle P.Y. Strain, Positive Direction, Mid-Section Bottom Outside
101	DAPYS-PMBI	1st Flr Angle P.Y. Strain, Positive Direction, Mid-Section Bottom Inside
102	DAPYS-PMTO	1st Flr Angle P.Y. Strain, Positive Direction, Mid-Section Top Outside Face
103	DAPYS-PMTI	1st Flr Angle P.Y. Strain, Positive Direction, Mid-Section Top Inside Face

Channel No.	Name	Description
0	T/R ACC-1	Command Horizontal Table Acceleration Signal
1	T/R ACC-2	Command Vertical Table Acceleration Signal
2	CMD H DISP	Command Horizontal Table Displacement Signal
3	CMD V DISP	Command Vertical Table Displacement Signal
4	AV H T DISP	Average Horizontal Table Displacement
5	AV V T DISP	Average Vertical Table Displacement
6	AV H T ACC	Average Horizontal Table Acceleration
7	AV V T ACC	Average Vertical Table Acceleration
8	PITCH	Angular Table Acceleration in Pitching Mode
9	ROLL	Angular Table Acceleration in Rolling Mode
10	TWIST	Angular Table Acceleration in Twisting Mode
11	FORCE H1	Force in Horizontal Actuator H1
12	FORCE H2	Force in Horizontal Actuator H2
13	FORCE H3	Force in Horizontal Actuator H3
14	ACC H1	Horizontal Table Acceleration at Actuator H1
15	ACC H2	Horizontal Table Acceleration at Actuator H2
16	ACC V1	Vertical Table Acceleration at Actuator V1
17	ACC V2	Vertical Table Acceleration at Actuator V2
18	ACC V3	Vertical Table Acceleration at Actuator V3
19	ACC V4	Vertical Table Acceleration at Actuator V4
20	FORCE V1	Force in Vertical Actuator V1

Table A-4 Dta channel listing for diagonal double angle bracing- Phase II

Channel No.	Name	Description
21	FORCE V2	Force in Vertical Actuator V2
22	FORCE V3	Force in Vertical Actuator V3
23	FORCE V4	Force in Vertical Actuator V4
24	DISP V1	Vertical Table Displacement at Actuator V1
25	DISP V2	Vertical Table Displacement at Actuator V2
26	DISP V3	Vertical Table Displacement at Actuator V3
27	DISP V4	Vertical Table Displacement at Actuator V4
28	DISP H1	Horizontal Table Displacement at Actuator H1
29	DISP H2	Horizontal Table Displacement at Actuator H2
30	DISP H3	Horizontal Table Displacement at Actuator H3
31	BLANK	
32	DAPYS-PBOS	1st Flr Angle P.Y.Strain, Pos. Direction, Bottom Outside Face, Frame S
33	DAPYS-PBIS	1st Flr Angle P.Y.Strain, Pos. Direction, Bottom Inside Face, Frame S
34	DAPYS-PTOS	1st Flr Angle P.Y.Strain, Pos. Direction, Top Outside Face, Frame S
35	DAPYS-PTIS	1st Flr Angle P.Y. Strain, Pos. Direction, Top Inside Face, Frame S
36	CLELG-NAOF	1st Floor Column NA DCDT, Outside Face
37	CLELG-NAIF	1st Floor Column NA DCDT, Inside Face
38	CLELG-NBOF	1st Floor Column NB DCDT, Outside Face
39	CLELG-NBIF	1st Floor Column NB DCDT, Inside Face
40	CLELG-SAOF	1st Floor Column SA DCDT, Outside Face
41	CLELG-SAIF	1st Floor Column SA DCDT, Inside Face
42	CLELG-SBOF	1st Floor Column SB DCDT, Outside Face

Channel No.	Name	Description
43	CLELG-SBIF	1st Floor Column SB DCDT, Inside Face
44	FLR DSP-MA1	1st Floor Absolute Displacement
45	FLR DSP-MA2	2nd Floor Absolute Displacement
46	FLR DSP-NA3	3rd Floor Absolute Displacement at Column NA
47	FLR DSP-SA3	3rd Floor Absolute Displacement at Column SA
48	FLR ACC-1	1st Floor Absolute Acceleration
49	FLR ACC-2	2nd Floor Absolute Acceleration
50	FLR ACC-N3	3rd Floor Absolute Acceleration, Frame N
51	FLR ACC-S3	3rd Floor Absolute Acceleration, Frame S
52	CPYS-NABO	1st Floor Column NA P.Y. Flexural Strain, Bottom End, Outside Face
53	CPYS-NABI	1st Floor Column NA P.Y. Flexural Strain, Bottom End, Inside Face
54	CPYS-NBBO	1st Floor Column NB P.Y. Flexural Strain, Bottom End, Outside Face
55	CPYS-NBBI	1st Floor Column NB P.Y. Flexural Strain, Bottom End, Inside Face
56	CESTR-NAB1	1st Floor Column NA Elastic Flexural Strain, Bottom End
57	CESTR-NAT1	1st Floor Column NA Elastic Flexural Strain, Top End
58	CESTR-NBB1	1st Floor Column NB Elastic Flexural Strain, Bottom End
59	CESTR-NBT1	1st Floor Column NB Elastic Flexural Strain, Top End
60	CESTR-SAB1	1st Floor Column SA Elastic Flexural Strain, Bottom End
61	CESTR-SAT1	1st Floor Column SA Elastic Flexural Strain, Top End
62	CESTR-SBB1	1st Floor Column SB Elastic Flexural Strain, Bottom End
63	CESTR-SBT1	1st Floor Column SB Elastic Flexural Strain, Top End
64	CESTR-NAB2	2nd Floor Column NA Elastic Flexural Strain, Bottom End

Channel No.	Name	Description
65	CESTR-NAT2	2nd Floor Column NA Elastic Flexural Strain, Top End
66	CESTR-NBB2	2nd Floor Column NB Elastic Flexural Strain, Bottom End
67	CESTR-NBT2	2nd Floor Column NB Elastic Flexural Strain, Top End
68	CESTR-SAB2	2nd Floor Column SA Elastic Flexural Strain, Bottom End
69	CESTR-SAT2	2nd Floor Column SA Elastic Flexural Strain, Top End
70	CESTR-SBB2	2nd Floor Column SB Elastic Flexural Strain, Bottom End
71	CESTR-SBT2	2nd Floor Column SB Elastic Flexural Strain, Top End
72	BESTR-LN1	1st Floor Beam Elastic Flexural Strain, Left End, Frame N
73	BESTR-RN1	1st Floor Beam Elastic Flexural Strain, Right End, Frame N
74	DAPYS-NN1	1st Flr Angle P.Y. Axial Strain, Negative Direction, Frame N
75	DAPYS-PN1	1st Flr Angle P.Y. Axial Strain, Positive Direction, Frame N
76	DAPYS-NS1	1st Flr Angle P.Y. Axial Strain, Negative Direction, Frame S
77	DAPYS-PS1	1st Flr Angle P.Y. Axial Strain, Positive Direction, Frame S
78	DAPYS-PN2	2nd Flr Angle P.Y. Axial Strain, Positive Direction, Frame N
79	DAPYS-NN2	2nd Flr Angle P.Y. Axial Strain, Negative Direction, Frame N
80	DAPYS-PS2	2nd Flr Angle P.Y. Axial Strain, Positive Direction, Frame S
81	DAPYS-NS2	2nd Flr Angle P.Y. Axial Strain, Negative Direction, Frame S
82	DAPYS-PN3	3rd Flr Angle P.Y. Axial Strain, Positive Direction, Frame N
83	DAPYS-NN3	3rd Flr Angle P.Y. Axial Strain, Negative Direction, Frame N
84	DAPYS-PS3	3rd Flr Angle P.Y. Axial Strain, Positive Direction, Frame S
85	DAPYS-NS3	3rd Flr Angle P.Y. Axial Strain, Negative Direction, Frame S
86	DAPYS-NBOS	1st Flr Angle P.Y. Strain, Neg. Direction, Bottom Outside Face, Frame S

Channel No.	Name	Description
87	DAPYS-NBIS	1st Flr Angle P.Y. Strain, Neg. Direction, Bottom Inside Face, Frame S
83	DAPYS-NTOS	1st Flr Angle P.Y. Strain, Neg. Direction, Top Outside Face, Frame S
89	DAPYS-NTIS	1st Flr Angle P.Y. Strain, Neg. Direction, Top Inside Face, Frame S
90	DAPYS-NBON	1st Flr Angle P.Y. Strain, Neg. Direction, Bottom Outside Face, Frame N
91	DAPYS-NBIN	1st Flr Angle P.Y. Strain, Neg. Direction, Bottom Inside Face, Frame N
92	DAPYS-NTON	1st Flr Angle P.Y. Strain, Neg. Direction, Top Outside Face, Frame N
93	DAPYS-NTIN	1st Flr Angle P.Y. Strain, Neg. Direction, Top Inside Face, Frame N
94	CLFRC-NA	1st Floor Column NA Elastic Axial Strain
95	CLFRC-NB	1st Floor Column NB Elastic Axial Strain
96	CLFRC-SA	1st Floor Column SA Elastic Axial Strain
97	CLFRC-SB	1st Floor Column SB Elastic Axial Strain
98	CPYS-NAT	1st Floor Column NA Post-Yield Flexural Strain, Top End
99	CPYS-NBT	1st Floor Column NB Post-Yield Flexural Strain, Top End
100	DAPYS-PBON	1st Flr Angle P.Y. Strain, Pos. Direction, Bottom Outside Face, Frame N
101	DAPYS-PBIN	1st Flr Angle P.Y. Strain, Pos. Direction, Bottom Inside Face, Frame N
102	DAPYS-PTON	1st Flr Angle P.Y. Strain, Pos. Direction, Top Outside Face, Frame N
103	DAPYS-PTIN	1st Flr Angle P.Y. Strain, Pos. Direction, Top Inside Face, Frame N

Channel No.	Name	Description
0	T/R ACC-1	Command Horizontal Table Acceleration Signal
1	T/R ACC-2	Command Vertical Table Acceleration Signal
2	CMD H DISP	Command Horizontal Table Displacement Signal
3	CMD V DISP	Command Vertical Table Displacement Signal
4	AV H T DISP	Average Horizontal Table Displacement
5	AV V T DISP	Average Vertical Table Displacement
6	AV H T ACC	Average Horizontal Table Acceleration
7	AV V T ACC	Average Vertical Table Acceleration
8	PITCH	Angular Table Acceleration in Pitching Mode
9	ROLL	Angular Table Acceleration in Rolling Mode
10	TWIST	Angular Table Acceleration in Twisting Mode
11	FORCE H1	Force in Horizontal Actuator H1
12	FORCE H2	Force in Horizontal Actuator H2
13	FORCE H3	Force in Horizontal Actuator H3
14	ACC H1	Horizontal Table Acceleration at Actuator H1
15	ACC H2	Horizontal Table Acceleration at Actuator H2
16	ACC V1	Vertical Table Acceleration at Actuator V1
17	ACC V2	Vertical Table Acceleration at Actuator V2
18	ACC V3	Vertical Table Acceleration at Actuator V3
19	ACC V4	Vertical Table Acceleration at Actuator V4
20	FORCE V1	Force in Vertical Actuator V1

Table A-5 Data Channel Listing for Unbraced Structure

Channel No.	Name	Description
21	FORCE V2	Force in Vertical Actuator V2
22	FORCE V3	Force in Vertical Actuator V3
23	FORCE V4	Force in Vertical Actuator V4
24	DISP V1	Vertical Table Displacement at Actuator V1
25	DISP V2	Vertical Table Displacement at Actuator V2
26	DISP V3	Vertical Table Displacement at Actuator V3
27	DISP V4	Vertical Table Displacement at Actuator V4
28	DISP H1	Horizontal Table Displacement at Actuator H1
29	DISP H2	Horizontal Table Displacement at Actuator H2
30	DISP H3	Horizontal Table Displacement at Actuator H3
31	BLANK	
⋮	⋮	
36	CLELG-NAOF	1st Floor Column NA DCDT, Outside Face
37	CLELG-NAIF	1st Floor Column NA DCDT, Inside Face
38	CLELG-NBOF	1st Floor Column NB DCDT, Outside Face
39	CLELG-NBIF	1st Floor Column NB DCDT, Inside Face
40	CLELG-SAOF	1st Floor Column SA DCDT, Outside Face
41	CLELG-SAIF	1st Floor Column SA DCDT, Inside Face
42	CLELG-SBOF	1st Floor Column SB DCDT, Outside Face
43	CLELG-SBIF	1st Floor Column SB DCDT, Inside Face
44	FLR DSP-MA1	1st Floor Absolute Displacement
45	FLR DSP-MA2	2nd Floor Absolute Displacement

Channel No.	Name	Description
46	FLR DSP-NA3	3rd Floor Absolute Displacement at Column NA
47	FLR DSP-SA3	3rd Floor Absolute Displacement at Column SA
48	FLR ACC-1	1st Floor Absolute Acceleration
49	FLR ACC-2	2nd Floor Absolute Acceleration
50	FLR ACC-N3	3rd Floor Absolute Acceleration, Frame N
51	FLR ACC-S3	3rd Floor Absolute Acceleration, Frame S
52	CPYS-NABO	1st Floor Column NA Post-Yield Flexural Strain, Bottom End, Outside Face
53	CPYS-NABI	1st Floor Column NA Post-Yield Flexural Strain, Bottom End, Inside Face
54	CPYS-NBBO	1st Floor Column NB Post-Yield Flexural Strain, Bottom End, Outside Face
55	CPYS-NBBI	1st Floor Column NB Post-Yield Flexural Strain, Bottom End, Inside Face
56	CESTR-NAB1	1st Floor Column NA Elastic Flexural Strain, Bottom End
57	CESTR-NAT1	1st Floor Column NA Elastic Flexural Strain, Top End
58	CESTR-NBB1	1st Floor Column NB Elastic Flexural Strain, Bottom End
59	CESTR-NBT1	1st Floor Column NB Elastic Flexural Strain, Top End
60	CESTR-SAB1	1st Floor Column SA Elastic Flexural Strain, Bottom End
61	CESTR-SAT1	1st Floor Column SA Elastic Flexural Strain, Top End
62	CESTR-SBB1	1st Floor Column SB Elastic Flexural Strain, Bottom End
63	CESTR-SBT1	1st Floor Column SB Elastic Flexural Strain, Top End
64	CESTR-NAB2	2nd Floor Column NA Elastic Flexural Strain, Bottom End
65	CESTR-NAT2	2nd Floor Column NA Elastic Flexural Strain, Top End
66	CESTR-NBB2	2nd Floor Column NB Elastic Flexural Strain, Bottom End
67	CESTR-NBT2	2nd Floor Column NB Elastic Flexural Strain, Top End
68	CESTR-SAB2	2nd Floor Column SA Elastic Flexural Strain, Bottom End

Channel No.	Name	Description
69	CESTR-SAT2	2nd Floor Column SA Elastic Flexural Strain, Top End
70	CESTR-SBB2	2nd Floor Column SB Elastic Flexural Strain, Bottom End
71	CESTR-SBT2	2nd Floor Column SB Elastic Flexural Strain, Top End
72	BESTR-LN1	1st Floor Beam Elastic Flexural Strain, Left End, Frame N
73	BESTR-RN1	1st Floor Beam Elastic Flexural Strain, Right End, Frame N
74	BLANK	
⋮	⋮	
94	CLFRC-NA	1st Floor Column NA Elastic Axial Strain
95	CLFRC-NB	1st Floor Column NB Elastic Axial Strain
96	CLFRC-SA	1st Floor Column SA Elastic Axial Strain
97	CLFRC-SB	1st Floor Column SB Elastic Axial Strain

EARTHQUAKE ENGINEERING RESEARCH CENTER REPORTS

NOTE: Numbers in parenthesis are Accession Numbers assigned by the National Technical Information Service; these are followed by a price code. Copies of the reports may be ordered from the National Technical Information Service, 5285 Port Royal Road, Springfield, Virginia, 22161. Accession Numbers should be quoted on orders for reports (PB --- ---) and remittance must accompany each order. Reports without this information were not available at time of printing. Upon request, EERC will mail inquirers this information when it becomes available.

EERC 67-1 "Feasibility Study Large-Scale Earthquake Simulator Facility," by J. Penzien, J.G. Bouwkamp, R.W. Clough and D. Rea - 1967 (PB 187 905)A07

EERC 68-1 Unassigned

EERC 68-2 "Inelastic Behavior of Beam-to-Column Subassemblages Under Repeated Loading," by V.V. Bertero - 1968 (PB 184 888)A05

EERC 68-3 "A Graphical Method for Solving the Wave Reflection-Refraction Problem," by H.D. McNiven and Y. Mengi - 1968 (PB 187 943)A03

EERC 68-4 "Dynamic Properties of McKinley School Buildings," by D. Rea, J.G. Bouwkamp and R.W. Clough - 1968 (PB 187 902)A07

EERC 68-5 "Characteristics of Rock Motions During Earthquakes," by H.B. Seed, I.M. Idriss and F.W. Kiefer - 1968 (PB 188 338)A03

EERC 69-1 "Earthquake Engineering Research at Berkeley," - 1969 (PB 187 906)A11

EERC 69-2 "Nonlinear Seismic Response of Earth Structures," by M. Dibaj and J. Penzien - 1969 (PB 187 904)A08

EERC 69-3 "Probabilistic Study of the Behavior of Structures During Earthquakes," by R. Ruiz and J. Penzien - 1969 (PB 187 886)A06

EERC 69-4 "Numerical Solution of Boundary Value Problems in Structural Mechanics by Reduction to an Initial Value Formulation," by N. Distefano and J. Schujman - 1969 (PB 187 942)A02

EERC 69-5 "Dynamic Programming and the Solution of the Biharmonic Equation," by N. Distefano - 1969 (PB 187 941)A03

EERC 69-6 "Stochastic Analysis of Offshore Tower Structures," by A.K. Malhotra and J. Penzien - 1969 (PB 187 903)A09

EERC 69-7 "Rock Motion Accelerograms for High Magnitude Earthquakes," by H.B. Seed and I.M. Idriss - 1969 (PB 187 940)A02

EERC 69-8 "Structural Dynamics Testing Facilities at the University of California, Berkeley," by R.M. Stephen, J.G. Bouwkamp, R.W. Clough and J. Penzien - 1969 (PB 189 111)A04

EERC 69-9 "Seismic Response of Soil Deposits Underlain by Sloping Rock Boundaries," by H. Dezfulian and H.B. Seed 1969 (PB 189 114)A03

EERC 69-10 "Dynamic Stress Analysis of Axisymmetric Structures Under Arbitrary Loading," by S. Ghosh and E.L. Wilson 1969 (PB 189 026)A10

EERC 69-11 "Seismic Behavior of Multistory Frames Designed by Different Philosophies," by J.C. Anderson and V. V. Bertero - 1969 (PB 190 662)A10

EERC 69-12 "Stiffness Degradation of Reinforcing Concrete Members Subjected to Cyclic Flexural Moments," by V.V. Bertero, B. Bresler and H. Ming Liao - 1969 (PB 202 942)A07

EERC 69-13 "Response of Non-Uniform Soil Deposits to Travelling Seismic Waves," by H. Dezfulian and H.B. Seed - 1969 (PB 191 023)A03

EERC 69-14 "Damping Capacity of a Model Steel Structure," by D. Rea, R.W. Clough and J.G. Bouwkamp - 1969 (PB 190 663)A06

EERC 69-15 "Influence of Local Soil Conditions on Building Damage Potential during Earthquakes," by H.B. Seed and I.M. Idriss - 1969 (PB 191 036)A03

EERC 69-16 "The Behavior of Sands Under Seismic Loading Conditions," by M.L. Silver and H.B. Seed - 1969 (AD 714 982)A07

EERC 70-1 "Earthquake Response of Gravity Dams," by A.K. Chopra - 1970 (AD 709 640)A03

EERC 70-2 "Relationships between Soil Conditions and Building Damage in the Caracas Earthquake of July 29, 1967," by H.B. Seed, I.M. Idriss and H. Dezfulian - 1970 (PB 195 762)A05

EERC 70-3 "Cyclic Loading of Full Size Steel Connections," by E.P. Popov and R.M. Stephen - 1970 (PB 213 545)A04

EERC 70-4 "Seismic Analysis of the Charaima Building, Caraballeda, Venezuela," by Subcommittee of the SEAONC Research Committee: V.V. Bertero, P.F. Fratessa, S.A. Mahin, J.H. Sexton, A.C. Scordelis, E.L. Wilson, L.A. Wyllie, H.B. Seed and J. Penzien, Chairman - 1970 (PB 201 455)A06

EERC 70-5 "A Computer Program for Earthquake Analysis of Dams," by A.K. Chopra and P. Chakrabarti - 1970 (AD 723 994)A05

EERC 70-6 "The Propagation of Love Waves Across Non-Horizontally Layered Structures," by J. Lysmer and L.A. Drake 1970 (PB 197 896)A03

EERC 70-7 "Influence of Base Rock Characteristics on Ground Response," by J. Lysmer, H.B. Seed and P.B. Schnabel 1970 (PB 197 897)A03

EERC 70-8 "Applicability of Laboratory Test Procedures for Measuring Soil Liquefaction Characteristics under Cyclic Loading," by H.B. Seed and W.H. Peacock - 1970 (PB 198 016)A03

EERC 70-9 "A Simplified Procedure for Evaluating Soil Liquefaction Potential," by H.B. Seed and I.M. Idriss - 1970 (PB 198 009)A03

EERC 70-10 "Soil Moduli and Damping Factors for Dynamic Response Analysis," by H.B. Seed and I.M. Idriss - 1970 (PB 197 869)A03

EERC 71-1 "Koyna Earthquake of December 11, 1967 and the Performance of Koyna Dam," by A.K. Chopra and P. Chakrabarti 1971 (AD 731 496)A06

EERC 71-2 "Preliminary In-Situ Measurements of Anelastic Absorption in Soils Using a Prototype Earthquake Simulator," by R.D. Borcherdt and P.W. Rodgers - 1971 (PB 201 454)A03

EERC 71-3 "Static and Dynamic Analysis of Inelastic Frame Structures," by F.L. Porter and G.H. Powell - 1971 (PB 210 135)A06

EERC 71-4 "Research Needs in Limit Design of Reinforced Concrete Structures," by V.V. Bertero - 1971 (PB 202 943)A04

EERC 71-5 "Dynamic Behavior of a High-Rise Diagonally Braced Steel Building," by D. Rea, A.A. Shah and J.G. Bouwkamp 1971 (PB 203 584)A06

EERC 71-6 "Dynamic Stress Analysis of Porous Elastic Solids Saturated with Compressible Fluids," by J. Ghaboussi and E. L. Wilson - 1971 (PB 211 396)A06

EERC 71-7 "Inelastic Behavior of Steel Beam-to-Column Subassemblages," by H. Krawinkler, V.V. Bertero and E.P. Popov 1971 (PB 211 335)A14

EERC 71-8 "Modification of Seismograph Records for Effects of Local Soil Conditions," by P. Schnabel, H.B. Seed and J. Lysmer - 1971 (PB 214 450)A03

EERC 72-1 "Static and Earthquake Analysis of Three Dimensional Frame and Shear Wall Buildings," by E.L. Wilson and H.H. Dovey - 1972 (PB 212 904)A05

EERC 72-2 "Accelerations in Rock for Earthquakes in the Western United States," by P.B. Schnabel and H.B. Seed - 1972 (PB 213 100)A03

EERC 72-3 "Elastic-Plastic Earthquake Response of Soil-Building Systems," by T. Minami - 1972 (PB 214 868)A08

EERC 72-4 "Stochastic Inelastic Response of Offshore Towers to Strong Motion Earthquakes," by M.K. Kaul - 1972 (PB 215 713)A05

EERC 72-5 "Cyclic Behavior of Three Reinforced Concrete Flexural Members with High Shear," by E.P. Popov, V.V. Bertero and H. Krawinkler - 1972 (PB 214 555)A05

EERC 72-6 "Earthquake Response of Gravity Dams Including Reservoir Interaction Effects," by P. Chakrabarti and A.K. Chopra - 1972 (AD 762 330)A08

EERC 72-7 "Dynamic Properties of Pine Flat Dam," by D. Rea, C.Y. Liaw and A.K. Chopra - 1972 (AD 763 928)A05

EERC 72-8 "Three Dimensional Analysis of Building Systems," by E.L. Wilson and H.H. Dovey - 1972 (PB 222 438)A06

EERC 72-9 "Rate of Loading Effects on Uncracked and Repaired Reinforced Concrete Members," by S. Mahin, V.V. Bertero, D. Rea and M. Atalay - 1972 (PB 224 520)A08

EERC 72-10 "Computer Program for Static and Dynamic Analysis of Linear Structural Systems," by E.L. Wilson, K.-J. Bathe, J.E. Peterson and H.H.Dovey - 1972 (PB 220 437)A04

EERC 72-11 "Literature Survey - Seismic Effects on Highway Bridges," by T. Iwasaki, J. Penzien and R.W. Clough - 1972 (PB 215 613)A19

EERC 72-12 "SHAKE-A Computer Program for Earthquake Response Analysis of Horizontally Layered Sites," by P.B. Schnabel and J. Lysmer - 1972 (PB 220 207)A06

EERC 73-1 "Optimal Seismic Design of Multistory Frames," by V.V. Bertero and H. Kamil - 1973

EERC 73-2 "Analysis of the Slides in the San Fernando Dams During the Earthquake of February 9, 1971," by H.B. Seed, K.L. Lee, I.M. Idriss and F. Makdisi - 1973 (PB 223 402)A14

EERC 73-3 "Computer Aided Ultimate Load Design of Unbraced Multistory Steel Frames," by M.B. El-Hafez and G.H. Powell 1973 (PB 248 315)A09

EERC 73-4 "Experimental Investigation into the Seismic Behavior of Critical Regions of Reinforced Concrete Components as Influenced by Moment and Shear," by M. Celebi and J. Penzien - 1973 (PB 215 884)A09

EERC 73-5 "Hysteretic Behavior of Epoxy-Repaired Reinforced Concrete Beams," by M. Celebi and J. Penzien - 1973 (PB 239 568)A03

EERC 73-6 "General Purpose Computer Program for Inelastic Dynamic Response of Plane Structures," by A. Kanaan and G.H. Powell - 1973 (PB 221 260)A08

EERC 73-7 "A Computer Program for Earthquake Analysis of Gravity Dams Including Reservoir Interaction," by P. Chakrabarti and A.K. Chopra - 1973 (AD 766 271)A04

EERC 73-8 "Behavior of Reinforced Concrete Deep Beam-Column Subassemblages Under Cyclic Loads," by O. Küstü and J.G. Bouwkamp - 1973 (PB 246 117)A12

EERC 73-9 "Earthquake Analysis of Structure-Foundation Systems," by A.K. Vaish and A.K. Chopra - 1973 (AD 766 272)A07

EERC 73-10 "Deconvolution of Seismic Response for Linear Systems," by R.B. Reimer - 1973 (PB 227 179)A08

EERC 73-11 "SAP IV: A Structural Analysis Program for Static and Dynamic Response of Linear Systems," by K.-J. Bathe, E.L. Wilson and F.E. Peterson - 1973 (PB 221 967)A09

EERC 73-12 "Analytical Investigations of the Seismic Response of Long, Multiple Span Highway Bridges," by W.S. Tseng and J. Penzien - 1973 (PB 227 816)A10

EERC 73-13 "Earthquake Analysis of Multi-Story Buildings Including Foundation Interaction," by A.K. Chopra and J.A. Gutierrez - 1973 (PB 222 970)A03

EERC 73-14 "ADAP: A Computer Program for Static and Dynamic Analysis of Arch Dams," by R.W. Clough, J.M. Raphael and S. Mojtahedi - 1973 (PB 223 763)A09

EERC 73-15 "Cyclic Plastic Analysis of Structural Steel Joints," by R.B. Pinkney and R.W. Clough - 1973 (PB 226 843)A08

EERC 73-16 "QUAD-4: A Computer Program for Evaluating the Seismic Response of Soil Structures by Variable Damping Finite Element Procedures," by I.M. Idriss, J. Lysmer, R. Hwang and H.B. Seed - 1973 (PB 229 424)A05

EERC 73-17 "Dynamic Behavior of a Multi-Story Pyramid Shaped Building," by R.M. Stephen, J.P. Hollings and J.G. Bouwkamp - 1973 (PB 240 718)A06

EERC 73-18 "Effect of Different Types of Reinforcing on Seismic Behavior of Short Concrete Columns," by V.V. Bertero, J. Hollings, O. Küstü, R.M. Stephen and J.G. Bouwkamp - 1973

EERC 73-19 "Olive View Medical Center Materials Studies, Phase I," by B. Bresler and V.V. Bertero - 1973 (PB 235 986)A06

EERC 73-20 "Linear and Nonlinear Seismic Analysis Computer Programs for Long Multiple-Span Highway Bridges," by W.S. Tseng and J. Penzien - 1973

EERC 73-21 "Constitutive Models for Cyclic Plastic Deformation of Engineering Materials," by J.M. Kelly and P.P. Gillis 1973 (PB 226 024)A03

EERC 73-22 "DRAIN - 2D User's Guide," by G.H. Powell - 1973 (PB 227 016)A05

EERC 73-23 "Earthquake Engineering at Berkeley - 1973," (PB 226 033)A11

EERC 73-24 Unassigned

EERC 73-25 "Earthquake Response of Axisymmetric Tower Structures Surrounded by Water," by C.Y. Liaw and A.K. Chopra 1973 (AD 773 052)A09

EERC 73-26 "Investigation of the Failures of the Olive View Stairtowers During the San Fernando Earthquake and Their Implications on Seismic Design," by V.V. Bertero and R.G. Collins - 1973 (PB 235 106)A13

EERC 73-27 "Further Studies on Seismic Behavior of Steel Beam-Column Subassemblages," by V.V. Bertero, H. Krawinkler and E.P. Popov - 1973 (PB 234 172)A06

EERC 74-1 "Seismic Risk Analysis," by C.S. Oliveira - 1974 (PB 235 920)A06

EERC 74-2 "Settlement and Liquefaction of Sands Under Multi-Directional Shaking," by R. Pyke, C.K. Chan and H.B. Seed 1974

EERC 74-3 "Optimum Design of Earthquake Resistant Shear Buildings," by D. Ray, K.S. Pister and A.K. Chopra - 1974 (PB 231 172)A06

EERC 74-4 "LUSH - A Computer Program for Complex Response Analysis of Soil-Structure Systems," by J. Lysmer, T. Udaka, H.B. Seed and R. Hwang - 1974 (PB 236 796)A05

EERC 74-5 "Sensitivity Analysis for Hysteretic Dynamic Systems: Applications to Earthquake Engineering," by D. Ray 1974 (PB 233 213)A06

EERC 74-6 "Soil Structure Interaction Analyses for Evaluating Seismic Response," by H.B. Seed, J. Lysmer and R. Hwang 1974 (PB 236 519)A04

EERC 74-7 Unassigned

EERC 74-8 "Shaking Table Tests of a Steel Frame - A Progress Report," by R.W. Clough and D. Tang - 1974 (PB 240 869)A03

EERC 74-9 "Hysteretic Behavior of Reinforced Concrete Flexural Members with Special Web Reinforcement," by V.V. Bertero, E.P. Popov and T.Y. Wang - 1974 (PB 236 797)A07

EERC 74-10 "Applications of Reliability-Based, Global Cost Optimization to Design of Earthquake Resistant Structures," by E. Vitiello and K.S. Pister - 1974 (PB 237 231)A06

EERC 74-11 "Liquefaction of Gravelly Soils Under Cyclic Loading Conditions," by R.T. Wong, H.B. Seed and C.K. Chan 1974 (PB 242 042)A03

EERC 74-12 "Site-Dependent Spectra for Earthquake-Resistant Design," by H.B. Seed, C. Ugas and J. Lysmer - 1974 (PB 240 953)A03

EERC 74-13 "Earthquake Simulator Study of a Reinforced Concrete Frame," by P. Hidalgo and R.W. Clough - 1974 (PB 241 944)A13

EERC 74-14 "Nonlinear Earthquake Response of Concrete Gravity Dams," by N. Pal - 1974 (AD/A 006 583)A06

EERC 74-15 "Modeling and Identification in Nonlinear Structural Dynamics - I. One Degree of Freedom Models," by N. Distefano and A. Rath - 1974 (PB 241 548)A06

EERC 75-1 "Determination of Seismic Design Criteria for the Dumbarton Bridge Replacement Structure, Vol. I: Description, Theory and Analytical Modeling of Bridge and Parameters," by F. Baron and S.-H. Pang - 1975 (PB 259 407)A15

EERC 75-2 "Determination of Seismic Design Criteria for the Dumbarton Bridge Replacement Structure, Vol. II: Numerical Studies and Establishment of Seismic Design Criteria," by F. Baron and S.-H. Pang - 1975 (PB 259 408)A11 (For set of EERC 75-1 and 75-2 (PB 259 406))

EERC 75-3 "Seismic Risk Analysis for a Site and a Metropolitan Area," by C.S. Oliveira - 1975 (PB 248 134)A09

EERC 75-4 "Analytical Investigations of Seismic Response of Short, Single or Multiple-Span Highway Bridges," by M.-C. Chen and J. Penzien - 1975 (PB 241 454)A09

EERC 75-5 "An Evaluation of Some Methods for Predicting Seismic Behavior of Reinforced Concrete Buildings," by S.A. Mahin and V.V. Bertero - 1975 (PB 246 306)A16

EERC 75-6 "Earthquake Simulator Study of a Steel Frame Structure, Vol. I: Experimental Results," by R.W. Clough and D.T. Tang - 1975 (PB 243 981)A13

EERC 75-7 "Dynamic Properties of San Bernardino Intake Tower," by D. Rea, C.-Y. Liaw and A.K. Chopra - 1975 (AD/A008 406) A05

EERC 75-8 "Seismic Studies of the Articulation for the Dumbarton Bridge Replacement Structure, Vol. I: Description, Theory and Analytical Modeling of Bridge Components," by F. Baron and R.E. Hamati - 1975 (PB 251 539)A07

EERC 75-9 "Seismic Studies of the Articulation for the Dumbarton Bridge Replacement Structure, Vol. 2: Numerical Studies of Steel and Concrete Girder Alternates," by F. Baron and R.E. Hamati - 1975 (PB 251 540)A10

EERC 75-10 "Static and Dynamic Analysis of Nonlinear Structures," by D.P. Mondkar and G.H. Powell - 1975 (PB 242 434)A08

EERC 75-11 "Hysteretic Behavior of Steel Columns," by E.P. Popov, V.V. Bertero and S. Chandramouli - 1975 (PB 252 365)A11

EERC 75-12 "Earthquake Engineering Research Center Library Printed Catalog," - 1975 (PB 243 711)A26

EERC 75-13 "Three Dimensional Analysis of Building Systems (Extended Version)," by E.L. Wilson, J.P. Hollings and H.H. Dovey - 1975 (PB 243 989)A07

EERC 75-14 "Determination of Soil Liquefaction Characteristics by Large-Scale Laboratory Tests," by P. De Alba, C.K. Chan and H.B. Seed - 1975 (NUREG 0027)A08

EERC 75-15 "A Literature Survey - Compressive, Tensile, Bond and Shear Strength of Masonry," by R.L. Mayes and R.W. Clough - 1975 (PB 246 292)A10

EERC 75-16 "Hysteretic Behavior of Ductile Moment Resisting Reinforced Concrete Frame Components," by V.V. Bertero and E.P. Popov - 1975 (PB 246 388)A05

EERC 75-17 "Relationships Between Maximum Acceleration, Maximum Velocity, Distance from Source, Local Site Conditions for Moderately Strong Earthquakes," by H.B. Seed, R. Murarka, J. Lysmer and I.M. Idriss - 1975 (PB 248 172)A03

EERC 75-18 "The Effects of Method of Sample Preparation on the Cyclic Stress-Strain Behavior of Sands," by J. Mulilis, C.K. Chan and H.B. Seed - 1975 (Summarized in EERC 75-28)

EERC 75-19 "The Seismic Behavior of Critical Regions of Reinforced Concrete Components as Influenced by Moment, Shear and Axial Force," by M.B. Atalay and J. Penzien - 1975 (PB 258 842)A11

EERC 75-20 "Dynamic Properties of an Eleven Story Masonry Building," by R.M. Stephen, J.P. Hollings, J.G. Bouwkamp and D. Jurukovski - 1975 (PB 246 945)A04

EERC 75-21 "State-of-the-Art in Seismic Strength of Masonry - An Evaluation and Review," by R.L. Mayes and R.W. Clough 1975 (PB 249 040)A07

EERC 75-22 "Frequency Dependent Stiffness Matrices for Viscoelastic Half-Plane Foundations," by A.K. Chopra, P. Chakrabarti and G. Dasgupta - 1975 (PB 248 121)A07

EERC 75-23 "Hysteretic Behavior of Reinforced Concrete Framed Walls," by T.Y. Wong, V.V. Bertero and E.P. Popov - 1975

EERC 75-24 "Testing Facility for Subassemblages of Frame-Wall Structural Systems," by V.V. Bertero, E.P. Popov and T. Endo - 1975

EERC 75-25 "Influence of Seismic History on the Liquefaction Characteristics of Sands," by H.B. Seed, K. Mori and C.K. Chan - 1975 (Summarized in EERC 75-28)

EERC 75-26 "The Generation and Dissipation of Pore Water Pressures during Soil Liquefaction," by H.B. Seed, P.P. Martin and J. Lysmer - 1975 (PB 252 648)A03

EERC 75-27 "Identification of Research Needs for Improving Aseismic Design of Building Structures," by V.V. Bertero 1975 (PB 248 136)A05

EERC 75-28 "Evaluation of Soil Liquefaction Potential during Earthquakes," by H.B. Seed, I. Arango and C.K. Chan - 1975 (NUREG 0026)A13

EERC 75-29 "Representation of Irregular Stress Time Histories by Equivalent Uniform Stress Series in Liquefaction Analyses," by H.B. Seed, I.M. Idriss, F. Makdisi and N. Banerjee - 1975 (PB 252 635)A03

EERC 75-30 "FLUSH - A Computer Program for Approximate 3-D Analysis of Soil-Structure Interaction Problems," by J. Lysmer, T. Udaka, C.-F. Tsai and H.B. Seed - 1975 (PB 259 332)A07

EERC 75-31 "ALUSH - A Computer Program for Seismic Response Analysis of Axisymmetric Soil-Structure Systems," by E. Berger, J. Lysmer and H.B. Seed - 1975

EERC 75-32 "TRIP and TRAVEL - Computer Programs for Soil-Structure Interaction Analysis with Horizontally Travelling Waves," by T. Udaka, J. Lysmer and H.B. Seed - 1975

EERC 75-33 "Predicting the Performance of Structures in Regions of High Seismicity," by J. Penzien - 1975 (PB 248 130)A03

EERC 75-34 "Efficient Finite Element Analysis of Seismic Structure - Soil - Direction," by J. Lysmer, H.B. Seed, T. Udaka, R.N. Hwang and C.-F. Tsai - 1975 (PB 253 570)A03

EERC 75-35 "The Dynamic Behavior of a First Story Girder of a Three-Story Steel Frame Subjected to Earthquake Loading," by R.W. Clough and L.-Y. Li - 1975 (PB 248 841)A05

EERC 75-36 "Earthquake Simulator Study of a Steel Frame Structure, Volume II - Analytical Results," by D.T. Tang - 1975 (PB 252 926)A10

EERC 75-37 "ANSR-I General Purpose Computer Program for Analysis of Non-Linear Structural Response," by D.P. Mondkar and G.H. Powell - 1975 (PB 252 386)A08

EERC 75-38 "Nonlinear Response Spectra for Probabilistic Seismic Design and Damage Assessment of Reinforced Concrete Structures," by M. Murakami and J. Penzien - 1975 (PB 259 530)A05

EERC 75-39 "Study of a Method of Feasible Directions for Optimal Elastic Design of Frame Structures Subjected to Earthquake Loading," by N.D. Walker and K.S. Pister - 1975 (PB 257 781)A06

EERC 75-40 "An Alternative Representation of the Elastic-Viscoelastic Analogy," by G. Dasgupta and J.L. Sackman - 1975 (PB 252 173)A03

EERC 75-41 "Effect of Multi-Directional Shaking on Liquefaction of Sands," by H.B. Seed, R. Pyke and G.R. Martin - 1975 (PB 258 781)A03

EERC 76-1 "Strength and Ductility Evaluation of Existing Low-Rise Reinforced Concrete Buildings - Screening Method," by T. Okada and B. Bresler - 1976 (PB 257 906)A11

EERC 76-2 "Experimental and Analytical Studies on the Hysteretic Behavior of Reinforced Concrete Rectangular and T-Beams," by S.-Y.M. Ma, E.P. Popov and V.V. Bertero - 1976 (PB 260 843)A12

EERC 76-3 "Dynamic Behavior of a Multistory Triangular-Shaped Building," by J. Petrovski, R.M. Stephen, E. Gartenbaum and J.G. Bouwkamp - 1976 (PB 273 279)A07

EERC 76-4 "Earthquake Induced Deformations of Earth Dams," by N. Serff, H.B. Seed, F.I. Makdisi & C.-Y. Chang - 1976 (PB 292 065)A08

EERC 76-5 "Analysis and Design of Tube-Type Tall Building Structures," by H. de Clercq and G.H. Powell - 1976 (PB 252 220) A10

EERC 76-6 "Time and Frequency Domain Analysis of Three-Dimensional Ground Motions, San Fernando Earthquake," by T. Kubo and J. Penzien (PB 260 556)A11

EERC 76-7 "Expected Performance of Uniform Building Code Design Masonry Structures," by R.L. Mayes, Y. Omote, S.W. Chen and R.W. Clough - 1976 (PB 270 098)A05

EERC 76-8 "Cyclic Shear Tests of Masonry Piers, Volume 1 - Test Results," by R.L. Mayes, Y. Omote, R.W. Clough - 1976 (PB 264 424)A06

EERC 76-9 "A Substructure Method for Earthquake Analysis of Structure - Soil Interaction," by J.A. Gutierrez and A.K. Chopra - 1976 (PB 257 783)A08

EERC 76-10 "Stabilization of Potentially Liquefiable Sand Deposits using Gravel Drain Systems," by H.B. Seed and J.R. Booker - 1976 (PB 258 820)A04

EERC 76-11 "Influence of Design and Analysis Assumptions on Computed Inelastic Response of Moderately Tall Frames," by G.H. Powell and D.G. Row - 1976 (PB 271 409)A06

EERC 76-12 "Sensitivity Analysis for Hysteretic Dynamic Systems: Theory and Applications," by D. Ray, K.S. Pister and E. Polak - 1976 (PB 262 859)A04

EERC 76-13 "Coupled Lateral Torsional Response of Buildings to Ground Shaking," by C.L. Kan and A.K. Chopra - 1976 (PB 257 907)A09

EERC 76-14 "Seismic Analyses of the Banco de America," by V.V. Bertero, S.A. Mahin and J.A. Hollings - 1976

EERC 76-15 "Reinforced Concrete Frame 2: Seismic Testing and Analytical Correlation," by R.W. Clough and J. Gidwani - 1976 (PB 261 323)A08

EERC 76-16 "Cyclic Shear Tests of Masonry Piers, Volume 2 - Analysis of Test Results," by R.L. Mayes, Y. Omote and R.W. Clough - 1976

EERC 76-17 "Structural Steel Bracing Systems: Behavior Under Cyclic Loading," by E.P. Popov, K. Takanashi and C.W. Roeder - 1976 (PB 260 715)A05

EERC 76-18 "Experimental Model Studies on Seismic Response of High Curved Overcrossings," by D. Williams and W.G. Godden - 1976 (PB 269 548)A08

EERC 76-19 "Effects of Non-Uniform Seismic Disturbances on the Dumbarton Bridge Replacement Structure," by F. Baron and R.E. Hamati - 1976 (PB 282 981)A16

EERC 76-20 "Investigation of the Inelastic Characteristics of a Single Story Steel Structure Using System Identification and Shaking Table Experiments," by V.C. Matzen and H.D. McNiven - 1976 (PB 258 453)A07

EERC 76-21 "Capacity of Columns with Splice Imperfections," by E.P. Popov, R.M. Stephen and R. Philbrick - 1976 (PB 260 378)A04

EERC 76-22 "Response of the Olive View Hospital Main Building during the San Fernando Earthquake," by S. A. Mahin, V.V. Bertero, A.K. Chopra and R. Collins - 1976 (PB 271 425)A14

EERC 76-23 "A Study on the Major Factors Influencing the Strength of Masonry Prisms," by N.M. Mostaghel, R.L. Mayes, R. W. Clough and S.W. Chen - 1976 (Not published)

EERC 76-24 "GADFLEA - A Computer Program for the Analysis of Pore Pressure Generation and Dissipation during Cyclic or Earthquake Loading," by J.R. Booker, M.S. Rahman and H.B. Seed - 1976 (PB 263 947)A04

EERC 76-25 "Seismic Safety Evaluation of a R/C School Building," by B. Bresler and J. Axley - 1976

EERC 76-26 "Correlative Investigations on Theoretical and Experimental Dynamic Behavior of a Model Bridge Structure," by K. Kawashima and J. Penzien - 1976 (PB 263 388)A11

EERC 76-27 "Earthquake Response of Coupled Shear Wall Buildings," by T. Srichatrapimuk - 1976 (PB 265 157)A07

EERC 76-28 "Tensile Capacity of Partial Penetration Welds," by E.P. Popov and R.M. Stephen - 1976 (PB 262 899)A03

EERC 76-29 "Analysis and Design of Numerical Integration Methods in Structural Dynamics," by H.M. Hilber - 1976 (PB 264 410)A06

EERC 76-30 "Contribution of a Floor System to the Dynamic Characteristics of Reinforced Concrete Buildings," by L.E. Malik and V.V. Bertero - 1976 (PB 272 247)A13

EERC 76-31 "The Effects of Seismic Disturbances on the Golden Gate Bridge," by F. Baron, M. Arikan and R.E. Hamati - 1976 (PB 272 279)A09

EERC 76-32 "Infilled Frames in Earthquake Resistant Construction," by R.E. Klingner and V.V. Bertero - 1976 (PB 265 892)A13

UCB/EERC-77/01 "PLUSH - A Computer Program for Probabilistic Finite Element Analysis of Seismic Soil-Structure Interaction," by M.P. Romo Organista, J. Lysmer and H.B. Seed - 1977

UCB/EERC-77/02 "Soil-Structure Interaction Effects at the Humboldt Bay Power Plant in the Ferndale Earthquake of June 7, 1975," by J.E. Valera, H.B. Seed, C.F. Tsai and J. Lysmer - 1977 (PB 265 795)A04

UCB/EERC-77/03 "Influence of Sample Disturbance on Sand Response to Cyclic Loading," by K. Mori, H.B. Seed and C.K. Chan - 1977 (PB 267 352)A04

UCB/EERC-77/04 "Seismological Studies of Strong Motion Records," by J. Shoja-Taheri - 1977 (PB 269 655)A10

UCB/EERC-77/05 "Testing Facility for Coupled-Shear Walls," by L. Li-Hyung, V.V. Bertero and E.P. Popov - 1977

UCB/EERC-77/06 "Developing Methodologies for Evaluating the Earthquake Safety of Existing Buildings," by No. 1 - B. Bresler; No. 2 - B. Bresler, T. Okada and D. Zisling; No. 3 - T. Okada and B. Bresler; No. 4 - V.V. Bertero and B. Bresler - 1977 (PB 267 354)A08

UCB/EERC-77/07 "A Literature Survey - Transverse Strength of Masonry Walls," by Y. Omote, R.L. Mayes, S.W. Chen and R.W. Clough - 1977 (PB 277 933)A07

UCB/EERC-77/08 "DRAIN-TABS: A Computer Program for Inelastic Earthquake Response of Three Dimensional Buildings," by R. Guendelman-Israel and G.H. Powell - 1977 (PB 270 693)A07

UCB/EERC-77/09 "SUBWALL: A Special Purpose Finite Element Computer Program for Practical Elastic Analysis and Design of Structural Walls with Substructure Option," by D.Q. Le, H. Peterson and E.P. Popov - 1977 (PB 270 567)A05

UCB/EERC-77/10 "Experimental Evaluation of Seismic Design Methods for Broad Cylindrical Tanks," by D.P. Clough (PB 272 280)A13

UCB/EERC-77/11 "Earthquake Engineering Research at Berkeley - 1976," - 1977 (PB 273 507)A09

UCB/EERC-77/12 "Automated Design of Earthquake Resistant Multistory Steel Building Frames," by N.D. Walker, Jr. - 1977 (PB 276 526)A09

UCB/EERC-77/13 "Concrete Confined by Rectangular Hoops Subjected to Axial Loads," by J. Vallenas, V.V. Bertero and E.P. Popov - 1977 (PB 275 165)A06

UCB/EERC-77/14 "Seismic Strain Induced in the Ground During Earthquakes," by Y. Sugimura - 1977 (PB 284 201)A04

UCB/EERC-77/15 "Bond Deterioration under Generalized Loading," by V.V. Bertero, E.P. Popov and S. Viwathanatepa - 1977

UCB/EERC-77/16 "Computer Aided Optimum Design of Ductile Reinforced Concrete Moment Resisting Frames," by S.W. Zagajeski and V.V. Bertero - 1977 (PB 280 137)A07

UCB/EERC-77/17 "Earthquake Simulation Testing of a Stepping Frame with Energy-Absorbing Devices," by J.M. Kelly and D.F. Tsztoo - 1977 (PB 273 506)A04

UCB/EERC-77/18 "Inelastic Behavior of Eccentrically Braced Steel Frames under Cyclic Loadings," by C.W. Roeder and E.P. Popov - 1977 (PB 275 526)A15

UCB/EERC-77/19 "A Simplified Procedure for Estimating Earthquake-Induced Deformations in Dams and Embankments," by F.I. Makdisi and H.B. Seed - 1977 (PB 276 820)A04

UCB/EERC-77/20 "The Performance of Earth Dams during Earthquakes," by H.B. Seed, F.I. Makdisi and P. de Alba - 1977 (PB 276 821)A04

UCB/EERC-77/21 "Dynamic Plastic Analysis Using Stress Resultant Finite Element Formulation," by P. Lukkunapvasit and J.M. Kelly - 1977 (PB 275 453)A04

UCB/EERC-77/22 "Preliminary Experimental Study of Seismic Uplift of a Steel Frame," by R.W. Clough and A.A. Huckelbridge 1977 (PB 278 769)A08

UCB/EERC-77/23 "Earthquake Simulator Tests of a Nine-Story Steel Frame with Columns Allowed to Uplift," by A.A. Huckelbridge - 1977 (PB 277 944)A09

UCB/EERC-77/24 "Nonlinear Soil-Structure Interaction of Skew Highway Bridges," by M.-C. Chen and J. Penzien - 1977 (PB 276 176)A07

UCB/EERC-77/25 "Seismic Analysis of an Offshore Structure Supported on Pile Foundations," by D.D.-N. Liou and J. Penzien 1977 (PB 283 180)A06

UCB/EERC-77/26 "Dynamic Stiffness Matrices for Homogeneous Viscoelastic Half-Planes," by G. Dasgupta and A.K. Chopra - 1977 (PB 279 654)A06

UCB/EERC-77/27 "A Practical Soft Story Earthquake Isolation System," by J.M. Kelly, J.M. Eidinger and C.J. Derham - 1977 (PB 276 814)A07

UCB/EERC-77/28 "Seismic Safety of Existing Buildings and Incentives for Hazard Mitigation in San Francisco: An Exploratory Study," by A.J. Meltsner - 1977 (PB 281 970)A05

UCB/EERC-77/29 "Dynamic Analysis of Electrohydraulic Shaking Tables," by D. Rea, S. Abedi-Hayati and Y. Takahashi 1977 (PB 282 569)A04

UCB/EERC-77/30 "An Approach for Improving Seismic - Resistant Behavior of Reinforced Concrete Interior Joints," by B. Galunic, V.V. Bertero and E.P. Popov - 1977 (PB 290 870)A06

UCB/EERC-78/01 "The Development of Energy-Absorbing Devices for Aseismic Base Isolation Systems," by J.M. Kelly and D.F. Tsztoo - 1978 (PB 284 978)A04

UCB/EERC-78/02 "Effect of Tensile Prestrain on the Cyclic Response of Structural Steel Connections, by J.G. Bouwkamp and A. Mukhopadhyay - 1978

UCB/EERC-78/03 "Experimental Results of an Earthquake Isolation System using Natural Rubber Bearings," by J.M. Eidinger and J.M. Kelly - 1978 (PB 281 686)A04

UCB/EERC-78/04 "Seismic Behavior of Tall Liquid Storage Tanks," by A. Niwa - 1978 (PB 284 017)A14

UCB/EERC-78/05 "Hysteretic Behavior of Reinforced Concrete Columns Subjected to High Axial and Cyclic Shear Forces," by S.W. Zagajeski, V.V. Bertero and J.G. Bouwkamp - 1978 (PB 283 858)A13

UCB/EERC-78/06 "Inelastic Beam-Column Elements for the ANSR-I Program," by A. Riahi, D.G. Row and G.H. Powell - 1978

UCB/EERC-78/07 "Studies of Structural Response to Earthquake Ground Motion," by O.A. Lopez and A.K. Chopra - 1978 (PB 282 790)A05

UCB/EERC-78/08 "A Laboratory Study of the Fluid-Structure Interaction of Submerged Tanks and Caissons in Earthquakes," by R.C. Byrd - 1978 (PB 284 957)A08

UCB/EERC-78/09 "Model for Evaluating Damageability of Structures," by I. Sakamoto and B. Bresler - 1978

UCB/EERC-78/10 "Seismic Performance of Nonstructural and Secondary Structural Elements," by I. Sakamoto - 1978

UCB/EERC-78/11 "Mathematical Modelling of Hysteresis Loops for Reinforced Concrete Columns," by S. Nakata, T. Sproul and J. Penzien - 1978

UCB/EERC-78/12 "Damageability in Existing Buildings," by T. Blejwas and B. Bresler - 1978

UCB/EERC-78/13 "Dynamic Behavior of a Pedestal Base Multistory Building," by R.M. Stephen, E.L. Wilson, J.G. Bouwkamp and M. Button - 1978 (PB 286 650)A08

UCB/EERC-78/14 "Seismic Response of Bridges - Case Studies," by R.A. Imbsen, V. Nutt and J. Penzien - 1978 (PB 286 503)A10

UCB/EERC-78/15 "A Substructure Technique for Nonlinear Static and Dynamic Analysis," by D.G. Row and G.H. Powell - 1978 (PB 288 077)A10

UCB/EERC-78/16 "Seismic Risk Studies for San Francisco and for the Greater San Francisco Bay Area," by C.S. Oliveira - 1978

UCB/EERC-78/17 "Strength of Timber Roof Connections Subjected to Cyclic Loads," by P. Gülkan, R.L. Mayes and R.W. Clough - 1978

UCB/EERC-78/18 "Response of K-Braced Steel Frame Models to Lateral Loads," by J.G. Bouwkamp, R.M. Stephen and E.P. Popov - 1978

UCB/EERC-78/19 "Rational Design Methods for Light Equipment in Structures Subjected to Ground Motion," by J.L. Sackman and J.M. Kelly - 1978 (PB 292 357)A04

UCB/EERC-78/20 "Testing of a Wind Restraint for Aseismic Base Isolation," by J.M. Kelly and D.E. Chitty - 1978 (PB 292 833)A03

UCB/EERC-78/21 "APOLLO - A Computer Program for the Analysis of Pore Pressure Generation and Dissipation in Horizontal Sand Layers During Cyclic or Earthquake Loading," by P.P. Martin and H.B. Seed - 1978 (PB 292 835)A04

UCB/EERC-78/22 "Optimal Design of an Earthquake Isolation System," by M.A. Bhatti, K.S. Pister and E. Polak - 1978 (PB 294 735)A06

UCB/EERC-78/23 "MASH - A Computer Program for the Non-Linear Analysis of Vertically Propagating Shear Waves in Horizontally Layered Deposits," by P.P. Martin and H.B. Seed - 1978 (PB 293 101)A05

UCB/EERC-78/24 "Investigation of the Elastic Characteristics of a Three Story Steel Frame Using System Identification," by I. Kaya and H.D. McNiven - 1978

UCB/EERC-78/25 "Investigation of the Nonlinear Characteristics of a Three-Story Steel Frame Using System Identification," by I. Kaya and H.D. McNiven - 1978

UCB/EERC-78/26 "Studies of Strong Ground Motion in Taiwan," by Y.M. Hsiung, B.A. Bolt and J. Penzien - 1978

UCB/EERC-78/27 "Cyclic Loading Tests of Masonry Single Piers: Volume 1 - Height to Width Ratio of 2," by P.A. Hidalgo, R.L. Mayes, H.D. McNiven and R.W. Clough - 1978

UCB/EERC-78/28 "Cyclic Loading Tests of Masonry Single Piers: Volume 2 - Height to Width Ratio of 1," by S.-W.J. Chen, P.A. Hidalgo, R.L. Mayes, R.W. Clough and H.D. McNiven - 1978

UCB/EERC-78/29 "Analytical Procedures in Soil Dynamics," by J. Lysmer - 1978

UCB/EERC-79/01 "Hysteretic Behavior of Lightweight Reinforced Concrete Beam-Column Subassemblages," by B. Forzani, E.P. Popov, and V.V. Bertero - 1979

UCB/EERC-79/02 "The Development of a Mathematical Model to Predict the Flexural Response of Reinforced Concrete Beams to Cyclic Loads, Using System Identification," by J.F. Stanton and H.D. McNiven - 1979

UCB/EERC-79/03 "Linear and Nonlinear Earthquake Response of Simple Torsionally Coupled Systems," by C.L. Kan and A.K. Chopra - 1979

UCB/EERC-79/04 "A Mathematical Model of Masonry for Predicting Its Linear Seismic Response Characteristics," by Y. Mengi and H.D. McNiven - 1979

UCB/EERC-79/05 "Mechanical Behavior of Lightweight Concrete Confined by Different Types of Lateral Reinforcement," by M.A. Manrique, V.V. Bertero, and E.P. Popov - 1979

UCB/EERC-79/06 "Static Tilt Tests of a Tall Cylindrical Liquid Storage Tank," by R.W. Clough and A. Niwa - 1979

UCB/EERC-79/07 "The Design of Steel Energy Absorbing Restrainers and Their Incorporation Into Nuclear Power Plants for Enhanced Safety: Volume 1 - Summary Report," by P.N. Spencer, V.F. Zackay, and E.R. Parker - 1979

UCB/EERC-79/08 "The Design of Steel Energy Absorbing Restrainers and Their Incorporation Into Nuclear Power Plants for Enhanced Safety: Volume 2 - The Development of Analyses for Reactor System Piping," "Simple Systems" by M.C. Lee, J. Penzien, A.K. Chopra, and K. Suzuki, "Complex Systems" by G.H. Powell, E.L. Wilson, R.W. Clough and D.G. Row - 1979

UCB/EERC-79/09 "The Design of Steel Energy Absorbing Restrainers and Their Incorporation Into Nuclear Power Plants for Enhanced Safety: Volume 3 - Evaluation of Commercial Steels," by W.S. Owen, R.M.N. Pelloux, R.O. Ritchie, M. Faral, T. Ohhashi, J. Toplosky, S.J. Hartman, V.F. Zackay, and E.R. Parker - 1979

UCB/EERC-79/10 "The Design of Steel Energy Absorbing Restrainers and Their Incorporation Into Nuclear Power Plants for Enhanced Safety: Volume 4 - A Review of Energy-Absorbing Devices," by J.M. Kelly and M.S. Skinner - 1979

UCB/EERC-79/11 "Conservatism In Summation Rules for Closely Spaced Modes," by J.M. Kelly and J.L. Sackman - 1979

UCB/EERC-79/12 "Cyclic Loading Tests of Masonry Single Piers Volume 3 - Height to Width Ratio of 0.5," by P.A. Hidalgo, R.L. Mayes, H.D. McNiven, and R.W. Clough - 1979

UCB/EERC-79/13 "Cyclic Behavior of Dense Coarse-Grained Materials in Relation to the Seismic Stability of Dams," by N.G. Banerjee, H.B. Seed, and C.K. Chan - 1979

UCB/EERC-79/14 "Seismic Behavior of Reinforced Concrete Interior Beam Column Subassemblages," by S. Viwathanatepa, E.P. Popov, and V.V. Bertero - 1979

UCB/EERC-79/15 "Optimal Design of Localized Nonlinear Systems with Dual Performance Criteria Under Earthquake Excitations," by M.A. Bhatti - 1979

UCB/EERC-79/16 "OPTDYN - A General Purpose Optimization Program for Problems with or without Dynamic Constraints," by M.A. Bhatti, E. Polak, and K.S. Pister - 1979

UCB/EERC-79/17 "ANSR-II, Analysis of Nonlinear Structural Response Users Manual," by D.P. Mondkar and G.H. Powell - 1979

UCB/EERC-79/18 "Soil Structure Interaction in Different Seismic Environments," A. Gomez-Masso, J. Lysmer, J.C. Chen, and H.B. Seed - 1979

UCB/EERC-79/19 "ARMA Models for Earthquake Ground Motions," by M.K. Chang, J.W. Kwiatkowski, R.F. Nau, R.M. Oliver, and K.S. Pister - 1979

UCB/EERC-79/20 "Hysteretic Behavior of Reinforced Concrete Structural Walls," by J.M. Vallenas, V.V. Bertero, and E.P. Popov - 1979

UCB/EERC-79/21 "Studies on High-Frequency Vibrations of Buildings I: The Column Effects," by J. Lubliner - 1979

UCB/EERC-79/22 "Effects of Generalized Loadings on Bond Reinforcing Bars Embedded in Confined Concrete Blocks," by S. Viwathanatepa, E.P. Popov, and V.V. Bertero - 1979

UCB/EERC-79/23 "Shaking Table Study of Single-Story Masonry Houses, Volume I: Test Structures 1 and 2," by P. Gülkan, R.L. Mayes, and R.W. Clough - 1979

UCB/EERC-79/24 "Shaking Table Study of Single-Story Masonry Houses, Volume 2: Tests Structures 3 and 4," by P. Gülkan, R.L. Mayes, and R.W. Clough - 1979

UCB/EERC-79/25 "Shaking Table Study of Single-Story Masonry Houses, Volume 3: Summary, Conclusions and Recommendations," by R.W. Clough, P. Gülkan, and R.L. Mayes

UCB/EERC-79/26	"Recommendations for a U.S.-Japan Cooperative Research Program Utilizing Large-Scale Testing Facilities," by U.S.-Japan Planning Group - 1979
UCB/EERC-79/27	"Earthquake-Induced Liquefaction Near Lake Amatitlan, Guatemala," by H.B. Seed, I. Arango, C.K. Chan, A. Gomez-Masso, and R. Grant de Ascoli - 1979
UCB/EERC-79/28	"Infill Panels: Their Influence on Seismic Response of Buildings," by J.W. Axley and V.V. Bertero - 1979
UCB/EERC-79/29	"3D Truss Bar Element (Type 1) for the ANSR-II Program," by D.P. Mondkar and G.H. Powell - 1979
UCB/EERC-79/30	"2D Beam-Column Element (Type 5 - Parallel Element Theory) for the ANSR-II Program," by D.G. Row, G.H. Powell, and D.P. Mondkar
UCB/EERC-79/31	"3D Beam-Column Element (Type 2 - Parallel Element Theory) for the ANSR-II Program," by A. Riahi, G.H. Powell, and D.P. Mondkar - 1979
UCB/EERC-79/32	"On Response of Structures to Stationary Excitation," by A. Der Kiureghian - 1979
UCB/EERC-79/33	"Undisturbed Sampling and Cyclic Load Testing of Sands," by S. Singh, H.B. Seed, and C.K. Chan - 1979
UCB/EERC-79/34	"Interaction Effects of Simultaneous Torsional and Compressional Cyclic Loading of Sand," by P.M. Griffin and W.N. Houston - 1979
UCB/EERC-80/01	"Earthquake Response of Concrete Gravity Dams Including Hydrodynamic and Foundation Interaction Effects," by A.K. Chopra, P. Charkabarti, and S. Gupta - 1980
UCB/EERC-80/02	"Rocking Response of Rigid Blocks to Earthquakes," by C.S. Yim, A.K. Chopra, and J. Penzien - 1980
UCB/EERC-80/03	"Optimum Inelastic Design of Seismic-Resistant Reinforced Concrete Frame Structures," by S.W. Zagajeski and V.V. Bertero - 1980
UCB/EERC-80/04	"Effects of Amount and Arrangement of Wall-Panel Reinforcement on Hysteretic Behavior of Reinforced Concrete Walls," by R. Iliya and V.V. Bertero - 1980
UCB/EERC-80/05	"Shaking Table Research on Concrete Dam Models," by R.W. Clough and A. Niwa - 1980
UCB/EERC-80/06	"Piping With Energy Absorbing Restrainers: Parameter Study on Small Systems," by G.H. Powell, C. Oughourlian and J. Simons - 1980

UCB/EERC-80/07 "Inelastic Torsional Response of Structures Subjected to Earthquake Ground Motions," by Y. Yamazaki - 1980

UCB/EERC-80/08 "Study of X-Braced Steel Frame Structures Under Earthquake Simulation," by Y. Ghanaat - 1980